A

T H E S I S

entitled

THE GEOCHEMISTRY OF FERROMANGANESE OXIDE DEPOSITS AND PELAGIC SEDIMENTS OF THE NORTH WEST INDIAN OCEAN.

submitted for the degree of

DOCTOR OF PHILOSOPHY

in the

FACULTY OF SCIENCE OF THE UNIVERSITY OF LONDON

by

NICHOLAS MARTIN COLLEY

Royal School of Mines,
Imperial College.

April, 1980.

A B S T R A C T

Ferromanganese encrustations and nodules from several sites in the N.W. Indian Ocean, and from certain other locations, have been investigated by several means. The composition of the deposits has been determined by atomic absorption spectrophotometry and the electron microprobe. The mineralogy has been determined using X- ray diffraction techniques. The scanning electron microscope has been used to try and relate chemistry and mineralogy to structure and morphology.

A suite of sediment samples has been analysed by atomic absorption spectrophotometry. The metals Al, Fe, and Ti are supplied to the sediments largely in terrigenous detritus. Hydrogenously derived metals are Mn, Ni and usually Cu. In elevated areas a biogenic control on Cu is evident.

A biogenic control on Cu distribution in ferromanganese oxide concretions is suggested by its variation in crusts and nodules from different water depths. A rapid increase in the Cu level is seen below the lysocline. In crusts from seamounts, Cu is significantly concentrated in detrital phases.

Volcanic influences on ferromanganese crusts, as indicated by high Fe/Mn ratios, high levels of aluminosilicate minerals, and high Al contents, are seen in two adjacent seamount locations. This may indicate relatively recent volcanic activity. A volcanic input to the sediment is seen only at the bottom of a few cores from the crest of the Carlsberg Ridge.

Two partially infilled cracks, in two of the crusts, have been studied, optically and chemically. At least one probably provided access for sea water and perhaps particulate matter to penetrate the crust. This caused diagenetic alteration of pre-existing oxides, resulting in metal enrichment in the crack vicinity.

The S.E.M. study revealed accumulations of sediment debris in the

hollows on crust surfaces. Bottom currents are thought to be responsible for this, carrying sediment particles along and depositing them in sheltered hollows, where reaction with oxide material may subsequently occur. Abrasion of the crust surface by particles suspended in the bottom current may be responsible for a later polishing and smoothing of crust surfaces.

A C K N O W L E D G E M E N T S

The research described in this thesis was carried out in the Applied Geochemistry Research Group, Imperial College, under the general direction of Professor J.S.Webb. The project was supervised throughout by Dr. D.S.Cronan, to whom I would like to express my gratitude.

The writer would like to acknowledge the many people who have been concerned with this project. In particular, I would like to thank:

The Master, officers and crew of the R.R.S.Shackleton for collecting most of the samples studied.

Mr. B.Foster and Miss. E.Morris for preparing polished sections.

Mr. P.Suddaby and Mr. N.Wilkinson for their invaluable help with the electron probe analyses.

Mr. Ray Curtis for his guidance and advice with the X- ray diffraction analyses.

Dr. R.Howarth and Messrs. S.Earle, M.Frost and S.Mancey for their assistance with the data processing.

Miss. P.Muttiah, Mr.M. Ahmed, Mr. J.Murphy, and Dr.B.Imber for atomic absorption analyses.

Mrs. H.Richardson for assistance in reproducing diagrams and photographs.

Miss. S.Shearme, Dr.S.Moorby and Mr.T.Cole for many fruitful discussions.

I am particularly grateful to Dr. Peter Rona, A.O.M.L.,Miami, for allowing me to participate in the 1976 cruise of the N.O.A.A. ship "Researcher" to the T.A.G. hydrothermal field.

Special thanks are due to Dr. Claude Lalou, C.N.R.S., Paris, for allowing me to participate in Colloque International du C.N.R.S. no. 289: Sur la Genèse des Nodules de Manganèse, September 1978.

Sincere thanks are also due to Mrs. Barbara Clark for typing the manuscript.

The work was supported by a Natural Environment Research Council grant, for which I am most grateful.

TABLE OF CONTENTS

LIST OF FIGURES

LIST OF TABLES

LIST OF PLATES

CHAPTER 1

INTRODUCTION

a) Introductory remarks

Deep sea ferromanganese oxide deposits have been a source of interest and controversy ever since their discovery during the Challenger Expedition of 1873-76 (Murray & Renard, 1891). Research on these deposits was sporadic until the late 1950s and early 60s, when more detailed sampling of the deposits in all three oceans revealed their great extent and highlighted their potential as ore deposits.

Despite the great amount of work which has now been carried out, many problems relating to marine ferromanganese oxide deposits are still unsolved. Among the unsolved geochemical problems which these deposits still pose are the relative importance of the sources of the major and trace elements in the authigenic phases, the rates and mechanisms of growth of the deposits, and the way in which the minor elements are incorporated into the deposits. Many reviews of the subject, covering one or more of these problems are to be found in the literature and the reader is referred to the following as giving fuller accounts of the problems: Murray & Renard,(1891), Goldberg, (1954),

Goldberg & Arrhenius, (1958); Goldberg,(1961);Arrhenius, (1963); Arrhenius & Bonatti, (1965); Bonatti & Nayudu, (1965); Mero (1965); Bonatti et al, (1972); Cronan,(1976); Glasby (1977).

Until relatively recently attempts were made to explain all ferromanganese oxide deposits as originating from one particular source over others throughout the World Ocean. Goldberg & Arrhenius (1958), Arrhenius et al.,(1964) and Glasby, (1973),all thought that terrigenous material contributed most to nodule formation, and that the seawater itself was a fairly inert transport medium to carry terrigenous material to the reaction site on the surface of the deposit. However, Bonatti & Nayudu(1965), cast serious doubts upon this theory and put forward a convincing argument that submarine volcanism was the main influence in nodule formation. Post-depositional remobilisation of manganese through the sediment column has not been proposed as a major influence on nodule composition on a world scale, although it may be important in near-shore nodules, where the organic content of the sediment is high, resulting in a low sediment redox potential.

When it was realised that single-source models could not be used to explain the phenomenon of ferromanganese oxide deposits, polygenetic models were proposed (e.g. Bonatti et al, 1972), where hydrogenous precipitation from sea water, submarine volcanism and, for nodules, diagenetic remobilisation all play a part in controlling the character of a deposit. Depending on the geochemical history of the environment of a deposit on the sea floor, then the

significance of each process will have fluctuated. If a series of nodules and crusts at varying distances from the crest of an active ridge could be investigated, then it may be possible to determine the relative importance of these three genetic influences on the character of the deposits, bearing in mind the geochemical criteria suggested by Bonatti et al., (1972) for distinguishing between these influences. Volcanic influences would be expected to predominate early in the history of a deposit, while hydrogenous and diagenetic influences will gradually predominate as the nodule moves away from the ridge crest under the influence of sea-floor spreading. Hopefully, chemical or mineralogical parameters might be found that can categorically be said to indicate a volcanic influence on the deposits.

In order to consider the problem of volcanism and the genesis of ferromanganese oxide deposits, factors other than the geochemistry should be considered.

In recent years, much detailed work has been done on specific aspects of deposits. Since the initial work of Buser and Grutter (Buser & Grutter,1956; Grutter & Buser, 1957), the mineralogy of the authigenic Mn and Fe oxide phases of the deposits has received detailed investigations by many workers (e.g. Andrushenko & Skornyakova, 1969; Herzenberg & Riley, 1969; Burns & Brown, 1972; Giovanoli et al, 1973). The present state of knowledge concerning the mineralogy of these deposits has been reviewed in detail by Burns & Burns (1977).

The internal structure of nodules and inter-element

associationson a microscopic scale within single samples has also been examined in detail (Burns & Fuerstenau,1966; Andrushenko & Skornyakova, 1969; Cronan & Tooms, 1968; Lalou et al.,1979). Attempts have been made to find relationships between the chemical composition of deposits and other factors such as their mineralogy (Crerar & Barnes, 1974), their growth rates (Heye & Marchig, 1977), the rate of accumulation of accompanying sediment (Price & Calvert 1970), the physical properties of the substrate (Horn et al., 1973) and the chemical composition of the underlying sediment (Calvert & Price, 1977). Yet other workers have tried to discover the mechanisms by which the trace metals are incorporated into the deposits (Goldberg,1954;Krauskopf, 1956; Stumm & Morgan,1970; Burns,1976; Hem, 1978a).

A full study of the genesis of marine ferromanganese oxide deposits therefore cannot be confined simply to the geochemistry and mineralogy. Consideration must also be given to the factors affecting the composition of the deposits. Thus factors such as rate of sedimentation, type and composition of sediment, element source, and degree of oxygenation of the bottom environment must all be considered in order to assess their effect on the composition of deposits. Although the study of these topics has greatly increased since the mid 1960's, our knowledge of some of these factors is still limited, particularly in the Indian Ocean.

In this thesis several topics of a non-geochemical nature are described and discussed as a background to the work so that their effects on the geochemistry and mineralogy

of the deposits can be taken into account. These topics are the structure and evolution of the N.W.Indian Ocean, the rate and type of sedimentation, the nature of the ocean currents, and the biological productivity of the overlying waters. Chapter 2 considers the sediment composition patterns in the N.W. Indian Ocean in detail. Chapter 3 considers the morphology of the present specimens and Chapter 4 describes their mineralogy. Chapter 5 discusses their bulk geochemistry, while Chapter 6 presents data on their chemical composition on a microscale. Chapter 7 describes the findings of an S.E.M. study of these deposits.

b) Structure and evolution of the N.W.Indian Ocean

Geographically, the Indian Ocean is the most remote of the three major oceans from the main centres of marine research, in the U.S.A. and Europe. As a result, it has received less study in the past than have the Atlantic and Pacific Oceans.

The N.W. Indian Ocean contains several prominant physiographic features which are shown in figure 1.1. The northern part of the study area is dominated by the Arabian Basin, lying between Arabia to the west and India to the east. To the north, it is bounded by Pakistan, through which runs the Indus River, the large sediment load of which is deposited in the Arabian Basin and forms the

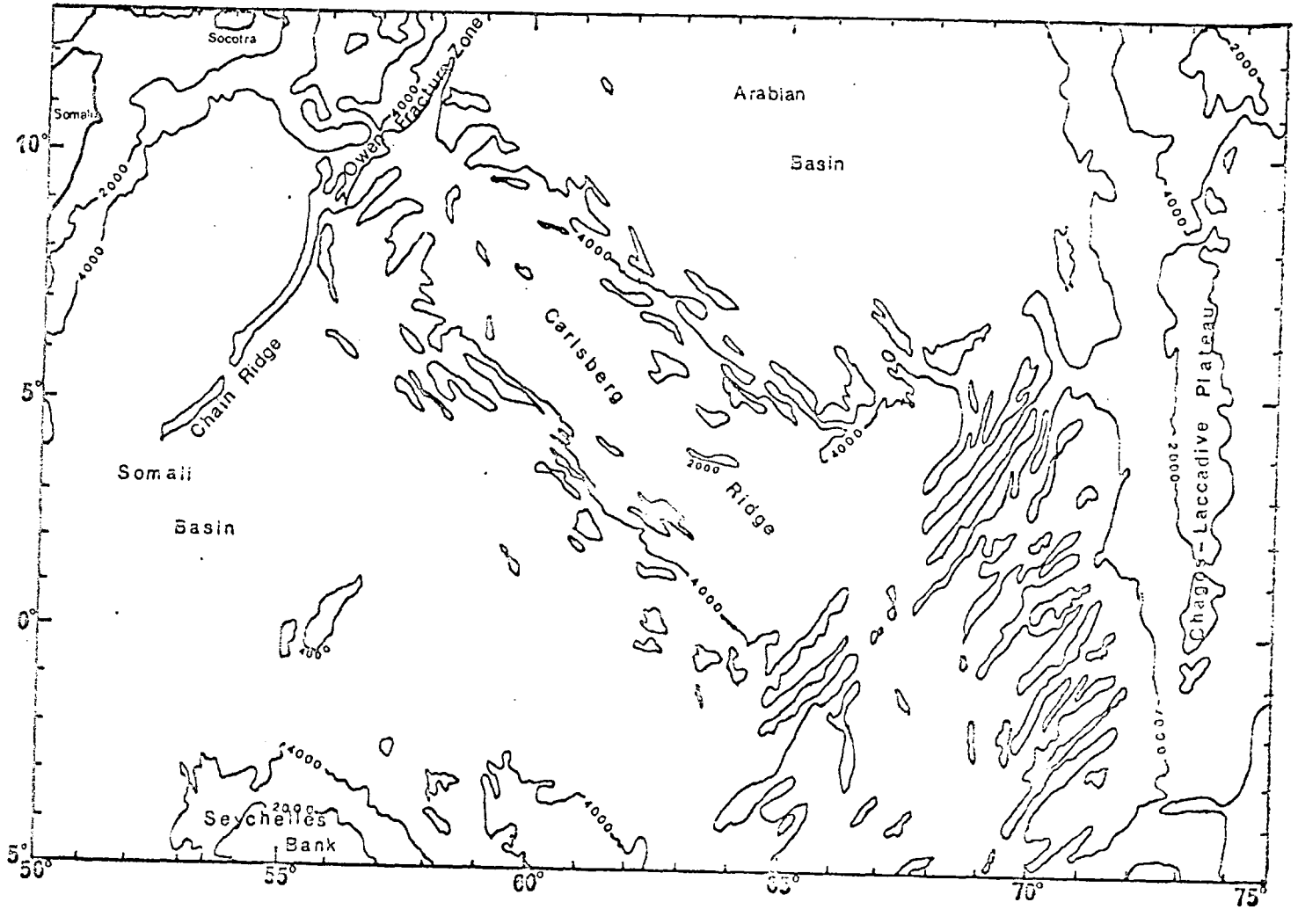

Figure 1.1: Map showing principle physiographic features in study area.

Indus Cone. In the study area, water depths in the Arabian Basin are generally greater than 4000m (Udintsev et al, 1975). The thickness of sediment in the Arabian Basin is directly related to the distance from the Indus River. The isopach map of Ewing et al.,(1969) shows more than 2.5 km. of sediment near the apex of the Indus Cone. This thickness decreases steadily southwards to less than ½ km. at the margins of the Carlsberg Ridge.

The southern half of the study area is dominated by the Somali Basin. This is split into two parts by the Chain Ridge, the south western extension of the Owen Fracture Zone. In the west, the Somali Basin extends from Socotra in the north to Madagascar in the south. In the east it extends southwards from the Carlsberg Ridge to the Seychelles Islands. In both parts, depths are generally greater than 4000m. In the eastern part however, there are several regions of seamounts which take the depth to less than 1000m in some instances. It is from two groups of seamounts that many of the specimens studied in this thesis came. The sediment thickness is very different in the two parts of the Basin. In the western part, adjacent to the African mainland, thicknesses exceed 2 kms.(Ewing et al., 1969). These thin eastwards to less than 200m at the foot of the Seychelles Plateau and remain at about this thickness in the eastern part of the Basin.

Separating the Arabian and Somali Basin is the Carlsberg Ridge. This is the north western extension of the Mid-Indian Ocean Ridge, and extends in a north westerly direction from the Central Indian Ocean Ridge as far as the

Owen Fracture Zone. At this point, the Ridge is offset 300km. northward. The mid-ocean ridge system then continues in a more westerly direction into the Gulf of Aden.

Muir & Tilley, (1964), and Aumento, (1969), have observed that ferromanganese oxide crusts generally appear to thicken with increasing distance from the crest of the Mid-Atlantic Ridge. This suggests that oxide deposition is initiated on new seafloor at an active ridge crest and continues as the encrustations move away from the crest due to seafloor spreading. Therefore the spreading history of the Carlsberg Ridge is of interest to the present work.

McKenzie & Sclater, (1971), describe how different interpretationsof available geophysical data give rise to different conclusions about the spreading history of the Carlsberg Ridge. The two spreading rates that they quote are 6.5 cms./yr. and 1.8 cms./yr. for the last 68 x 10^6 years. They explain the discrepancy by suggesting that spreading must have stopped or become very slow between 55 and 10 x 10^6 yrs.ago. Le Pichon & Heirtzler (1968), using the same magnetic profiles as McKenzie & Sclater came to the same conclusion, only with a shorter pause in the spreading.

Radiometric dating of rocks from the Amirante Ridge (Fisher et al., 1968) and Chain Ridge (Bunce et al., 1967) has given then an age of 82 and 89.6 x 10^6 years respectively. They suggest that these dates are compatible with the formation of the N.W. Indian Ocean since the Cretaceous period. After the formation of the oldest magnetic anomaly, i.e. when spreading was initiated (just after the Middle

Cretaceous, McKenzie & Sclater, 1971; Helsley & Steiner, 1969), the spreading half-rate increased to 6.5 cms/year until 55 x 10^6 years ago. Spreading was then very slow for the next 20 to 25 x 10^6 years. Then over the last 30 to 35 x 10^6 years, McKenzie & Sclater (1971) conclude that spreading has been more or less continuous at 1.2 to 1.3 cms./year.

Ewing et al., (1969), failed to detect any sediment cover on the Carlsberg Ridge: they reported that the crestal area of the mid-ocean ridge is consistently bare of sediment to a distance of at least 100 km. from the axis. This is erroneous since many sediment samples analysed in this work camefrom near the Ridge crest. Their conclusion probably arose from the very irregular distribution of sediment cover on the Ridge and also from the problems of detecting thin sediment cover by seismic techniques in areas of rugged topography.

The Seychelles Bank or Plateau is one of several continental fragments entrapped in the Indian Ocean. It lies about half way between Madagascar and the Carlsberg Ridge. The Plateau is predominantly of Pre-Cambrian age, and the islands of the Seychelles group form the only granite mid-oceanic islands in the world (Baker, 1963). Much of the movement of this Plateau seems to have occurred early in the history of the Indian Ocean, and its arrival at its present position and its fit in the reconstruction of Gondwanaland are still not fully understood.

Lying between the Carlsberg Ridge and the Indian mainland is the aseismic Chagos-Laccadive Ridge. This is a

north-south trending feature at about 70-75°E. and 10°S. to 15°N.,where it runs close to India, and sub-parallel with the coast. This ridge, and the Mascerene Ridge to the south west of the Carlsberg Ridge, are both about equi-distant from the Indian Ocean ridge system, and the fracture zones associated with the active ridge all terminate against these two features. On the assumption that the Central Indian Ridge and Carlsberg Ridge have spread symmetrically then the Mascarene and Chagos-Laccadive Ridges must have been contiguous at the start of spreading at the active ridges (McKenzie & Sclater, 1971). As the ridges became volcanically active, the Chagos-Laccadive and Mascarene Ridges began to form, either by volcanic events along the "leaky" transform fault which formed the western analogue of the Ninety East Ridge or by drift over a hotspot area. Some segments of the Chagos-Laccadive Ridge, especially the Maldive Islands segment, may be microcontinents rifted away from India during the early phases of movement of the Indian Plate. (Avraham & Bunce, 1977).

c. Sedimentation

Two sedimentary parameters seem to be important in affecting the distribution and composition of marine ferromanganese deposits. These are sedimentation rate and sediment type (Price & Calvert, 1970; Greenslate et al., 1973; Horn et al., 1973; Lyle et al., 1977). These parameters and their variability in the N.W. Indian Ocean are discussed.

Sedimentation rate

No detailed studies of sedimentation rates in the N.W.

Indian Ocean have been carried out. The data which are available from this area are part of oceanwide studies of sedimentation rates. For example, Opdyke & Glass,(1969), used 40 cores from throughout the Indian Ocean to try and gain some knowledge of sedimentation rates. They found rates in pelagic areas of between 3 and 7 mm. per thousand years. On elevated ridge areas however, they observed sedimentation rates of 10 mm. to 20 mm. per thousand years.

Udintsev et al., (1975), have compiled a map showing variation in sedimentation rates throughout the Indian Ocean. From this, three areas of high sedimentation rate occur in the N.W. Indian Ocean. There is an area of very high sedimentation in the northern part of the ocean around the coastline of India. This includes the Indus Cone where rates exceed 10mm. per thousand years. This is because of the very large input of terrigenous material brought down by the Indus River (435 million tons of sediment/year; Rateev et al.,1969). A second area of equally rapid sedimentation extends from this northern area down the east coast of Africa and Arabia. No precise details of sedimentation rates in this near-coastal area are known at present. A third zone of high sedimentation occupies the southern part of the Somali Basin and the Seychelles Plateau. In view of the location of the Seychelles Plateau, remote from major continental inputs, the high sedimentation rate is probably due to rapid deposition of biogenic carbonate material in an area where the sea floor is shallower than the carbonate compensation depth and lies beneath a zone of high biological productivity (see section iv).

Areas of slow sedimentation rates occur in the deep basins below the carbonate compensation depth and beyond the limits of transport of land derived material by turbidity currents. Such areas occur in the northern Somali Basin and the southern parts of the Arabian Basin (Moorby, 1978). Most of the elevated areas of the Indian Ocean, especially the Mid-Ocean Ridge system are characterised by high sedimentation rates (Opdyke & Glass, 1969), mainly by virtue of their being above the lysocline, and thus receiving large amounts of biogenic carbonate debris. Because of the very rugged nature of the topography of these regions, sedimentation rates can fluctuate widely over comparatively short distances. The north-west part of the Indian Ocean is probably not an exception to this observation.

Sediment type

Early ocean wide studies of sediment type by Griffin et al., (1968), and Rateev et al., (1969), were limited by the relatively small number of samples used. Moreover, these studies were concerned primarily with the clay mineral assemblages of the surface sediments rather than with overall sediment type. Later work carried out by Goldberg & Griffin, (1970), Venkatarathnam & Biscaye, (1973), and Kolla et al., (1976b)was more detailed but again concentrated on the clay mineral assemblages. A study of the clay fraction of sediments provides no information of overall sediment composition and therefore of the relative importance of different types of sediment. However, clay minerals usually form a significant component of deep-sea

sediments. A knowledge of the clay mineral assemblages of samples therefore proves a useful guide to the relative importance of modes of transport and supply of sediment to the sea bed i.e. aeolian transport, continental run-off and submarine volcanism. Based on the distribution of characteristic mineral assemblages, Kolla et al., (1976b) recognised three different types of sedimentary province in the Indian Ocean.

These are as follows:

Type 1

Montmorillonite rich provinces, the montmorillonite being derived from the in-situ alteration of basalts and showing no evidence of long distance transport of materials. The only area in the N.W. Indian Ocean in this category is in the N.E. Somali Basin, between the Seychelles Plateau and the Carlsberg Ridge (Moorby, 1978).

Type 2

These are provinces enriched in a particular mineral or minerals which have been derived from continents or submarine volcanic areas, and which show evidence of long-distance sediment transport. In the N.W. Indian Ocean, the areas falling in this category are the Arabian and Indus provinces of Kolla et al., (1976b). The Indus province is illite-rich and contains clays derived primarily from the continental run-off from the Indus River. The Arabian Province, to the south of the Indus Province, includes much of the Carlsberg Ridge. There are appreciable amounts of palygorskite in the sediments of this province, probably brought by aeolian transport from Arabia (Weser, 1972).

Type 3

This type of area contains no clay mineral in particularly high amounts, and the origin of the sediment is therefore more obscure, probably because of the ad-mixing of material from several other provinces. The only area in the N.W. Indian Ocean falling in this category is to the east of the Horn of Africa. Lack of accurate knowledge of bottom currents in this area prevents detailed understanding of the relative importance of other sedimentary provinces in supplying material to these areas.

d) Oceanography

Currents

Ocean currents, particularly bottom currents by their influence on the bottom environment, play an important role in the development of marine ferromanganese oxide deposits. To investigate this role fully, detailed knowledge of present day and palaeo-bottom currents is needed, and for the N.W. Indian Ocean, no such information is available.

The most important source of major bottom currents in the Indian Ocean is Antarctic Bottom Water (AABW). (Payne & Connolly, 1972; Kennett & Watkins, 1975; Kolla et al., 1976c). This water can have a very marked effect on the bottom environment.Where the current is strong it can erode the sediment by winnowing (Watkins & Kennett, 1977).Where the current velocity slackens, it can redeposit suspended material (Burckle et al., 1974). In all areas, it has a marked effect on carbonate dissolution rates because of its marked undersaturation in $CaCO_3$ (Kolla et al.,

1976a).

Le Pichon (1960), Wyrtki (1971), Kennett & Watkins (1975), and Kolla et al., (1976c) have shown that AABW finds its way into all parts of the Indian Ocean. From its formation off Antarctica, it appears to move northwards by three major routes (Kolla et al., 1976c), one of which takes it as far north as the Arabian Basin: AABW travels from the eastern Atlantic-Indian Basin directly into the Crozet Basin, where strong northward-flowing bottom currents caused by the spreading of AABW have been observed. From the Crozet Basin, AABW crosses the S.W. Indian Ridge into the Madagascar Basin (Wyrtki, 1971; Burckle et al., 1974; Warren, 1974; Kolla et al., 1976c). From the Madagascar Basin, AABW flows northwards into the Mascarene Basin and then into the Somali Basin. Bottom potential temperature, and salinity measurements (Wyrtki, 1971) indicate that AABW traverses the Carlsberg Ridge through a passage in the region of the Chain Ridge and then flows into the Southern Arabian Basin. However, the vigour of the AABW in the Somali and Arabian Basins is greatly diminished compared to the southern part of the ocean.

Strong bottom current activity occurs in several areas of the Indian Ocean which are at depths too shallow for the current to be caused by AABW. However, no detailed work has been done on such shallow currents in the N.W. Indian Ocean. Therefore, the source of such currents here cannot be established.

Productivity

Greenslate et al., (1973) suggested that the composition

of ferromanganese oxide deposits might be affected by biological productivity of the overlying ocean. They inferred that biogenic debris forms an important source of trace metals, especially Ni and Cu in the bottom water.

Kobletz-Mishke, (1970), and Qasim (1977) drew up maps of the primary productivity of the Indian Ocean. From these it is apparent that the most productive areas of the ocean are the coastal areas of India, Arabia, and parts of Africa and Indonesia. These regions are areas of upwelling (Krey, 1973), where nutrient-rich water is brought to the surface, encouraging high productivity. In the area under consideration in the present study, the primary water column production from 60°E to 72°E and from the Equator to about 15°N is quite low (less than 50 tonnes of organic carbon/km^2/yr.; Qasim, 1977). East of 72°E, it increases rapidly because of the influence of upwelling off the Indian coast.West of 60°E productivity increases to over 100 tonnes C/km^2/yr. Thus to summarise, primary production in the study area is low in the middle and moderate to high in the western and eastern parts of the study area.

There is no marked equatorial zone of high biological productivity in the Indian Ocean, as there is in the Pacific Ocean. The Equatorial undercurrent, which is associated with the upwelling of nutrient-rich water in the Pacific persists throughout the year. It is this current which is responsible for the high biological productivity in equatorial ocean water in the Pacific. In the Indian Ocean, this current is subject to the seasonally varying monsoon wind system. This causes it to disappear during the

south-west monsoon period (May-October) and reappear during the north-east monsoon(November-April) (Sharma,1968). Thus biological productivity is high during the north-east monsoon and low during the south-west monsoon. When the average productivity of the equatorial region for the whole year is computed, no region of high productivity is observed.

According to the theories of Greenslate et al.,(1973), and Piper & Williamson,(1977), the carbonate compensation depth (C.C.D.) and the lysocline depth are important factors in controlling the regional compositional variations of ferromanganese oxide deposits since significant dissolution of carbonate debris occurs between these two depths. This dissolution process leads to the release into the deep water of trace metals contained in the carbonate organisms. In the Somali Basin, the C.C.D. is at 5100m.; inthe northern Arabian Basin it is at 4800m. because of dilution of carbonate material by terrigenous material (Kolla et al., 1976c). According to Kolla et al., (op.cit.), excluding areas where dilution by terrigenous material occurs, variations in the depths of the C.C.D. and the lysocline are caused partly by factors such as deep-water turbulence and degree of undersaturation, and partly by variations in surface productivity.

CHAPTER 2

The Geochemistry of recent sediments from the North West Indian Ocean.

Introduction

Previous Geochemical Studies of Indian Ocean Sediments

There have been relatively few geochemical studies of the sediments of the Indian Ocean, compared with the Atlantic and Pacific Oceans. Bostrom et al., (1969), described the chemistry of 543 sediment samples from the three major oceans and drew two conclusions about the processes affecting the geochemistry of pelagic sediments. They showed that the values of Al/Al + Mn+Fe were lowest on the mid-ocean ridges and highest furthest away from the ridges, nearest the continents. Their conclusions were that:

1) the sedimentation rate of the detrital portion of pelagic sediments decreases from the continents towards the mid-ocean ridges.

2) the rate of deposition of the ferromanganese component of these sediments was greatest along the mid-ocean ridges and decreased to the lowest values at points furthest from the ridges.

They considered that submarine volcanism producing hydrothermal emanations, which when released into the bottom waters precipitate Fe and Mn oxides, was a process contributing to Fe and Mn enrichment in mid-ocean ridge crest sediments. They showed that the areal extent of these Fe-Mn rich sediments is a reflection of the volcanic activity along the ridges.

Bender & Schultz (1969) reported values of Mn, Ni, Co, Cu, Zn, Fe and $CaCO_3$ in 22 surface sediments from the Southern Indian Ocean. They showed that the Mn, Co, Ni and Cu values were greatest in the centre of the basin and lowest at its fringes. The metal values were three times higher in the east than in the west. They concluded that this enrichment was due to the presence of a fine grained silicate fraction which preferentially concentrated these metals.

Horowitz (1970) analysed a set of eighteen widely spaced surface sediments from the Indian Ocean for Pb, Sn, Zn, Ag and Tl. He was able to make three observations. Firstly, there was an association between high concentrations of Pb, Zn, and Ag with high heat-flow values, proximity to an active ridge, and high Fe, Mn, and V. This led him to suggest that these elements were derived from an active ridge source. Secondly the association of these elements with Fe and Mn indicated that they were in part concentrated by adsorption on hydrous ferromanganese oxides (Krauskopf, 1956). Thirdly, the negative correlation of Pb, Zn and Tl with $CaCO_3$ suggested that these elements were not concentrated by skeletal remains.

Bostrom & Fisher (1971) analysed 100 surface sediments

from sites throughout the Indian Ocean for Fe, U and V. They showed that Fe is concentrated in two areas. Firstly, along the Indian Ocean Ridge system, where it is probably supplied by volcanic activity. Secondly, on elevated inactive areas, e.g. the Broken Ridge, where there is a tendency for authigenic Fe deposits to form in the absence of terrigenous material.

Vergès (1979) studied sediments from the southern half of the Indian Ocean west of 90°E and came to the conclusion that Ni, Cu and Co were transported to the sediment by calcareous skeletal remains. However, there is doubt about whether her data are corrected for Ca interference or not (Appendix 1); consequently, the validity of this observation is in question. She applied a different chemical attack to her samples (hot 4N HCl) compared to that used in this work ($HF/HNO_3/HClO_4$, Appendix 1). This is likely to leave much of the clays and detrital minerals unattacked, so her data are not strictly comparable to those obtained in the present work.

These studies have described the distribution of particular elements over very wide areas. They provide a general survey of the geochemistry of Indian Ocean sediments as a whole, but none of them give detailed studies of any relatively small area of the Indian Ocean. In contrast, Horder (1979) studied 80 surface sediments from a relatively small area of the Central Indian Ridge, to the N. and N.E. of Mauritius. This was an attempt to further the understanding of the influence of an active mid-ocean ridge on the distribution of various metals in the sediments on the

ridge. He concluded that Mn and associated metals appear to be precipitated from seawater throughout the area as authigenic Mn oxides, while Fe is relatively uniformly distributed in all non-crest sediments by the incorporation of basaltic weathering products. Both Fe and Mn and associated trace elements are enriched in crest sediments by hydrothermal leaching of these metals from underlying basalts and coprecipitation as Fe and Mn oxyhydroxides and possibly iron silicates. He proposes that the elements Pb, Cd, Co and Li are biogenically concentrated, and that Li may also be linked to continental detrital material.

The present work is concerned with a suite of samples on and around an active spreading ridge (the Carlsberg Ridge), in an attempt to define some of the chemical sedimentary processes occurring in the area. It is hoped that the information thus gained will be useful in characterising the sources of the metals in ferromanganese oxide deposits from the same area. Very little geochemical work has been done in the North West Indian Ocean.

Sample location and distribution

In the present study, 164 samples have been analysed for Ca, $CaCO_3$, Mn, Fe, Ni, Co, Ti, Al, Mg, Cu, Zn, Pb and Cd. They have been taken from the Somali Basin (46 samples), the Seychelles seamount province (46 samples), the Arabian Basin (14 samples), the Chagos-Laccadive Plateau (5 samples), the Carlsberg Ridge and Owen Fracture zone (28 samples) and the Seychelles Bank (26 samples). The data are tabulated in Addendum Ia. Details of the analytical methods used and the precisions and accuracies obtained are given in Appendix 2. The data for Co, Pb and Cd appear to

be neither very accurate nor very precise, probably because of the serious interference by Ca in their determination. Consequently, little emphasis will be placed on these elements in the forthcoming description and discussion.

The data set can be divided into two parts: surface sediments and subsurface sediments. 91 of the samples are surface sediments, 22 from the Carlsberg Ridge, five from the Chagos-Laccadive Plateau, ten from the Arabian Basin, 46 from the Somali Basin, and eight from the Seychelles seamount province. The remaining 73 samples have been obtained from fifteen cores. Of these, seven were from the seamounts, one from the bottom of the Seychelles Bank, one from the Arabian Basin, near the Carlsberg Ridge, three from the Ridge crest (area 4a), and three from the Somali Basin near the Ridge flank (area 4c).

At a very late stage in the work, five short cores from the median valley of the Carlsberg Ridge were collected and made available by Dr. Peter Rona of N.O.A.A. 23 samples were obtained and analysed; they are treated as a separate data group.

Sources of sediments to the N.W.Indian Ocean

Introduction

Metals can be introduced to the marine environment in solid or colloïdal phases, or as dissolved material (Chester, 1976). The dissolved metals may subsequently precipitate out of solution and become part of the sediment. In the North West Indian Ocean, the most significant sources of the solid phase are:

1. Biogenous. e.g. skeletal remains
2. Lithogenous i.e. continentally derived

material transported by rivers, wind and, (important in the Indus Cone), turbidity currents (Seibold, 1972).

3. Volcanic: high temperature alteration of newly extruded rocks produces basalt fragments. Low temperature alteration produces alteration products such as montmorillonite, and mobilises metals contained in the basalt (e.g. Corliss, 1971; Bischoff & Dickson, 1975; Mottl & Holland, 1978). Metals in solution are introduced by rivers, and by hydrothermal solutions.

The most important source of lithogenous material to the N.W. Indian Ocean is the Indus River, discharging 48×10^{10} kgms/yr. of suspended sediment to the Arabian Sea (Holeman, 1968). Seibold (1972) states that the sediment cone of the Indus now reaches outward more than 2000 kms to the Carlsberg Ridge, and reports that the participation of present-day active turbidity currents is beyond question. He also suggests that sediment redistribution is associated with deep-sea currents in the area, and the extreme monsoon storms, which can resuspend shelf material and transport it to the deep sea. Therefore the particle size separation process which affects river-transported sediment on its introduction to the marine system, (Turekian, 1967) is probably greatly confused by these redistribution processes. Much coarse-grained material (relatively metal-poor, Chester & Aston(1976)) which settles out of suspension earlier than fine-grained material (relatively metal-rich, Chester & Aston(op.cit.)) is redeposited in deep-sea areas. As well as rock fragments and mineral weathering residues transported by the Indus, the solids also contain

phases precipitated from weathering solutions, e.g. hydrous oxides of manganese and iron. These are present as either discrete particles or as coatings on rock fragments. Krauskopf (1957) has described how important these oxides are in adsorbing dissolved trace elements from solution, and can be important in transporting trace elements in this fashion from a river environment to deep-sea areas.

Wind-borne transport of continental material to the N.W.Indian Ocean may be widely effective, though Kolla et al., (1976b) suggest it is dominant only in the western part. The north east monsoon, blowing from the Indian mainland seems likely to contribute a strong seasonal eolian input to the eastern part of the ocean, either from the Indian peninsular (Deccan Traps) or the Rajasthan Desert. Using mineralogical source tracers, Goldberg & Griffin (1970) suggest an eolian contribution from both areas while Aston et al., (1973) present data on dust samples taken during the N.E. Monsoon which indicate the Rajasthan Desert as the source. Kolla et al., (1976b) suggest the main input from the Deccan Traps is fluvial, via the Narmada and Tapti rivers which drain the area. A further zone of eolian input occurs in the western Arabian Sea, adjacent to the Arabian peninsula. The sediments here are derived from the deserts of Somalia and Arabia by prevailing monsoon and north-westerly winds (Heezen & Tharpe 1965; Goldberg & Griffin, 1970; Kolla et al., 1976b).

Results given in the literature show that some trace elements are enhanced in marine plankton by several orders of magnitude relative to sea water (Nicholls et al., 1959;

Turekian, 1965; Thompson & Bowen, 1969; Martin, 1970; Martin & Knauer, 1973; Greenslate et al., 1973; Moore & Bostrom, 1978). This ability to concentrate metals makes marine organisms a supply of these metals to sediments. They can act in three ways to transport metals to the sea floor. Firstly, they can assimilate metals into their bodies from their food and water, so that when the organisms die and sink to the sea floor, the metals contained in their bodies are added to the sediment. The distinction ought to be made here between metals which are present in the hard parts of organisms (skeletons), partially resistant to decomposition, and metals present in their soft parts. The soft tissues decompose rapidly under bacterial action, releasing the metals held therein to solution, probably as organic complexes. Since it is essentially only the hard parts which reach the sediment surface relatively unchanged (above the lysocline), then it is only the metals in the hard parts which become assimilated into the sediment. Secondly, metals can be associated with body processes e.g. digestive and excretory functions, which may result in the organism expelling the metals in faecal pellets (Chester & Aston, 1976; Honjo, 1978). Thirdly, tests act as a substrate for iron and manganese oxyhydroxides as they fall through the water column. These oxyhydroxides are capable of scavenging trace metals from sea water (Krauskopf, 1957) and consequently this may be a significant route for these metals to the seabed. In the present group of samples, this was well seen in core SH1315 (page 74) which had a calcite content of 96%, consisting mostly of foram tests. Many

of these tests had black flocs of manganese oxides adhering to them, and it can be seen from fig. 2.20 that these are probably responsible for the high Mn and Ni values in the core.

Present-day volcanism is likely to be present on the Carlsberg Ridge, associated with the tectonic activity of an active spreading centre. Past investigations have found large amounts of basaltic debris on the Ridge (Matthews et al., 1965; Cann & Vine, 1966; Hekinian, 1968; Cann, 1969). A recent cruise by the American vessel "Researcher" found considerable quantities of relatively fresh basalts at several locations on the Ridge crest (Cole, pers. comm.). Therefore, there is potentially a plentiful supply of metals released by the alteration of these rocks by seawater. There has been only one report of possible hydrothermal activity on the Carlsberg Ridge. This was inferred from the lack of magnetic anomalies in a fault at the Ridge crest (Matthews et al., 1965) and not from any sedimentary geochemical evidence. The scientists of the "Researcher", on the same cruise which returned the fresh rocks, could find no sign of any current hydrothermal activity on the Ridge crest between 10°N and the Equator (Cole, pers. comm.). Therefore it seems unlikely that hydrothermal activity is acting as a significant source of metals to the surface sediments on this part of the Carlsberg Ridge at present.

Bulk Geochemistry of Surface Sediments

The lysocline

The lysocline is the depth in the water column at which

the rate of dissolution of calcium carbonate increases rapidly, and is consequently of major oceanographic and geochemical interest. The depth of the lysocline varies from area to area throughout the World Ocean, and it has a marked effect on sediments. Those taken from above the lysocline are generally rich in calcium carbonate, and those from below are generally poorer in calcium carbonate.

Fig. 2.1 shows a plot of calcium carbonate content of sediments from the North West Indian Ocean. Apart from five outlying samples below the main trend, which are discussed below, most of the samples fall on a plot such that the rate of decrease of $CaCO_3$ with depth increases sharply at about 3800-4000m. This is identified as the lysocline in this part of the ocean. This is in excellent agreement with Kolla et al., (1976a), who also found that the lysocline here was at about 3800-4000m.

Of the five anomalous samples mentioned above, four are associated with the Chagos-Laccadive Plateau, three from the top and one near the bottom. Weser (1972) has described the sedimentation history at D.S.D.P. site 219, on the Chagos-Laccadive Plateau. He has pointed out an increase in the terrigenous contribution to the sediments here since India rose above sea-level, which appears to persist to the present day. He attributes this terrigenous input to the Indus River, the Deccan Traps and an eolian source. Dilution of calcareous sediment by a relatively high rate of detrital sedimentation would explain why these samples do not plot on the main trend in figure 2.1.

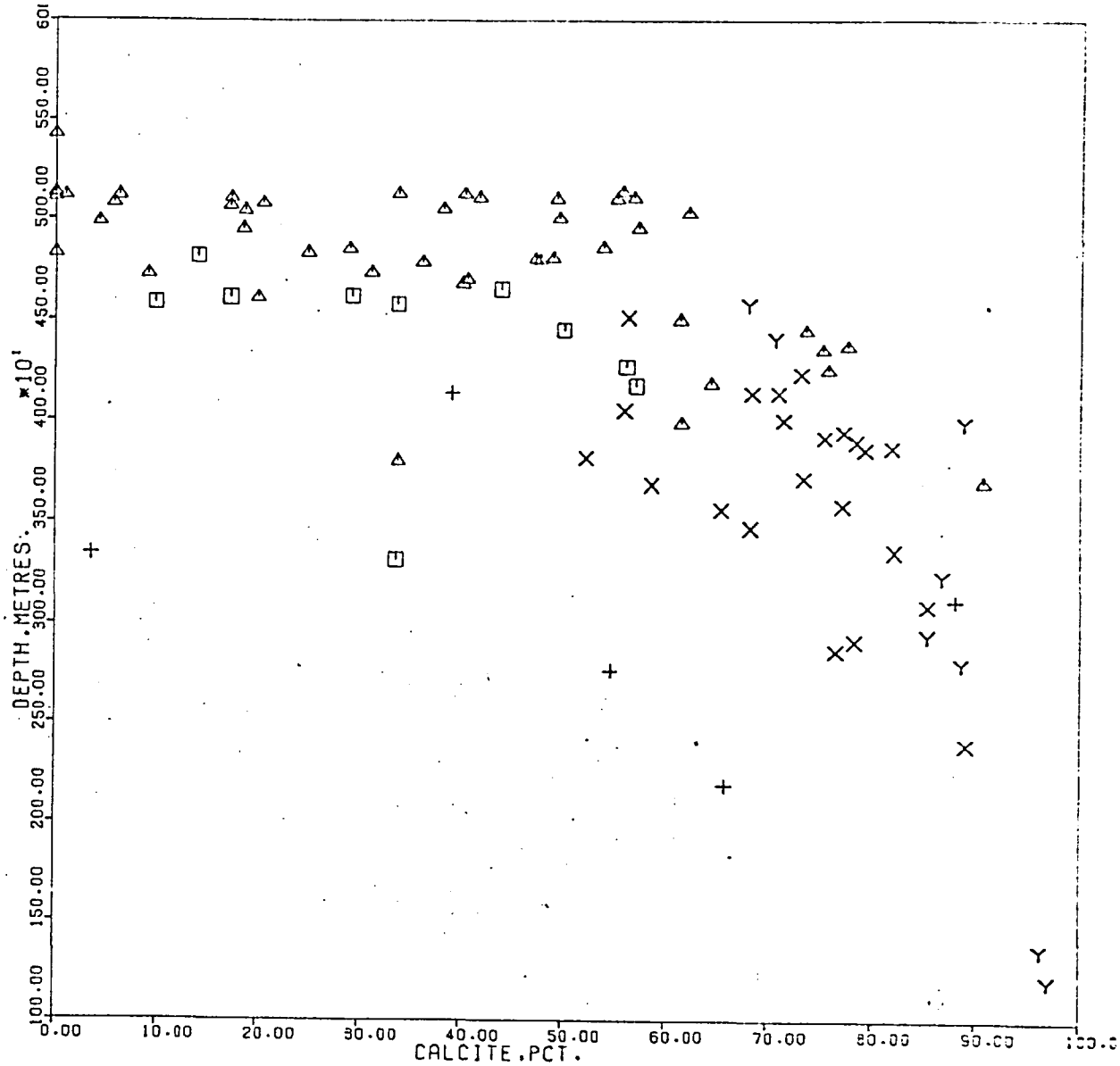

Fig.2.1: Plot of calcite content vs. water depth, surface sediments.

GROUP	SYMBOL	NO. OBS.	R
ALL	-	91	-0.67
RIDGE	X	22	-0.55
C.L.P.	+	5	-0.42
ARABIAN BASIN	□	10	-0.33
SOMALI BASIN	△	46	-0.58
SEAMOUNTS	Y	8	-0.88

Geochemical variations in the sample area.

Introduction

While the sample coverage of the area is far from detailed, it has been possible to draw some conclusions regarding the regional variations of particular elements by relating them to the sedimentary inputs to the area. The areal distributions of Ca and Mg, expressed on a total sediment basis are shown in figures 2.2 and 2.3. Distributions for Fe, Al, Ti, Mn, Ni, Zn and Cu in the carbonate-free fraction of the surface sediments are shown in figures 2.4 to 2.10.

Calcium, Figure 2.2

The distribution of calcium is largely controlled by biological processes, and is present as the carbonates calcite and aragonite. The distribution of Ca in the North West Indian Ocean reflects essentially the distribution of calcium carbonate and the depth of the lysocline in the area. This was described in detail earlier, so it is sufficient to say here that Ca is generally high on topographic highs, such as the seamounts and the Carlsberg Ridge, where these lie above the lysocline. Ca is generally low in the Somali and Arabian Basins, below the lysocline.

Ca is found in many crustal minerals and is transported to the oceans in terrestrial detritus. Volcanically derived minerals may also contribute significant amounts of both Ca and Mg to sediments (Chester & Aston,1976). This non-biogenic contribution of Ca to sediments already consisting largely of skeletal remains (e.g. on topographic highs such as the seamounts and the Carlsberg Ridge) will be hidden. In the

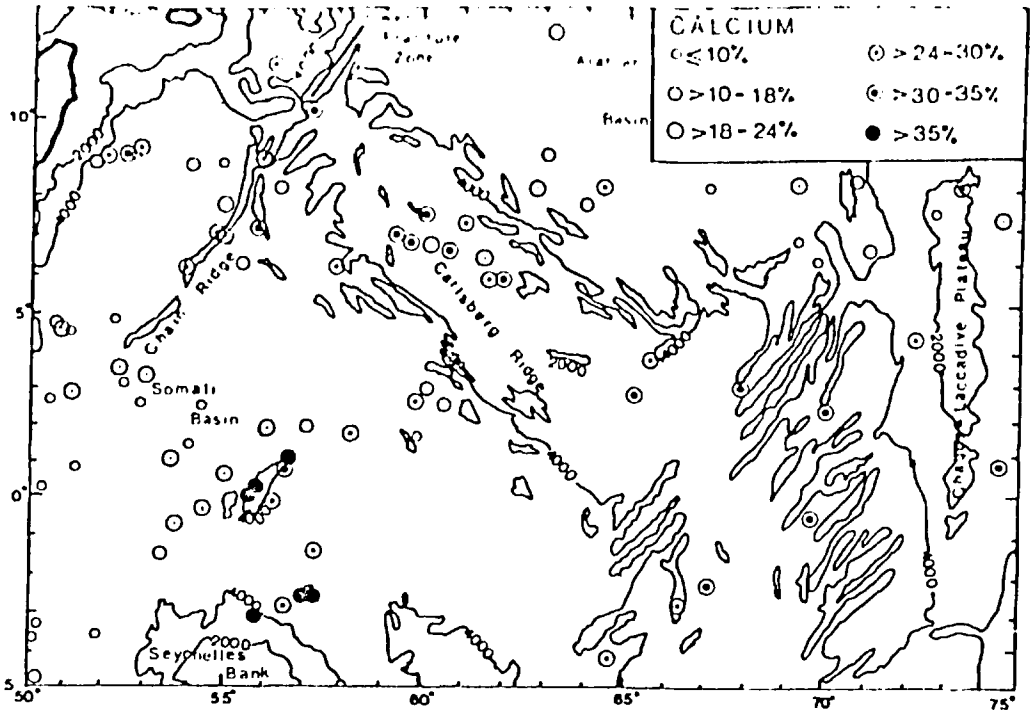

Figure 2.2: Distribution of calcium in the surface sediments of the North West Indian Ocean.

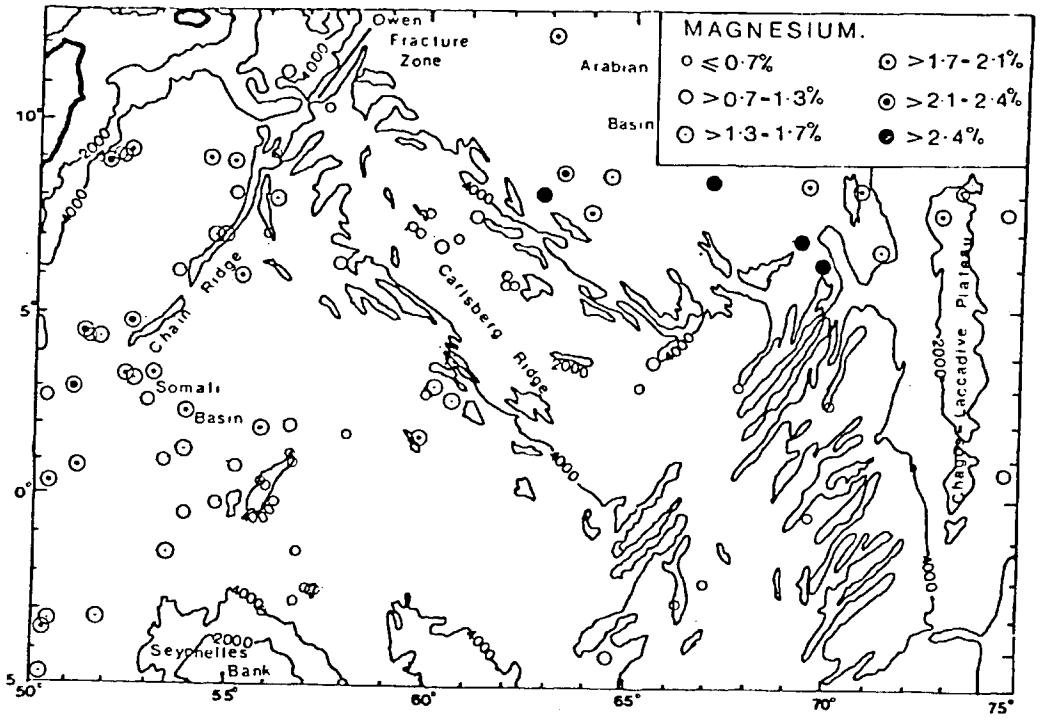

Figure 2.3: Distribution of magnesium in the surface sediments of the North West Indian Ocean.

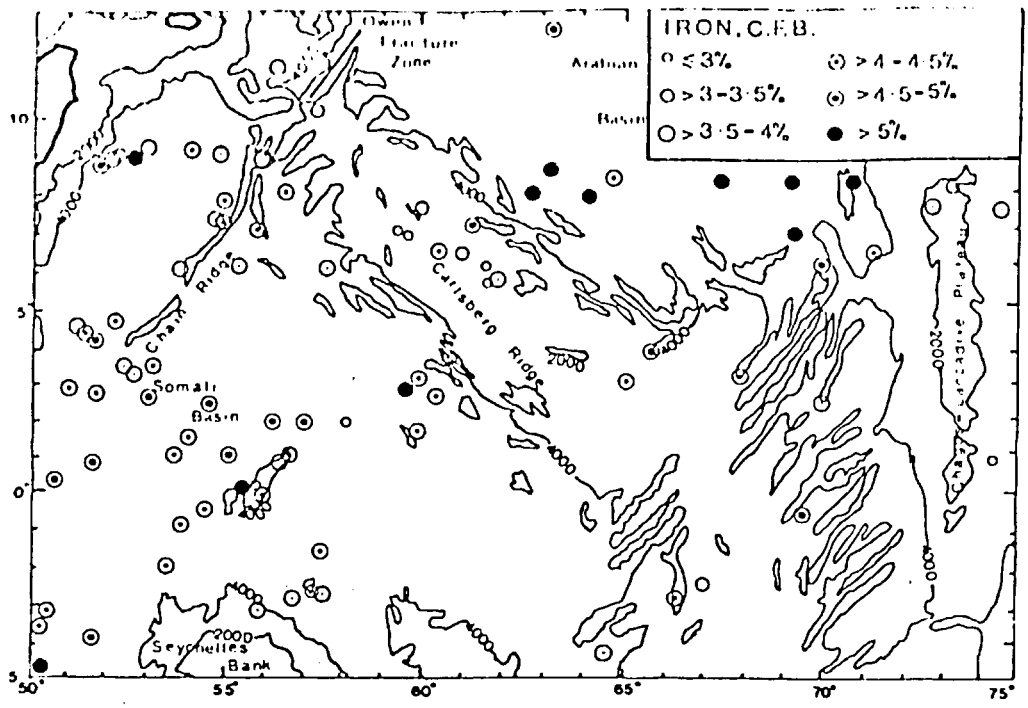

Fig.2.4:Distribution of iron in the carbonate-free fraction of surface sediments of the North West Indian Ocean.

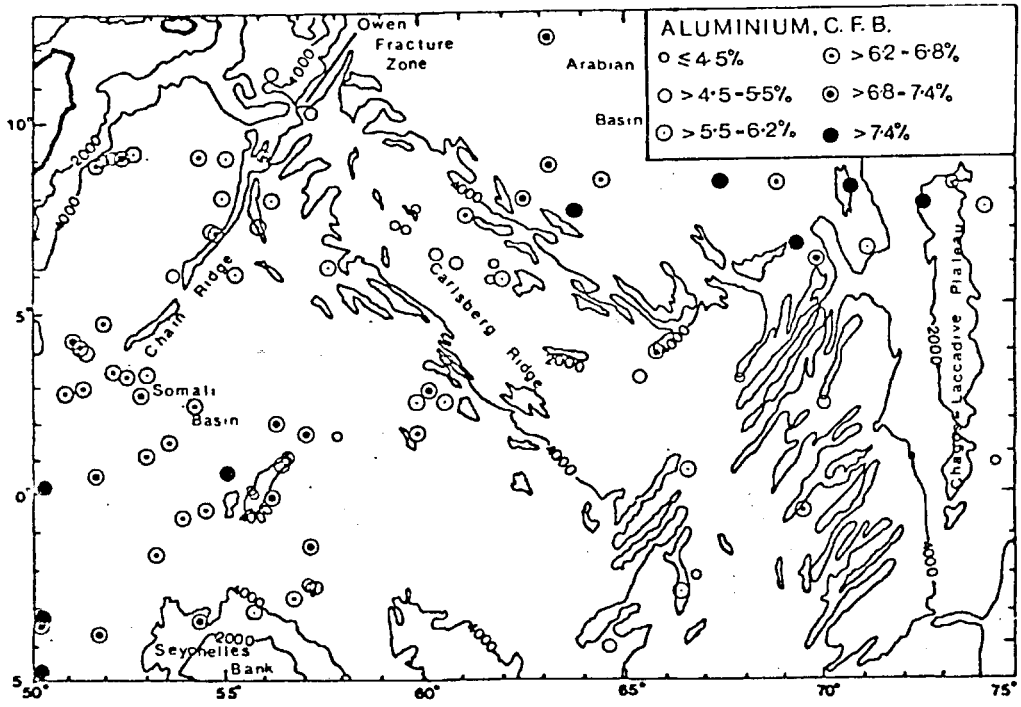

Fig.2.5:Distibution of aluminium in the carbonate-free fraction of surface sediments of the North West Indian Ocean.

Basins, where the depths are mainly below the lysocline, the overall level of Ca is reduced as the biogenic contribution becomes smaller because skeletal material is dissolved. Consequently, the terrigenous contribution becomes relatively larger.

Magnesium, Figure 2.3

Wiseman (1965) found $MgCO_3$ contents of Indian Ocean sediments between 0.65% and 4.77% and suggested that the bulk of this originates in the tests of benthonic foraminifera. It is for this reason that the Mg distribution in figure 2.3 is plotted using Mg values on a total sediment basis. If there was a significant biological source of Mg to the sediments in this way, then some correlation between the Ca and Mg distribution would appear. A comparison of figures 2.2 and 2.3 shows that this is not so. On the topographic highs of the Carlsberg Ridge and the seamounts, Mg is markedly lower than in the Basins. This probably indicates that the main source of Mg is in a non-biogenic i.e. largely terrigenous form. This is diluted by biogenic sediment on topographic highs. In the Basins, below the lysocline, the calcareous debris (relatively Mg-poor) dissolves rapidly, leaving the non-calcareous material (relatively Mg-rich) as the increasingly dominant contribution of Mg to the sediment. Having established that the Mg is largely in the terrigenous, non-biogenic phase, all future references to the Mg content of the sediments will be on a carbonate-free basis unless otherwise stated.

Iron, figure 2.4

Chester & Aston(1976)lists three main sources of Fe in

marine sediments.

1. It may be transported to the oceans in association with terrigenous solids, particularly clay minerals. According to Carroll (1958), iron may be associated with the clay minerals a) as an essential constituent within the crystal lattice b) as a minor constituent within the crystal lattice c) as iron oxide coatings on the surfaces of clay particles.

2. It may be deposited through the agency of a biological mechanism e.g. as oxide coatings on skeletal parts.

3. It may be deposited through processes involving the authigenic removal of iron from seawater.

The similarity of the distribution of Fe to that of Al indicates that the first of these origins is the most likely to be dominant in the present samples. (figures 2.4 and 2.5) Certainly the generally lower values on the Ridge, above the lysocline, where the biogenic input would be potentially high, and the volcanic influence strongest, indicate that these sources of Fe appear to be weak in the N.W. Indian Ocean. The higher values in the Basins, particularly in the Arabian Basin, where the Indus River input is dominant, suggest that terrigenous material is the source of the iron here. Terrigenous input would be weakest on the Ridge, furthest from the continents. This is probably why the Fe values on the Ridge are lower than those in the Basins. From the data presented so far, it is impossible to say whether the Fe is present within the mineral lattice of the terrigenous material or as oxide coatings.

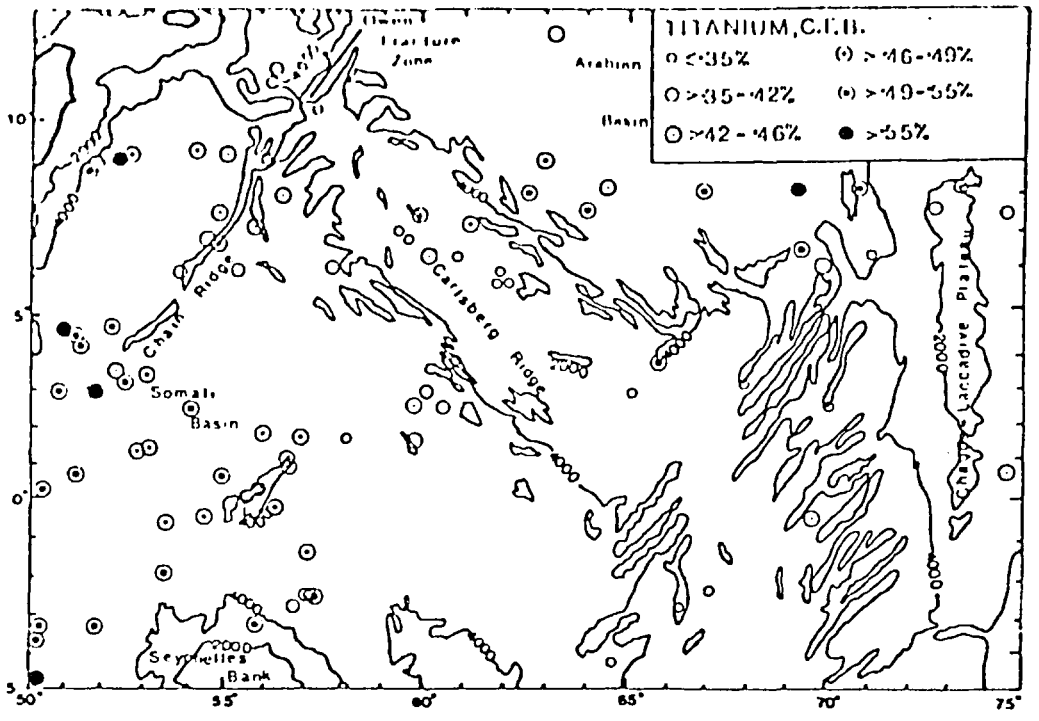

Fig.2.6:Distribution of titanium in the carbonate-free fraction of surface sediments from the North West Indian Ocean.

Aluminium Figure 2.5

Because Al in deep sea sediments is largely located in aluminosilicate material it has been used as an indicator of the amount of terrigenous debris in the sediment (Arrhenius, 1952; Landergren 1964). On the Carlsberg Ridge, relatively remote from continental landmasses, the Al may come more from incorporation of basaltic weathering products into the sediments than from terrigenous debris. However, palygorskite is present in the Carlsberg Ridge sediments, probably brought by eolian transport from Arabia (Weser, 1972). Some of the Al will be from this mineral, and therefore will have a terrigenous origin. The overall distribution of Al is similar to that of Fe i.e. higher in the Arabian Basin than the Somali Basin. This pattern is in accord with strong fluvial continental sources viz: the Indus River dominant in the Arabian Basin, and the African mainland acting as a weaker terrigenous source to the Somali Basin than the Indus River to the Arabian Basin.

Titanium Figure 2.6

Chester & Aston(1976) lists titanium as a minor constituent in many aluminosilicates e.g. clays, feldspars and micas. He suggests that continentally derived minerals such as these account for most of the Ti in deep sea sediments. This would explain why Ti is higher in the Arabian and Somali Basins which have a dominantly terrigenous input, than on the Ridge, remote from the continents. It may also explain the frequent association of high values of Ti with high values of Al in the Basins. However, Goldberg & Arrhenius (1958) have pointed

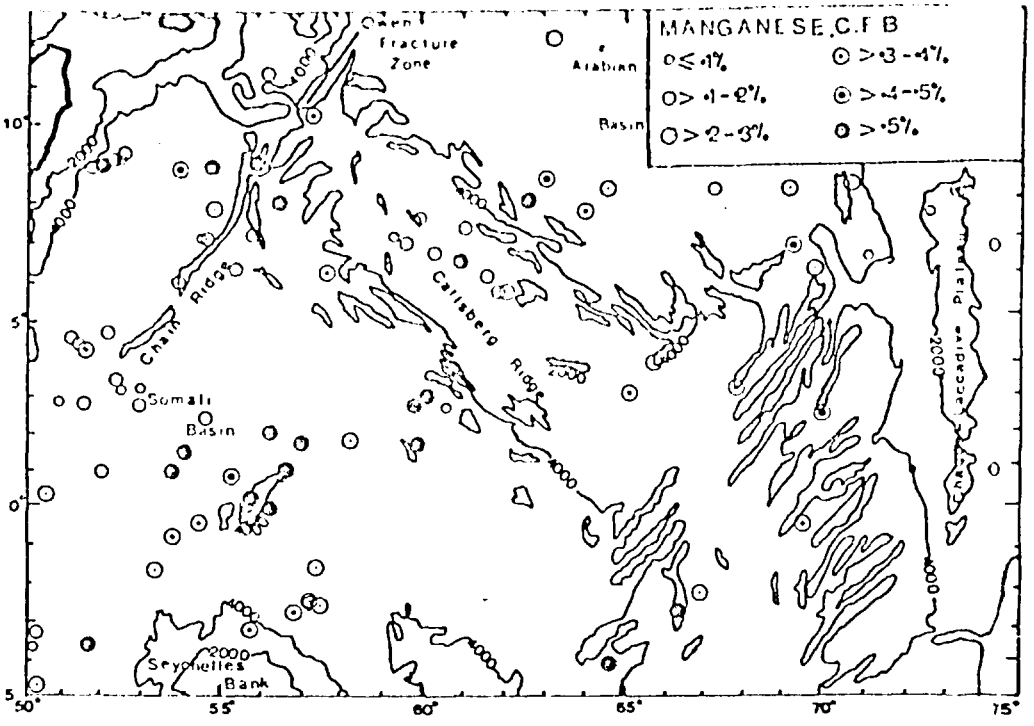

Fig.2.7:Distribution of manganese in the carbonate-free fraction of surface sediments from the North West Indian Ocean.

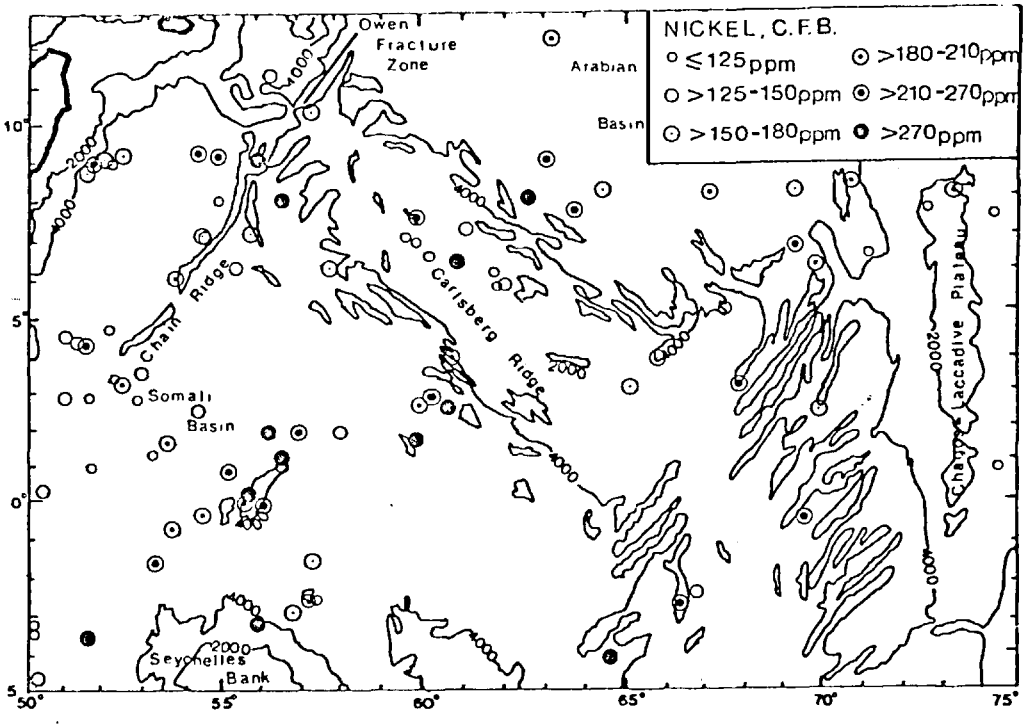

Fig.2.8:Distribution of nickel in the carbonate-free fraction of surface sediments from the North West Indian Ocean.

out that in those sediments containing relatively high levels of Ti(greater than about 0.7%), it is almost invariably associated with basaltic debris from a volcanic source. Levels of Ti much lower than this are seen in the Carlsberg Ridge samples. This suggests the absence of a volcanic input of material in the vicinity of the sediments sampled.

Manganese Figure 2.7

Four main sources of Mn to surface sediments have been described in the literature.

1. A continental source:

a. In particulate form either within the lattice of lithogenous minerals or as discrete particles of hydrous manganese oxides.

b. In solution through river run-off.

2. A biological source, as oxide coatings on skeletal remains.

3. A diagenetic source, through post-depositional migration from deeper sediments.

4. A volcanic source, either from hydrothermal solutions or from alteration of basalt extruded onto the sea floor.

Chester & Aston(1976) considered these and concluded that the relative importance of each source varies locally.

Continental sources, already established as the main sedimentary input to the Somali and Arabian Basins, do not appear to contribute very much to the manganese contents of the surface sediments in these Basins, since the overall levels of Mn are low. Much of the Basins is below the

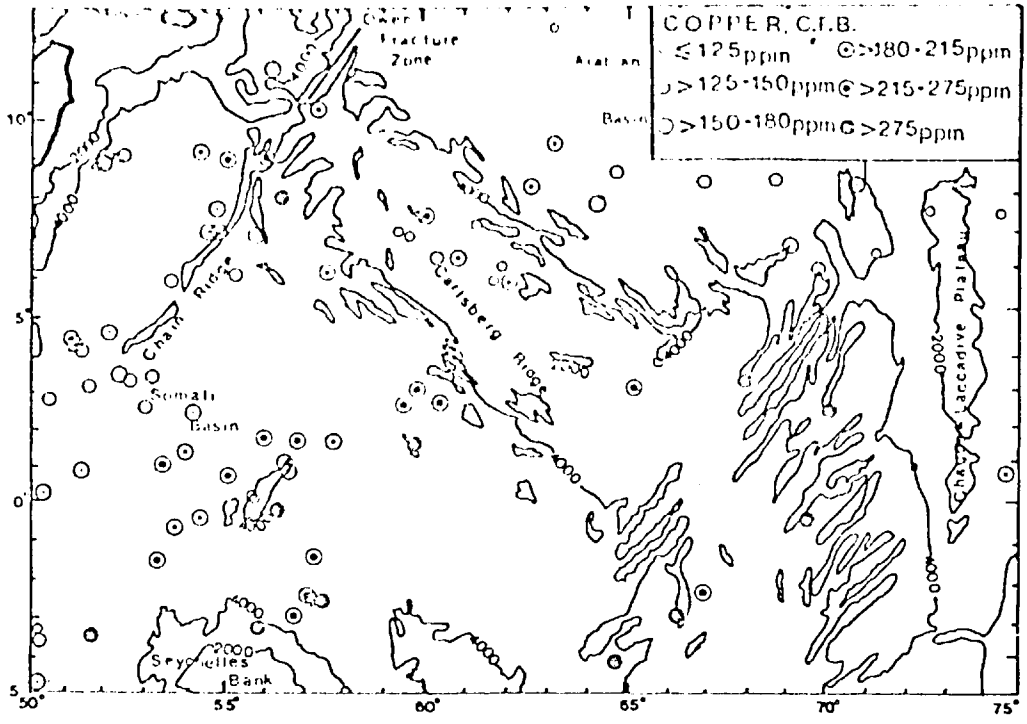

Fig.2.9:Distribution of copper in the carbonate-free fraction of surface sediments from the North West Indian Ocean.

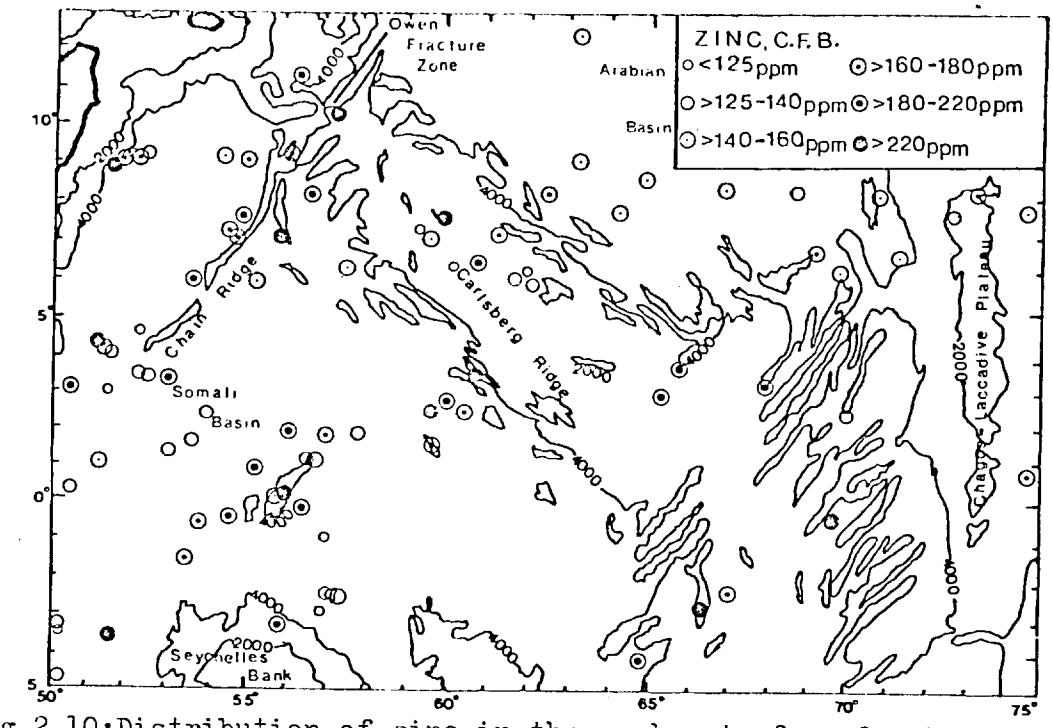

Fig.2.10:Distribution of zinc in the carbonate free fraction of surface sediments from the North West Indian Ocean.

lysocline so a biogenic route for Mn to the sediment is unlikely. The Basins are remote from centres of active volcanism so a volcanic contribution is improbable. The low levels of Mn in the Basin sediments directly reflect low levels of Mn in the continental source material. There are a few samples, mainly in the Somali Basin showing high Mn contents (>0.5%). Diagenetic remobilisation is not considered an important source of Mn here because it is unlikely that conditions favouring mobility of Mn (e.g. low Eh) exist close to the surface of the sedimentary column in an oxidising open ocean basin under a normal sedimentation regime. Indeed at D.S.D.P. site 234 in the north west Somali Basin, reducing conditions in the sediment were found to be present 10m. below the surface.
Oxidising surface conditions were indicated by the presence of manganese nodules (Fisher et al., 1974).

In several of the cores from which the present samples came, manganese micronodules were noted. It seems likely therefore that the presence of manganese micronodules probably accounts for most of the high Mn values in the sediments.

Nickel and copper Figures 2.8 and 2.9

Enhanced levels of Cu and Ni occur with high Mn values in the Somali Basin and on the Carlsberg Ridge, and may be attributed to the presence of manganese micronodules. The high values of copper, nickel and manganese in the Somali Basin are located more in the eastern and central parts than in the western part. This is probably because sedimentation is more rapid in the western part, being

closer to the African mainland which is the main source of its sediment supply. Rapid sedimentation buries micronodules before they are able to accrete a significant amount of manganese oxide from sea water. On the Chagos-Laccadive Plateau and in the Arabian Basin, Cu and Ni values are quite low, but increase towards the Ridge. This reflects either an increasing volcanic contribution or a decreasing rate of sedimentation of metal-poor terrigenous material with increasing distance from the Indus River and Indian peninsula. The first is not considered likely since quite low values of Cu and Ni are generally found on the Ridge, which indicates that a volcanic or hydrothermal contribution to these elements is not large. Therefore a decreasing sedimentation rate is considered more likely as the cause of the increasing metal concentration near the Ridge. This allows micronodule nuclei to continue accreting oxide material, relatively rich in Ni and Cu, from sea water before being buried. In two calcareous cores from the seamounts north of the Seychelles the foram tests were seen to have black flocs of manganese oxide adhering to them. It is probable that in these sediments the Ni was incorporated in the Mn oxide (page 77). Cu levels did not appear to be affected by the presence of the Mn oxide. (figures 2.20 and 2.23).

Zinc Figure 2.10

The distribution of zinc is similar to that of Ni, Cu and Mn. Zinc values are low in the Arabian Basin and on the Chagos-Laccadive Plateau, so biogenic and continental sedimentary inputs probably contain only low levels of

zinc. The level of zinc is generally higher in the Somali Basin, although differences between the east and central parts, and the western part,as noted in the case of other elements are not seen for zinc. Values on the Carlsberg Ridge are very variable. Some of the high values in the Somali Basin and on the Ridge correspond to high Mn and Ni values, so it is probable that the presence of manganese micronodules is responsible for these. There appears to be no correspondence between high Al and Ti values on the Ridge with high zinc values, so a significant volcanic contribution seems unlikely.

A comparison of crest and non-crest sediments

In order to obtain a clearer picture of the influence of submarine volcanism on the sediments, the samples from the Carlsberg Ridge were divided into crest and non-crest sediments. The crest regions of active ridges are known to be volcanic and so sediments from there would be expected to show enrichments in iron and manganese from volcanic emanations. The left hand side of table 2.1 compares the mean values for the elements in the two data sets.

Far from being enriched in transition metals,Table 2.1 shows the crest samples contain lower average concentration except for lead than the non-crest sediments. The two values for lead are about the same, within analytical error.

The right hand side presents data from the cores supplied by Dr.Rona. These are from the median valley of the Carlsberg Ridge and confirm the lack of metal enrichment observed above. There is some increase in the contents of Al, Fe and Mg and Ti at depth in the cores, compared to the

surface samples. Since the subsurface samples are nearer to the basement rock, then perhaps the increased values of these metals are caused by incorporation of basaltic weathering products into the sediment.

Conclusions

Present day sediment sources in the North West Indian Ocean are identifiable as fluvial and eolian (terrigenous), biogenic, authigenic and volcanic. The Arabian and Somali Basins would be expected to be different sedimentologically since the Carlsberg Ridge probably acts as an efficient barrier to fluvial detritus from the Indian subcontinent. The main terrigenous input to the Somali Basin is eolian from the African and Arabian mainland. Eolian input from India to the Arabian Basin is small compared to the Indus River input (Weser, 1972). These different sediment inputs to the two Basins are clearly seen in the sediment chemistry, the Arabian Basin having higher levels of terrigenously supplied elements such as Al, and lower levels of hydrogenously precipitated elements such as Mn, Ni and Cu, than the Somali Basin. Volcanic and hydrothermal activity associated with an active spreading ridge, which are said to have such a profound effect on sediments from other parts of the Mid-Ocean Ridge system (Bostrom et al., 1969; Bostrom, 1973) are only apparent perhaps, in the down-core samples from the cores supplied by Dr. Rona. Here, the increased levels of Al, Fe and Mg may indicate the incorporation of basaltic weathering products into the sediment.

Metal accumulation rates

Metal accumulation rates have been used in the past to

Table 2.1

Comparison of average metal contents of crest and non-crest sediments from the Carlsberg Ridge.

	Crest(n=8)	Non-Crest (n = 14)	Rona cores(median valley) Surface (n = 5)	Rona cores(median valley) All samples (n = 23)
Ca%	29.39	30.09	27.4	27.5
Mn	2756	3907	2455	2328
Fe%	3.32	3.56	3.12	3.83
Ni	165	195	114	110
Co	44	42	48	42
Ti	3283	3455	2845	3647
Al%	4.62	4.91	3.48	4.67
Mg%	2.78	2.76	2.19	2.61
Cu	181	223	155	141
Zn	178	240	86	105
Pb	71	66	47	58
Cd	7	7	--	--
Depth(m)	3566	3746	--	--

All concentrations are expressed on a carbonate-free basis except Ca, which is expressed on a total sediment basis.

determine if sediments are undergoing an anomalously high input of one or more metals (e.g. McMurtry, 1974; McMurtry & Burnett, 1974). The metal accumulation rate is derived by multiplying together the metal concentration, the sedimentation rate and the dry bulk density of the sediment.

In the past various authors have employed a constant value of 0.70 gms. cm^{-3} for the dry bulk density of marine sediments (McMurtry, 1974; McMurtry & Burnett, 1974; Dymond & Veeh, 1975; Sayles et al., 1975). However some caution should be exercised when using this approach, since considerable errors can be introduced in the calculation of the metal accumulation rates for water-rich, low carbonate pelagic sediments if such a value is assumed (Dymond & Veeh, 1975; Sayles et al., 1975, 1976). Lyle & Dymond (1976) have reported errors of between 300 and 400% in the calculation of metal accumulation rates for south east Pacific sediments using this method. Broecker & Broecker (1974) recognised that there is a relationship between the $CaCO_3$ content and the dry sediment density of marine sediments, and thus Lyle & Dymond (1976) derived an expression for estimating the dry bulk density of marine sediments from determination of their $CaCO_3$ content. The work of Lyle & Dymond (op.cit.) is used as the basis for the following estimation and discussion of metal accumulation rates. The sedimentation rates are estimated using the data presented by Kolla et al (1976a). The data are presented in Table 2.2. The estimated metal accumulation rates are presented in Table 2.3.

Table 2.2 Sedimentation rates in different areas of the N.W.Indian Ocean.

Data group	$CaCO_3$ content, wt. %	Wet bulk density gms. cm^{-3} *	Water content*	Dry bulk density, gms cm^{-3}*	Sedimentation rate, cms/10^3yrs. **
CREST	72.42	1.347	.57	.58	2.5
NON-CREST	72.54	1.348	.57	.58	2.5
ARABIAN BASIN	34.51	1.20	.71	.35	1.7
SOMALI BASIN	36.78	1.21	.70	.36	1.8
SEAMOUNTS	85.16	1.41	.52	.68	4.0
CHAGOS-LACCADIVE PLATEAU	50.26	1.255	.65	.44	1.9

*Estimated using the equations of Lyle & Dymond, 1976.

**Estimated using the data of Kolla et al., (1976a).

	CREST	NON-CREST	ARABIAN BASIN	SOMALI BASIN	SEAMOUNTS	CHAGOS-LACCADIVE PLATEAU	CREST (Horder,1979)	NON-CREST (Horder,1979)
Mn	.110	.157	.11	.137	.158	.088	.166	.071
Fe	1.33	1.42	1.95	1.76	1.54	1.53	1.1	.354
Ni	.007	.008	.008	.008	.008	.005	.002	.001
Co	.002	.002	.002	.002	.005	.002	--	--
Ti	.131	.138	.188	.203	.239	.17	.026	.028
Al	1.84	1.96	2.79	2.62	1.92	2.51	.255	.552
Mg	1.11	1.1	1.26	0.98	1.17	1.52	.33	.291
Cu	.007	.009	.006	.008	.009	.005	.005	.002
Zn	.007	.01	.006	.007	.007	.006	.006	.003
Pb	.003	.003	.002	.002	.007	.002	.002	.0005
Cd	.0003	.0003	.0001	.0001	.002	.0002	--	--

Table 2.3 Metal accumulation rates, gms. $cm^{-2}/10^3$ years, in different areas of the N.W.Indian Ocean.

There is great similarity between metal accumulation rates on the Ridge crest and on the Ridge flanks. It might be expected that they would be higher on the crest from incorporation of metals from volcanic activity (Bostrom et al., 1973). Compared to the data of Horder(1979), the accumulation rates of Ti, Al and Mg are high in both crest and non-crest sediments. The area studied by Horder (op. cit.) is on the Central Indian Ridge, remote from terrestrial sources of sediment. This is reflected in sedimentation rates there, which are lower than those on the Carlsberg Ridge (Horder, 1979). The north-west part of the Indian Ocean is surrounded by land on three sides, consequently it is more likely to have a higher terrestrial sedimentation rate than the Central Indian Ridge. Since Ti, Al, and Mg are largely terrigenous in origin (previous section), this probably accounts for the higher rates of accumulation of these metals in the N.W. Indian Ocean than on the central Indian Ridge. Mn, Ni, Cu, Zn, Pb and Co all have similar accumulation rates from area to area throughout the N.W. Indian Ocean. This is probably because they are added to the sediment mostly by authigenic precipitation from seawater. Accumulation rates for Pb and Zn are similar to those found by Horder (1979) on the Central Indian Ridge. The lack of any significant enrichment of any metal on the Ridge compared to elsewhere in the N.W. Indian Ocean, remote from likely centres of active volcanism clearly indicates that a significant volcanic or hydrothermal contribution to present-day sedimentation has not been found on this part of the Ridge.

Data Handling

Introduction

The use of computers to facilitate the manipulation and interpretation of geological and geochemical data is well established. Correlation coefficients have been calculated for the present data in an attempt to understand the inter-element associations in the surface sediments of the N.W.Indian Ocean, and to elucidate the effect of different sediment sources on sediment geochemistry.

The correlation matrix for the whole sediment data group, described below, will only bring out average correlations for the whole of the N.W.Indian Ocean, and cannot show how element associations vary from area to area. This is particularly important in assessing any volcanic contribution to the sediments, since this should only be apparent in the samples from the Carlsberg Ridge and Owen Fracture Zone. Also, different element correlations in the Somali and Arabian Basins may indicate how the different sediment inputs affect sediment chemistry.

The five cores supplied by Dr.P.Rona from the west of the Carlsberg Ridge, arrived too late for inclusion of their analyses in the statistical study of the rest of the sediments. There are 23 samples of which five are surface sediments; they are treated as a separate data group.

In order to take account of the factors described above, the primary sample group has been divided into groups from five physiographic provinces. These are the Carlsberg Ridge, the Arabian Basin, the Somali Basin, the

Chagos-Laccadive Plateau, and the seamounts. Correlation matrices have been calculated for these sample groups in an attempt to determine how the sediment geochemistry varies from province to province. These variations are discussed in terms of the changing significance of each of the sediment sources.

Firstly, in an attempt to establish geochemically the characteristics of the sediment sources in the North West Indian Ocean as a whole, the complete surface data set (91 samples) is considered. Table 2.4 shows the correlation matrix for this data set.

Variations in Fe and Mn, Al, Ca and depth would be expected to reflect the main controls on sediment composition, representing the hydrogenous, detrital, and biogenic components respectively. The elements correlating significantly positively with Ca are Mg, Pb, Cd and Zn. None of these correlations is very strong. Depth, Al, and Fe vary negatively with Ca. This is probably because calcite decreases with depth, and if this is so, the detrital content, measured by Al, must increase with depth. Fe also increases with depth, and varies strongly positively with Al. Fe might be expected to correlate with Mn in the hydrogenous phase, but no significant correlation is observed. Nickel and copper are the only elements to correlate significantly with manganese in the hydrogenous phase.

Initially, then, the following groups of elements are identified as being associated with the various sources of the sediment components:

Biogenic: Ca, Mg, Pb, Cd and Zn.

Detrital: Al, Fe

Hydrogenous: Mn, Ni, Cu.

Carlsberg Ridge and Owen Fracture Zone

Table 2.1 shows the average levels of metals in the present sediments from the crest and non-crest regions of the Carlsberg Ridge. To try and elucidate the controls on the metal contents of the sediments from the two areas, correlation matrices have been computed for the two data sets. These are shown in Tables 2.5 and 2.6.

In the crest samples (Table 2.5), Ni and Cu are significantly correlated with Ca at the 99% confidence level, and Ni is correlated with Mn at the 95% confidence level. Mn shows a weak but not significant correlation with Ca, so perhaps biogenic sedimentation is a route for authigenic oxides to the sediment, perhaps as a coating on calcareous tests, or as flocs adhering to the tests. In the non-crest sediments (Table 2.6), Ni and Cu are clearly correlated with Mn and show no relation with Ca. The authigenic fraction is clearly separate from the biogenic fraction. The detrital component is characterised by Fe, Al, and Ti in both crest and non-crest samples. Mg shows a strong correlation with Ti in the crest samples, which may suggest a common source, perhaps from incorporation of basaltic weathering products.

Arabian Basin

There are significant differences in the element associations in this sample set compared to the Ridge sediments. Table 2.7 shows its correlation matrix.

	Ca	Mn	Fe	Ni	Co	Ti	Al	Mg	Cu	Zn	Pb	Cd	Depth
Ca	1												
Mn	.071	1											
Fe	-.564	.111	1										
Ni	.025	.791	.215	1									
Co	.179	.232	.087	.179	1								
Ti	-.271	-.015	.491	.078	.596	1							
Al	-.663	-.014	.828	.064	-.287	.230	1						
Mg	.389	-.107	-.115	.005	.214	.166	.294	1					
Cu	.148	.583	.024	.524	-.124	-.232	.024	-.178	1				
Zn	.261	.153	-.102	.236	.032	-.010	-.163	.094	.219	1			
Pb	.364	.042	-.241	.090	.615	.475	-.449	.275	-.115	.197	1		
Cd	.456	.024	-.14	.011	.434	.260	-.354	.239	.103	.037	.491	1	
Depth	-.663	.033	.489	-.048	-.386	.018	.648	-.429	.213	-.183	-.591	-.537	1

Table 2.4 Correlation matrix for the surface sediment samples.

n = 91

Significance levels are $r = .242$ at 99%

and $r = .173$ at 95% (from Fisher & Yates, 1964)

None of the metals seem to be associated with the biogenic fraction of the sediment. Fe, Ni, Cu and possibly Cd and Zn, are associated with Mn, possibly in the hydrogenous phase. The most striking aspect of these samples is the correlations between Al and Mn, and Al and Fe, significant at the 95% confidence level. This can be interpreted in two ways: either the detrital phase contains within the structural lattice most of the metals normally associated with the hydrogenous phase, or the detrital material is acting as the transport mechanism of the hydrogenous phase to the sediment, perhaps as oxide coatings on clay particles.

Somali Basin

The element associations here revert to those seen in the whole data set. Table 2.8 shows the correlation matrix for this sample set. Cd again correlates with Ca in the biogenic component. The hydrogenous fraction is again characterised by the close correlations between Mn and Ni, and Mn and Cu. Fe, Ti and Al appear to constitute the detrital elements.

Chagos-Laccadive Plateau

The correlation matrix for these samples is shown in Table 2.9. Zn, Cd and possibly Cu are associated with Ca. Zn also appears to be associated with Mn, although the correlation with Ca is stronger. Ni and Pb are also correlated with Mn, but Cu is not. Fe again seems to be contributed mainly by the detrital phase, being correlated with Al.

	Ca	Mn	Fe	Ni	Co	Ti	Al	Mg	Cu	Zn	Pb	Cd	Depth
Ca	1												
Mn	.536	1											
Fe	.291	.355	1										
Ni	.813	.626	.259	1									
Co	.077	.291	.230	-.295	1								
Ti	.363	-.09	.660	.403	-.159	1							
Al	.279	.347	.951	.114	.445	.527	1						
Mg	.560	.228	.678	.681	-.229	.919	.491	1					
Cu	.875	.555	.563	.661	.259	.358	.570	.524	1				
Zn	.852	.198	.146	.762	-.112	.560	.040	.688	.672	1			
Pb	.620	.458	.231	.348	.588	-.015	.318	.099	.805	.487	1		
Cd	.668	-.175	.103	.573	-.42	.549	.013	.565	.563	.813	.277	1	
Depth	-.593	.192	.047	-.588	.602	-.545	.176	-.583	-.309	-.773	.062	-.899	1

Table 2.5 Correlation matrix for the crest samples.

n= 8 Significance limit for 99% confidence level r = .75

95% confidence level r =.582 (from Fisher & Yates,1964)

	Ca	Mn	Fe	Ni	Co	Ti	Al	Mg	Cu	Zn	Pb	Cd	Depth
Ca	1												
Mn	-.635	1											
Fe	-.525	.196	1										
Ni	-.563	.923	.267	1									
Co	.151	.208	.159	.389	1								
Ti	-.48	.026	.829	.133	.169	1							
Al	-.516	.159	.963	.175	.082	.876	1						
Mg	.023	-.586	.163	-.500	-.274	.377	.199	1					
Cu	-.35	.851	.264	.827	.248	-.071	.161	-.572	1				
Zn	.190	.089	.008	.162	.130	.056	-.046	-.276	.247	1			
Pb	.211	-.171	.011	-.292	-.141	-.089	.008	.147	.083	.401	1		
Cd	.09	-.227	-.039	-.123	-.58	-.002	-.048	.052	-.170	.290	.061	1	
Depth	-.663	.639	.658	.608	.104	.403	.601	-.181	.718	.005	.229	-.187	1

Table 2.6 Correlation matrix for the non-crest sediments.

n = 14

Significance limit for 99% confidence level r = .592

95% confidence level r = .441 (from Fisher & Yates,1964)

Seamounts

The correlation matrix for these samples is shown in Table 2.10. Again, Pb is positively correlated with Ca, indicating an association with the biogenic fraction of the sediment. Fe appears to be of a hydrogenous origin, correlating with Mn rather than Al. Ni correlates very strongly with Mn, but Cu is more strongly correlated with Al than Mn, probably indicating a mainly detrital source for this metal.

Rona samples

The correlation matrix for these samples is shown in Table 2.11. The correlations here fall into three groups. Cd correlates with Ca and therefore appears to have a biogenic origin. Mn, Ni and Cu form a group on their own. This indicates a similar mode of incorporation into the sediment; these elements are probably hydrogenous in origin. Fe, Ti, Al and Mg correlate strongly with each other. These elements may be derived from terrigenous aluminosilicate material or from the incorporation of local volcanic weathering products into the sediments. The latter possibility is more likely in view of the core locations in the median valley of the Carlsberg Ridge.

Discussion

Table 2.12 shows the groups of elements associated with each component in each sample group. The Arabian Basin samples are clearly different from the rest in that the detrital and hydrogenous inputs appear to be intimately associated with each other. The main source of sedimentary material here is the Indus River. Elsewhere in the N.W.Indian

	Ca	Mn	Fe	Ni	Co	Ti	Al	Mg	Cu	Zn	Pb	Cd	Depth
Ca	1												
Mn	.056	1											
Fe	-.289	.529	1										
Ni	-.059	.972	.548	1									
Co	-.419	.183	.164	.30	1								
Ti	-.012	.605	.938	.571	-.039	1							
Al	-.483	.629	.674	.725	.535	.493	1						
Mg	.206	.547	.653	.546	.297	.674	.627	1					
Cu	-.084	.886	.458	.876	-.009	.54	.451	.273	1				
Zn	-.021	.644	.00	.733	.394	-.011	.405	.073	.617	1			
Pb	.125	.161	-.114	.149	.157	-.158	.420	.387	-.187	.025	1		
Cd	.205	.654	.022	.712	-.036	.096	.287	.113	.689	.804	.137	1	
Depth	-.322	.625	.879	.604	.145	.842	.710	.704	.563	.019	.052	.04	1

Table 2.7 Correlation matrix for Arabian Basin surface sediments.

n = 10

Significance limits are r = .685 for 99% confidence level

r = .521 for 95% confidence level (From Fisher & Yates,1964)

	Ca	Mn	Fe	Ni	Co	Ti	Al	Mg	Cu	Zn	Pb	Cd	Depth
Ca	1												
Mn	.074	1											
Fe	-.575	-.002	1										
Ni	.096	.761	-.013	1									
Co	.221	.303	-.073	.102	1								
Ti	-.507	-.227	.691	-.229	.047	1							
Al	-.507	.030	.832	-.070	.046	.594	1						
Mg	.613	-.177	-.393	-.012	-.139	-.209	-.581	1					
Cu	.028	.68	.028	.704	.360	-.326	.08	-.274	1				
Zn	.296	.185	.085	.250	.154	-.074	-.047	.277	.148	1			
Pb	.265	.162	-.046	.350	.364	-.099	-.071	.228	.423	.104	1		
Cd	.440	.034	-.177	.146	.499	-.071	-.14	.332	.265	.178	.734	1	
Depth	-.565	-.137	.199	-.203	-.305	.083	.266	-.375	.00	-.416	-.523	-.493	1

Table 2.8 Correlation matrix for the Somali Basin surface sediments.

n = 46

Significance limits are r = .338 for 99% confidence level

r = .243 for 95% confidence level (Fisher & Yates, 1964)

	Ca	Mn	Fe	Ni	Co	Ti	Al	Mg	Cu	Zn	Pb	Cd	Depth
Ca	1												
Mn	.57	1											
Fe	-.626	.00	1										
Ni	.242	.876	.466	1									
Co	.013	-.608	-.319	-.591	1								
Ti	-.087	-.032	.570	.337	.41	1							
Al	-.907	-.243	.878	.168	-.265	.277	1						
Mg	.675	-.037	-.637	-.237	.744	.267	-.788	1					
Cu	.664	.158	-.20	.148	.535	.629	-.568	.843	1				
Zn	.889	.846	-.41	.589	.172	.010	-.685	.489	.544	1			
Pb	-.085	.739	.598	.890	-.838	.067	.450	-.646	-.301	.274	1		
Cd	.749	-.003	-.833	-.326	.626	-.027	-.914	.955	-.695	.527	-.672	1	
Depth	-.479	-.403	.672	.037	.479	.898	.548	.047	.324	-.424	-.075	-.236	1

Table 2.9 Correlation matrix for the Chagos-Laccadive Plateau samples.

n = 5

Significance limits are r = .882 for 99% confidence level

r = .729 for 95% confidence level (Fisher & Yates,1964)

	Ca	Mn	Fe	Ni	Co	Ti	Al	Mg	Cu	Zn	Pb	Cd	Depth
Ca	1												
Mn	-.065	1											
Fe	-.389	.683	1										
Ni	-.029	.909	.456	1									
Co	.48	.621	.299	.639	1								
Ti	.569	.211	-.156	.346	.851	1							
Al	-.868	-.133	.372	-.236	-.729	.871	1						
Mg	.698	.168	-.254	.407	.734	.877	-.867	1					
Cu	-.435	-.208	.117	-.491	-.657	.650	.58	-.786	1				
Zn	.177	-.222	-.681	.065	.163	.58	-.495	.554	-.355	1			
Pb	.624	.094	-.532	.172	.602	.894	-.861	.893	-.733	.753	1		
Cd	.557	-.163	.111	-.219	.225	.228	-.302	.395	-.163	-.170	.143	1	
Depth	-.831	-.156	.24	-.321	-.778	.840	.911	-.928	.825	-.389	-.851	-.441	1

Table 2.10 Correlation matrix for the seamount surface sediments.

n = 8

Significance limits are r = .75 for 99% confidence level

r = .58 for 95% confidence level (Fisher & Yates 1964)

	Ca	Mn	Fe	Ni	Co	Ti	Al	Mg	Cu	Zn	Pb	Cd
Ca	1											
Mn	.267	1										
Fe	-.448	.032	1									
Ni	.032	.500	.005	1								
Co	.198	-.173	.178	.000	1							
Ti	-.124	-.145	.722	.049	.506	1						
Al	-.402	-.217	.866	.071	.230	.825	1					
Mg	.047	.146	.815	.134	.273	.732	.753	1				
Cu	.083	.543	.314	-.134	.259	.219	.008	.211	1			
Zn	-.383	-.083	.426	.278	-.296	.070	.433	.311	-.342	1		
Pb	-.105	.243	.176	-.008	-.059	.010	.144	.170	.078	.031	1	
Cd	.488	.012	-.683	-.070	.292	-.284	-.553	-.461	-.090	-.406	.116	1

Table 2.11 Correlation matrix for the Rona samples

n = 23

Significance limit for 99% confidence level r = 0.46

95% confidence level r = 0.34 (Fisher & Yates, 1964)

Table 2.12

Element groupings in surface sediment components.

Data set	Av.depth.	Biogenic	Detrital	Hydrogenous
All	4250m	Ca,Pb,Cd,Zn.	Fe, Al	Mn,Ni,Cu
Ridge	3681	Ca, Cd	Fe, Al	Mn, Ni, Cu.
Arabian	4405	Ca	Fe,Mn,Al,Ni,Cu,Cd,Zn,Mg,Ti	
Somali	4820	Ca,Cd	Fe,Al,Ti	Mn,Ni,Cu.
Chagos-Laccadive Plateau	3110	Ca,Cd,Cu,Zn.	Fe,Al.	Ni,Mn,Pb.
Seamounts	3061	Ca,Pb.	Al,Cu.	Fe,Ni,Mn.

Ocean, the detrital input is primarily eolian(Weser,1972). The most important difference between fluvial and eolian input is that eolian material is introduced directly into the open ocean, whereas river-borne material passes through estuarine environment, being subjected to large changes of ionic strength and redox potential in its passage. Also, it is in contact with water for longer and consequently has more time in which to accumulate an oxide coating, which has the ability to scavenge other metals from sea water such as Ni, Cu, and Zn (Krauskopf, 1956). A dominance of river-borne material may explain why the sediments of the Arabian Basin are so obviously geochemically different from other parts of the North West Indian Ocean.

Another striking aspect about the samples is the lack of any apparent difference between the samples from the Carlsberg Ridge, where volcanic activity might be expected to influence sediment composition, and the Somali Basin,

an area remote from active volcanism. The Rona cores probably penetrated the whole sediment column in the median valley of the Carlsberg Ridge (Cole, pers.comm.), so it may be that the increased Fe, Ti, Al and Mg values observed at depth in these cores are attributable to the incorporation of basaltic weathering products. This is the only discernible influence which volcanic activity has had on any of the sediments studied in this work.

The element groupings undergo a change in the shallower samples from the Chagos-Laccadive Plateau and the seamounts, the most significant of which is the presence of Cu not in the hydrogenously-derived group of metals, but in the biogenic group in the Chagos-Laccadive Plateau samples, and more importantly, in the detrital component on the seamounts. Colley et al., (1979) have estimated that a relatively large proportion (9%) of the Cu in ferromanganese oxide deposits from these seamounts is associated with aluminosilicate detritus. The quite high correlation between Cu and Al in the seamount sediments seems to support this observation.

Bulk Geochemistry of Sediment Cores

Introduction

Nine cores from the North West Indian Ocean were opened, sampled, and analysed by the author and are described in detail below.

Core SH1300G 42 cms. Figure 2.11

The core was taken in the Arabian Basin from a depth of 4615m., well below the lysocline. This is reflected by the low calcite content of the core, which varies from nearly 30% at the top, to 3% at 32 cms., to 13% at 41cms.

Figure 2.11: Variation of calcite, iron, manganese, copper and nickel with depth in core SH1300.

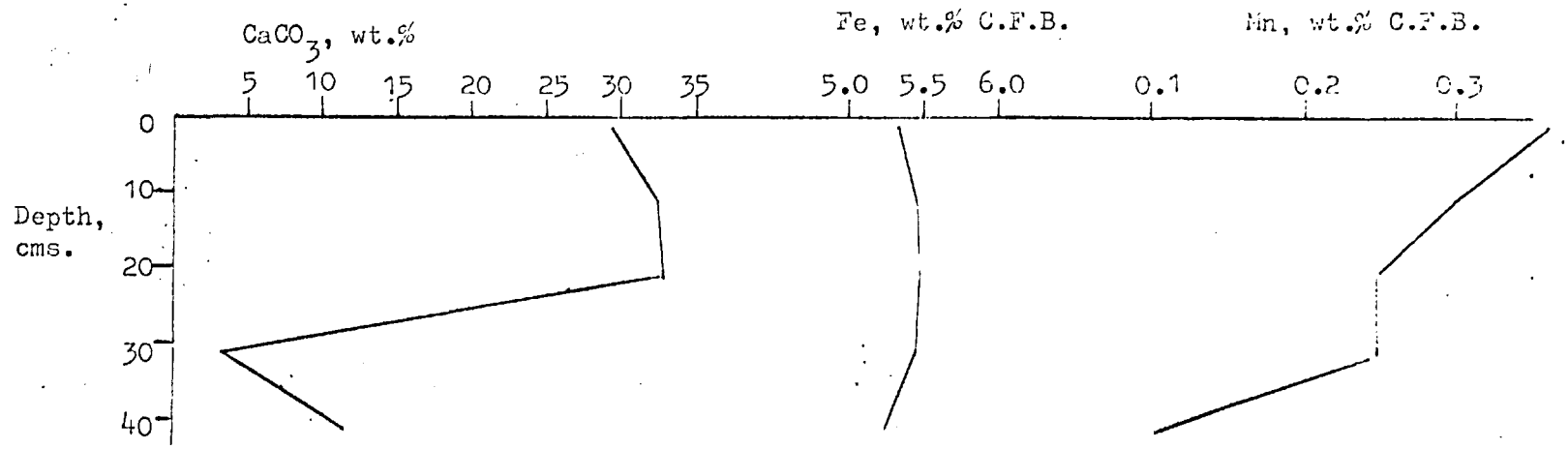

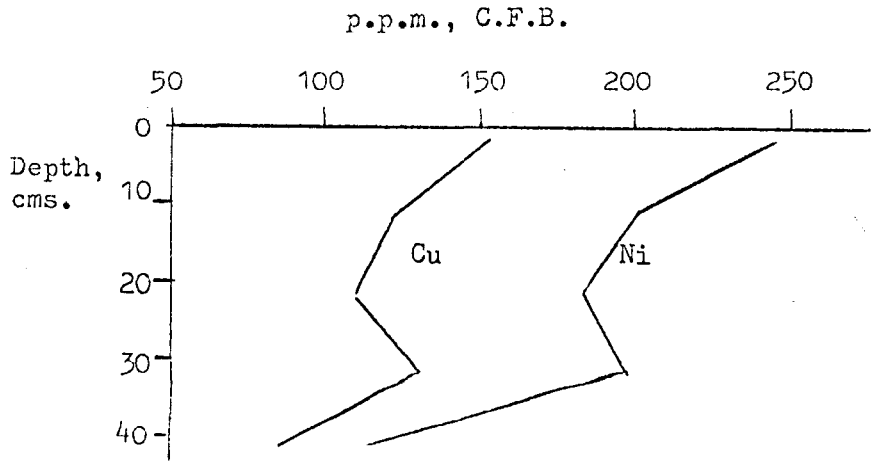

The Fe, Ti and Al do not vary significantly down the core, being about 5.4%, 0.53% and 8% respectively. The clearest trend to be seen in this core is the close association of Cu and Ni with Mn. The contents of both Cu and Ni approximately double from the bottom of the top of the core, while Mn increases from 1012 ppm to 3630 ppm.

Core SH1305G Figs. 2.12 - 2.15; 254cms.

This core was taken in the Somali Basin from a depth of 4,369m. near the bottom of the Seychelles Bank. It has quite a varied lithology, showing frequent minor colour changes and changes in texture. The most obvious feature is a calcareous turbidite at 175-200 cms., presumably derived from the shallow water sediments around the Seychelles Islands. 26 samples were taken altogether and a correlation matrix computed (Table 2.13).

The calcite content is high (average 74%) considering the depth the core was taken from, 400 metres or so below the lysocline. The maximum value of 88% is reached in the middle of the turbidite, and the minimum of 55% at 70 cms. (Fig.2.12). The only element which appears to be associated with calcite is Cd. Iron, titanium and lithium are associated together with aluminium in what is probably the detrital phase. Copper and zinc are more strongly correlated with iron and the detrital phase than with manganese and the hydrogenous phase. Nickel is more strongly associated with manganese than with iron. The manganese content exceeds 1% at 12 cms and the Ni, Cu, and Zn values all show marked increases here (fig. 2.13). This may be caused by the presence of manganese micronodules.

Figure 2.12: Core SH1305: Variation of calcite and cadmium with depth.

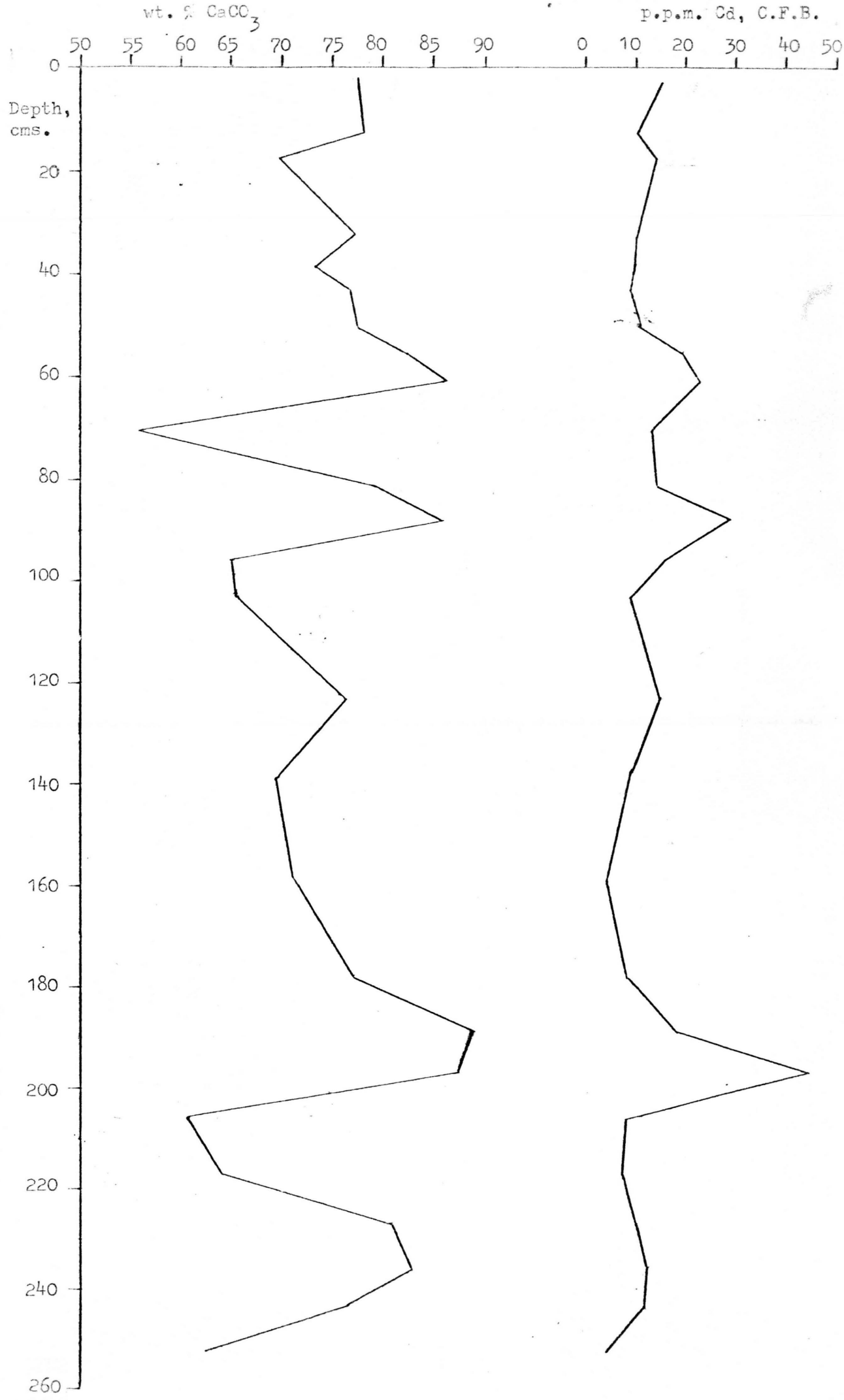

Figure 2.13: Core SH1305: Variation of Mn and Ni with depth.

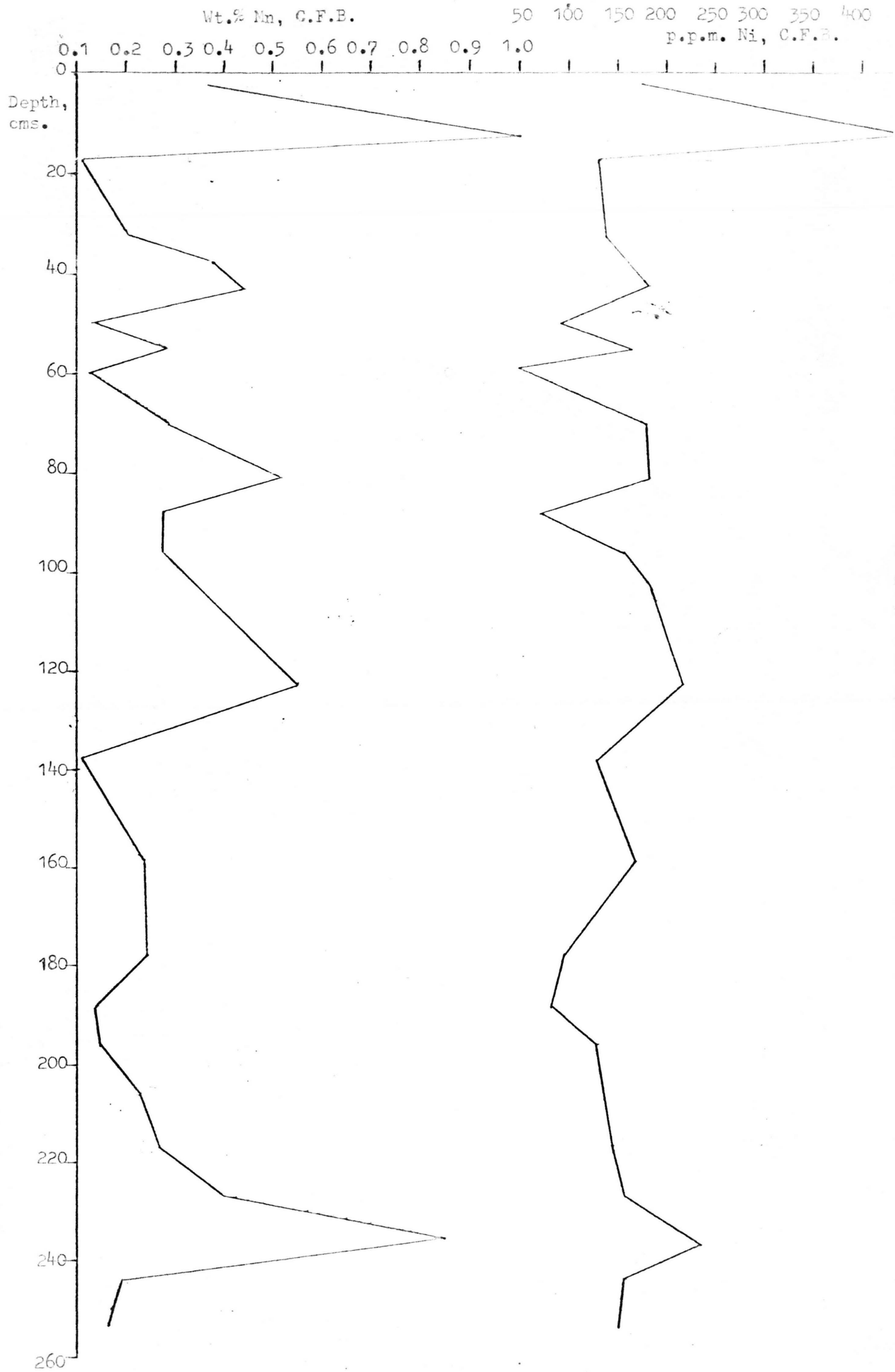

Figure 7.14: Core SH1305: Variation of iron and aluminium with depth.

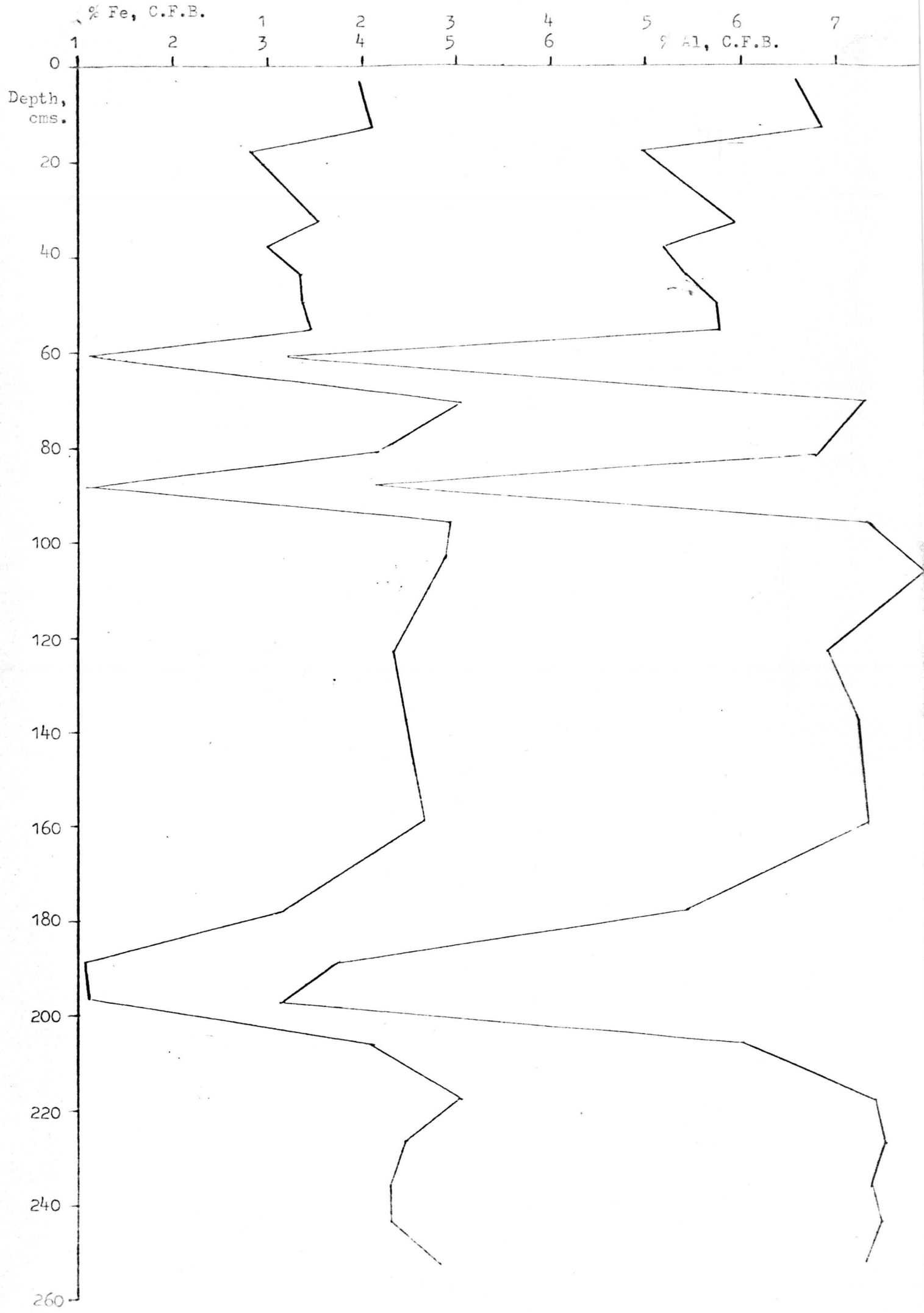

Figure 2.15: Core SM1305: Variation of titanium and lithium with depth.

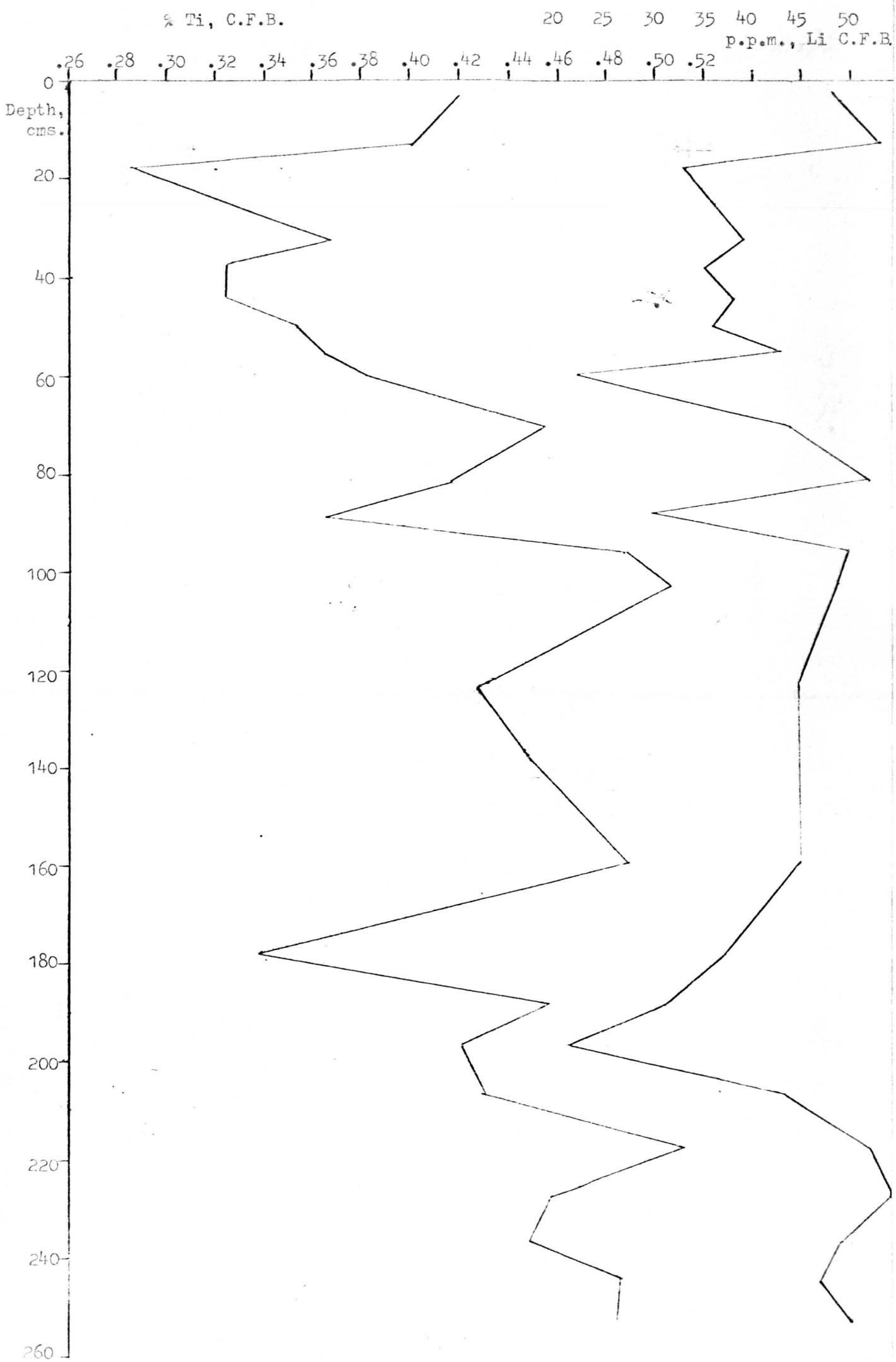

	Ca	Mn	Fe	Ni	Co	Ti	Al	Mg	Cu	Zn	Pb	Cd	Li
Ca	1												
Mn	.046	1											
Fe	-.766	.288	1										
Ni	-.210	.865	.463	1									
Co	.197	.393	.101	.176	1								
Ti	-.449	.015	.957	.083	.231	1							
Al	-.68	.334	.981	.493	.152	.951	1						
Mg	.407	-.004	-.288	-.003	.070	.648	-.298	1					
Cu	-.504	.694	.842	.700	.309	.602	.853	-.230	1				
Zn	-.494	.627	.808	.766	.245	.580	.818	-.027	.867	1			
Pb	-.237	.261	.326	.115	.068	.165	.337	-.047	.383	.310	1		
Cd	.55	-.165	-.724	-.264	-.187	-.213	-.766	.344	-.578	-.679	-.318	1	
Li	-.547	.503	.901	.580	.190	.803	.906	-.121	.920	.908	.462	-.661	1

Table 2.13 Correlation matrix for the samples from Core 1305

n = 26

Significance limit for 99% confidence level r = .44

95% confidence level r = .32 (Fisher & Yates, 1964)

The effect of the turbidite layer on the composition of the core is quite clear. Mg increases from 2.5% outside the layer to 4.5% in the middle. The contents of Fe, Al, Ti, Cu, Zn, Pb and Li are all markedly lower (Figs.2.14 and 2.15). Cd, on the other hand, increases from less than 10 ppm outside the layer to over 40 ppm.

Core SH1306G 190 cms. Figs. 2.16 and 2.17

This core was taken from the foot of a seamount to the N.E. of the Seychelles, in a water depth of 3983m. The core does not vary very much in appearance: there are no marked changes in texture or colour. The calcite content does not vary very much down the core, lying mostly between 85 and 87%. Cu and Ni tend to follow Mn in what is probably the hydrogenous fraction. Mg and Fe seem to follow Al, in the detrital phase.

Core SH1308 37cms. Fig.2.18

This was a box core taken from the same seamount as the gravity core 1306, only further up the slope at a depth of 3231m. It consists throughout of a visually uniform calcareous sand, with an essentially constant calcite content of 87%. Ni, Cu, Zn and Pb show marked minima at 11 cms, coincident with a Mn minimum. Fe again follows Al in the detrital phase.

Core SH1313G 65 cms. Fig. 2.19

This core was collected from the Somali Basin, to the north of the seamount where cores 1308 and 1306 were taken, at a depth of 4404 metres. It consists of a uniform foraminiferal ooze throughout. The calcite content is quite high for its depth. The surface contains 70% calcite,

Figure 2.16: Core SH1306: Variation of iron, aluminium and magnesium with depth.

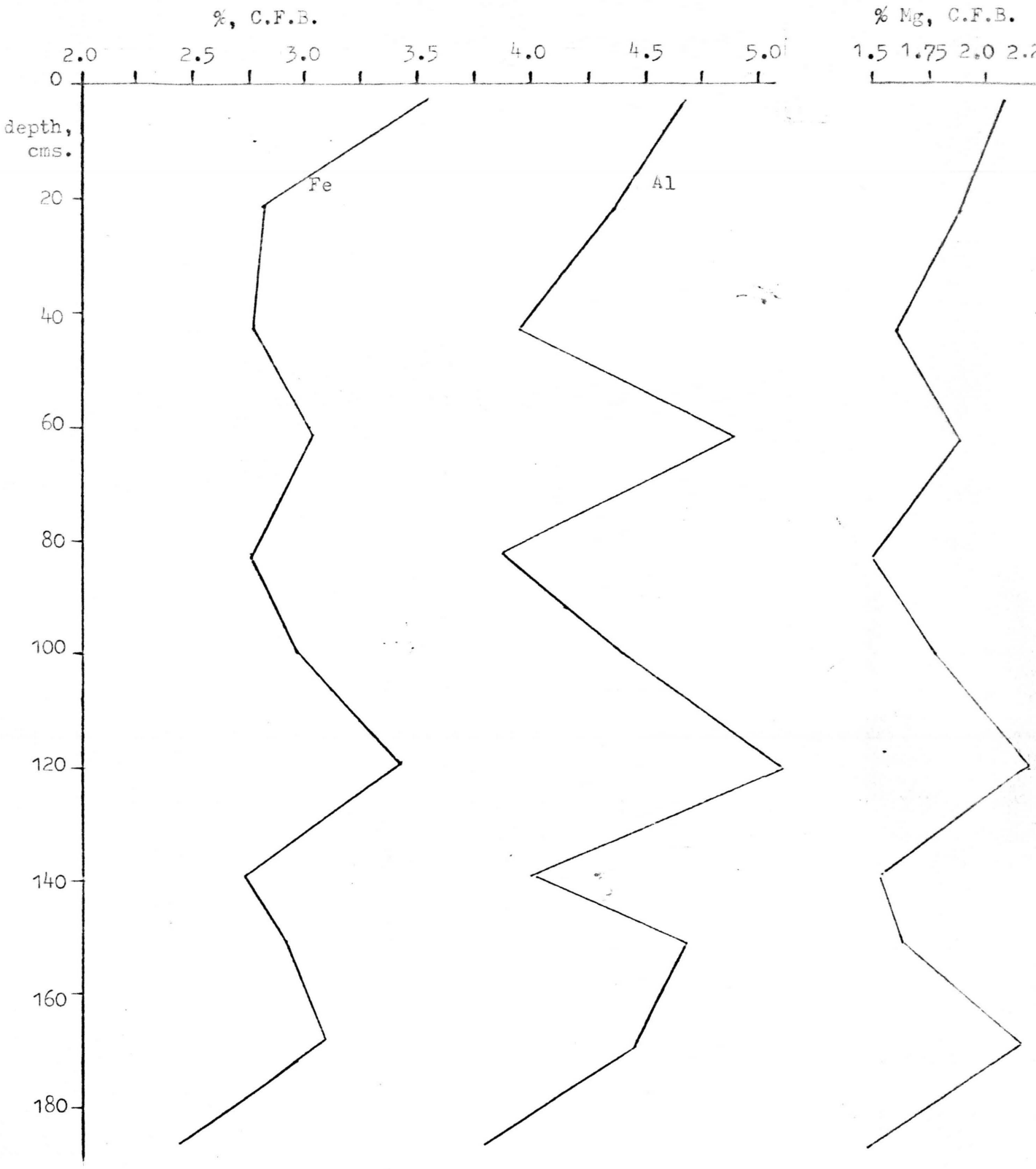

Figure 2.17: Core SH1306: Variation of manganese, nickel and copper with depth.

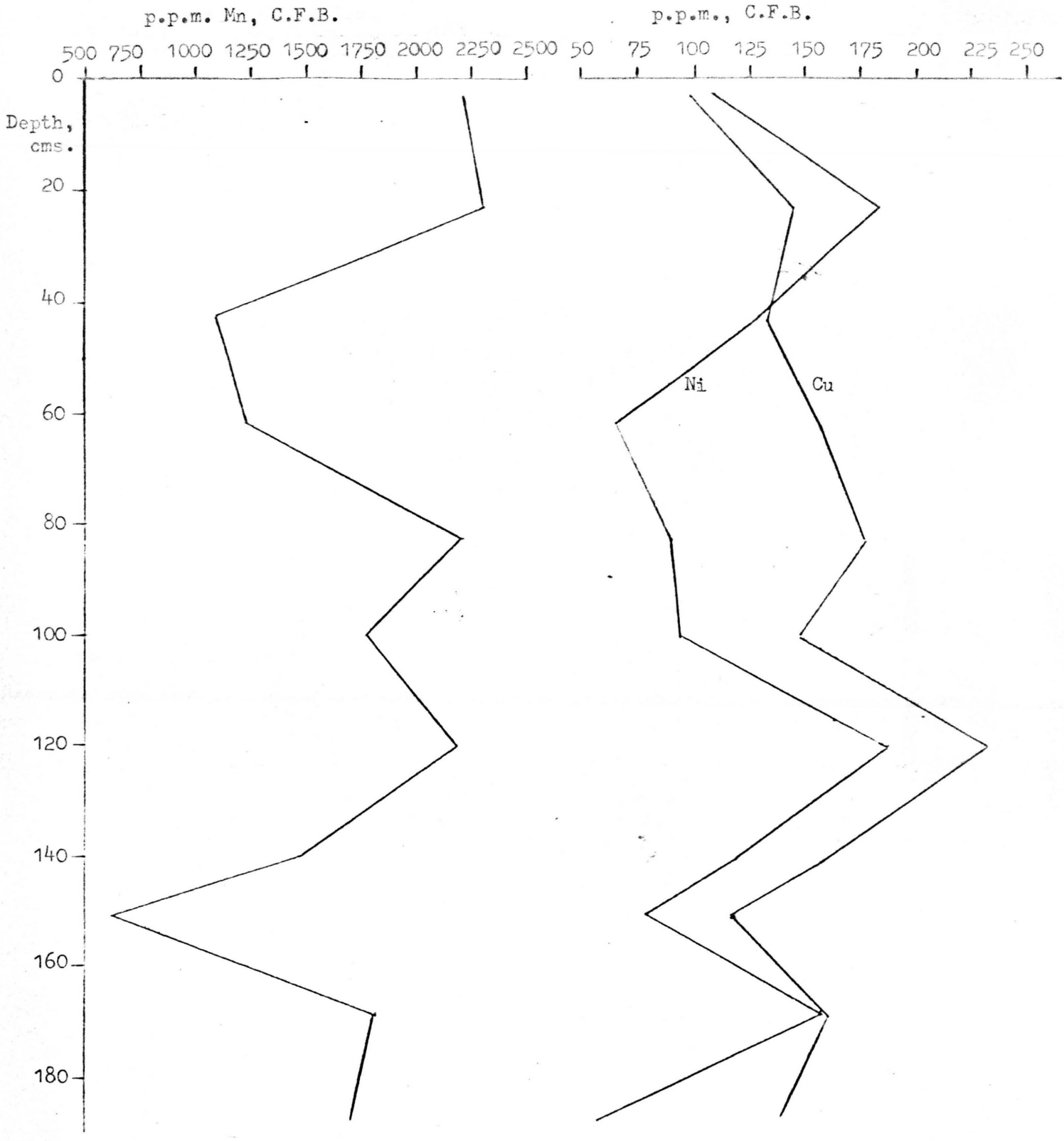

Figure 2.18: Core SH1308: Variation of manganese, lead, zinc, nickel, copper, iron and aluminium with depth.

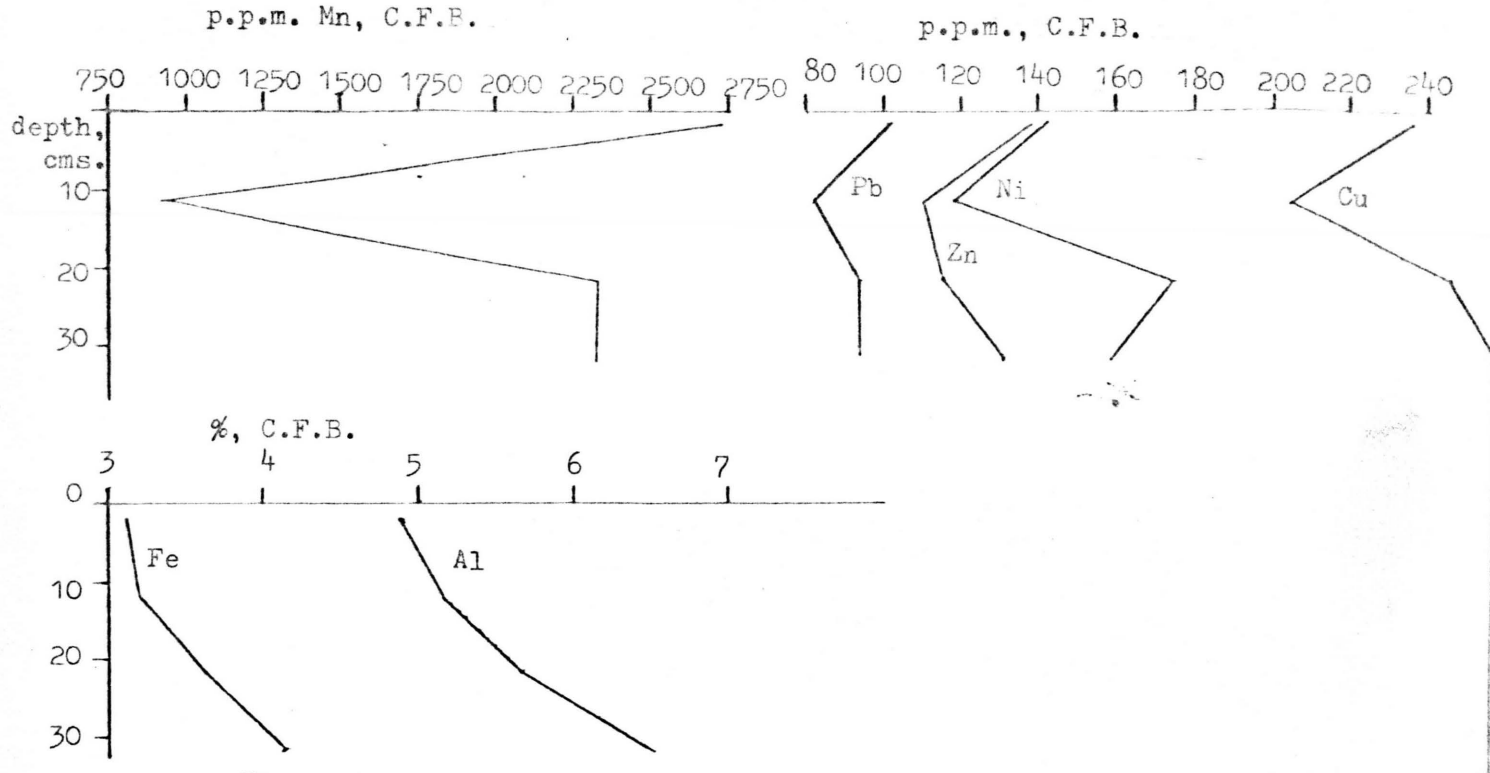

Figure 2.19: Core SH1313: Variation of iron, aluminium, titanium, nickel, manganese and calcite with depth.

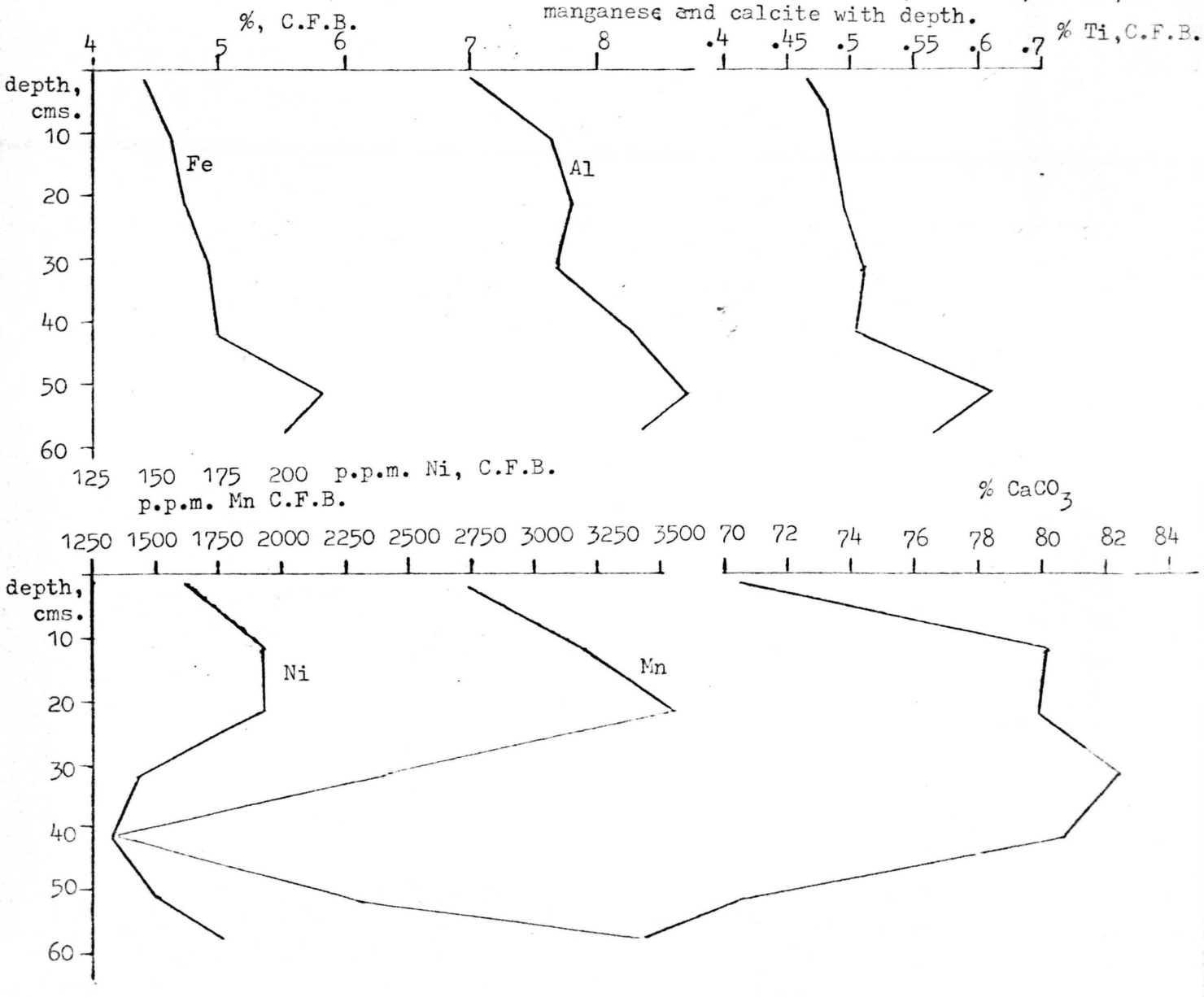

increasing to 80-82% from 10 to 40 cms., and reverts to 70% or less to the bottom. Mn is quite variable, and nickel seems to follow it. Fe and Ti seem to follow Al quite closely.

Core SH 1315 36 cms. Fig.2.20

This is a core consisting of foram sand taken from near the top of a seamount to the north of the Seychelles, at a depth of 1200m. The calcite content is therefore very high, and fairly constant at around 96%. Ferromanganese oxide staining of the forams was a very common occurrence throughout the core. This is reflected in the very high Fe and Mn contents for such a high calcite content. Fe reaches 5.9% at the bottom, where Mn reaches 1.05%. Ni and Pb also reach very high values (greater than 400ppm. at the bottom). Cu levels are fairly normal near the top, although it follows Mn, increasing towards the bottom.

Core SH1318 31cms. Fig.2.21

Like SH1315, this consists of a foram sand throughout, and has a high calcite content(94-96%). It was taken close to SH1315, from a depth of 1358m. However there is no ferromanganese oxide staining, and the low Fe and Mn values reflect this (about 2% and 0.11% respectively). Al shows a large increase towards the bottom of the core.

Core SH 1323A 85 cms. Fig.2.22

This core was taken at a depth of 2800 m. from another seamount to the north of the Seychelles. It is a calcareous ooze throughout, and the consistently high calcite content (86-89%) reflects its fairly shallow

Figure 2.20: Core SH1315: Variation of manganese, copper, lead, nickel aluminium and iron with depth.

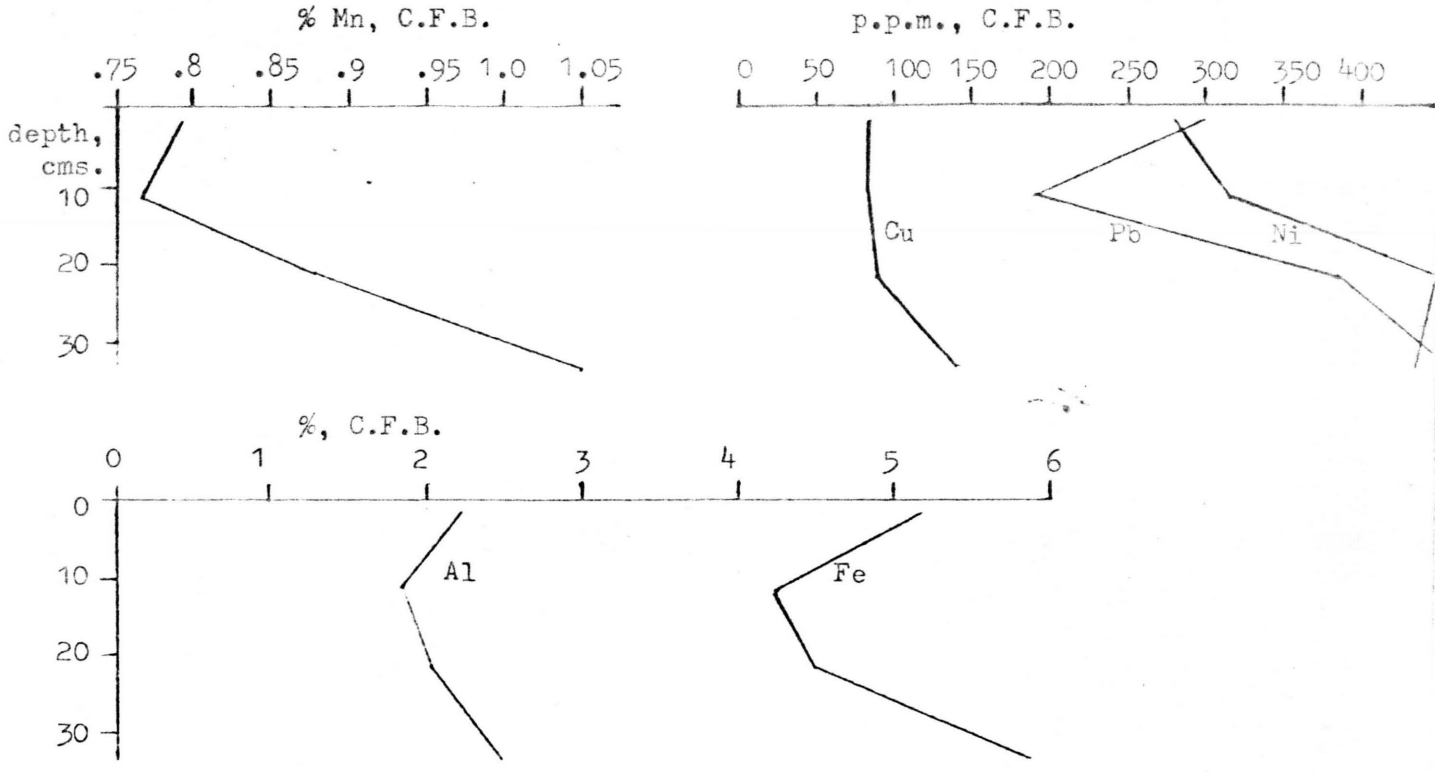

Figure 2.21: Core SH1318: Variation of manganese, copper, nickel, aluminium and iron with depth.

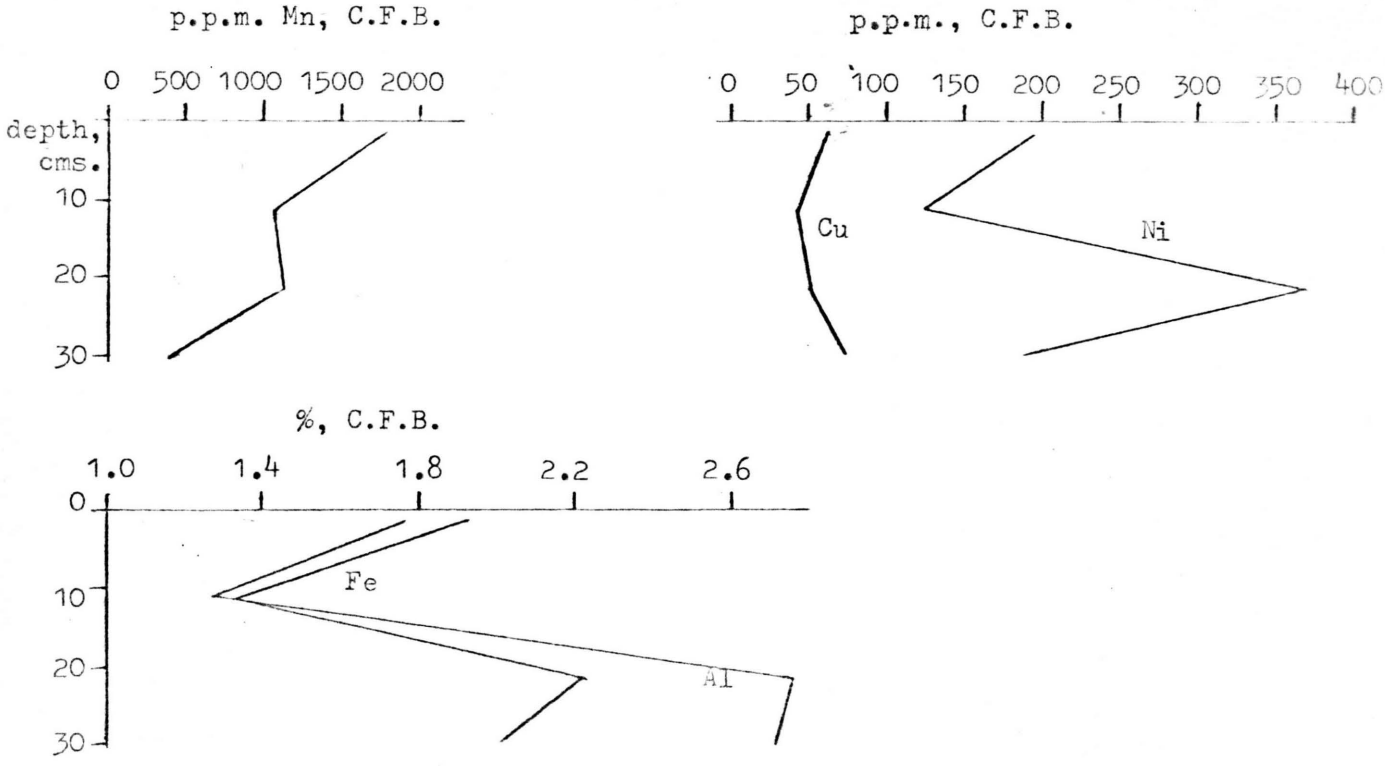

Figure 2.22: Variation of manganese, nickel, copper, magnesium, iron and aluminium with depth in core SH13234.

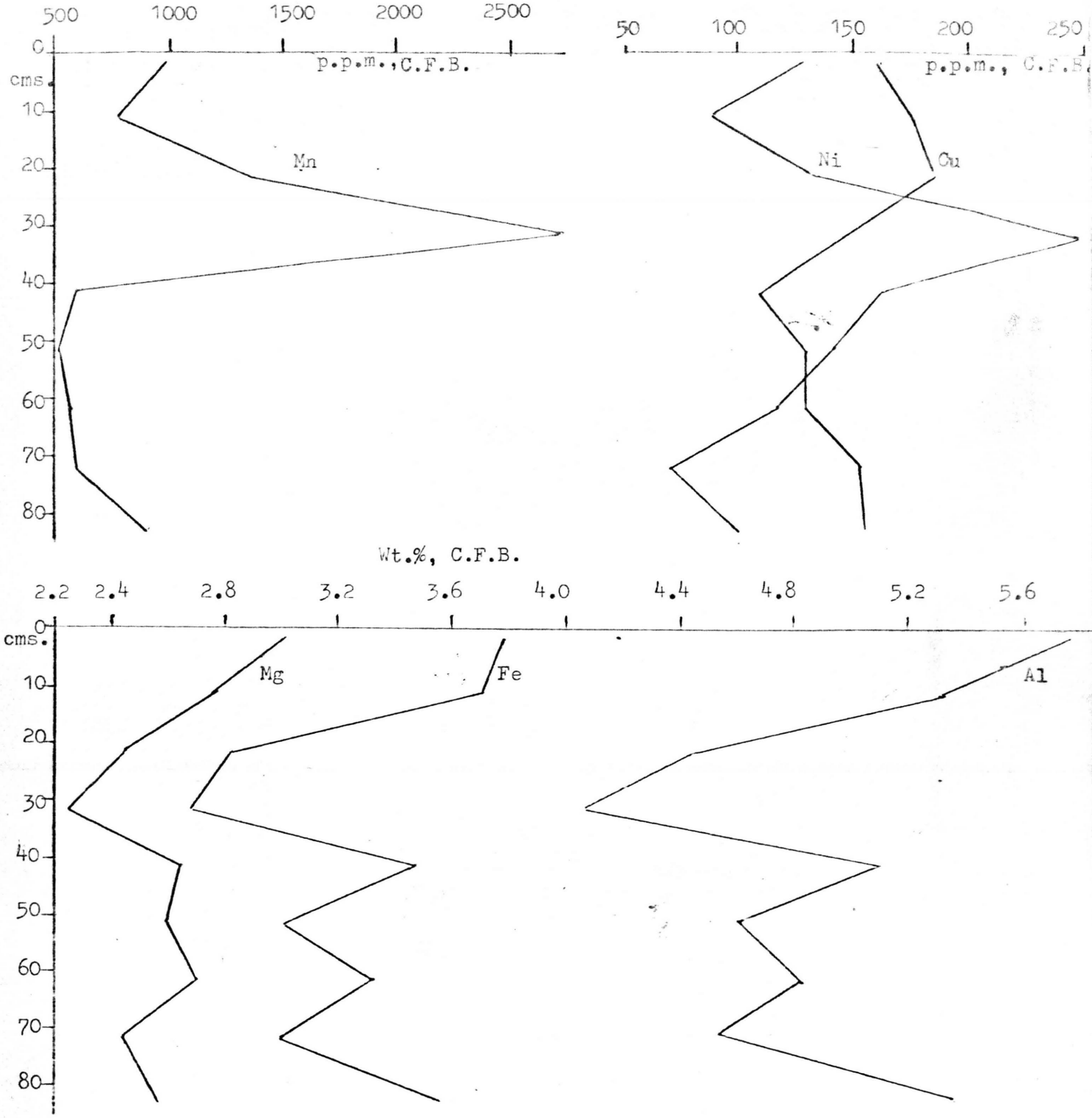

depth. Mn shows a distinctly high zone between 20 and 40 cms. Outside this zone, the values lie between 500 and 1000 ppm; inside, they reach 2700 ppm. Ni shows this peak also, but Cu does not. Fe and Mg follow Al in the detrital phase; these metals show clear minima between 20 and 40 cms. where the hydrogenous phase showed a maximum.

Core SH1323B 57 cms. Fig.2.23

This core was taken very close to 1323A, from a depth of 2940m. Again, it consists of a calcareous ooze throughout, calcite varying from 85-90%. Manganese oxide staining was observed on the foram tests. This is probably what accounts for the higher values of Mn and Ni in this core than in 1323A, varying from 285 to 455 ppm. and from 5400 to 7600 ppm. respectively. Mn shows a maximum at 21 cms. and Ni at 32 cms. Cu also reaches a maximum at 32 cms. Fe is slightly higher than in 1323A, and seems to covary with Al, which is no higher in general than in 1323A. Mg, Cd, Pb and Zn appear to covary with calcite.

Inter-element associations

The same statistical method used for the surface sediments has been applied to the core samples. The top (surface) samples have been included to get a more realistic picture about the sediment geochemistry of these cores, which were taken from an area of extensive ferromanganese oxide crust sampling. Consequently, this approach may shed some light on the sources of metals to the sediments during the formation of the crusts. Table 2.14 shows the correlation matrix for the samples from all the cores described in the previous section.

Figure 2.23: Variation of calcite, cadmium, zinc, lead, magnesium, manganese, copper, nickel, iron and aluminium with depth in core SH1323B.

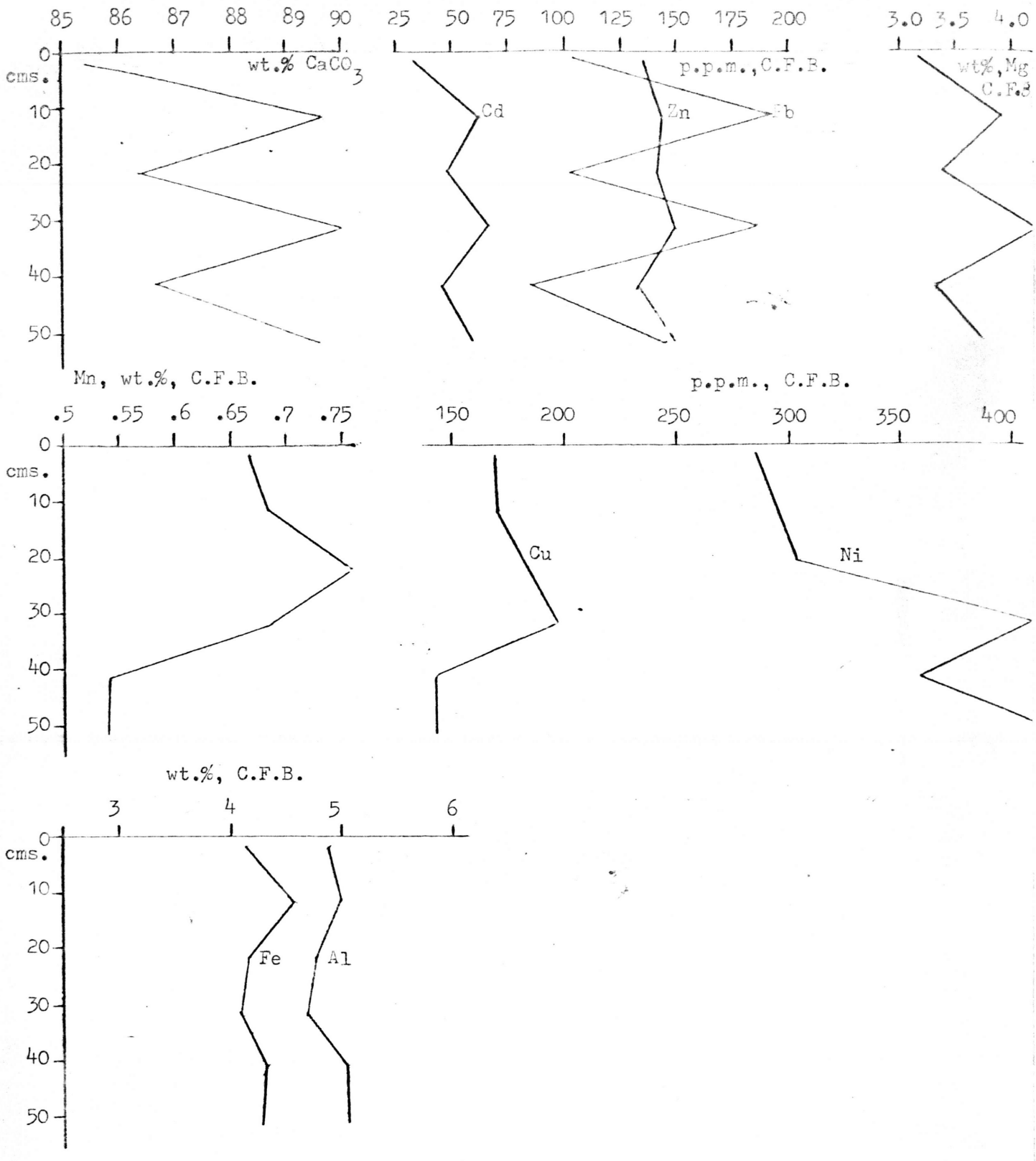

The elements associated with Ca in the biogenic fraction appear to be Pb and Cd, and some of the Co. Mg shows a weaker correlation with Mn, which may mean that some of it is associated with the hydrogenous manganese oxide fraction. Co shows a stronger correlation with Mn than with Ca. The data presented in Appendix 2 seem to suggest the analytical method is poor for Pb and Cd and Co because of the positive interference of Ca with these metals. Consequently the positive associations seen here between these metals and Ca may be analytical artefacts to some extent.

When the surface samples only were considered earlier, it was seen that Mn and Fe were associated together in the seamount samples, in the hydrogenous fraction. Elsewhere they had appeared to be segregated, with the iron in the detrital fraction. In the subsurface samples, some Fe still appears to be associated with Mn in the hydrogenous phase, but most of it is detrital, the correlation with Al being stronger than with Mn. Ni and Co are strongly correlated with Mn, and Zn shows small but significant correlations with the hydrogenous elements.

Cu is perhaps the most surprising element; in the surface samples from this area, it appeared to be present in the detrital phase, being correlated with Al, rather than Mn. Because of the small size of that data set, this could conceivably have been a statistical artefact. With the present, much larger, data set the correlation is maintained so it appears that in this area, most of the copper is detrital and not hydrogenous. This again

	Ca	Mn	Fe	Ni	Co	Ti	Al	Mg	Cu	Zn	Pb	Cd
Ca	1											
Mn	.097	1										
Fe	-.461	.475	1									
Ni	.218	.80	.396	1								
Co	.455	.601	.218	.627	1							
Ti	.208	.215	.298	.266	.732	1						
Al	-.737	-.001	.719	-.082	-.449	-.196	1					
Mg	.50	.354	-.001	.617	.671	.729	-.433	1				
Cu	-.454	.177	.553	-.018	-.352	-.093	.717	-.409	1			
Zn	.039	.327	.394	.477	.368	.715	.169	.471	.176	1		
Pb	.494	.297	.033	.471	.753	.775	-.451	.730	-.389	.627	1	
Cd	.560	.167	-.131	.296	.381	.113	-.485	.354	-.296	.042	.355	1

Table 2.14 Correlation matrix for the seamount-Somali Basin core samples.

n = 71 except for Ti, where n = 47.

n = 71: r =.195 at 95% confidence level n = 47: r = .242 at 95% confidence level
r =.274 at 99% confidence level r = .339 at 99% confidence level
(Fisher & Yates, 1964).

supports the observation of Colley et al., (1979), who found that a significant amount of Cu in the ferromanganese oxide crusts from this area appeared to be detrital rather than hydrogenous.

Summary

In general, the metals in the present suite of samples can be divided into three groups on the basis of their sources: biogenic, detrital, and hydrogenous.

The only metal which can confidently be identified as biogenic is Ca.

The detritally derived metals are Al, nearly always Fe, and usually Ti. The hydrogenously derived metals are Mn, Ni, and usually Cu. In elevated areas such as the Ridge crest, the Chagos-Laccadive Plateau, and the seamounts, Cu seems to be present mostly in the detrital phase(seamounts) or biogenic phase (Ridge crest and Chagos-Laccadive Plateau), rather than the hydrogenous phase (Rona Samples).

Of all of these groups of elements, it was thought that volcanic influences were present only in the Rona Samples at depth in the sediment column, near to the basalt basement. On the Ridge, where volcanic activity would be expected to be greatest, concentrations of metals which might be supplied by volcanism were higher in the non-crest sediments than in the crest sediments. This may, in part, reflect a paucity of samples from the crest area.

The division of the sedimentary components into biogenic, detrital and hydrogenous sources breaks down in the Arabian Basin, where the metals previously described as detrital and hydrogenous appear to be closely associated.

This is probably a characteristic of the Indus River input, which is the most important source of sediments to the Arabian Basin (Weser,1972). The cause of this association is likely to be detrital aluminosilicate material such as clays acting as the transporting agent for the hydrogenous oxides, which are probably present as coatings on this material.

CHAPTER 3

FERROMANGANESE OXIDE SPECIMEN DISTRIBUTION AND MORPHOLOGY

Introduction

A total of 45 ferromanganese oxide specimens from the N.W. Indian Ocean were examined during the course of this study. Most of them were obtained during a cruise of the R.R.S. Shackleton in 1975. Other samples were taken from two stations occupied by the R.R.S. Discovery in 1967. Some of the samples are from the Carlsberg Ridge area and the rest are from a group of seamounts north of the Seychelles. Figure 3.1 shows the station locations.

Two types of ferromanganese oxide material were studied.

a) Nodules

Carlsberg Ridge: D6273

Fragments of two small nodules from a dredge haul were obtained. These had previously been studied by Glasby(1970).

Seamounts: SH1323

A single spheroidal nodule, 1.5 cms in diameter was obtained from a calcareous sediment core and examined. Its position in the core is not known since it was found trapped in the catcher.

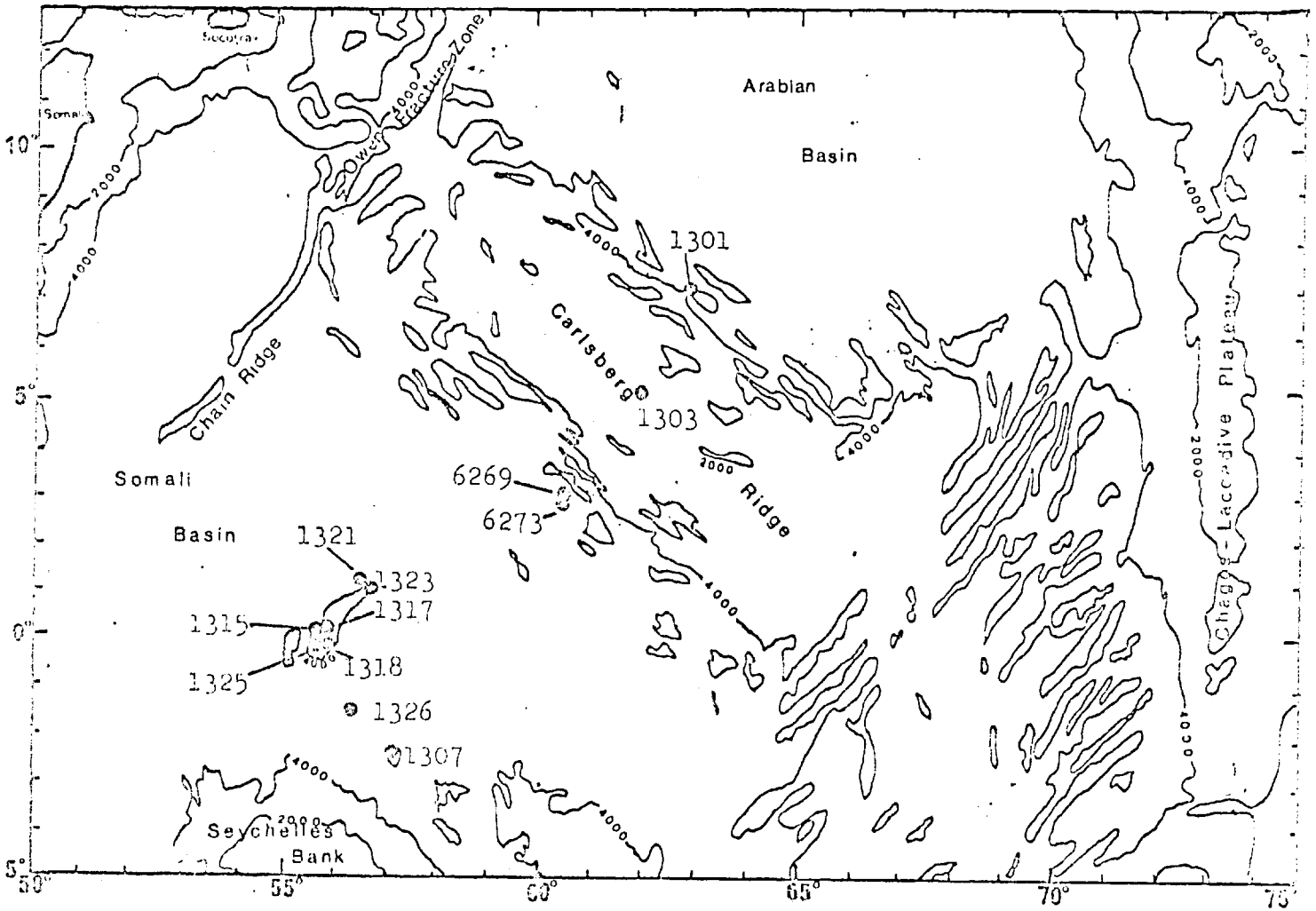

Figure 3.1: Map of the North West Indian Ocean showing the locations of the sampling stations.

East Pacific Rise : SH1564

A single tabular nodule 4.3 cms long was found on the surface of a calcareous sediment core from the station.

Bauer Deep : SH1578

A single spheroidal nodule 5.5 cms in diameter was found on the surface of a siliceous clay sediment core from this station.

S.W. Indian Ridge

A single pear-shaped nodule 4.5 cms. high was acquired from a dredge haul at station 45 of the OSIRIS cruise of the "Marion Dufesne".

b) Crusts

Crusts were obtained from all N.W. Indian Ocean stations except D6273. They were generally irregular and granular. Those from 1315, from the top of a seamount were smooth and polished. They varied in thickness from 2-3 mms. to 7 cms.. They were taken from a variety of localities and environments. Consequently they show a wide range of physical characteristics, described in detail below.

a) External form

The wide variations in texture and appearance noted in deposits from the N.W. Indian Ocean by previous workers (Glasby, 1970; Moorby, 1978) were also seen in the specimens studied in this work. Specimens from individual stations are described below in terms of size, shape, surface texture and type of substrate.

Station SH1301 $6^{o}52.3'$N. $62^{o}53.3'$E. 3645-4290m.

This was a dredge station on the lowest part of the northern flank of the Carlsberg Ridge. Two populations of

crust were obtained at this station. One population (Type A) was irregular with a micro-botryoidal surface and a very hard macro-granular(bubbly) surface. Below about 5-6 mms, the crusts were very soft and easily drilled and crushed. These crusts were generally no thicker than 35-40 mms. The other population (Type B), also irregular in shape, had a much smoother and much more even surface, with a micro-granular texture. They had a constant hardness, being fairly soft and easy to sample throughout their thickness. These were generally greater than 40mms.thick. None of the specimens from either population were attached to substrates on retrieval.

Station SH 1303 5°00.2'N, 61°32'E, 2930-2945m.

Two crusts were obtained from this dredge haul on the Ridge crest. Both were granular, irregular, fairly soft, and about 5mms. thick. One of the crusts had a substrate which contained calcite and clay minerals.

Station SH 1307. 2°35.1'S. 57°16E. 3155-3710m

This station was on the flank of a seamount in the Somali Basin. Again, two types of crust were obtained. Type 1 was friable, microgranular, flat, and up to 70mms thick, with no substrate attached. Type 2 was much harder, with a microgranular texture, locally smooth, and adhering to basalt substrates with a well-developed palagonite rind. These were generally thinner, about 20-25 mms thick. Angular basalt fragments were also obtained, with only a veneer of oxide coating.

Station SH 1315 0°15.5'S. 55°41'E. 1200m-1330m.

This station was also located on a seamount. Two

smooth, polished crusts were obtained, both of which were flat. They were both 8 mms thick and attached to an altered volcanic rock substrate.

Station SH1317 0°14 N. 55°34.5'E. 2179-2450m.

This was a dredge station close to SH1315. The four crusts examined were irregular and botryoidal. Traces of volcanic substrate were seen on two of the crusts examined; all of the crusts studied were about 25-30 mms thick, and consisted of three distinct layers. The top and bottom layers (each about 8 mms thick) were similar, being quite hard and black, with a shiny fracture surface. Between these layers was a very soft, brown dull layer. This seemed to have a flat interface with the bottom layer, and a botryoidal interface with the top layer.

Station SH1318 0°11.5N. 55°36'E. 1214-1637m.

Four specimens were obtained in this dredge from near the top of a seamount. All of them were crusts up to 7mms. thick, on limestone rocks, some of which appeared altered.

Station SH1321 1°19.2'N. 50°35.6'E. 1600-2180m.

The specimens examined from this dredge haul were botryoidal and microgranular. Two were attached to substrates of a greenish-grey, clay-like material. Two others(without substrates) had hard and shiny surfaces, and dull oxide material at the bottom. All the crusts were between 10 and 25 mms. thick.

Station SH1323 1°20.9'N. 56°36.4'E. 2800-3000m.

The crusts from this station were botryoidal and granular, and tended to be very friable. A granular spheroidal nodule was obtained from a gravity core close by.

Station SH1325 0°8.7'N. 55°9.9'E. 1400-2100m.

This station was near the top of a seamount and several crusts were obtained. They tended to be irregular and granular, but a few were smooth and some were botryoidal. They were quite soft and easily drilled and crushed.

Station SH1326 1°14'N. 56°2'E. 3530m-4480m.

Only one specimen was acquired at this dredge station in the Somali Basin, north of the Seychelles. It was 25mms thick, with a vesiculated structure and a granular surface. No substrate was obtained.

The other two stations from which material was obtained were on the southern flank of the Carlsberg Ridge.

Station D6269 2°56.5'N. 60°2.8'E 3926-4259m.

The only specimen examined from this station was a medium-hard, botryoidal, granular crust around a large, basalt boulder. This varied in thickness from about 30mms at the "equator", (above which there was no sediment adhering to the crust), to 15 mms. on the top to 10mms on the bottom.

Station D6273 2°54.9'N. 60°3.5'E. 3895-4890m.

No crusts from this station were examined in this work. Fragments of two small soft, granular nodules were studied, however.

Two nodules were also studied from the East Pacific, and one from the S.W.Indian Ocean.

SH1564 11°29.2'S, 87°57.9'W. 4107m.

A tabular oblate nodule, 4.3cms x 3.3 cms x 1.7cms was taken from the top of a sediment core from the East Pacific Rise. It had a sub-botryoidal surface form, and a granular texture. It had no core visible.

SH1578 9°59.7'S, 101°49.3'W. 4546m.

This nodule was taken from the top of a sediment core from the Bauer Deep. It was 5.5 cms. wide by 3.4 cms.high, a slightly flattened sphere with a regular surface form and a granular texture. It had no core visible.

Station 45, "OSIRIS" 29°54'S, 61°56'E. 4400m.

This nodule was kindly supplied by Mlle.C.Lalou of C.N.R.S. and is known in this work as the Lalou nodule. It was pear-shaped and slightly flattened on the top and bottom, with dimensions of 4.5 cms. high x 3-5 cms. wide. The core appeared to be a crystal of silicate material. This station was located on the southwest branch of the Indian Ocean ridge system.

Station SH1370 12°30'S. 60°54'E. 3620m

Two crusts, 1370A and 1370B, were kindly donated by Dr.Roy Chester,from this dredge station located near the Vema Trench. 1370A was a flat crust, 10 mms. thick, with a microgranular surface texture. 1370B had an irregular, microbotryoidal surface, and varied from 12 to 18 mms thick. It also had a microgranular surface texture.

Discussion

A total of 45 ferromanganese oxide specimens from the N.W. Indian Ocean were examined during the course of this study. The specimen sites are plotted in figure 3.1. The specimens came from a wide range of bottom environments and show a wide range of physical characteristics.

Many authors (Cronan & Tooms, 1969; Crerar & Barnes, 1974; Calvert & Price, 1977) have suggested that variations in the bottom environment may cause variations in the

chemical and mineralogical composition of marine ferromanganese oxide deposits. Few authors have investigated the role of environmental factors in controlling the morphology of these deposits, although such a study has been carried out, with some success, in a freshwater lake (Sozanski & Cronan,1976). Goodell et al.,(1970), working on samples from the South Pacific and Atlantic Oceans recognised four different morphological types of concretion on the basis of type of nucleii, thickness of deposit, and external shape. They suggested that morphology was dependent on the nature and proximity of element source and the rate of accretion. It seems likely (Cronan 1976) that the shape and nature of the nucleus is also an important factor in determining the shape of nodules, particularly when the overlying oxide layers are thin.

Compared to the amount of work published on the internal features of nodules, very little attention has been paid to external features. This is surprising, since, if as suggested by Goodell et al.,(1970), the morphology is partly controlled by element source, it may in turn reflect compositional trends. In discussing the specimens analysed in this investigation, three major parameters were recognised : thickness, shape and surface texture.

Thickness

It has been noted by earlier workers (Muir & Tilley, 1964; Aumento, 1969) that ferromanganese oxide crusts generally appear to thicken with increasing distance from a ridge crest. This suggests that ferromanganese oxide deposition is initiated on new sea floor at the ridge crest

and continues as the encrustation moves away from the crest due to sea floor spreading. Some of the thickest crusts found (70 mms thick) were indeed at the location furthest from the ridge crest (type 1 crusts at 1307), but so also were some of the thinnest. Evidently, some process other than that of the simple model outlined above must be operating. This suggestion is supported by the observation that there is no correlation between crust thickness and distance from the Carlsberg Ridge. This implies that some crusts grew more slowly, or they were deposited at the same rate, with periods of zero or negative growth (erosion). A third alternative is that for any given distance from the Ridge, some substrates have been exposed to favourable conditions for ferromanganese oxide deposition for much longer periods than other substrates at the same distance from the Ridge. This is probably a result of submarine erosional processes which, in the rugged environment under consideration, will continually produce new fragments of basalt about which accretion can take place.

Shape

Where substrates were attached to the specimens, it was clear that the crust followed the shape of the substrate. Where the crusts were thin (e.g. at 1303, 1318, 1325, some fragments from 1307), and the substrate irregular, then the crust was also irregular. With thicker crusts, such irregularities tended to become smooth, for example at 1323 and 6269. On some specimens where no substrate was attached, there was usually evidence, such as traces of palagonite on the crust bottoms, that the crusts had grown on a

substrate and the dredge had pulled them off. This was seen with type 1 crusts from 1307, both types of crust from 1301, and two crusts from 1317. Some crusts were found that had grown on sediment(1303), where the sediment substrate surface was quite flat, and the crust surface was distinctly botryoidal. Other specimens were also found which had begun as flat crusts on a flat surface but which had developed a botryoidal surface as they grew thicker, e.g. 1317, two crusts from 1321, 1323 and 1325. There is no evidence to suggest why these crusts had departed from a regular surface as they had grown progressively thicker.

Texture of surface

The surface textures of the nodules and encrustations examined varied from smooth and polished to coarsely granular. Raab(1972) noted that in Pacific Ocean nodules, a granular surface texture tends to develop on that part of the nodule which is in contact with the sediment whilst the upper parts of nodules, which are in direct contact with seawater tend to have a smooth surface. On this basis, a granular surface texture on ferromanganese nodules suggests their growth is by element precipitation from interstitial pore waters at or very near the sediment-water interface. A smooth surface texture, on the other hand indicates accretion by direct precipitation from sea water(Calvert, quoted by Moorby, 1978). Of the nodules studied, four were spheroidal and granular all over and one was oblate and granular all over. The East Pacific nodules were known to come from the tops of cores i.e. they were resting on the sediment surface. The orientation of the others is not

known (1323,6273). If Calvert's suggestion (op.cit.) is true then it is difficult to visualise how these nodules could have accreted all over from the sediment when only a maximum of about half of the nodule is in contact with the sediment. Sorem et al., (1979) have postulated the existence of a "boundary layer" at the sediment-water interface. They visualise the first part of a nodule's depositional history as taking place while totally immersed in this boundary layer. Only as it becomes larger does it become anchored to the sediment proper. It is at this point that Sorem et al.,(op. cit.) suggest that asymmetric growth starts. If this theory is correct then the homogeneous appearance of the outside of the nodules from 1564 and 1578 could be accounted for by postulating that they had grown while completely immersed in this boundary layer.

In this investigation, many encrustations were examined which had a granular surface texture, yet these deposits must, by their very nature, have accreted by direct precipitation from seawater. The nature of the surface texture does not therefore appear to be a reliable guide to the way in which the encrustations accreted. In any event, whatever the original nature of the surface texture of a sample, it may be altered by subsequent changes in the bottom environment. Moorby (1978) has produced evidence in support of this by finding depressions in the surface of some nodules where a granular texture occurs, whilst the rest of the nodule surface is smooth and polished. He suggests that the whole surface of the deposit was originally granular but that strong bottom

currents, perhaps operating when conditions were otherwise unfavourable for nodule growth, have subsequently physically eroded the nodules surfaces. This process may be affected by the abrasive action of the suspended sediment load in the bottom current. It is interesting to note that samples from areas of strong bottom current activity, near the top of seamounts, tend to have smoothed surfaces (1315, type 2 crusts from 1307, two crusts from 1321).

Other work on the surface texture of ferromanganese oxide deposits has been done by Heye(1975) who, in a detailed study of Pacific Ocean nodule structures and growth rates, reached the conclusion that rough granular outer surfaces on nodules indicated accretion under favourable circumstances. Smooth surfaces were formed as a result of growth under unfavourable circumstances. This is in accord with the suggestion above, concerning the present specimens, that smooth surfaces are produced under unfavourable depositional (in fact, possibly erosional) circumstances.

Heye & Marchig (1977) reached the conclusion that the granular layers within nodules are rapidly accreted layers. They found that these layers were enriched in Mn, Ni, and Cu, and that more massive internal layers, those which produced a smooth surface texture tended to be depleted in these metals. They thought that these layers accreted more slowly. If these theories are correct then the Cu-Ni rich nodules in the Pacific and Indian Oceans are likely to have grown relatively quickly, unless growth has consisted of short bursts of rapid growth interspersed with long periods of no growth. Several workers, however, (Ku & Broecker,1969;

Tooms et al.,1969; Bhat et al.,1973; Anderson, 1978) have shown that pelagic nodules appear to grow very slowly. The surface texture of ferromanganese oxide deposits and its implication in nodule and encrustation genesis must therefore be regarded as another unsolved problem of marine ferromanganese oxide deposits.

Conclusions

One of the main objectives of the investigation was to assess the influence of volcanic activity on the genesis of ferromanganese oxide deposits in the deep ocean. No definite trends in thickness, shape or surface texture have been observed that could be attributed to regional volcanic influences. The crusts most likely to show volcanic influences (those at station 1303 from the Ridge crest) were similar in texture and shape to many crusts from elsewhere, both from the Ridge and the seamounts. The presence of two distinct populations of crusts in two dredge hauls from stations 1301 and 1307, indicates that crust morphology and texture are probably controlled by local conditions such as bottom current activity, and suspended sediment load. The latter are likely to smooth and scour crust surfaces, eroding a granular surface to produce a smooth surface. The presence of crusts which are granular over part of their surface, and smooth in others (type 2 crusts from 1307) indicates how variable, on a scale of a few cms. bottom currents and suspended sediment loads may be.

CHAPTER 4

MINERALOGY

Introduction

Great confusion exists in the literature on ferromanganese oxide deposits over the nomenclature of the constituent manganese and iron oxide phases. This is attributable directly to the minute grain sizes of some of the phases. Attempts have been made to correlate nodule and crust phases with terrestrial minerals on the one hand, and with products of laboratory synthesis on the other. As a result, at least three classification schemes exist on ferromanganese oxide deposits, leading to ambiguities between variously named species. Burns & Burns(1977) have reviewed this controversy in detail, and it is unnecessary to repeat a review of it here. However, their recommendations concerning nomenclature are accepted here. The name "δ-MnO_2" is used for the phase in these deposits giving rise to X-ray diffractions around 2.4-2.45 Å, and 1.42 Å. The name todorokite is used for the mineral giving rise to reflections at about 9.6 Å and 4.8 Å as well as 2.4 Å and 1.42 Å. Table 4.1 gives the detailed X-ray powder pattern data used for identifying the minerals.

Many authors believe the iron phases play a vital role

Table 4.1

X-ray diffraction data of the manganese minerals recognised in the North West Indian Ocean samples.

Todorokite		δMnO_2	
d, Å	I%	d, Å	I.
9.59-9.65	100		
6.98-7.2	15		
4.76-4.81	80		
4.42-4.45	10		
3.4	5		
3.19-3.20	30		
3.10-3.11	10		
2.45-2.46	25	2.43	broad,medium
2.39-2.4	45		
2.33-2.36	15		
2.21-2.23	30		
2.13-2.16	10		
1.42-1.43	30	1.41	broad,weak
1.38-1.40	15		

in the nucleation and authigenesis of marine ferromanganese oxides (e.g. Burns & Brown, 1972; Burns & Burns 1977). However, little is known about the iron compounds present in these oxides, mainly because the iron appears to be present largely as X-ray amorphous material.

Moorby(1978) has reviewed the occurrence of iron compounds in ferromanganese oxide deposits and has come to the conclusion that there are three possible sites for the iron in these oxides.

1. Within the lattices of the manganese phases, substituting for Mn ions.

2. As an unidentified random mixed-layer iron-manganese oxide.

3. As a discrete iron phase:

a) of sufficiently large particle size and sufficiently well-ordered structure as to be identifiable by X-ray diffraction techniques.

b) of very small particle size and/or disordered structure, and thus essentially amorphous.

Of these, only those phases of type 3(a) are likely to be amenable to the standard X-ray diffraction methods used with the present samples. Of the various iron minerals listed in the literature as being found in marine ferromanganese oxide deposits, only goethite was identified in the samples analysed in this investigation. Table 4.2 gives the X-ray diffraction data for goethite. In samples where no goethite peaks were observed, the iron phase or phases were regarded as being amorphous.

Table 4.2

X-ray diffraction data for goethite.

d, Å	I
4.98	10
4.18	100
3.38	10
2.69	30
2.49	16
2.45	25
2.25	10
2.19	20
1.72	20
1.69	10
1.56	16
1.51	10
1.45	10

Mineralogy of the ferromanganese phases of the North West Indian Ocean samples.

All the samples analysed chemically during this study were also subjected to mineralogical investigation by X-ray diffraction techniques using a Phillips diffractometer. Details of the method are given in Appendix 3, and typical traces are shown in Addendum 2.

Mineralogy of the Manganese phases.

(a) Todorokite

Twelve of the 114 oxide samples analysed contained todorokite in discernible amounts. Nine of these were from specimens from station 1301 where it was present in the top 7 or 8 mm. of several crusts. Two more samples were from station 1321 where it was found on the bottom of two crusts. The last sample was found on the bottom of a crust from station 1317.

(b) Birnessite

The diagnostic line for this mineral is a strong reflection at 7.2 to 7.3Å. No samples containing this reflection were found.

(c) δ-MnO_2

This was the most common manganese mineral present. It was found in all samples from all stations, and in 102 of the 114 samples, it was the only identifiable manganese mineral.

Mineralogy of the iron phases

Goethite was the only iron mineral found. It was identified beyond any reasonable doubt in only one sample, from station 1301. This was a flat crust fragment with no visible difference between top and bottom: it was crushed

and analysed whole. All other samples exhibited no lines attributable to a discrete iron phase. The iron compounds in these samples were therefore regarded as amorphous.

Other minerals

Burns & Burns (1977) have reviewed the occurrence of accessory minerals in ferromanganese oxide deposits. Quartz, felspar, hornblende, zeolites and montmorillonite appear to have been reported most frequently.

In the present suite of samples, quartz is the most common accessory mineral, and appears in all but a very few samples. Feldspars occur in the middle layers of the specimens from 1317. Also in these layers, the broad unresolved hump between 4½ and 3Å of volcanic glass was seen. Calcite was found in small amounts in a few samples.

Discussion

The occurrence and distribution of todorokite in the present suite of samples requires some comment. Of the crusts examined from 1321 (four crusts) and 1317 (three crusts), three contained todorokite on the bottom, but δ-MnO_2 at the top. Clearly a change in the bottom environment had occurred and this is reflected in the change of mineralogy of the ferromanganese oxides being deposited. Since δ-MnO_2 is in a more oxidised state than todorokite, then perhaps the change in mineralogy is explained by the bottom environment becoming more oxidising with time.

A change in the redox potential of the bottom environment also seems to have occurred at station 1301, where several crusts have todorokite in the top layers, but not in the bottom. This may have been caused by the bottom

environment becoming more reducing in nature perhaps due to sediment covering the site.

If a change in the redox potential of the bottom environment is indeed the cause of these changes in the mineral composition of the ferromanganese oxides which are being formed, then the changes must be very local: the rest of the crusts from 1321 and 1317, and those from stations nearby (1315, 1318, 1325 and 1323) contain no detectable todorokite, and at 1301, only some of the crusts in the dredge haul contained todorokite.

Influence of mineralogy on minor element composition.

Twelve specimens were taken from station 1301, and from these, 43 samples were obtained. Nine samples containing todorokite and δ-MnO_2 (group 1) and eleven samples containing δ-MnO_2 and no todorokite (group 2) were extracted from five of the specimens. The remaining 23 samples from the other seven specimens contained only δ-MnO_2 (group 3). Table 4.3 shows the average composition for the three sample groups. The variations of metal content with mineralogy are described below and discussed.

Nickel and copper

Todorokite is known to contain about 8 wt.% Mn^{2+} (Levinson, 1960; Frondell et al., 1960; Straczek et al., 1960). Since atomic substitution of Mn^{2+} by Ni^{2+} and Cu^{2+} occurs in the todorokite structure (Burns & Burns, 1978a), the upper limit of (Ni+Cu) concentrations in todorokite-bearing deposits is likely to be approximately 8 wt. %. This is probably why group 1 samples are Cu and Ni-enriched compared to groups 2 and 3. Electron probe

Table 4.3 Variation of chemical composition with mineralogy

	Fe%	Mn%	Mn/Fe	Co ppm.	Pb ppm.	Ni ppm.	Cu ppm.	Zn ppm.	Al%	Ti ppm.	Ca%
Todorokite group 1	13.8	22.77	1.65	2095	734	4509	2181	637	1.75	4007	1.13
δ-MnO_2 group 2	22.59	10.92	.48	1902	1165	2007	1077	669	1.77	5582	1.26
δ-MnO_2 group 3	19.92	14.74	.74	1904	964	1931	700	485	1.55	5253	1.85

	Mg %	Cd,ppm.	Li, ppm.
Todorokite group 1	1.76	6	33
δ-MnO_2 group 2	1.11	5	9
δ-MnO_2 group 3	1.07	5	7

The nominal compositions of todorokite and δMnO_2 are as follows (Burns & Burns, 1977):

Todorokite: $(Na, Ca, K, Ba, Mn^{2+})_2Mn_5O_{12} \cdot 3H_2O$

δMnO_2: MnO_2

analysis (Chapter 6) of a todorokite-bearing crust from station 1301 indicates that such crusts have much less than 8 wt.% (Ni + Cu) and are therefore undersaturated with respect to Ni and Cu..

Cobalt and Lead

It can be seen from Table 4.3 that changes in mineralogy appear to have little effect on the cobalt content of the sample. The level of Co seems to be maintained irrespective of the mineralogy of the host phase.

On the Ridge, the main route of Pb into the deposits is with the iron oxides (Chapter 5). Since the Fe content in todorokite-bearing samples is lower than in δ-MnO_2-bearing samples, then the lead content is also lower. Pb follows Fe proportionately: between groups 1 and 2, the Fe content drops by 39% and the Pb content drops by 37%.

Zinc

Zinc is more abundant in the specimens comprising groups 1 and 2 than in specimens comprising group 3. There is no significant difference between the Zn levels in the todorokite-containing samples (group 1) and the δMnO_2-containing samples(group 2). This is surprising since Zn^{2+} has an ionic radius close to that of Mn^{2+} and might be expected to substitute for it (Moorby, 1978), and give rise to higher Zn levels in the todorokite-containing samples.

Cadmium

The mineralogy appears to exert little influence over the amount of Cd in the deposits. Since the Cd^{2+} ion is quite large, then perhaps it is equally unfavourable to fit into both the todorokite lattice and the δ-MnO_2 lattice.

Lithium

The todorokite-containing samples contain more Li than the δ-MnO_2-containing samples. This excess lithium

appears to be associated with the oxide fraction of the samples (page 144). Lithiophorite has the formula (Al, Li) $MnO_2(OH)_2$ (Wadsley, 1952). This contains about 3 wt. % Li. This mineral would therefore only have to be present at the 0.1% level to account for the Li-excess in the todorokite-containing samples. An alternative possibility arises out of the uncertainty concerning the structure of todorokite. Wadsley, (1964), suggests that todorokite may be related to the tunnel structure of hollandite and psilomelane. These tunnels are known to accommodate large Group I and Group II cations (Na,K,Ba), (Burns & Burns, 1977), so small quantities of Li may also be accommodated here.

Titanium

Since Ti is correlated with Fe (Chapter 5), then todorokite-containing samples (group 1), which have less Fe than δ-MnO_2-containing samples (Groups 2 and 3), also have less Ti than δ-MnO_2-containing samples. While the Fe content drops by 39% from group 1 to group 2, the Ti content drops by 28%. This suggests that some of the Ti is not associated with the iron. Perhaps some of the Ti is in a phase other than the authigenic oxides; this portion of the Ti would be unaffected by a change in oxide mineralogy.

Calcium

The mineralogy of the host phase seems to have little effect on the Ca content of the samples. The Ca content of group 3 is much higher than in group 2, despite the fact that they contain ostensibly the same oxide mineral. Since a depth dependence for the Ca content of the deposits is seen (Chapter 5), then perhaps the specimens constituting group 3 are from a shallower depth than those constituting groups 1 and 2. Since all the specimens considered here were from one

dredge station (1301), the depths of individual specimens are not known.

Magnesium

Magnesium is clearly enriched in group 1 samples compared with groups 2 and 3. Calvert & Price, (1977), also found higher levels of Mg in nodules where todorokite was the dominant mineral phase. The Mg content is higher in todorokite-bearing specimens perhaps because the todorokite crystal structure may be more favourable to the uptake of magnesium than is the structure of δ-MnO_2.

Summary

In the suite of samples under investigation, two manganese minerals have been identified. These are δ-MnO_2, present in all samples, and todorokite, present in 12 samples. The todorokite occurs in the bottom of three crusts from the seamounts, and in the top layers of five crusts from 1301 on the Ridge flank.

One iron oxide mineral was found in the samples, goethite. This was found in a specimen from 1301 (not associated with todorokite). The iron phases in all other samples are regarded as amorphous.

Nickel, copper, lithium and magnesium are concentrated in todorokite-containing samples. Cobalt is not significantly enriched in any sample group, while lead, titanium and calcium are more abundant in δ-MnO_2-only samples. Cadmium and zinc seem to be equally abundant in specimens containing both todorokite and δ-MnO_2. They appear to vary independently of mineralogy in the present sample suite.

CHAPTER 5

BULK GEOCHEMISTRY OF FERROMANGANESE OXIDE DEPOSITS.

Introduction

During the course of the present study, 114 samples of ferromanganese oxide material were obtained from 45 specimens taken from the Carlsberg Ridge and adjacent seamounts. Seventeen specimens were taken from the Carlsberg Ridge and 28 from the seamounts. They were analysed for Mn, Fe, Co, Ni, Pb, Cu, Zn, Al, Ti, Ca, Mg, Cd and some for Li. The analyses were all carried out by atomic absorption spectrophotometry. Details of the techniques used and the precisions and accuracies obtained are given in Appendix 1. The data are tabulated in Addendum Ib.

The material studied consisted of three nodules, one from station 1323, and two from station 6273, and 42 crusts. The nodule from 1323 was sawn in half; one half was kept, and the other was ground for analysis. The nodules from 6273 were easily split by hand. This facilitated layer sampling, which was carried out. The crusts varied in thickness from less than 2mm., for example, on some fragments of basalt from 1307, to several centimetres

at stations 1301 and 1307. Samples were drilled out at points of varying depth within the specimens using a hand-drill with a 2 mm. stainless steel bit. Analysis of such a bit has shown that no serious contamination problems should arise from this procedure. Where substrates were attached to the crusts, these were sampled also.

Data processing

Fifty seven samples were obtained from the seamount specimen set and 57 from the Ridge specimens. The data from these two areas were prepared separately, to facilitate a comparison of the two groups. By performing such a comparison, it was hoped that it might be possible to distinguish volcanic influences present in a tectonically active area such as the Carlsberg Ridge, from non-volcanic influences present in a volcanically quiet area such as the seamounts.

The statistical treatment of the data was performed on C.D.C. computers in the Imperial College Computer Centre. The programme used was written by Earle (unpublished Ph.D Thesis, in preparation), and designed to operate interactively. The arithmetic and log. means, standard deviation, skewness and kurtosis of each element were calculated and correlation matrices were computed using log. and arithmetic data.

Tables 5.1 and 5.2 show the skewness of the elements in the two data sets. Some elements tend towards log. normal distributions and some towards normal distributions. Correlation matrices for both log. transformed and untransformed data are presented in tables 5.3 and 5.4. Log. data are to the right of the diagonal. Little difference is

is found in significant correlations. Those which are significant in one set are significant in the other. Table 5.5 shows the values of the correlation coefficients which are significant at the 95% and 99% confidence levels.

Moorby (1978) has discussed the problems of the production and use of correlation matrices made from manganese nodule data. Chayes (1960) has described the problems of correlating variables of constant sum. The problems arising from a "closed system" (the total element concentration must sum to 100%) can be ignored when correlations between variables whose contribution to the total variance of the data set is small (Chayes, 1960). The elements Cu, Zn, Ni, Co, Pb, Ti, Cd, and Li fall into this category. Al, Ca and Mg have higher concentrations and comparisons involving these elements may not be so secure. Fe and Mn are major elements and there should always be a negative correlation between them. This negative correlation is observed in both data sets. Correlation with variables which are not part of the closed system are not subject to the drawbacks imposed by it. (Chayes, 1960). In this context, the only variable not part of the closed system is depth.

Iron, manganese and aluminium

Iron and manganese, metals associated with the authigenic oxide minerals, will probably show negative correlations with Al, which is associated with detrital minerals. In the Ridge samples, Mn and Al show a negative correlation, significant at the 95% but not the 99% confidence level. When the data are plotted, the scatter is broad,

Table 5.1

Skewness of each element distribution in the Ridge sample set.

Element	Untransformed data	Log-transformed data
Fe	-.885	-1.478
Mn	.307	- .188
Co	1.206	- .114
Pb	-.896	-1.50
Ni	1.673	.826
Cu	.851	- .194
Zn	.684	.034
Al	1.249	- .80
Ti	.799	- .068
Ca	1.819	.516
Mg	1.566	1.307
Cd	1.04	.096
Li	1.08	.370

Table 5.2

Skewness of each element distribution in the seamount sample set.

Element	Untransformed data	Log-transformed data
Fe	.774	.158
Mn	-.587	-1.382
Co	1.462	.587
Pb	.391	-.422
Ni	2.463	.701
Cu	2.037	.238
Zn	2.056	1.243
Al	.923	-.219
Ti	1.415	.969
Ca	3.232	1.94
Mg	2.926	2.25
Cd	.518	-.936
Li	1.80	-.037

	Fe	Mn	Co	Pb	Ni	Cu	Zn	Al	Ti	Ca	Mg	Cd	Li	Mn/Fe
Fe	1	-.707	.202	.758	-.703	-.622	-.107	-.236	.424	.199	-.765	-.072	-.776	-.919
Mn	-.766	1	.110	-.444	.709	.332	.054	-.301	-.323	-.038	.590	.379	.608	.929
Co	.163	.08	1	.382	.040	-.06	.025	-.090	.416	-.083	.143	.135	-.017	-.045
Pb	.724	-.528	.352	1	-.345	-.343	.173	-.258	.617	.219	-.632	-.010	-.49	-.643
Ni	-.699	.697	.023	-.366	1	.785	.584	.156	-.127	-.304	.731	.337	.886	.764
Cu	-.722	.568	-.068	-.418	.883	1	.575	.570	-.17	-.521	.736	.051	.859	.511
Zn	-.100	.098	.008	.169	.643	.617	1	.128	.037	-.447	.308	.201	.514	.088
Al	-.212	-.28	-.104	-.281	.089	.315	.027	1	.055	-.257	.365	.226	.366	-.044
Ti	.238	-.298	.517	.517	-.102	-.221	.005	.061	1	.308	-.448	.068	-.24	-.394
Ca	.092	-.109	-.063	.100	-.244	-.419	-.402	-.069	.232	1	-.515	-.03	-.369	-.124
Mg	-.742	.678	.158	-.625	.655	.774	.267	.265	-.378	-.414	1	.098	.812	.720
Cd	-.078	.331	.124	-.07	.384	.181	.260	-.227	.036	-.039	.059	1	.227	.247
Li	-.816	.753	.003	-.540	.875	.885	.456	.186	-.243	-.294	.819	.259	1	.733
Mn/Fe	-.913	.879	-.08	-.693	.676	.699	.121	-.007	-.378	-.216	.808	.15	.217	1

Table 5.3

Correlation matrix for the Ridge sample set.

Arithmetic data are to the left, log. data are to the right of the diagonal.

	Fe	Mn	Co	Pb	Ni	Cu	Zn	Al	Ti	Ca	Mg	Cd	Li	Mn/Fe	Depth
Fe	1	-.527	-.458	-.037	-.695	-.097	-.015	.172	.235	-.422	-.368	-.361	-.28	-.759	.583
Mn	-.591	1	.588	.394	.725	-.007	.224	-.658	.397	.171	.145	.564	-.28	.953	-.352
Co	-.492	.619	1	.748	.491	.435	-.015	-.655	.046	.429	.191	.352	-.158	.612	-.619
Pb	-.104	.470	.767	1	.295	-.476	.227	-.651	-.186	.103	.087	.143	-.302	.313	-.756
Ni	-.587	.610	.320	.210	1	.205	.495	-.313	.245	.14	.702	.544	.33	.802	-.604
Cu	-.22	-.011	-.359	-.453	.404	1	.196	.633	.126	-.541	.412	.171	.603	.029	.651
Zn	-.066	.247	-087	.114	.708	.358	1	-.091	.368	-.245	.647	.307	.302	.178	-.213
Al	.024	-.717	-.565	-.609	-.191	.452	-.116	1	.359	-.357	.163	-.227	.67	-.565	.541
Ti	.218	-.344	.006	-.202	-.232	.099	-.332	-.299	1	.082	.019	.285	.183	-.395	.350
Ca	-.367	.059	.465	.150	-.010	-.342	-.236	-.027	.192	1	.162	.059	.221	.281	-.526
Mg	-.325	.214	.139	.052	-.862	.561	.753	.081	-.053	-.128	1	.420	.683	.243	-.386
Cd	-.394	.514	.316	.152	.558	.201	.389	-.286	-.302	-.133	.479	1	.194	.568	-.295
Li	-.375	-.031	-.088	-.203	.729	.626	.626	.437	.016	-.045	.862	.401	1	-.128	.182
Mn/Fe	.771	.933	.704	.473	.715	.063	.243	-.555	-.326	.152	.369	.542	.190	1	-.491
Depth	.492	-.338	-.55	-.751	-.561	.536	.279	.375	.42	-.472	-.355	-.303	-.005	-.503	1

Table 5.4 Correlation matrix for the seamount sample set.

Arithmetic data are to the left, log. data to the right of the diagonal.

Table 5.5

Values of correlation coefficients which are significant at the 95% and 99% confidence levels. (From Fisher and Yates, 1964).

No. of samples used in matrix, seamount samples.	95%	99%
22 (Depth)	.36	.492
42 (Li)	.257	.357
46 (Cd)	.243	.338
47 (Mg,Ti)	.24	.33
57	.211	.295
No of samples used in matrix, Ridge samples.		
49 (Li)	.231	.322
53 (Cd, Mg, Ti)	.220	.31
57	.21	.295

and the overall relationship is poor (fig.5.1). If the todorokite-containing samples from the station 1301 are omitted, with their high Mn content, then the negative correlation is much clearer. In the seamount sample group, the correlation between Mn and Al is much more strongly negative (Fig.5.2.).

Fe and Al are not negatively correlated: neither in the Ridge samples nor the seamount samples does a clear correlation emerge between these two elements. When the two sample groups are combined, it appears that Fe and Al vary independently of each other. (Fig.5.3.). It might be expected that these two elements would be negatively correlated in a set of ferromanganese oxide analyses because they are major contributors to the data array (Chayes,1960). The inference therefore is that there is a process working to counteract the expected negative correlation. Since Fe is associated with the authigenic minerals and Al with the detrital minerals, then perhaps some Fe is associated with the detrital minerals or some of the Al occurs in authigenic minerals. A contribution of iron to the samples from detrital minerals is unlikely since there are no peaks in the X-ray diffractograms of Fe-containing detrital minerals such as Fe-rich clays. Authigenically-derived aluminium is possible, for example in zeolites, but again, there are no signs of such minerals in X-ray diffractograms of the samples. An alternative possibility is that iron is being incorporated into the encrustation as oxide coatings on clay particles (Carroll, 1958; Fordham, 1970 ; Aston & Chester, 1973).

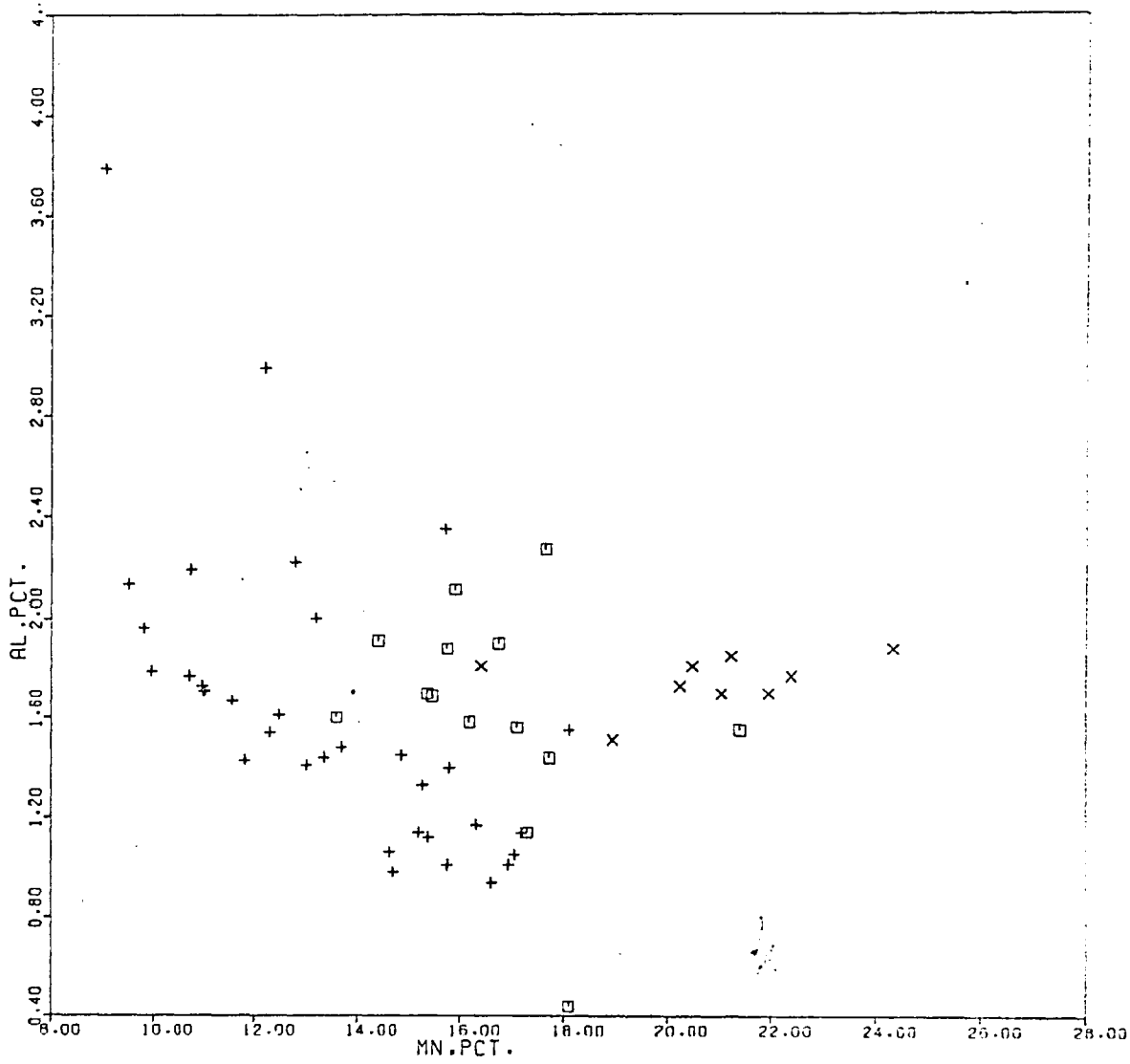

Figure 5.1 Plot of manganese vs. aluminium, Ridge samples.

GROUP	SYMBOL	NO. OBS.	R
ALL	-	57	-0.28
TODOROKITE	X	9	0.33
1301	+	34	-0.63
REST	⊡	14	-0.30

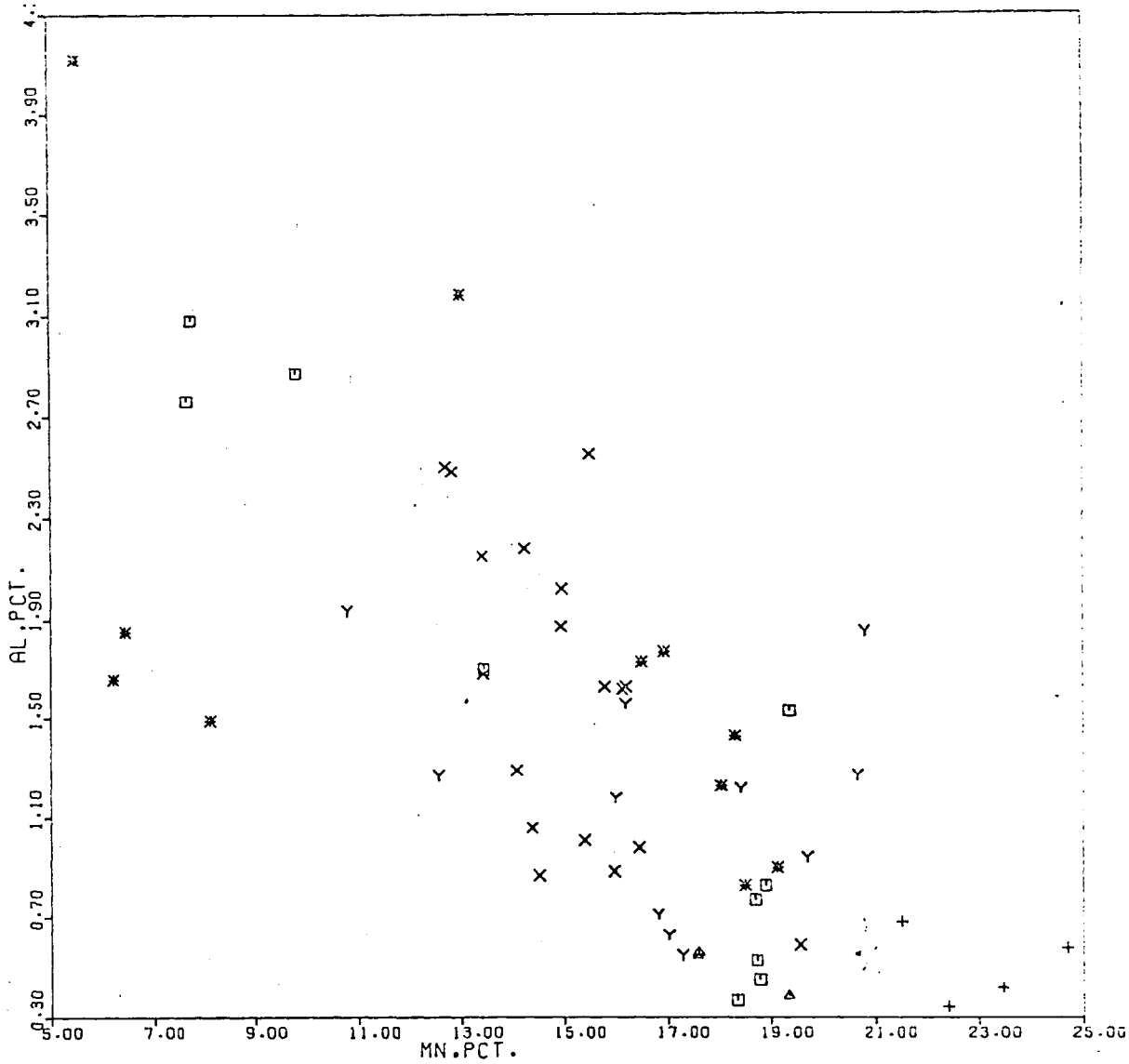

Figure 5.2 Plot of manganese vs. aluminium, seamount samples.

GROUP	SYMBOL	NO. OBS.	R
ALL	-	57	-0.72
1307	X	18	-0.60
1315	+□	4	-0.12
1317	□	10	-0.93
1318	△	3	-1.00
1321	Y	11	-0.22
REST	✱	11	-0.57

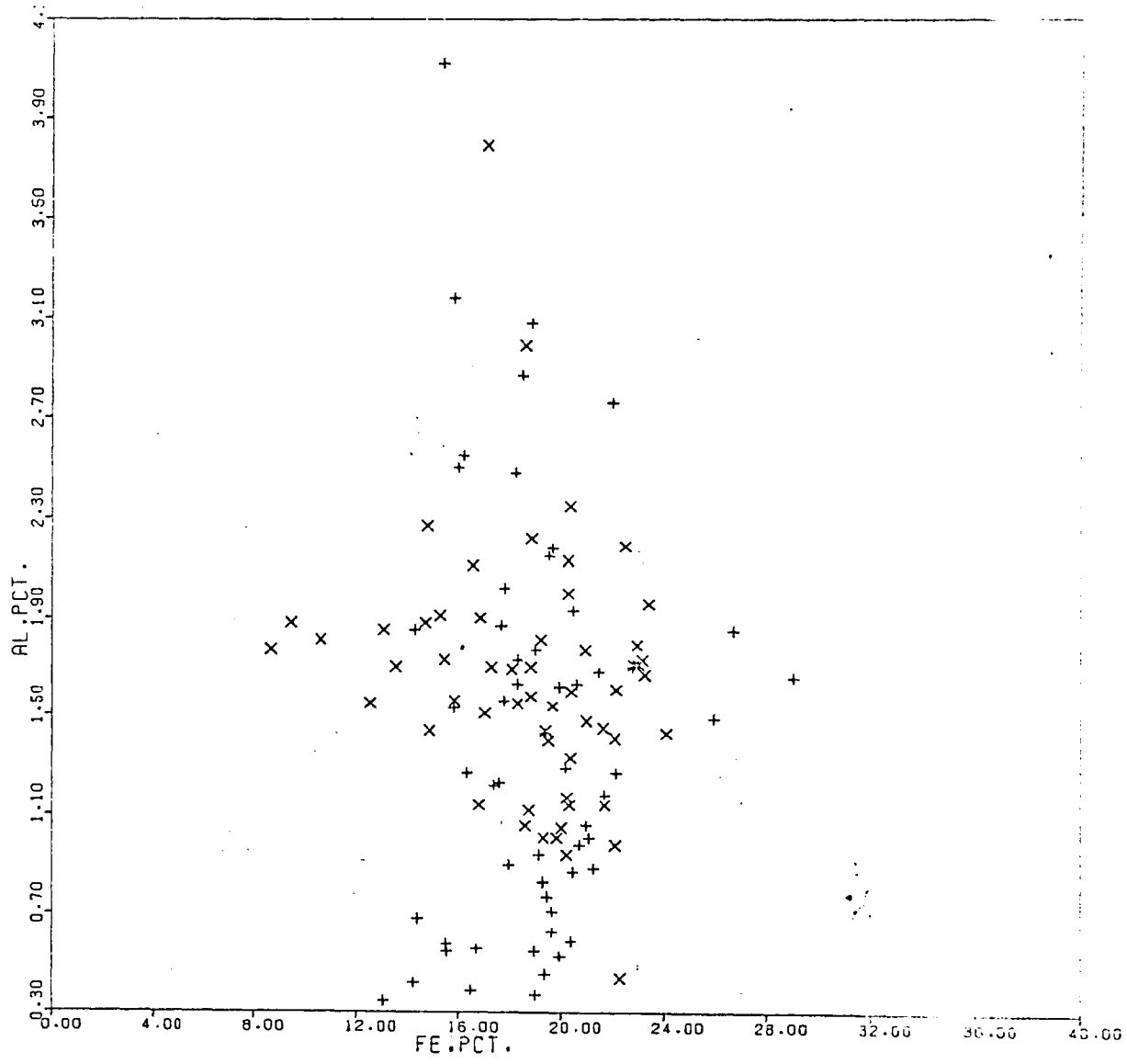

Figure 5.3 Plot of iron vs. aluminium, all oxide samples.

GROUP	SYMBOL	NO. OBS.	R
[illegible]	-	114	-0.08
[illegible]	X	57	-0.21
SEAMOUNTS	+	57	0.02

Copper and Nickel

Copper and nickel show different correlations to each other in the Ridge area and the seamount area. On the Ridge, they show a strong positive correlation (Fig.5.4). On the seamounts they show no clear correlation with each other. Other workers have found as a general rule that these elements correlate positively together with manganese (Goldberg, 1954; Cronan, 1967, 1975; Glasby, 1970; Calvert & Price, 1977; Moorby, 1978) Nickel correlates strongly with manganese on the Ridge and the seamounts, whereas copper correlates with manganese only on the Ridge. Nickel and iron show a strong negative correlation in both areas, whereas copper only does so on the Ridge. No clear relation exists between Cu and Fe on the seamounts. In the seamount province, Ni correlates negatively and copper positively, with depth. Specimens from only four different depths are available from the Ridge, so no useful observations can be made in this regard. Ni shows no relationship with Al in either area. Cu shows a positive relationship with Al on the seamounts which is weaker on the Ridge.

The association between Ni, Cu and Mn in marine ferromanganese oxide deposits is well established. Some workers (Burns & Fuerstenau, 1966; Cronan & Tooms, 1969) have suggested that ionic substitution of Ni^{2+} and Cu^{2+} for Mn^{2+} in the manganese oxide lattice is the explanation for this association. On the other hand, Fuerstenau et al., (1973), have suggested that Ni and Cu may not be lattice-held but simply adsorbed onto colloid-size manganese oxide particles. These explanations break down with the seamount

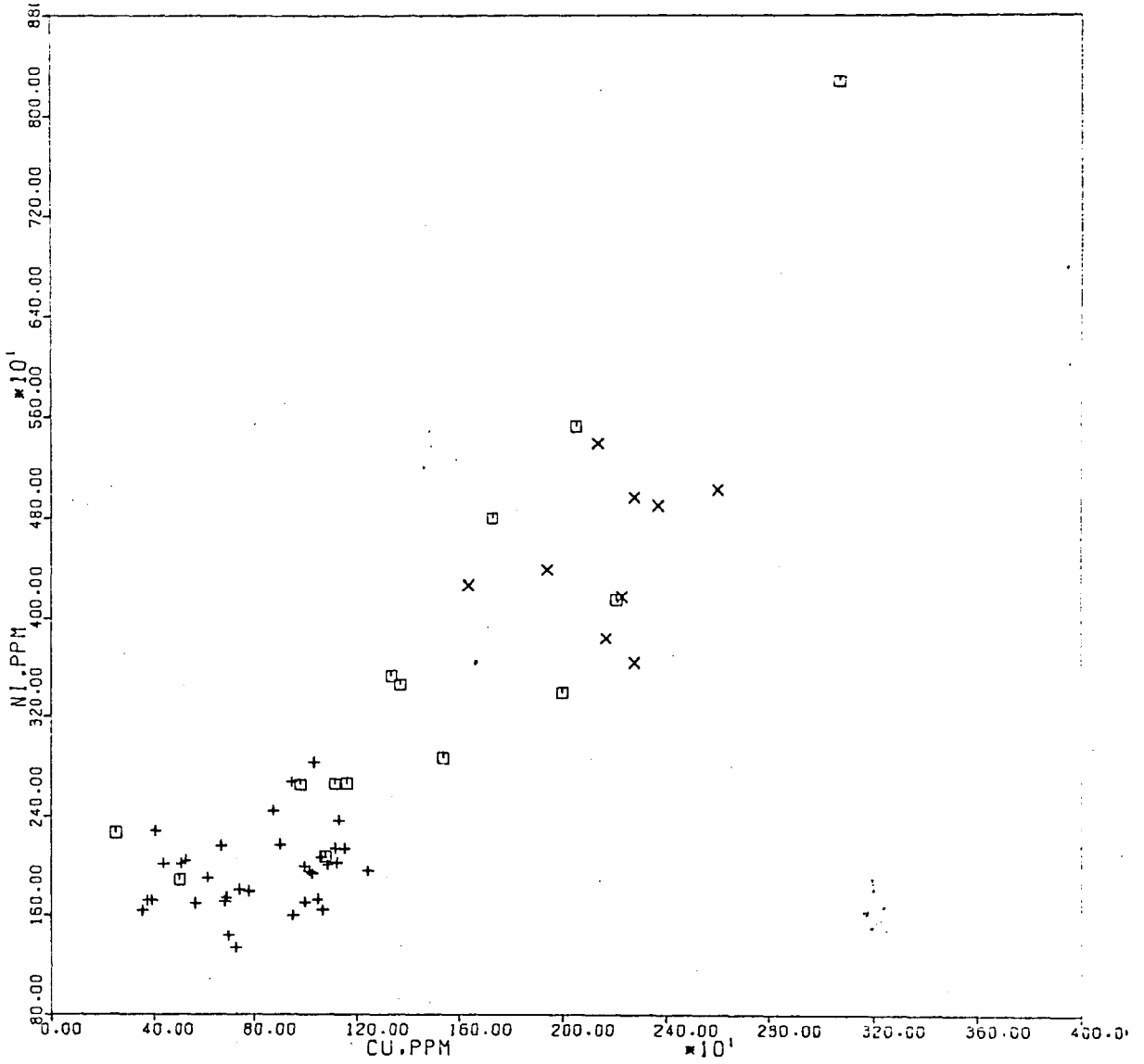

Figure 5.4 Plot of copper vs. nickel, Ridge samples.

GROUP	SYMBOL	NO. OBS.	R
ALL	-	57	0.66
TODOROKITE	X	9	0.29
1301	+	34	0.29
REST	□	14	0.88

samples, where the Ni-Cu-Mn association is not present. While they serve to explain the Ni-Mn correlation, some other explanation must be sought for the behaviour of Cu.

Moorby(1978) has shown that copper values in shallow water samples from the Indian Ocean are up to an order of magnitude lower than the nickel values. In contrast he found nodules from depths below the lysocline containing almost as much Cu as Ni. Bezrukov & Andrushenko (1974) also found this in the Indian Ocean. Cronan(1972) and Horn et al.,(1973) have shown that the same phenomenon is also observed in the Pacific Ocean.

In the seamount samples from the N.W.Indian Ocean, the main differences in behaviour between Ni and Cu with respect to the controlling variables are that Cu correlates positively with depth and Al while Ni correlates negatively with depth and not at all with Al. Colley et al.,(1979) have shown that no more than about 10% of the Cu and 2½% of the Ni in the seamount samples is associated with the detrital phase. So while the detrital contribution of Cu is relatively high, it is not the major control on it. The significance of the detrital contribution to the Ni content of the deposits is quite small. Consequently, some other controls must be invoked to account for the marked fractionation of the elements on the seamounts, and their correlation together in the Ridge samples.

Moorby(1978), and Colley et al.,(1979) have suggested that biological productivity, linked with the effect of depth on biological material may be responsible for this fractionation of Ni from Cu. Copper and nickel are considerably

enriched in many marine organisms compared to their concentrations in normal sea water (Nicholls et al.,1959; Fujita, 1971; Greenslate et al., 1973; Leatherland et al., 1973; Oldnall, 1975; Horder, 1979). Some of these authors also show that Cu is considerably more enriched in many of these organisms than is nickel. Sclater et al.,(1976) have shown that Ni is involved in the biogeochemical cycle and that its concentration in seawater is fairly constant with depth. Boyle et al., (1977) have shown that dissolved Cu increases with depth. In areas of high biological productivity, the upper part of the water column may exhibit lower Cu/Ni ratios than seawater in areas of lower productivity. At depths below the lysocline, substantial dissolution of dead organisms occurs, and the Cu/Ni ratio of the seawater may increase. This could influence the composition of ferromanganese oxide deposits from these depths. From the oceanwide maps of productivity by Qasim (1977) it seems that primary production is moderately high, but varies greatly over short distances in the area considered here. Marine organisms may take up sufficient Cu to cause its depletion in shallow water samples compared to Ni, and provide an enhanced supply of Cu below the lysocline, where the rate of dissolution of dead organisms rapidly increases. The effect of depth on the Cu content of ferromanganese oxide deposits can be seen by comparing the average depths and average Cu values of deposits from each station. Figure 5.5 is a plot of Cu versus depth, and shows how Cu increases rapidly with depth after the lysocline is reached(3800-4000m., Kolla et al., 1976a; 3700-4000m., this work).

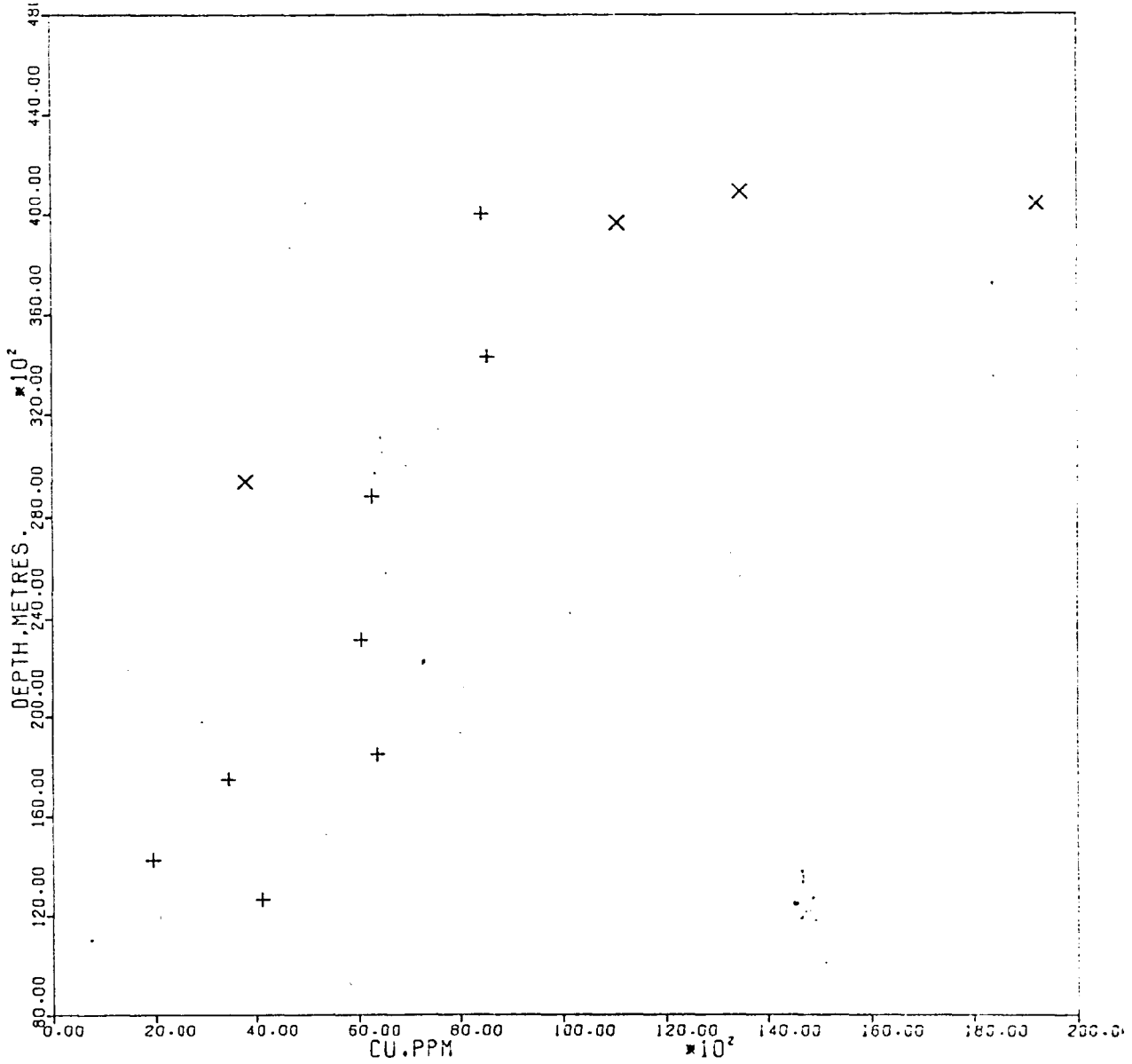

Figure 5.5 Plot of copper vs. station depth.

GROUP	SYMBOL	NO. OBS.	R
ALL	-	12	0.79
RIDGE	×	4	0.86
SEAMOUNT	+	8	0.87

Thus the most probable explanation for the differences in the behaviour of Cu and Ni in the present samples is one of biological fractionation, with Cu being taken up by the deposits after liberation from the dissolution of organic remains below the lysocline.

If the fractionation of Cu from Ni in the present samples is indeed caused by biological activity, then the same phenomenon should be seen throughout the World Ocean. A method to check this is to take Cu and Ni data from ferromanganese oxide deposits throughout the World Ocean, and plot their variations with sample depth-lysocline depth. Table 5.6 summarises the Cu and Ni contents of ferromanganese oxide deposits from various areas of the World Ocean. Figures 5.6 and 5.7 show these data graphically. The graph for Cu starts to turn at the lysocline. Nickel is less affected by this and the scatter is much wider.

It is reasonable to conclude therefore, that biological activity does play an important role in the distribution of Cu and Ni in ferromanganese oxide deposits, not only in the N.W. Indian Ocean, but also worldwide.

Cobalt and Lead

On an oceanwide basis Co and Pb often correlate together and usually correlate with iron (Goldberg, 1954; Burns & Fuerstenau, 1966; Willis, 1970; Calvert et al., 1978). Cronan (1967) noted that they were very closely related in one factor of a factor analysis of a large amount of nodule data. He concluded that this was a depth factor because of the high negative correlations between Co and depth and lead and depth. He did not observe any strong relationships

Table 5.6 Average content of Cu and Ni in ferromanganese oxide deposits from various parts of the World Ocean.

Indian Ocean (Adapted from Colley et al., 1979).

	Average sample depth, m.	Depth of lysocline (Kolla et al.,1976a)	Sample depth— lysocline depth	Cu,ppm	Ni,ppm
Central Indian Basin	5090	4050	+1040	9910	10300
Crozet Basin	4600	4250	+ 350	1500	3390
Madagascar Basin	5010	4000	+1010	1150	2280
Mozambique Basin	5277	4350	+ 927	1660	3150
Somali Basin	4435	4000	+ 435	2410	4810
Wharton Basin	5320	3900	+1420	3550	5570
Mozambique Channel	3120	4300	-1180	2040	8000
South African Plateaux	3180	4350	-1170	940	2850
Carlsberg Ridge	3925	3900	+ 25	1192	2760
Seychelles Seamounts	2638	3900	-1262	659	2918

Table 5.6 cont'd.

Atlantic Ocean (From Cronan, 1975; Lysocline data from Biscaye et al., 1976)

	Average sample depth, m.	Depth of lysocline	Sample depth − lysocline depth	Cu,ppm	Ni,ppm
N.W. Atlantic Basin	4339	4300	+ 39	1300	2700
Mid-Atlantic Ridge,45°N	2388	4200	-1812	480	1880
Central Mid-Atlantic Ridge	2440	4800	-2360	470	2250
N.Mid-Atlantic Ridge	2877	4200	-1323	700	1400
N.E.Atlantic Basin	3107	4300	-1193	1260	3610
Cape Verde Basin	3934	4800	- 866	1050	2490
Argentine Basin	3802	3700	+ 102	1820	5490
Brazil Basin	4258	4500	- 242	1180	2660
Drake Passage-Scotia Sea	3696	2500	+1196	1050	2440
Cape Basin	4924	4400	+ 529	5000	9520
Walvis Ridge	1836	4500	-2669	780	4820
South of South Africa	2718	4600	-1882	580	2560

Table 5.6 Cont'd.

Pacific Ocean (from Cronan, 1972; Lysocline data from Berger et al., 1976)

Area	Average depth of samples,m.	Depth of lysocline ,m.	Sample depth - lysocline depth ,m.	Cu,ppm.	Ni,ppm
N.E. Pacific	4537	3900	+ 637	6270	10800
S.E.Pacific	4324	4200	+ 124	1640	9610
Central N. Pacific	5049	3200	+1849	7110	9560
Central S. Pacific	3539	4150	- 611	1850	4330
W.Pacific	5001	4250	+ 751	3930	5640
Mid. Pacific Mts.	1757	3000	-1243	610	3930
N. Pacific	4990	3200	+1790	2940	4220

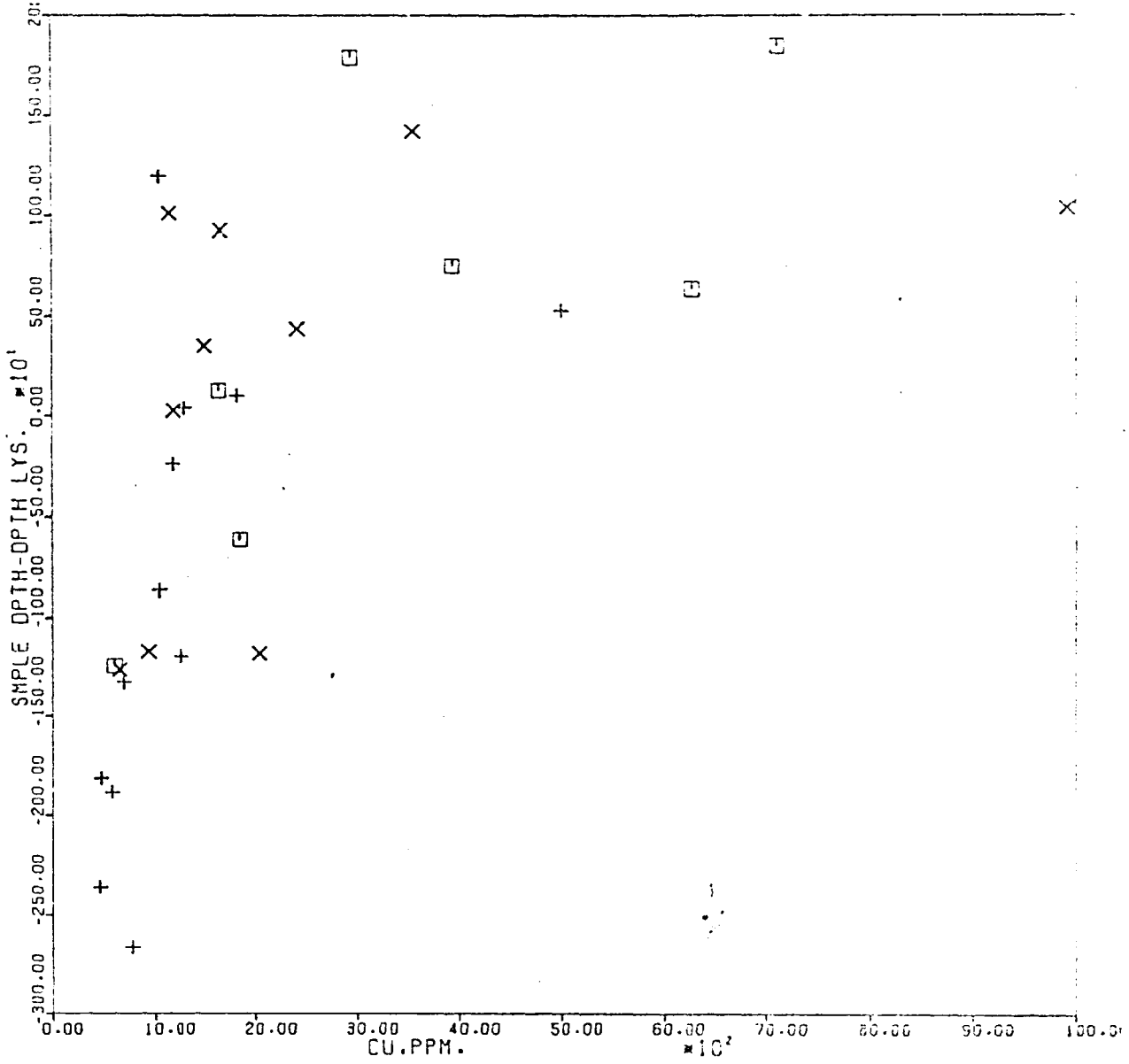

Figure 5.6 Plot of copper vs.sample depth-lysocline depth.

GROUP	SYMBOL	NO. OBS.	R
ATL	-	29	0.60
INDIAN	×	10	0.45
ATLANTIC	+	12	0.55
PACIFIC	⊡	7	0.72

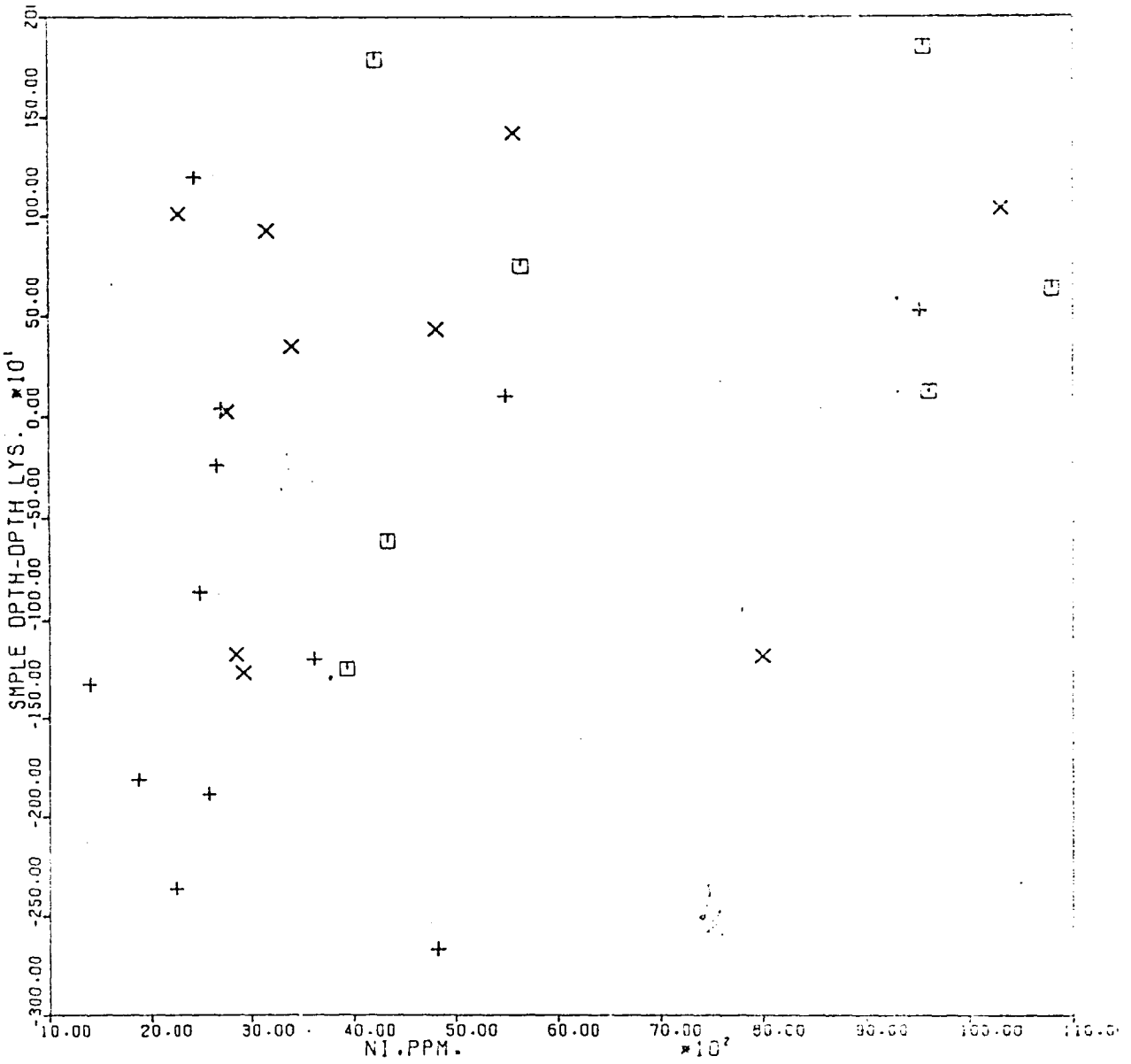

Figure 5.7 Plot of nickel vs. sample depth-lysocline depth.

GROUP	SYMBOL	NO. OBS.	R
ALL		28	0.41
INDIAN	+	9	0.14
ATLANTIC	×	12	0.53
PACIFIC	□	7	0.36

between these elements and Fe.

Cobalt and lead in the present samples correlate strongly positively on the seamounts, but only weakly on the Ridge. Their associations with other elements also vary between the two areas. On the Ridge, Co tends to be correlated with the Fe content. In the seamount area, Co is clearly correlated with the manganese concentration (Fig.5.8). Both Pb and Co show strong negative correlations with depth (Figs. 5.9 and 5.10), in agreement with the findings of Cronan, (1967). In contrast to Co, Pb on the Ridge shows a strong correlation with Fe and Mn, the first positive, and the second negative. In the seamount samples, Pb behaves differently. It appears to be independent of the iron content, but is strongly correlated with Mn.

Burns & Burns (1977) have pointed out that the ionic radius of Co^{3+} (0.525Å) is very much less than Fe^{3+}(0.645Å) and hence is not easily tolerated in the iron phase. They also claim that Co OOH. xH_2O is not isostructural with FeOOH and hence will not form a solid solution. The radius of Co^{3+} is close to that of Mn^{4+} (0.54Å). This is a more favourable situation for substitution, and might account for the positive correlations between Mn and Co in the present samples, and as seen by Barnes (1967), Cronan & Tooms (1968), Jenkyns (1970), and Ostwald & Fraser (1973).

The iron content of the samples increases with increasing depth (Table 5.4). The effect of this is twofold : 1. Iron may block reaction sites in the manganese oxide lattice to cobalt substitution (Burns & Burns, 1977). 2. Increasing iron content will probably decrease the amount of manganese

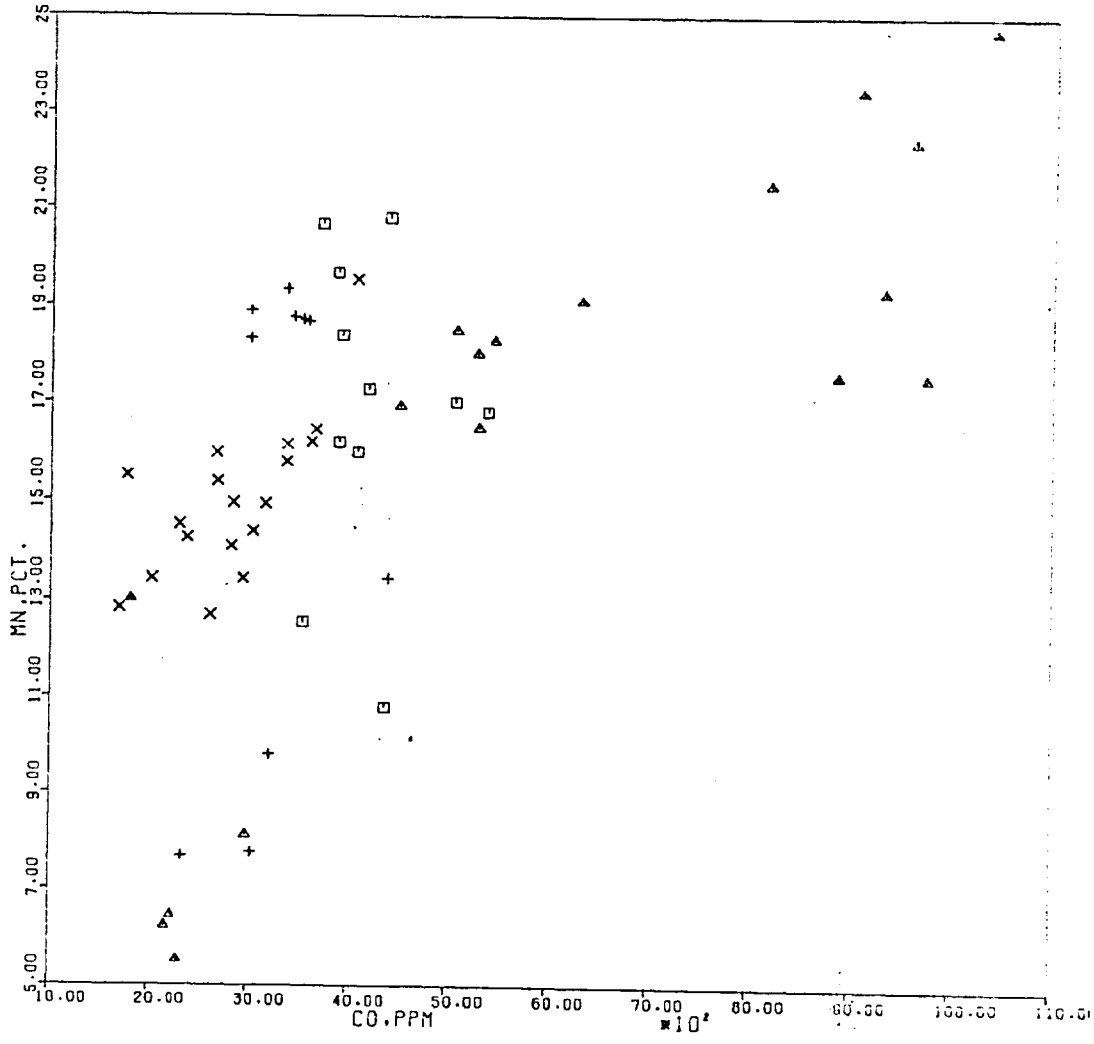

Figure 5.8 Plot of cobalt vs. manganese, seamount samples.

GROUP	SYMBOL	NO. OBS.	R
ALL	-	57	0.62
1307	×	18	0.70
1317	+	10	0.35
1321	⊡	11	-0.02
REST	△	18	0.65

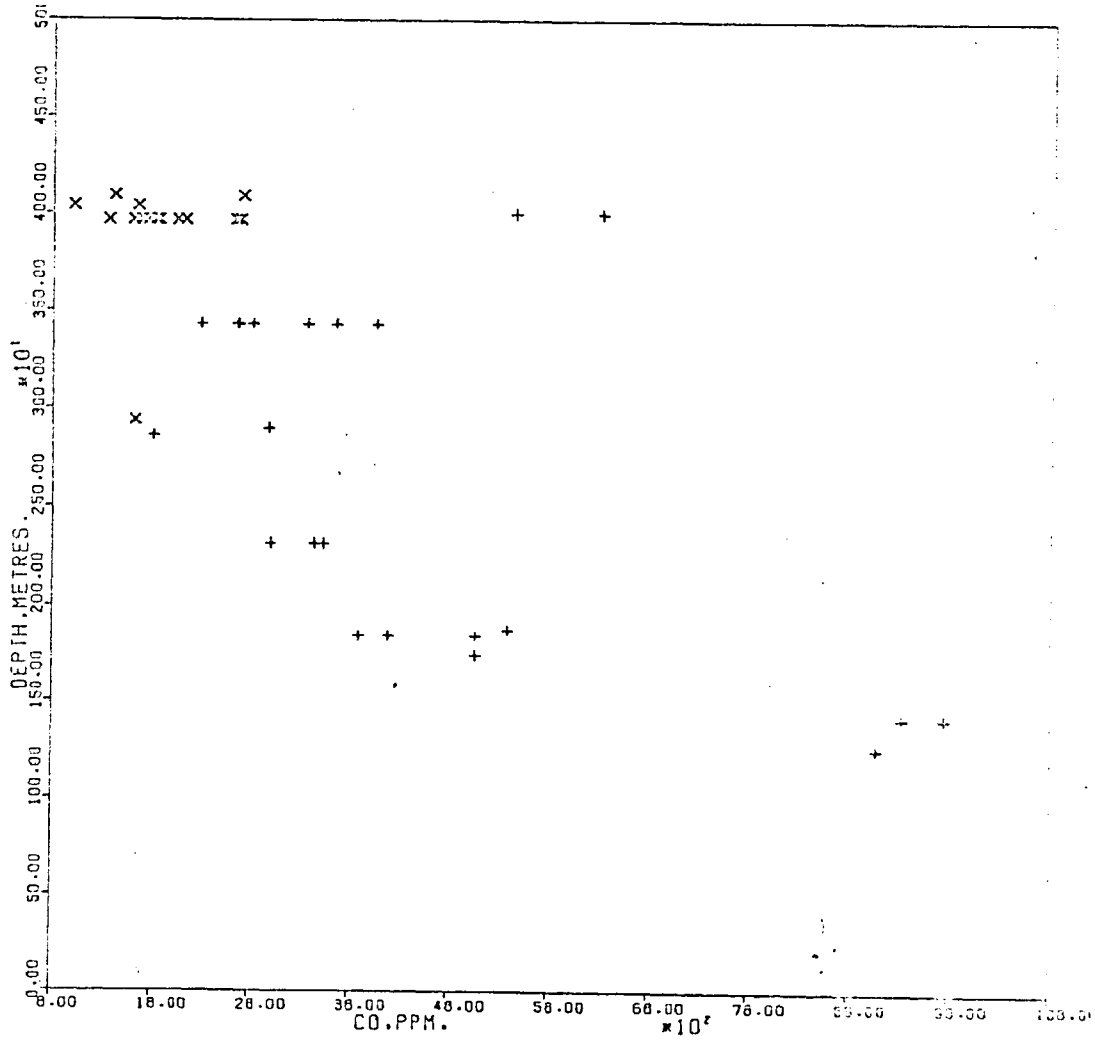

Figure 5.9 Plot of cobalt vs. depth, all oxide samples.

GROUP	SYMBOL	NO. OBS.	R
ALL	-	37	-0.71
RIDGE	X	15	0.11
SEAMOUNTS	+	22	-0.55

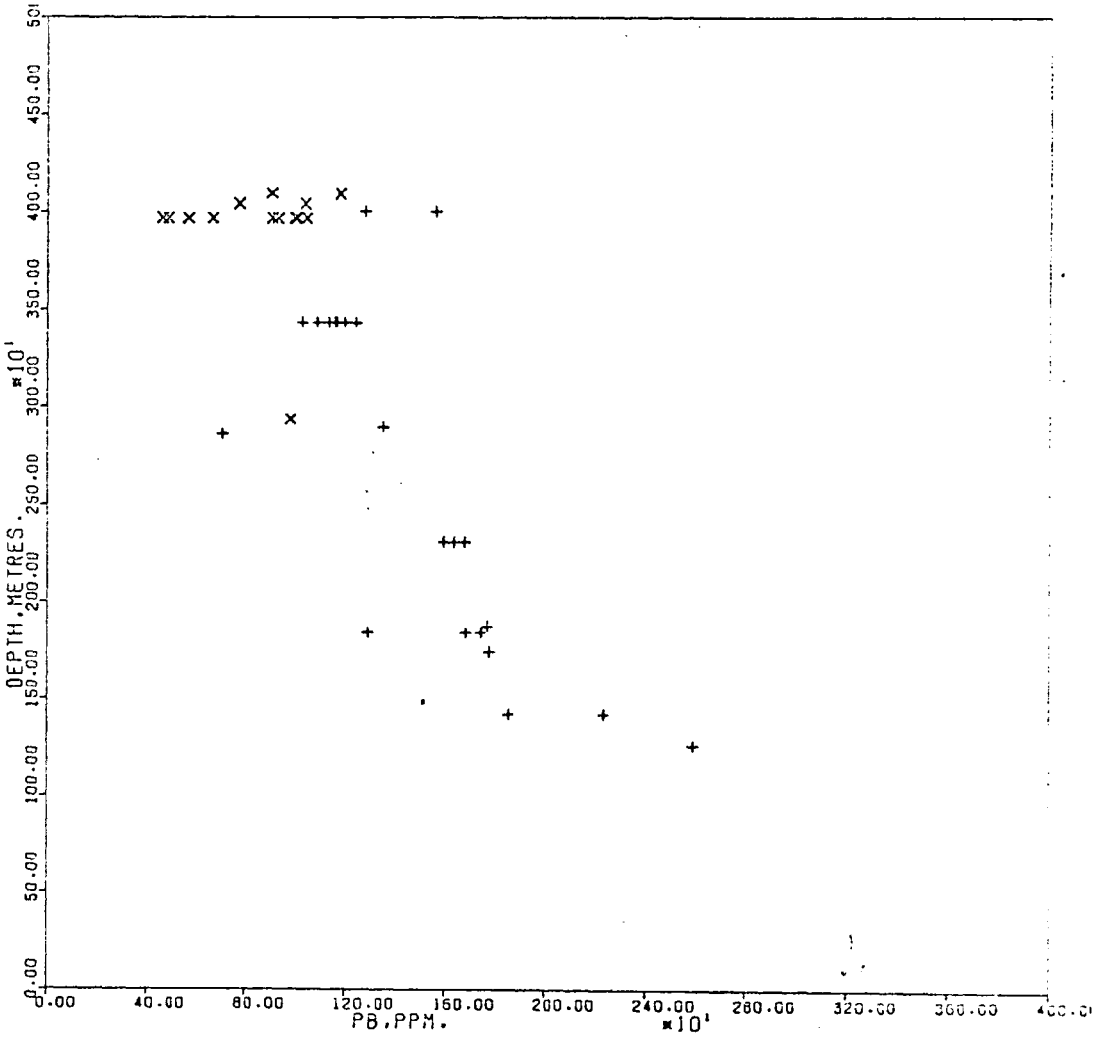

Figure 5.10 Plot of lead vs. depth, all oxide samples.

GROUP	SYMBOL	NO. OBS.	R
ALL	-	37	-0.82
RIDGE	×	15	-0.08
SEAMOUNTS	+	22	-0.75

present in the sample. If the dominant process of incorporation of Co into these deposits is indeed by substitution into the manganese oxide lattice, then these effects could account for the decrease of Co with increasing depth in the seamount samples.

Co correlates with neither Mn nor Fe in the Ridge samples.

In the seamount samples, the behaviour of lead with respect to Fe and Mn is similar to cobalt. While it seems crystal substitution of Co(II) into the manganese oxide lattice appears to be the main method of incorporation of Co into the deposits on the seamounts, it is unlikely that Pb substitutes for Mn in this way because of the large differences in ionic radii (0.84Å for Pb^{4+} and 1.2Å for Pb^{2+} compared with 0.54Å for Mn^{4+}. Goldberg (1965) suggested that in highly oxygenated marine environments (for example, on top of seamounts), lead may be oxidised to the tetravalent ion. Sillén (1961) proposed on this basis that $(Mn,Pb)O_2$ solid solutions may form and this would account for the enrichment of Pb in deposits from oxygenated shallow water. Van der Weijden & Kruissink (1977) has discussed this suggestion and rejected it. He found that oxygen is not very active as an oxidising agent for Pb(II)→Pb(IV). He came to the conclusion that the uptake of Pb in manganese oxides can be explained by adsorption of Pb^{2+} without having recourse to oxidation to Pb(IV).

In the Ridge samples Pb reverses its behaviour, correlating positively with Fe (fig.5.11) and negatively with Mn.

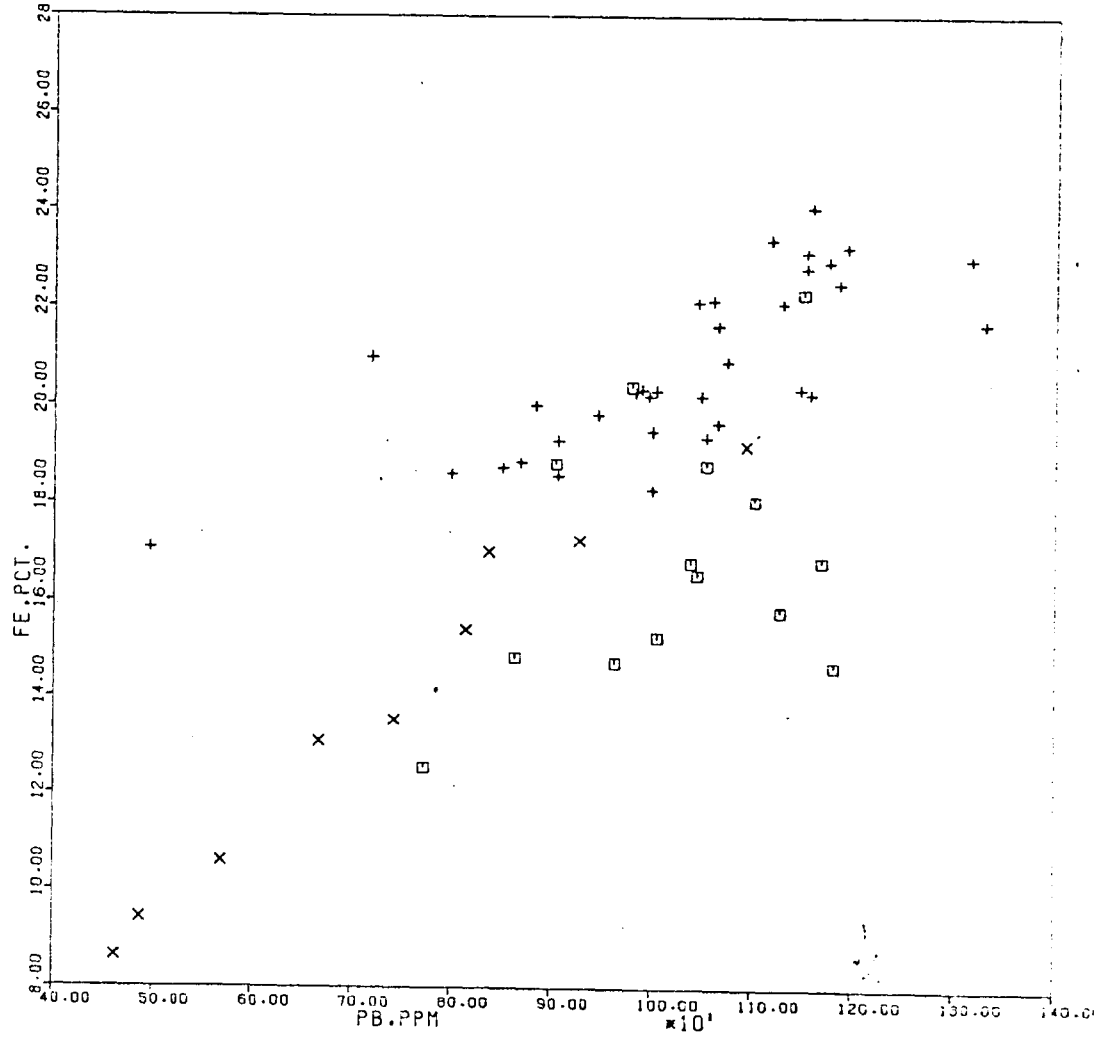

Figure 5.11 Plot of lead vs. iron, Ridge samples.

GROUP	SYMBOL	NO. OBS.	R
ALL	-	57	0.72
[illegible]	X	9	0.98
[illegible]	+	34	0.74
[illegible]	□	14	0.38

Zinc

Zinc is another element to show ambivalent behaviour towards Fe and Mn. It has usually been found to correlate with Mn by other workers (Glasby, 1970; Cronan, 1975a,b; Calvert & Price, 1977; Calvert et al., 1978; Moorby, 1978). There have been no previously reported Zn-Fe correlations. In the Ridge samples, Zn is correlated with Fe in the samples from station 1301, including those containing todorokite (Fig.5.12). At the other stations it correlates with Mn (Fig.5.13). In the seamount samples, Zn shows a positive correlation to Mn, although none of the correlations are statistically significant. There appears to be no relation between Zn and depth.

The association of Zn with Mn is thought to be brought about by substitution of Mn^{2+} by Zn^{2+} in the todorokite lattice (Moorby, 1978). This is not adequate to explain the Zn-Mn correlation at 6269, 6273 and 1303, because there are no samples from these stations which contain todorokite. However, Hem (1978) has suggested Zn^{2+} may easily enter the manganese oxide lattice during the early stages of formation of the manganese oxide material. This could account for the observed Zn-Mn correlation here. Krauskopf(1956) showed that hydrated ferric oxide is an efficient scavenger of Zn from solution, so perhaps adsorption of zinc in this way might account for the Zn-Fe correlation in the samples from 1301.

Cadmium

Very little work has been done on this metal in ferromanganese oxide deposits. Ahrens et al.,(1967), found

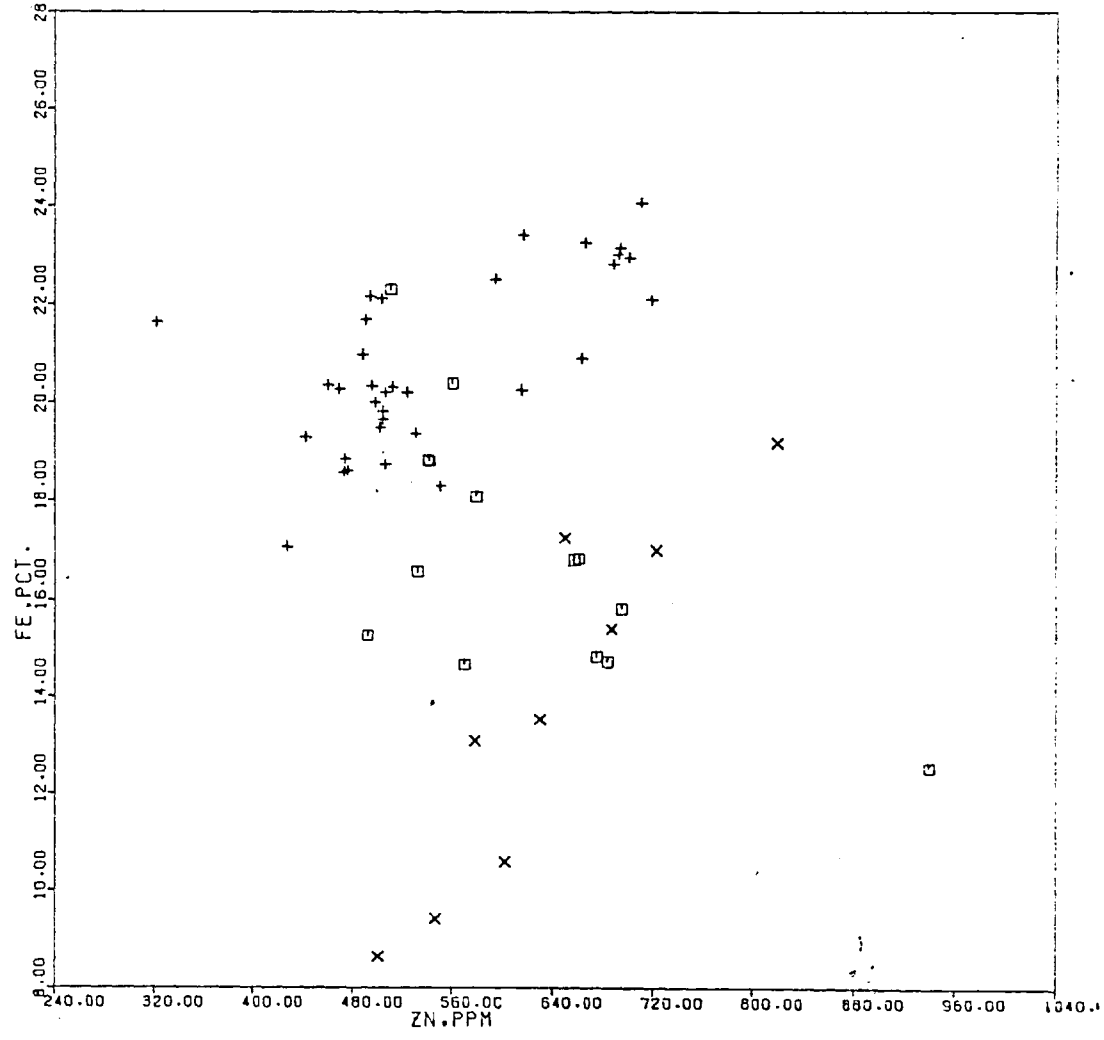

Figure 5.12 Plot of zinc vs. iron, Ridge samples.

GROUP	SYMBOL	NO. OBS.	R
ALL	-	57	-0.10
TODOROKITE	X	9	0.92
1301	⊞	34	0.65
REST	⊡	14	-0.65

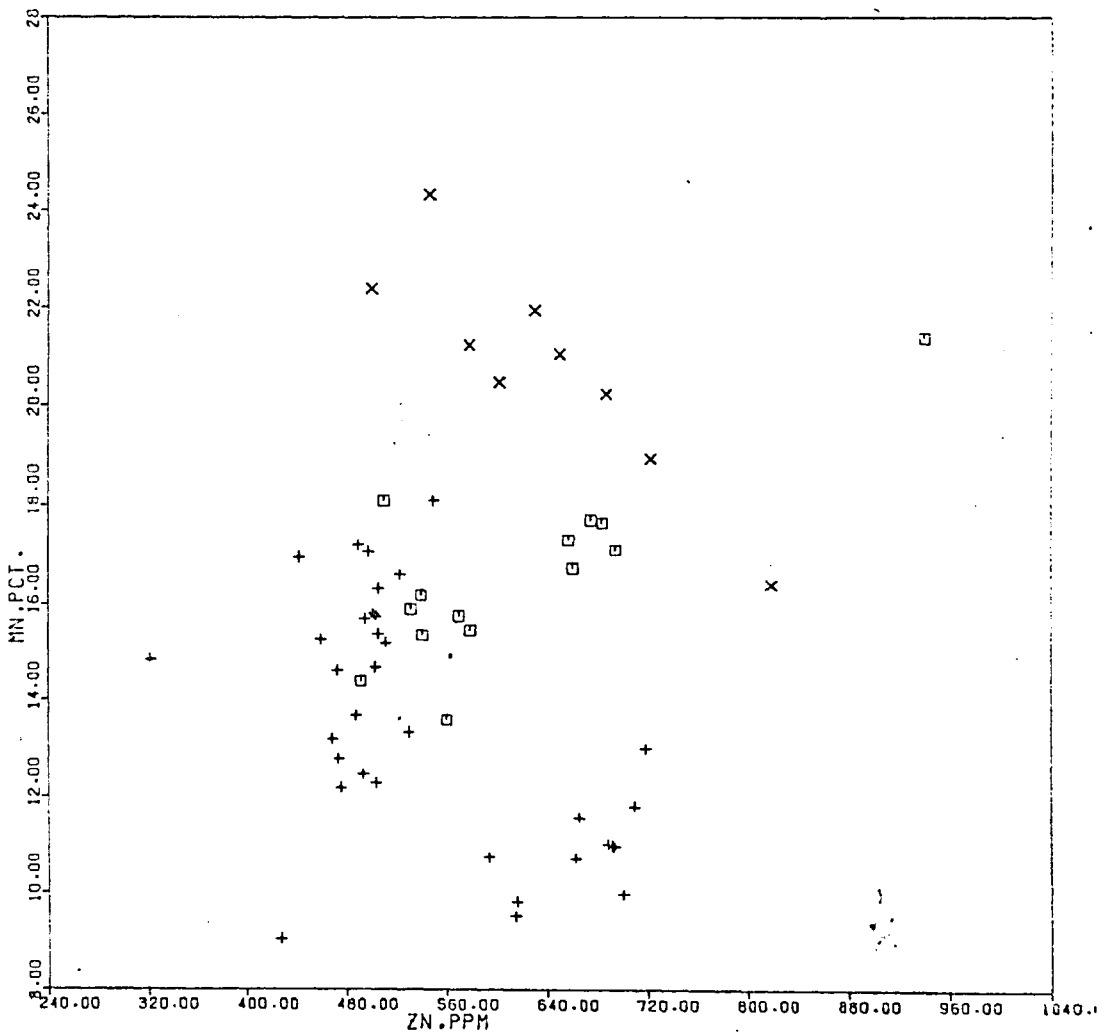

Figure 5.13 Plot of zinc vs manganese, Ridge samples.

GROUP	SYMBOL	NO. OBS.	R
ALL	-	57	0.10
TODOROKITE	X	9	-0.89
[illegible]	+	34	-0.53
REST	[illegible]	14	0.81

a positive correlation with Zn, and Moorby(1978) found positive correlations with Cu, Ni, Zn, and Mn. In the present samples, the mineralogy of the host phase seems to control the behaviour of Cd. In the specimens which contain δ-MnO_2 only, from both the Ridge and the seamounts, Cd is correlated with Mn. In the specimens of mixed-mineralogy from 1301, Cd is correlated with Fe, both in the todorokite-bearing samples and in the samples containing δ-MnO_2-only (group 1301 MXMIN in Fig.5.14).

Moorby (op.cit.) has suggested that the Cd^{2+} ion is too large to fit well into a manganese oxide lattice. This could account for the low concentration of this metal in these deposits (6 ppm average). So perhaps the metal is adsorbed onto the surface of the oxide particles. The change in behaviour of Cd with mineralogy is difficult to explain.

Lithium

No previous work has been done on the Li content of ferromanganese oxide deposits. In the seamount samples, the main pathway of Li into the deposits appears to be via aluminosilicate debris, because of the significant correlation between Li and Al(Fig.5.15). In the Ridge samples, two controls seem to be operating. In the δMnO_2-only specimens from 1301, (group 1301 DMNO2 in Fig.5.16), aluminosilicate debris is again the main route (Fig.5.16). In the other samples, the Mn content appears to control the Li content, especially in the todorokite-containing samples (Fig.5.17).

The average Li content of a deep sea clay is 57 ppm.

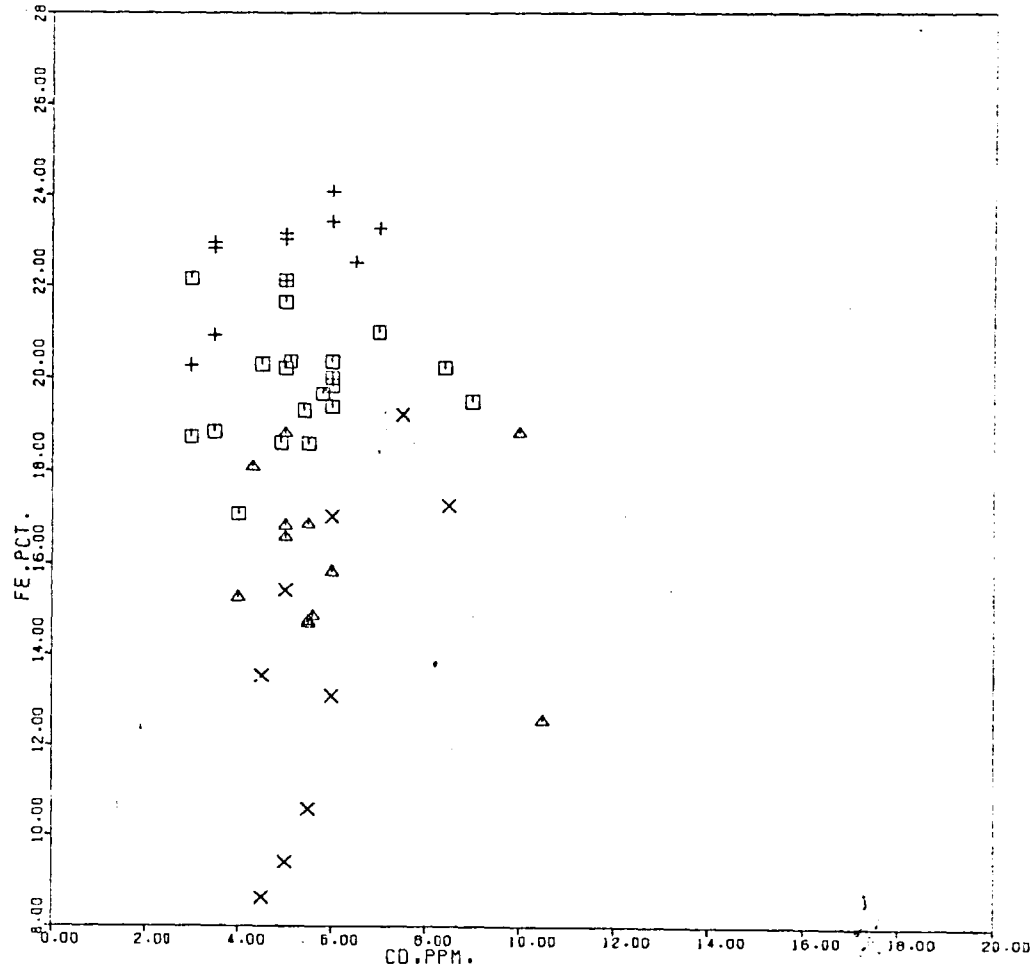

Figure 5.14 Plot of cadmium vs. iron, Ridge samples.

GROUP	SYMBOL	NO. OBS.	R
ALL	-	53	-0.08
TODOROKITE	X	9	0.72
1301MXMIN	+	11	0.64
1301DMNO2	□	21	0.08
REST	△	12	-0.22

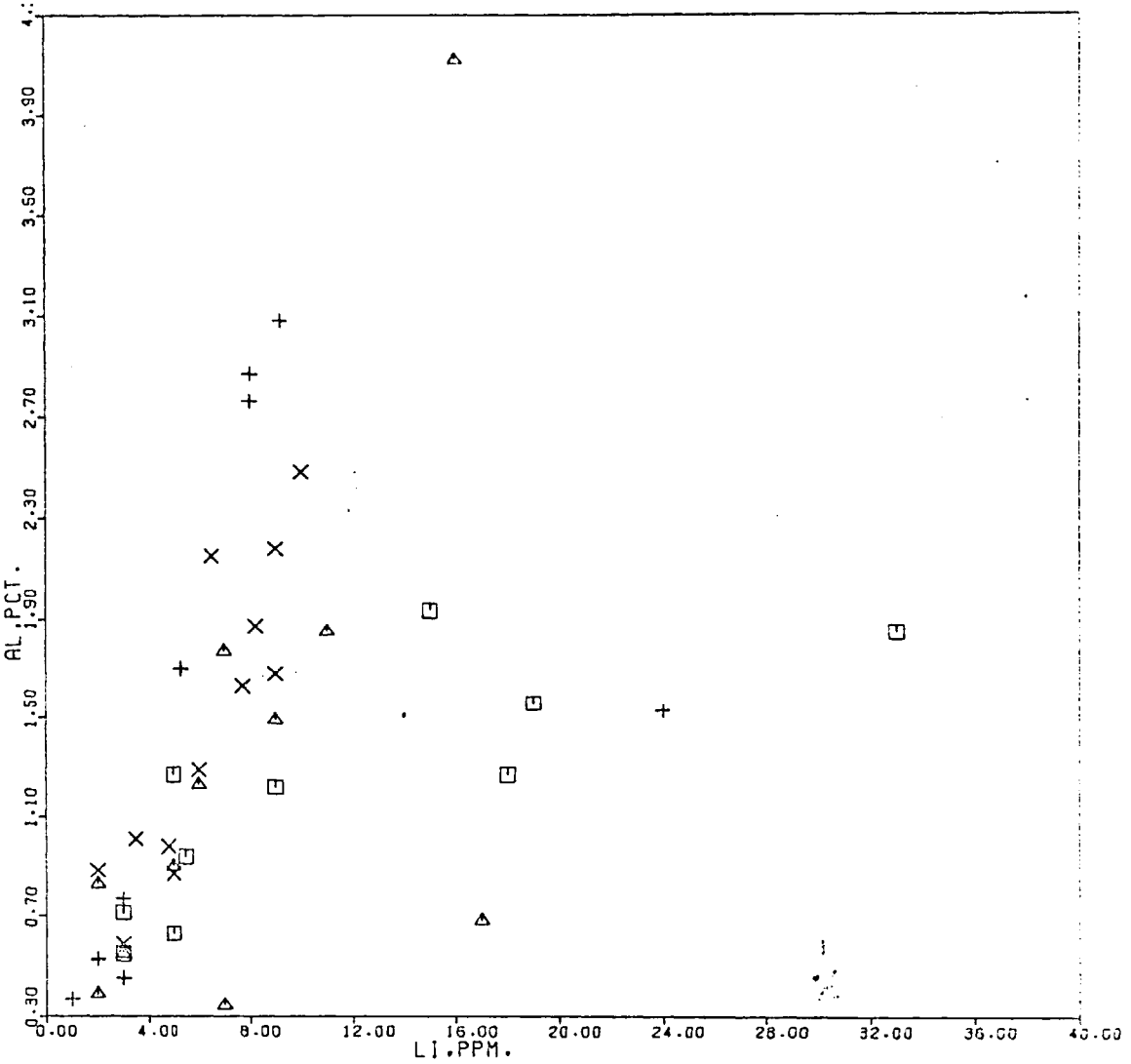

Figure 5.15 Plot of lithium vs. aluminium, seamount samples.

GROUP	SYMBOL	NO. OBS.	R
ALL	-	42	0.44
[illegible]	×	12	0.88
[illegible]	+	9	0.40
[illegible]	□	10	0.60
REST	△	11	0.59

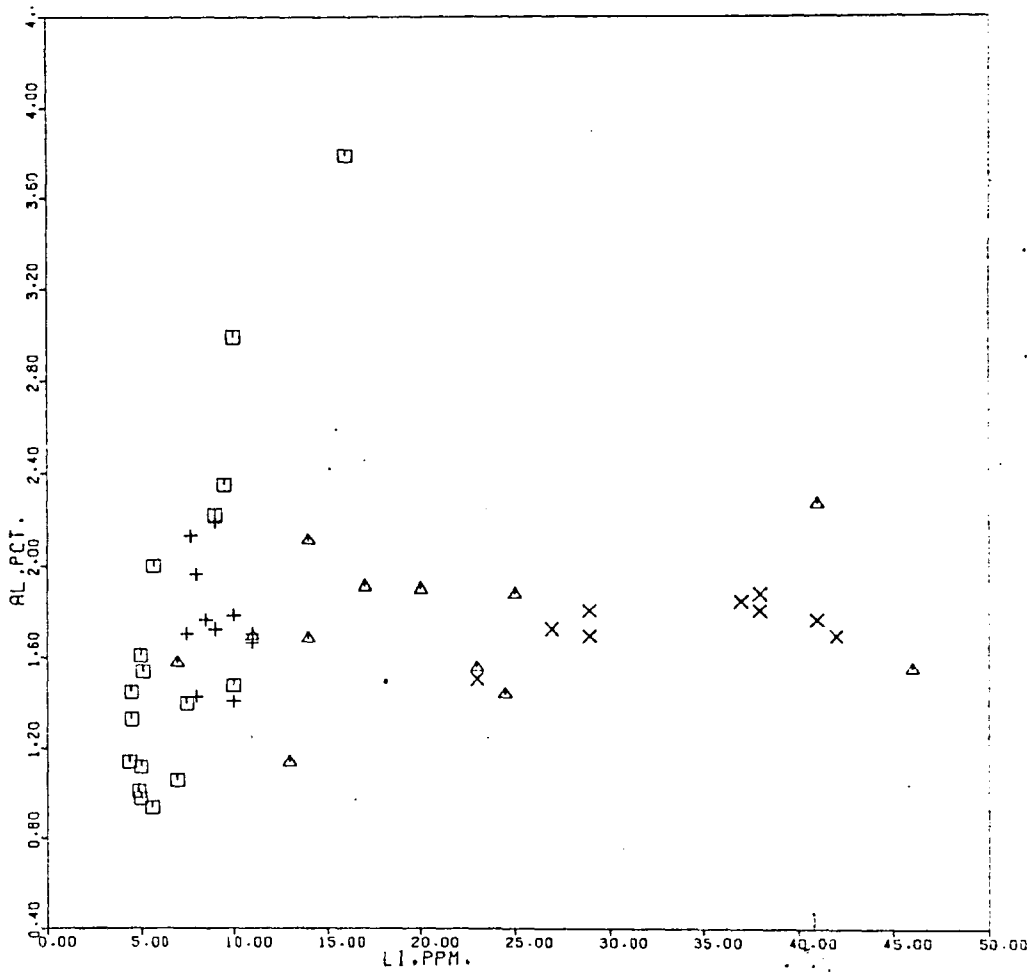

Figure 5.16 Plot of lithium vs. aluminium, Ridge samples.

GROUP	SYMBOL	NO. OBS.	R
ALL	-	49	0.19
TODOROKITE	×	9	0.59
1301MIXMN	+	11	-0.28
1301OMNO2	□	17	0.85
REST	△	12	0.24

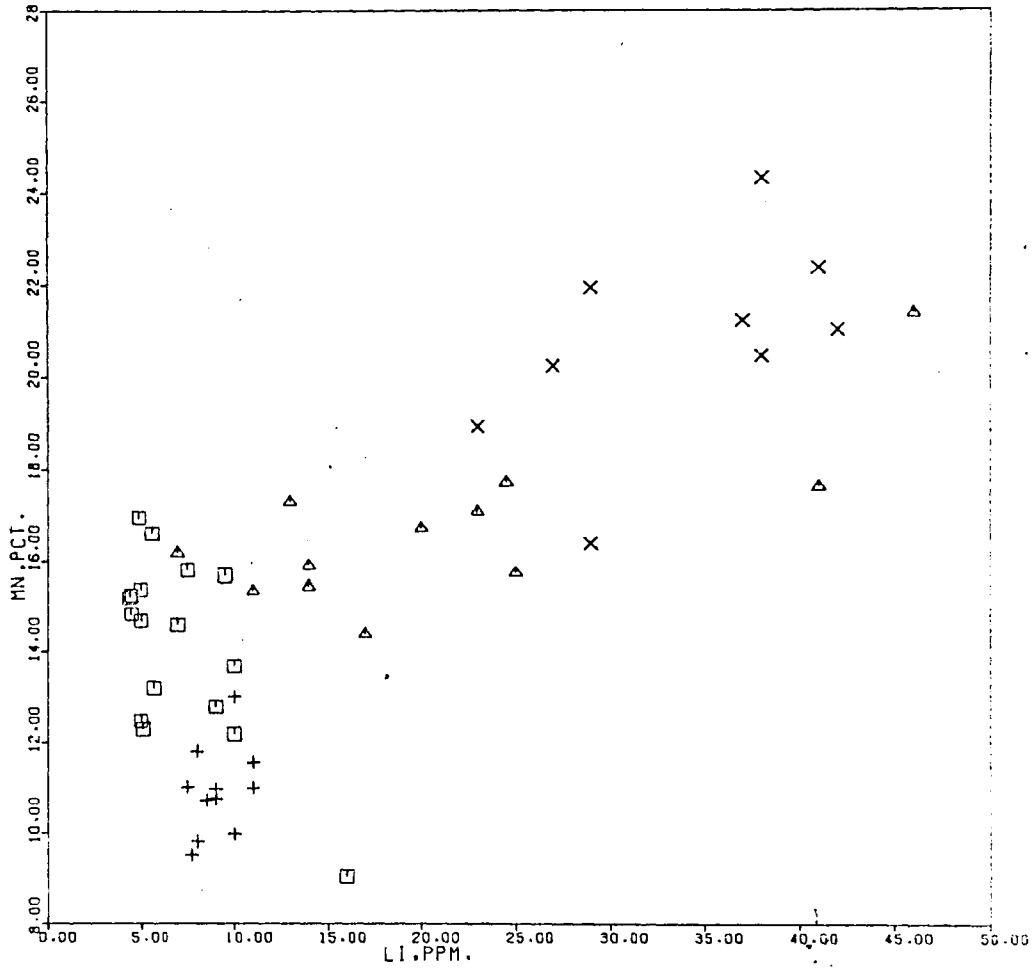

Figure 5.17 Plot of lithium vs. manganese, Ridge samples.

GROUP	SYMBOL	NO. OBS.	R
ALL	-	49	0.76
TODOROKITE	X	9	0.56
1301MXMIN	+	11	0.37
1301OMNO2	⊡	17	-0.65
REST	△	12	0.76

(Turekian & Wedepohl, 1961). The average Li content of the δMnO_2-only samples is 7ppm. If only 10-12% of the samples is composed of clay, the clearly all the Li in these samples would be detrital. This is not so in the todorokite-containing samples, which have an average Li content of 34 ppm. Consequently there is a large non-detrital contribution of Li in the todorokite-containing samples. Lithium has an ionic radius of .68Å and at first glance this might seem suitable for substitution of Mn^{4+} (radius .6Å). However-this is not likely since Li^{+} cannot assume the octahedral coordination necessary for such substitution. It was suggested earlier (Chapter 4) that this lithium excess in the todorokite-containing samples could be accounted for by the presence of a small amount of lithiophorite.

Titanium

Titanium correlates positively with Fe and negatively with Mn in both the seamount samples and the Ridge samples. In the seamount samples there is also a weak correlation with Al, although on the Ridge there is no correlation. Ti seems to be independent of depth. Goldberg(1954), Cronan(1967) and Moorby (1978), also found positive correlations between Fe and Ti. Goldberg attributed it to scavenging of Ti by colloidal iron oxides. However, Moorby (1978), using selective leach techniques, found only 10-30% of the Ti was removed while 60-80% of the Fe was removed with acetic acid-hydroxylamine hydrochloride reagent. Therefore it seems that some of the Ti is in a different phase to the authigenic oxides. The correlation with Al in the seamount samples suggest a detrital contribution to the Ti content.

Calcium

Calcium shows no significant correlations in the Ridge samples. On the seamounts, there is a significant negative correlation with depth.

Calcium has been reported as an important constituent of marine ferromanganese deposits (Straczek et al., 1960). Electron microprobe studies have shown that within some deposits, Ca is enriched in Mn-rich areas (Cronan & Tooms, 1968; this work). Also, some of the Ca present in the samples may be in the form of authigenic carbonate material.

Magnesium

Magnesium behaves oddly in the seamount samples. It shows no significant correlations with any of the major input controls such as Fe, Mn, Al and depth, but correlates strongly positively with Ni, Cu, Zn, and Li. In the Ridge samples, Mg correlates with Mn, and appears subject to a strong mineralogical influence, the todorokite-containing samples containing higher than average Mg concentrations.

Local variations in specimen composition

Variations in specimen composition, both within a single specimen, and between separate specimens from the same site, have been investigated by several workers (Cronan & Tooms, 1967; Glasby,1970, 1973; Raab, 1972; Moorby, 1978). Some significant variations were observed by these authors.

From the present suite of specimens, those from 1301 show a distinct compositional variation between individual specimens. This variation appears to be related to a change in morphology. The specimens from 1317 show a distinct

compositional variation within the specimens. These stations are considered separately.

Geochemistry at station 1301

There appear to be two populations of crusts at this station, morphologically, mineralogically and chemically. The specimens containing todorokite are morphologically and chemically distinct from those containing no todorokite. Those containing todorokite have a hard surface 4-6 mm. deep, with a bubbly appearance. This material gave the strongest todorokite peaks. This zone was followed by a thin black laminar layer, which gave weaker todorokite peaks. Below this, the rest of these crusts were homogeneously brown-black, and showed only δ-MnO_2. Those specimens containing only δ-MnO_2 as their primary manganese mineral have flat microgranular surfaces, and have no visible zoning. The chemical differences between these two populations have already been discussed in Chapter 4. From a study of these differences, it appears the depositional histories of the two populations are quite different. The Cu, Pb, Zn, and Al values in group 2 are higher than in group 3 (Table 4.3), and the Ca is much lower in spite of the fact that they are mineralogically similar. Consequently, the two populations must have been obtained from different environments. This is possible since the dredge was on the sea floor for five hours, traversed some rugged topography, and passed through the lysocline. The first population, containing both todorokite and δ-MnO_2 contains high Cu and low Ca levels. This might suggest that it was obtained from below the lysocline, near the bottom end of the dredge traverse(4300m).

The second population, with lower Cu and higher Ca values may have come from the top of the traverse, above the lysocline (3600m).

Geochemistry at station 1317

The three crusts examined from this station all show a zone of low Mn/Fe ratio and high Al in the middle. Table 5.7 summarises the data. The following factors point to proximity to a volcanic eruption causing the change in chemistry in the middle of these crusts.

1) Increased Al concentration in the middle layer indicates a higher level of aluminosilicate debris.

2) The occurrence of strong quartz and felspar peaks in the X.R.D. traces (Chapter 4).

3) The occurrence of the broad unresolved "hump" of amorphous silica, which may be volcanic glass, in the X.R.D. traces.

4) The lack of this layer in crusts from stations close by (1315, 1318, 1325) indicates a local source for the event or events which created the layer.

Locations other than the North West Indian Ocean

Three nodules and two crusts from other parts of the world have been examined.

One nodule was the OSIRIS Specimen (Chapter 3), from the S.W. Indian Ridge. The chemical analysis is shown in Table 5.9. It has a low Mn/Fe ratio (0.62), and is low in nickel (1500 ppm). Cobalt is also quite low (2200 ppm). Lead and zinc are about the same as in the North West Indian Ocean samples, and copper is higher (1000 ppm). There is a large amount of aluminosilicate material incorporated in the nodule. This is shown by a high Al value (2.63%)

Table 5.7

Averaged analyses of 1317 A, B and C (first 2 columns) and 1317 A and B (last column)

Depth of Crust	0-5mm.	9-13 mm.	20-25 mm.
Mineralogy	δ-MnO_2	δ-MnO_2 quartz, felspars, clays.	δ-MnO_2. 1317C has some todorokite
Fe%	19.42	19.79	21.12
Mn%	18.61	8.42	16.07
Mn/Fe	.97	.43	.76
Co	3324	2863	3991
Pb	1638	1530	1828
Ni	2598	1367	2013
Cu	284	649	636
Zn	596	529	680
Al%	0.45	2.90	1.23
Ti	5925	7219	7222
Ca%	2.15	1.42	1.97
Mg%	0.96	1.00	1.01
Cd	5	4	6
Li	2	8	11

All concentrations are in p.p.m. unless otherwise stated.

and the marked presence of quartz, felspar and clay peaks in the X.R.D. trace. δ-MnO_2 is the only oxide phase to be distinguished. The other two nodules are from the East Pacific, one from the East Pacific Rise (1564) and one from the Bauer Deep (1578) (Chapter 3). They are mineralogically very similar, showing todorokite as the main oxide phase, with significant quantities of phillipsite incorporated. Table 5.8 compares the composition of 1564 and 1578 to the compositions of Bauer Deep nodules (Lyle et al., 1977).

The only differences between the composition of 1578 and the data of Lyle, et al. are in Co, Cu and Al. None of these are very large. 1564 is similar, but here the Fe is low compared with the Bauer Deep samples.

Two of the crusts (1370A and B) were from the Vema Trench area on the Central Indian Ridge. (Chapter 3). Their analyses are presented in Table 5.9.

Despite some morphological variation through them, their chemical composition hardly varies from top to bottom. Copper is the only element to show a coherent trend, increasing from 600 ppm in the surface to 1050 ppm in the bottom of 1370A, a distance of 10 mm. The levels of Mn, Fe, Zn, Ni, Pb and Co are similar to those in the N.W.Indian Ocean crusts. Al is quite low (.5-.6%) and remains about constant. δ-MnO_2 was the only oxide mineral identified.

1370B is very similar to 1370A. Cu increases from 900 ppm in the surface to 1500 ppm in the bottom, a distance of 15 mms. Thus both 1370A and 1370B appear to have the same copper concentration gradient of 40-45 ppm/mm. δ-MnO_2 is again the only oxide mineral present.

Table 5.8

Comparison of the compositions of 1564, 1578 and Bauer Deep nodules.

	1564	1578	Bulk composition of Bauer Deep Nodules (Lyle et al., 1977).		
			Average	Minimum	Maximum
Fe%	7.47	10.05	10.09	8.26	13.1
Mn%	29.12	30.70	29.5	27.0	33.8
Co	1198	455	960	640	1130
Pb	322	109	--	--	--
Ni%	1.18	1.06	1.47	1.36	1.59
Cu%	.64	.68	.724	.625	.829
Zn	1506	1558	1790	1490	2390
Al%	1.8	.98	1.68	1.14	1.91
Ti	2536	1024	--	--	--
Ca%	1.51	1.44	1.63	1.35	1.91

Table 5.9

Compositions of S.W.Indian Ocean nodule, and crusts from 1370

	S.W. Indian Ocean	1370A				1370B			
		0-2mm.	3-6mm.	7-8mm.	8-10mm.	0-4mm.	4-6mm.	8-12mm.	12-15mm.
Fe %	19.86	20.89	21.36	20.11	21.79	21.77	22.09	22.79	24.21
Mn %	12.26	14.90	15.86	16.48	15.45	16.18	16.02	16.31	14.32
Co	2160	2294	2125	1958	1957	1564	1411	1320	1067
Pb	1000	669	594	600	569	575	559	482	465
Ni	1456	1912	2072	2164	2036	1842	1825	1852	1594
Cu	953	618	795	970	1053	892	983	1257	1459
Zn	539	524	510	504	513	534	541	524	637
Al%	2.63	0.51	0.57	0.48	0.59	0.53	0.54	0.60	0.82
Ti%	1.11	0.52	0.49	0.38	0.47	0.37	0.36	0.30	0.28
Ca%	1.8	3.50	2.92	1.82	2.87	3.0	2.98	2.28	2.87
Mg%	1.37	0.88	0.89	0.71	0.91	0.88	0.93	0.92	0.91

Discussion

There are three sources of the constituent metals of marine ferromanganese oxide deposits. These have long been accepted as continental weathering and river run-off, submarine volcanic activity, and migration from sub-surface sediments. One of the major aims of this work is to try and evaluate the importance of the second of these sources, volcanic activity. By comparing the seamount samples with the Ridge samples, it was hoped that it might be possible to distinguish volcanic influences present in a tectonically active area such as the Carlsberg Ridge from non-volcanic influences present in a volcanically quiet area such as the seamounts. Depending on the geochemical history of the depositional environment of ferromanganese oxide deposits on the seafloor, then the significance of each source will have fluctuated. If a series of deposits at known distances from the crest of an active Ridge are investigated then it may be possible to determine the relative importance of each source on the character of the deposits.

Bonatti et al., (1972) have suggested chemical criteria for distinguishing between the influences of each source. They state that volcanically influenced deposits are characterised by generally low Mn/Fe ratios and contain low concentrations of Cu, Ni and Co relative to hydrogenous deposits. If the three variables Fe, Mn, and (Cu+Ni+Co)X10 are plotted on a ternary diagram, then it can be seen that only a few of the seamount samples and none of the ridge samples appear to be volcanically derived (Figs. 5.18 and 5.19).

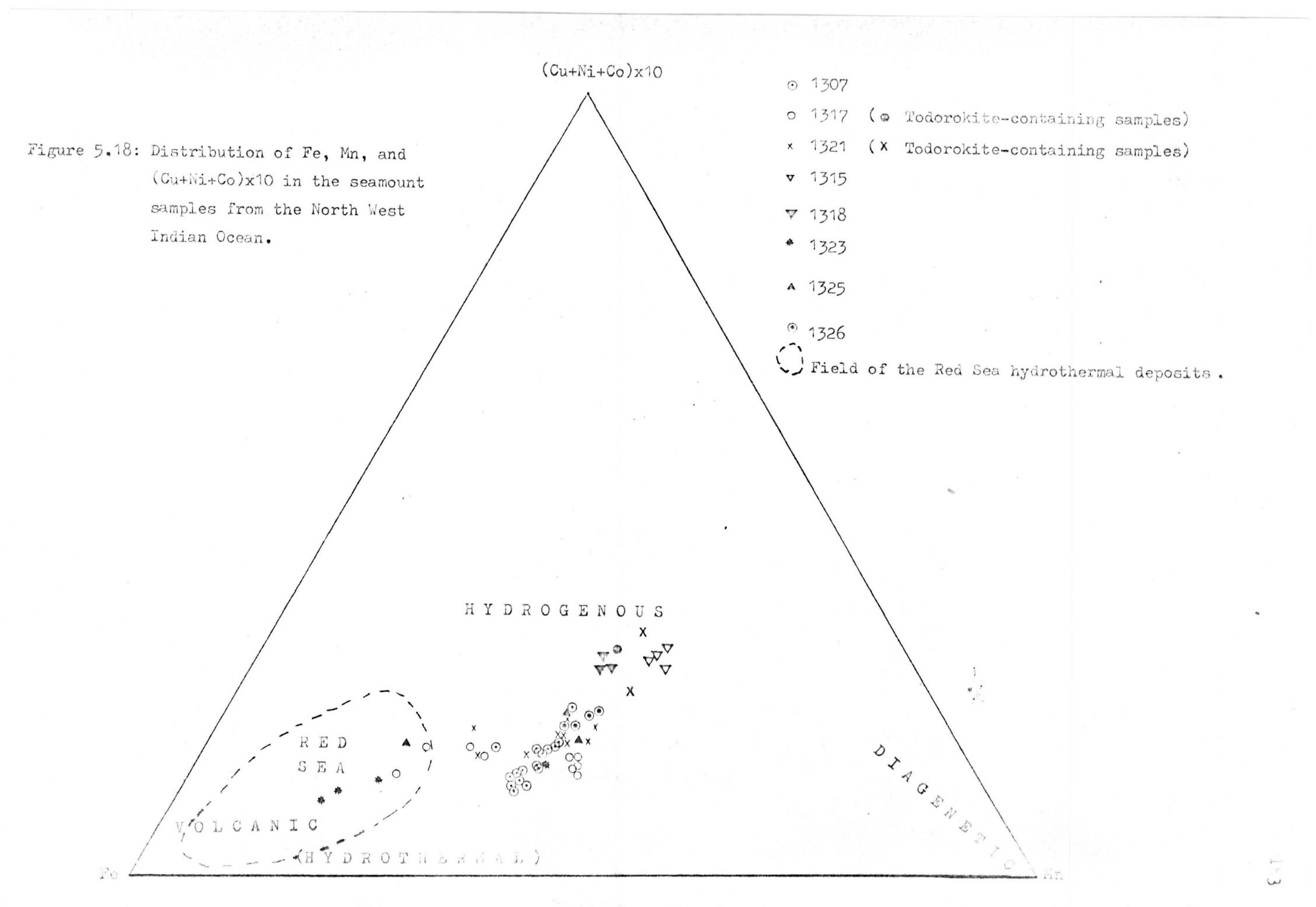

Figure 5.18: Distribution of Fe, Mn, and (Cu+Ni+Co)x10 in the seamount samples from the North West Indian Ocean.

Figure 5.19: Distribution of Fe, Mn, and (Cu+Ni+Co)x10 in the Ridge samples from the North West Indian Ocean.

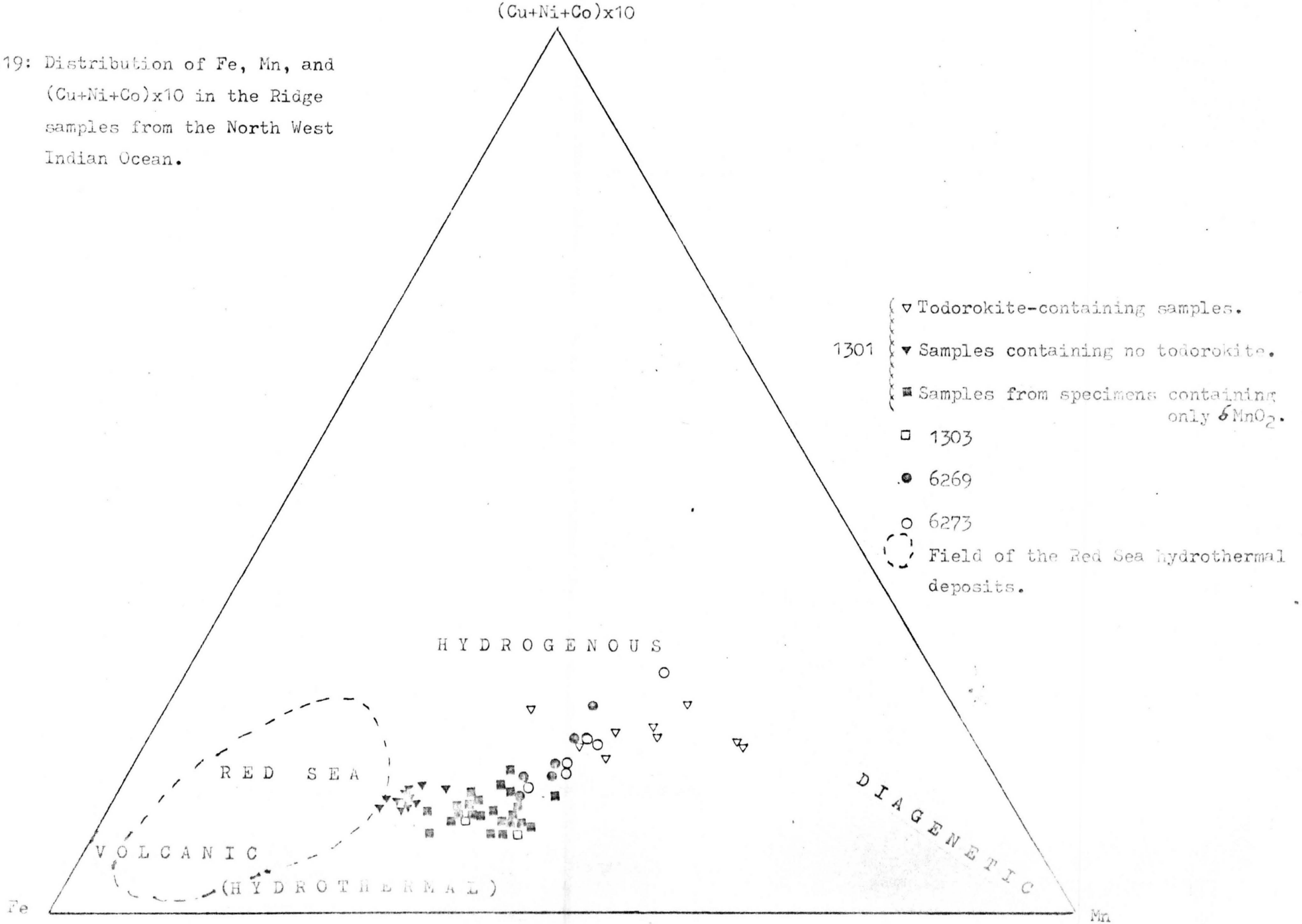

If we consider the samples plotting in the Red Sea field as hydrothermal in origin, there are three samples from station 1323, two from 1317 and one from 1325 which are similar and might also exhibit hydrothermal influences. It was described on page 47 how the samples from 1317 are thought to have been volcanically derived. The samples from 1323 lack three of the characteristics which those from 1317 possess.

1. The Al concentration of the three samples in question are about average for the group, indicating no excess aluminosilicate material.

2. There are no strong quartz or felspar peaks in the X.R.D. traces.

3. The broad, unresolved hump of volcanic glass or opaline silica is absent from the X.R.D. trace. Therefore while some chemical characteristics indicate hydrothermal influences on these samples the mineralogical characteristics do not indicate a volcanic origin for them.

The sample from 1325 has a high Al content (4.12%), and this is reflected in the high levels of detrital minerals indicated in the X.R.D. pattern. This sample fulfills both chemical and mineralogical criteria for volcanic influences, and so it may have suffered some hydrothermal input.

1317 and 1325 are two of a cluster of four stations taken close together on the southern seamount group (Fig. 3.1). The crust samples from the other two sations (1315 and 1318) plot well inside the hydrogenous zone of Figure 5.18 and appear to have no identifiable volcanic

contributions. The volcanic effects on the crusts in this area of the southern seamount group therefore appear to be localised to 1317 and 1325.

In conclusion, bulk chemical analyses of whole encrustation sections have shown no regional trends that can be related specifically to submarine volcanic activity. However, with a more detailed study of the layer-by-layer composition of encrustations, possible submarine volcanic influences have been found in some seamount samples, but not in any Ridge samples, where they might be most expected. The duration of a volcanic eruption is probably short compared with the period of deposition of a ferromanganese oxide deposit. Therefore a volcanic source will only be reflected in the deposits formed during and immediately after the eruption. Those deposits precipitated between eruptions should be similar to those formed in non-volcanic areas, and comprise the bulk of the samples examined in this study.

CHAPTER 6

ELECTRON PROBE MICROANALYSIS OF FERROMANGANESE OXIDE CRUSTS

Introduction

Electron probe microanalysis techniques have been used by previous workers to obtain information concerning inter-element relationships and the chemical composition of ferromanganese oxide deposits (Burns & Fuerstenau, 1966; Cronan, 1967; Winterhalter & Siivola, 1967; Glasby, 1970; Fein & Morgenstein, 1973; Burns et al., 1975). Burns & Fuerstenau (1966), used semi-quantitative one-dimensional line scans to show inter-element relationships in a nodule. Cronan, (1967), used the X-ray image intensity to show such relationships qualitatively in two dimensions. The line scan approach was also favoured by Glasby,(1970). Fein & Morgenstein, (1973), made comprehensive use of quantitative spot analyses to examine the relationship between ferro-manganese oxide crusts and basalt weathering.

The reason for using the electron microprobe in this work was to enable a chemical study of the microstructure of the deposits to be made. From the information thus

obtained, it may be possible to determine the origin of a particular part of a crust.

Instrumental methods

Two electron probes were available and the techniques used varied with each machine because of the different facilities available on each. The machine used initially was a Cambridge Geoscan equipped with a wavelength dispersive detection system. The machine used later was a Cambridge Microscan Mk5 fitted with an energy-dispersive(E.D.) detection system. The details of operating conditions are given in Appendix 4. The detection limits for most of the elements studied on the Geoscan were between 100 and 1000 p.p.m., depending on the counting time and the actual concentration of the element. The E.D. system had poorer detection limits; in the present study, they mostly fell between 500 and 2000 p.p.m. Two techniques were used to investigate the specimens. These were as follows:

a. A regular matrix of point analyses was carried out on selected areas of certain specimens to try and obtain a chemical map. This was carried out using the automatic facilities available using a Digico Micro 16 minicomputer interfaced with the Geoscan. It was possible to carry out a regular grid of several hundred analyses by this means. The grid origin, dimensions, and the number of analyses in each dimension were input at the beginning of each grid. A detailed description of both hardware and software available on the Imperial College Geoscan is given in Frost et al., (1976). Output of the data was by means of paper tape. Because of the small size of the core (only

4K of 16 bit words) of the computer, the only on-line data processing was subtraction of the background counts from the analysis counts. The raw data thus obtained were processed on the Imperial College computers using the Mk7 interactive program described by Frost (1977).

It has been found that on the Geoscan, the specimen relocation under the electron beam is more efficient than spectrometer relocation on the element peak angle. (Suddaby, pers.comm.). Consequently, the control programme used was designed to set the two spectrometers on the element peak angles and move the specimen through a complete grid for the two elements in question, rather than analyse each point for all the elements desired before moving to the next point. The advantage is that this approach gives a grid of analyses for any particular pair of elements which is internally consistent (machine drift notwithstanding). Therefore the grids had to be traversed a number of times to obtain data for all the elements desired. While relocation of the grid origin was quite accurate, it was not perfect. Therefore, instead of analysing exactly the same grid a number of times, a series of grids very close to one another were analysed (to within about 4-5μ). Therefore quantitative analyses for individual spots were not possible. Consequently, the atomic number, fluorescence and absorption corrections usually applied to probe data could not be carried out. The concentrations thus measured are only semi-quantitative. The only correction applied was that of counter dead time. The final data were therefore uncorrected concentrations of the elements calculated from the formula:

$$\text{wt.\% element} = \frac{\text{Specimen pk. count rate} - \text{specimen bgnd. count rate}}{\text{std. pk. count rate} - \text{std. bgnd. count rate}} \times \text{wt. \% element in standard}$$

The concentrations calculated in this manner were plotted using an interactive three-dimensional matrix mapping package available on the Imperial College computer graphics network. This program (called MATMAP) plots the element concentrations on the z-axis, and the x and y axes of the plots are the x and y areas of the analysis grid. The advantage of this plotting technique over X-ray image intensity scanning (Cronan & Tooms, 1968) and line scans (Glasby, 1970; Sorem & Fewkes, 1977) is that this method provides a much more quantitative estimate of element concentrations than the areal concentration of dots on an oscilloscope image. It also provides it in two dimensions rather than the single dimension of a line scan.

b. A number of quantitative point analyses were carried out on specimens selected on the basis of the results of the grid analysis and from inspection with a microscope. These analyses were carried out on the Microscan Mk.5 using the energy-dispersive detection system and on-line data processing with a Link Systems System 290 modular software package. This enabled a full analysis, (except for H_2O) of each spot to be made, and so the usual ZAF corrections were applied.

Results

The most interesting grids were obtained from crusts from stations 1301, 1317 and 1321, from where crusts were found which contained todorokite as well a δ-MnO_2. (Chapter

4). The results are presented and discussed station by station.

Station 1301

A todorokite-bearing crust from this station was selected for preparation for probe analysis. Visually, the crust showed a bright massive layer about ½ mm. to 1 mm. wide on the top surface, sharply separated from the interior of the crust which showed a cusp-type growth form Plate 6.1 shows the backscattered electron (B.S.E.) image of the grid area. An exploratory grid of spacing 80μ was carried out from the interior to the outside. The length was 4.72 mms. (59 analyses) and the width was 0.96 mms. (12 analyses). Four pairs of elements were analysed : Fe and Mn, Ca and Al, Ti and Si, and Ni and Co. The plots are shown in figures 6.1 to 6.11.

Figure 6.1 shows the map of the Mn concentration. Apart from one spurious point, the concentrations in the interior range from about 10% to 15%. In the outer zone concentrations are generally 35-45%. Ni is also much higher here (Fig.6.2), generally between 1 and 1½%, while inside it is only 0.2 to 0.3%. Co shows no such demarcation (fig.6.3). Fe is low in this outer zone, generally about 2% (Fig.6.4). Inside it is about 16-20%; it shows an increasing trend with depth in the crust (Fig. 6.5). Ti tends to follow Fe: there is a greater number of analyses greater than 0.4% at depth in the crust then there is at the outside (Fig.6.6). Ti is present at a lower level in the outer zone (.1 to.2%) than in the inside (.3 to .7%) (Fig. 6.7). Al shows an erratic distribution (Fig. 6.11). There appear to be two

Figure 6.1: Mn, 1301, First Grid.

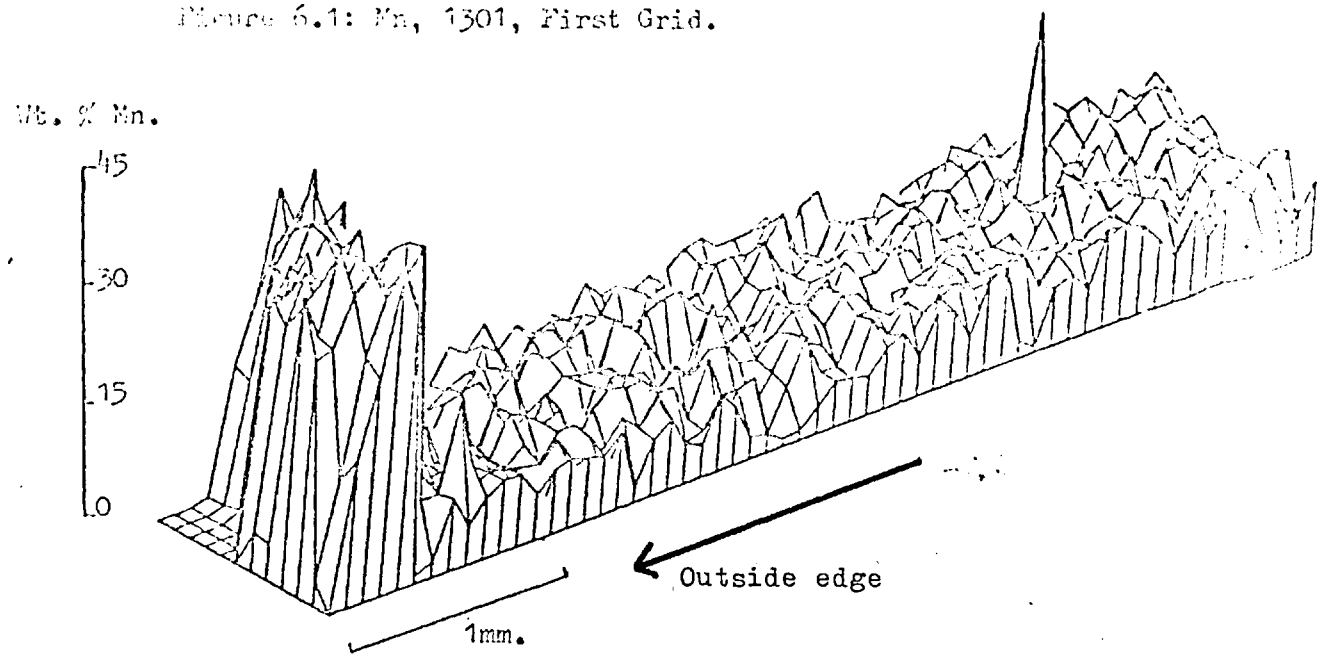

Figure 6.2: Ni, 1301, First Grid.

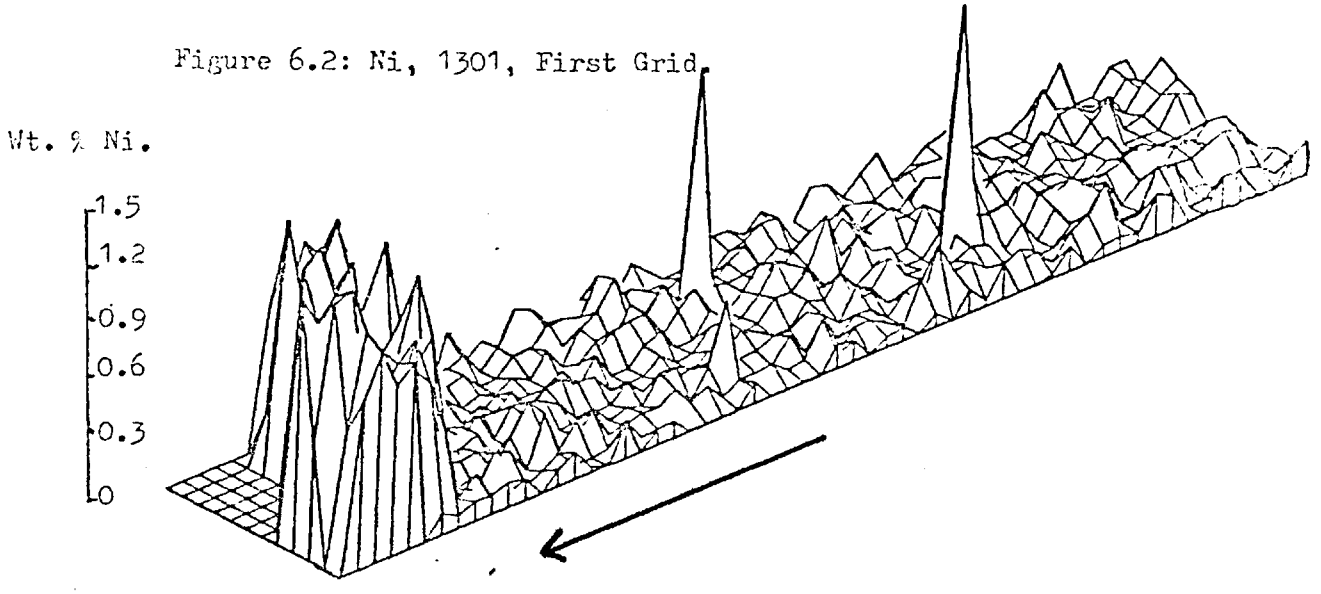

Figure 6.3: Co, 1301, First Grid.

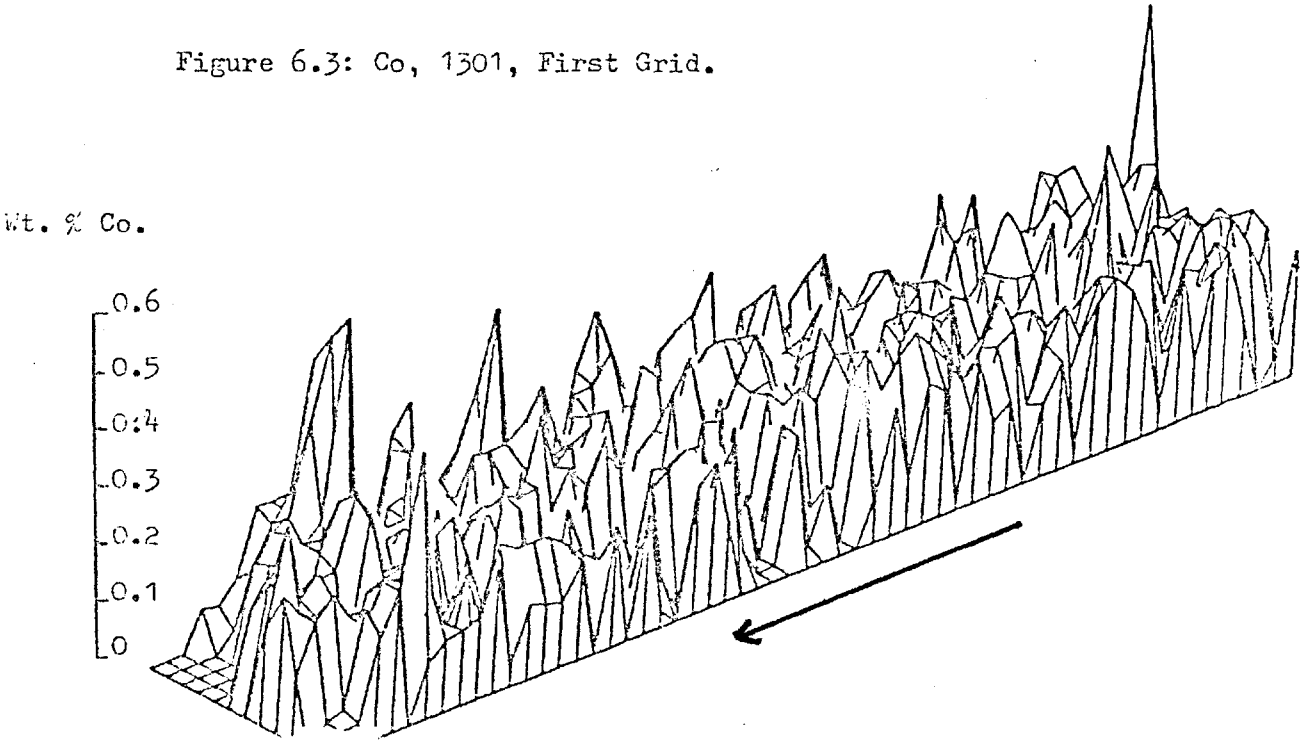

Figure 6.4: Fe, 1301, First Grid.

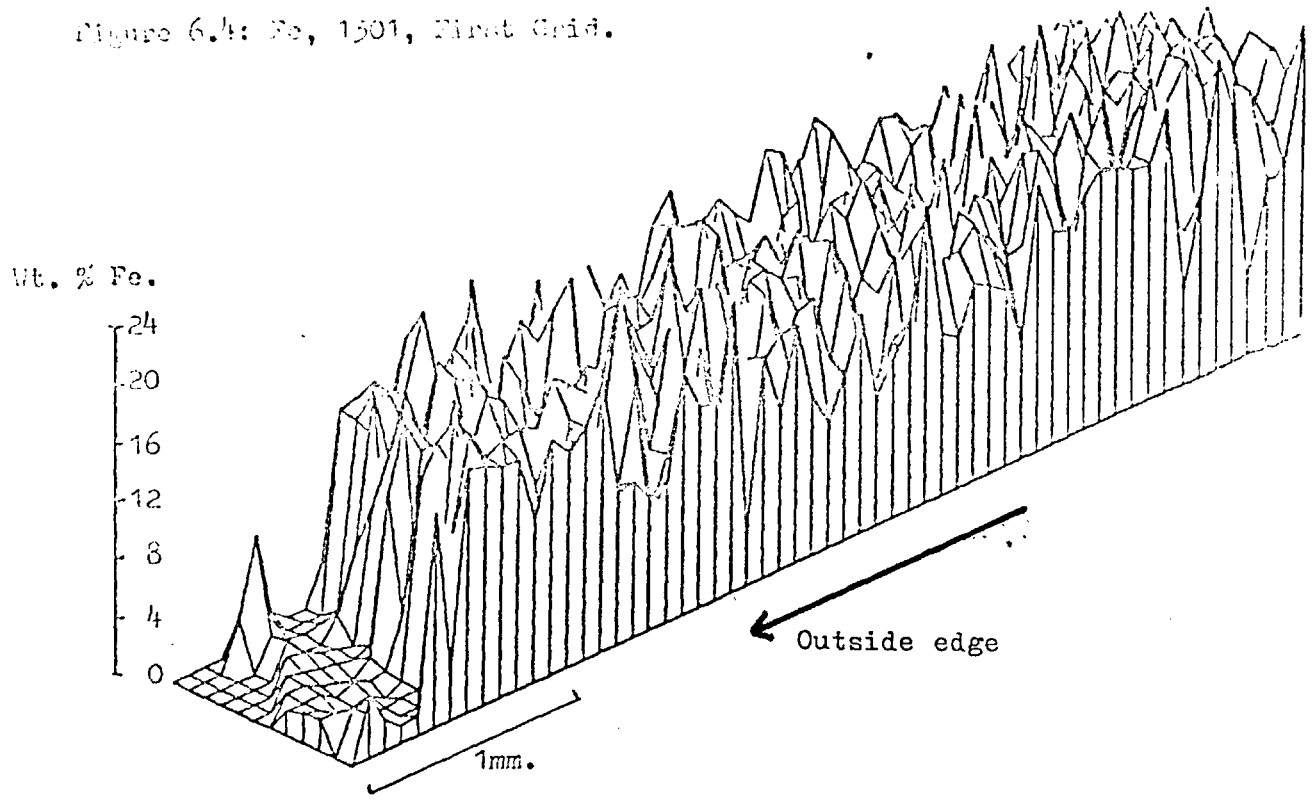

Figure 6.5: Fe, 1301, First Grid; Cut-off= 16%.

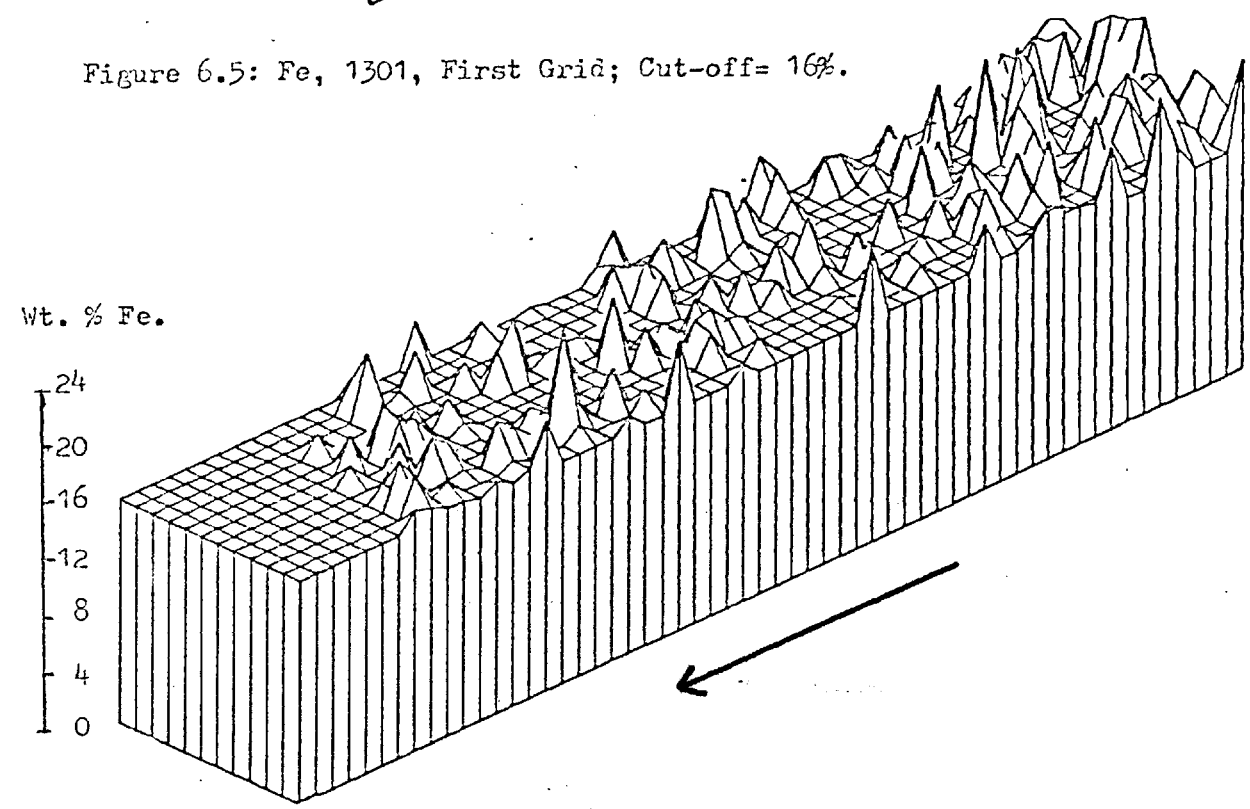

Figure 6.6: Ti, 1301, First Grid.

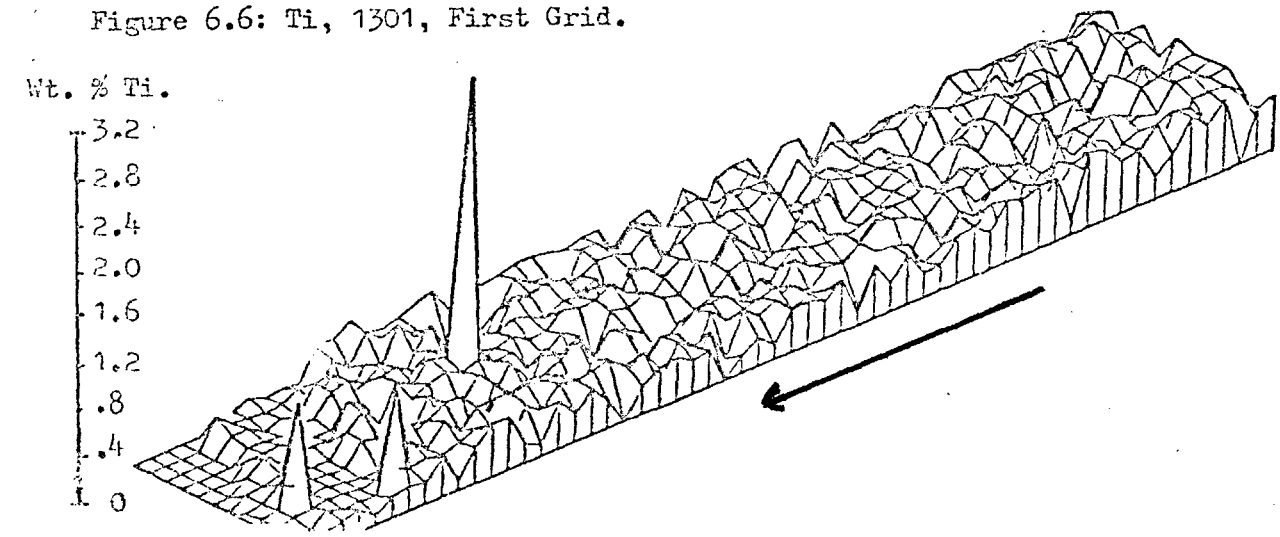

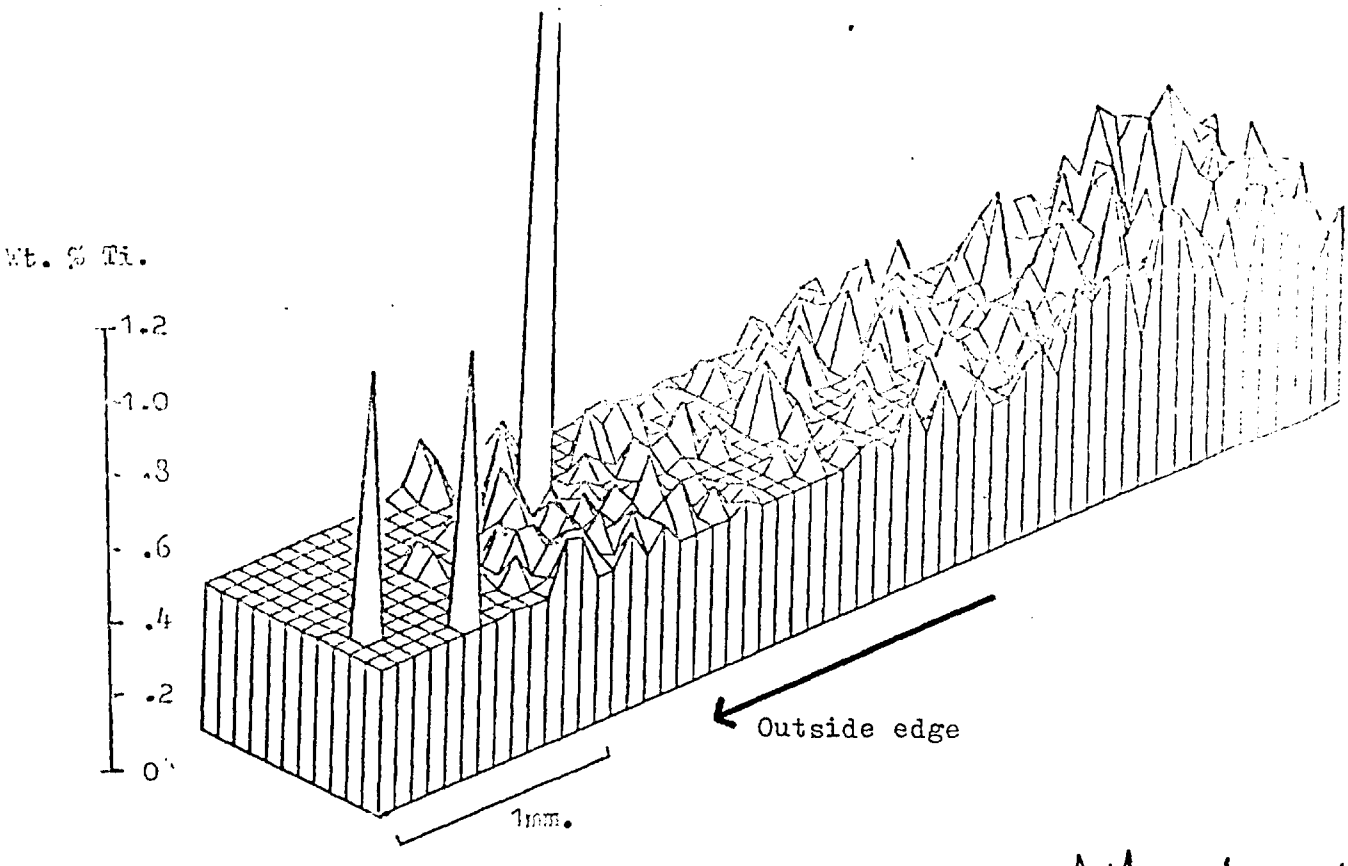

Figure 6.8: Si, 1301, First Grid.

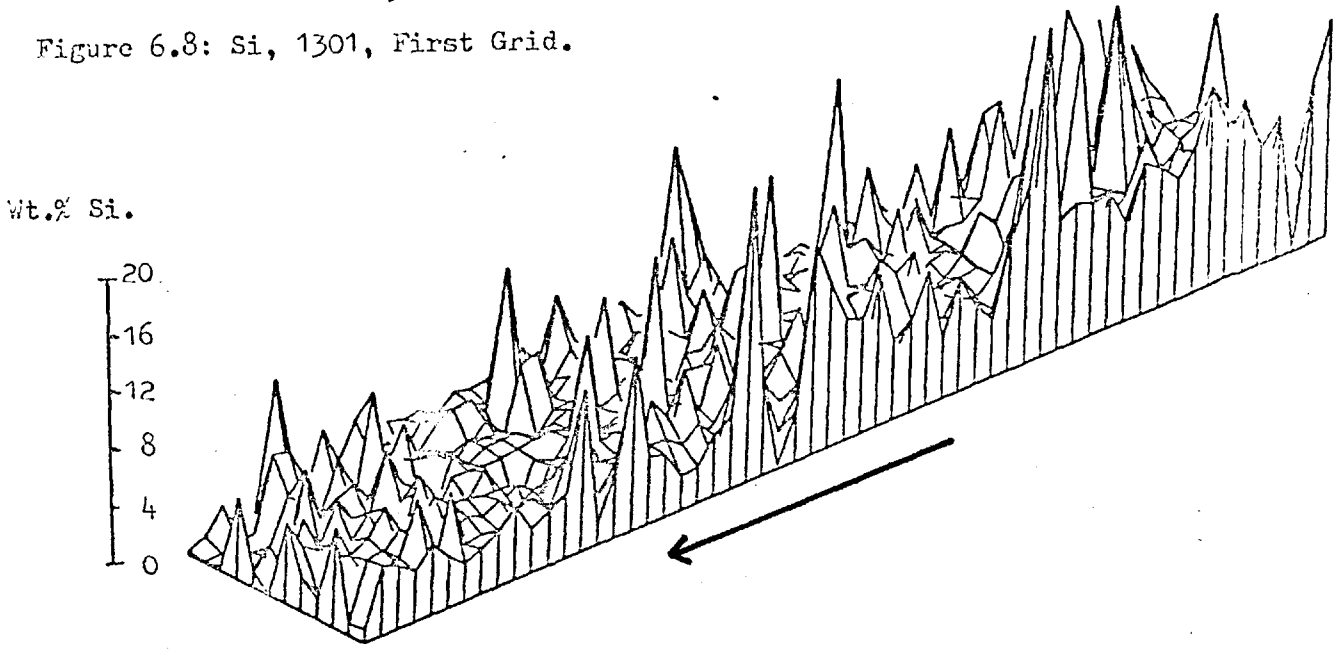

Figure 6.9: Ca, 1301, First Grid.

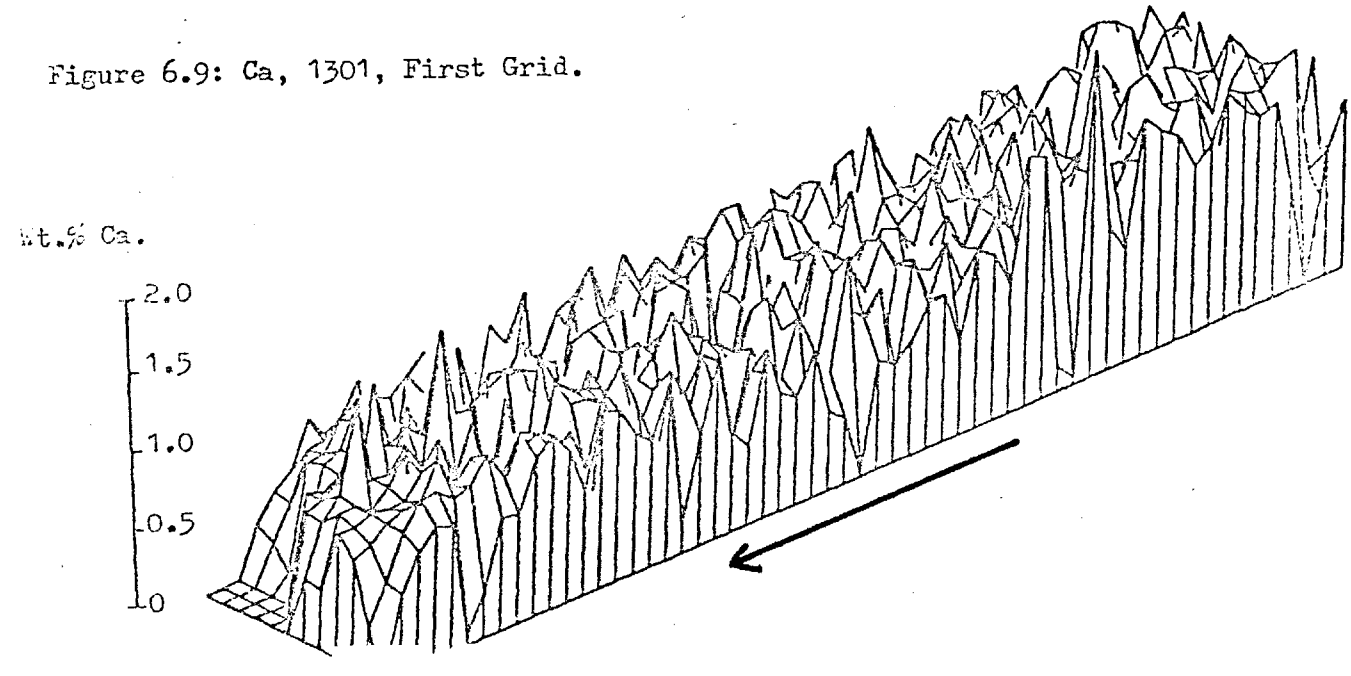

Figure 6.10: Ca,1301, First Grid; Cut-off= 1%

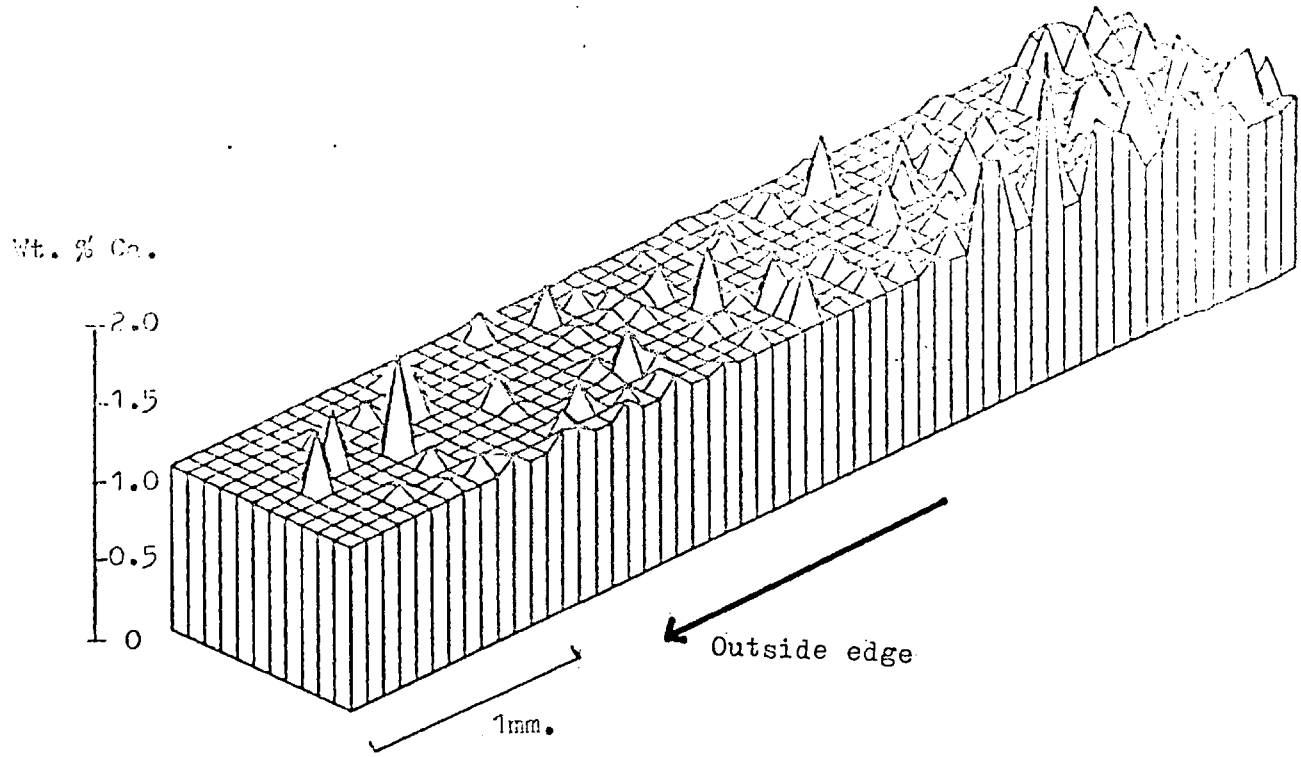

Figure 6.11: Al, 1301, First Grid.

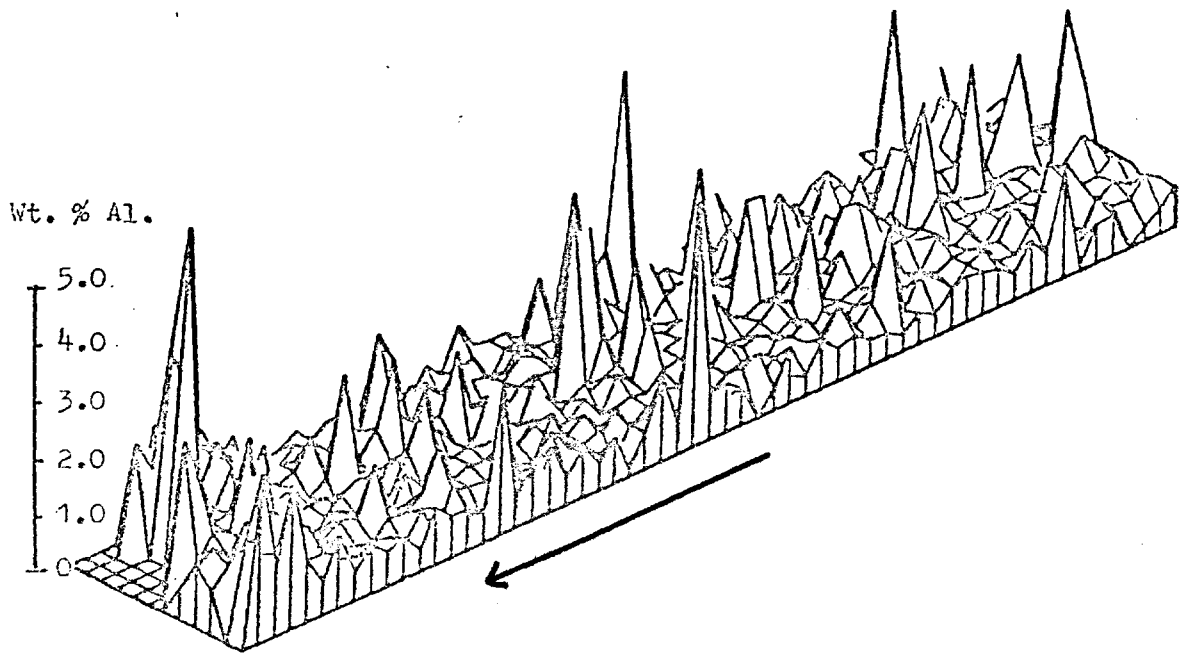

components to the aluminium. One component is about 0.5 to 1% Al, and the other is about 2 to 4% Al. The first component is probably Al associated with the oxide phase, and the second is probably Al associated with detrital aluminosilicate material. It is these analyses which appear to be erratic, and may be explained by the presence of detrital particles which have become trapped between the cusps of ferromanganese oxides as they have accreted (Dunham & Glasby , 1974). The level of Al in the outer zone appears to be generally higher than in the inner zone. Si also has an erratic distribution (Figure 6.8), probably for the same reason that Al does. Ca has a fairly even distribution (Fig.6.9), but shows higher concentrations deeper into the crust. (Fig.6.10).

The data obtained from the energy dispersive system on the Microscan (i.e. the point analyses) can be split into analyses from four zones:

Zone 1 is the thin massive outer zone (18 analyses).

Zone 2 is the interior of the crust showing a cuspate pod growth structure (i.e. essentially the rest of the crust) (37 analyses).

Zone 3 is the clay infilling of a healed fracture at depth in the crust (13 analyses).

Zone 4 is the oxide infilling of the same fracture (23 analyses).

Table 6.1 summarises the data. Figure 6.12 presents the differences between the element abundances in Zones 1 and 2. The mean element values from each zone have been subtracted from each other and the differences plotted

Element	Means, wt.%				Maxima				Minima			
	Zone 1	Zone 2	Zone 3	Zone 4	Zone 1	Zone 2	Zone 3	Zone 4	Zone 1	Zone 2	Zone 3	Zone 4
Na	..63	1.04	0.75	1.09	1.39	3.46	.88	1.50	0.38	0.28	0.64	0.47
Mg	2.16	0.89	2.64	2.44	2.41	3.39	2.98	3.63	1.74	0.41	2.34	1.70
Al	1.14	1.26	4.48	1.60	2.11	4.71	5.03	3.08	0.62	0.37	4.07	0.09
Si	3.12	6.62	21.9	4.32	13.6	18.9	22.8	12.80	0.98	1.51	19.9	0.14
P	N.D.	0.15	N.D.	N.D.	N.D.	0.23	N.D.	N.D.	N.D.	0.09	N.D.	N.D.
Ca	1.05	1.14	.13	0.65	1.38	1.97	0.23	1.61	0.61	0.23	0.08	0.43
Mn	47.3	11.5	1.07	43.1	53.2	24.4	1.23	56.0	34.3	1.20	0.91	14.9
Fe	1.89	19.6	10.6	3.16	3.63	26.8	13.8	10.5	0.58	8.68	8.24	0.61
Co	0.29	0.46	N.D.	0.31	0.50	0.71	N.D.	0.41	0.20	0.27	N.D.	0.25
Ni	0.69	0.40	N.D.	0.92	1.17	1.37	N.D.	2.06	0.35	0.13	N.D.	0.28
Cu	0.40	0.21	N.D.	0.42	0.58	0.40	N.D.	0.62	0.27	0.14	N.D.	0.29

Table 6.1 E.D.S. probe data for 1301.

N.D. : not detected.

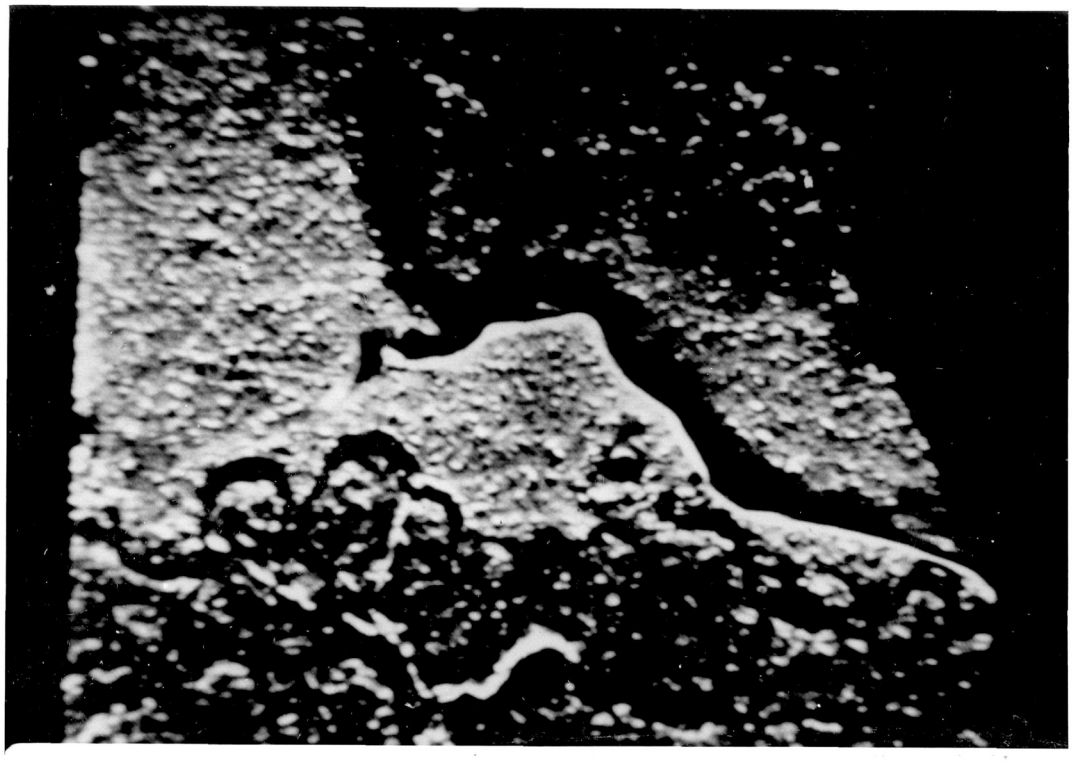

Plate 6.1: Back-scattered electron image of part of first grid area. specimen from 1301. ⊢——⊣ 100μ

Plate 6.2: Back-scattered electron image of the second grid area, specimen from 1301. ⊢——⊣ 100μ

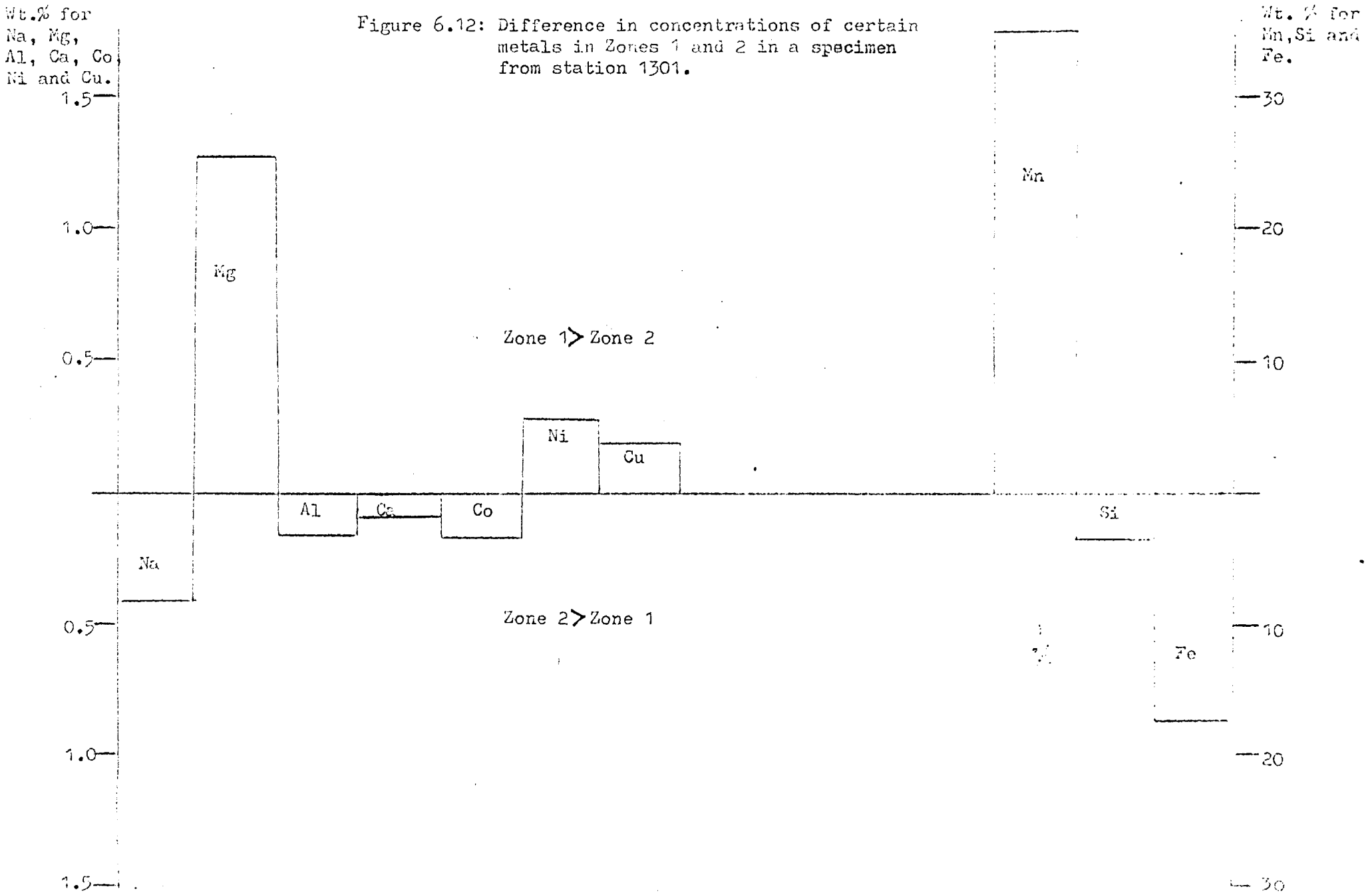

Figure 6.12: Difference in concentrations of certain metals in Zones 1 and 2 in a specimen from station 1301.

either below the zero line if there is more of the metal in zone 2 or above the line if there is more of the metal in Zone 1. All the metals except Al and Ca show significant differences between the two zones. There is a very high level of Mn in Zone 1 (47%) and this is accompanied by higher values of Cu (0.4%), Ni (0.7%) and Mg(2.1%) than in Zone 2. Fe and Co are much higher in Zone 2 (20% and 0.46%) than in Zone 1. Si and Na are also much higher and Al and Ca are marginally higher in Zone 1.

A further grid was analysed across the healed fracture in this sample, described in detail later in this chapter. The grid was carried out across the interface of the normal crust interior and the filling of the fracture. Plate 6.2 shows the B.S.E. image of the grid setting. The grid consisted of a square of 400 points (20 x 20) with a spacing of 20μ. Figures 6.13 to 6.22 show the element maps for this grid. Mn is shown in figure 6.13. The bright vein of massive oxide material (plate 6.2) corresponds to Mn values of 30 to 50%, while the cuspate pod structures have Mn at about the 10-15% level. The grid for Ni was offset from the grids for the other elements by about 150μ. The vein cuts the top edge of the grid instead of running through the top half of the grid. This is why the high Ni values seen in figure 6.14 do not correspond exactly with the high Mn values in Figure 6.13. Ni is high in the vein, averaging about 1%, (fig. 6.14). It is often not detectable in the pod structures.Cu is around the .2 to .3% level in the latter, rising to .5 to 1%, and occasionally 1.5% in the vein (Fig. 6.15).Cobalt (Figs.6.17 and 6.18) appears

Figure 6.13: Mn, 1301, Second Grid.

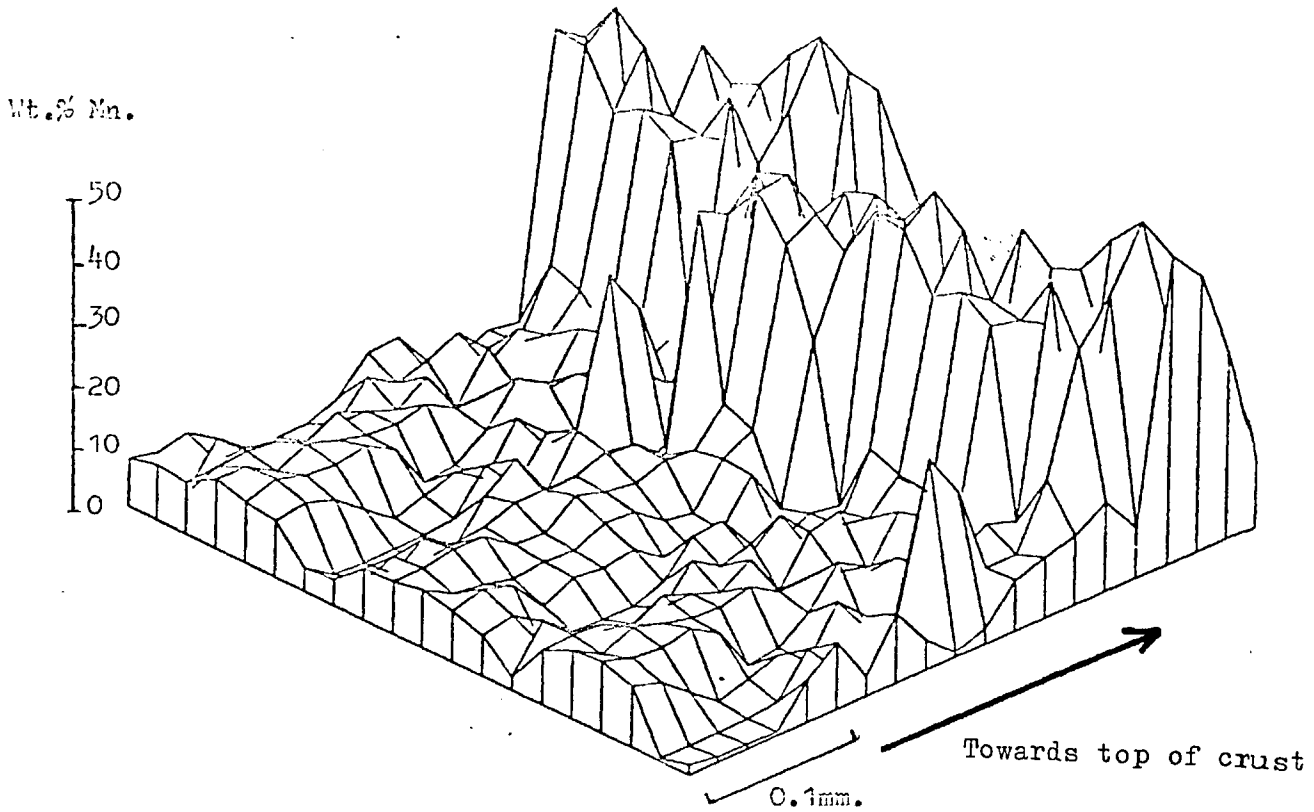

Figure 6.14: Ni, 1301, Second Grid.

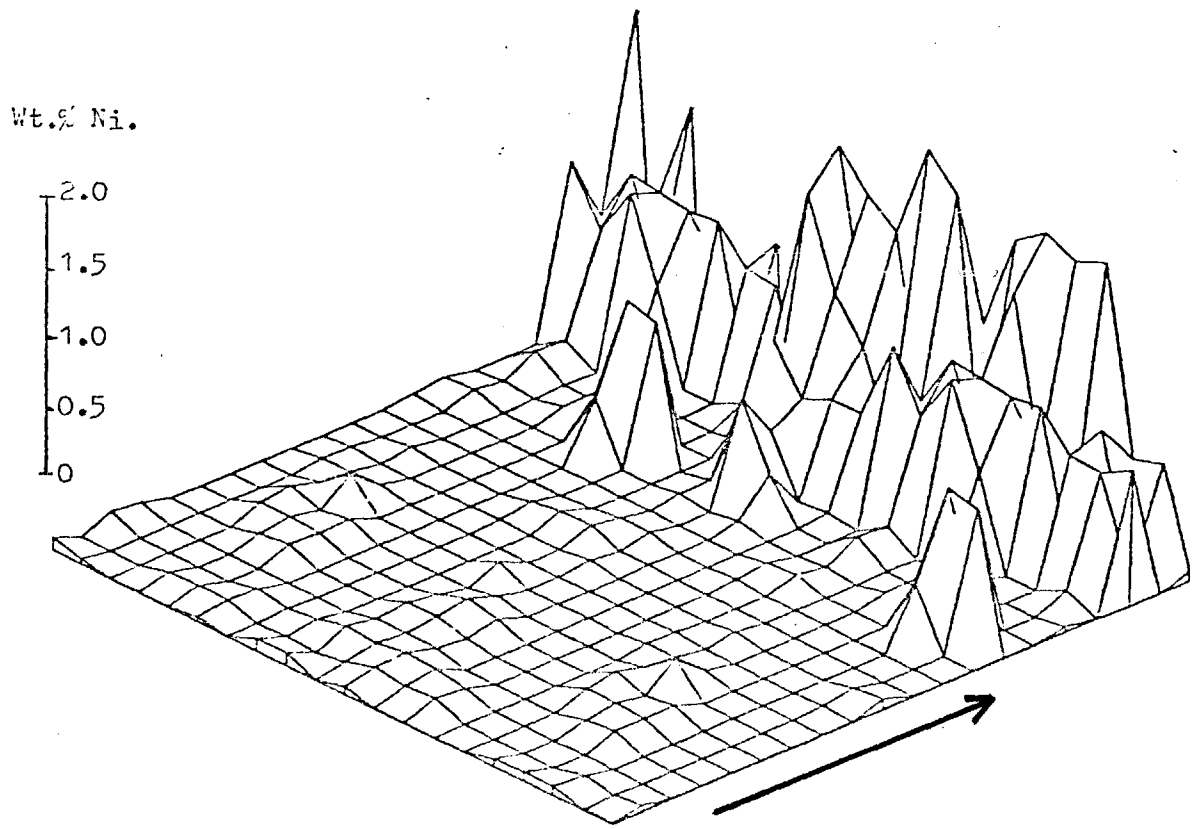

Figure 6.15: Cu, 1301, Second Grid.

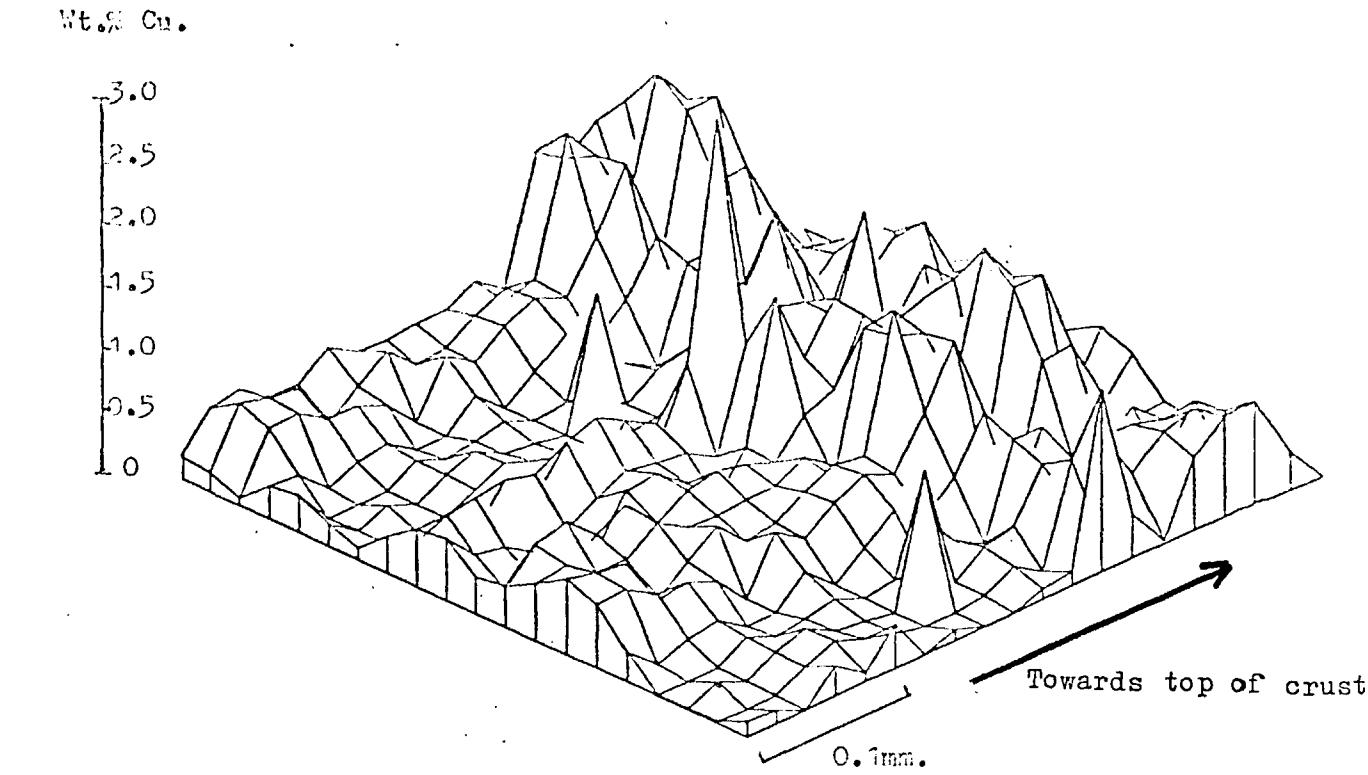

Figure 6.16: Fe, 1301, Second Grid.

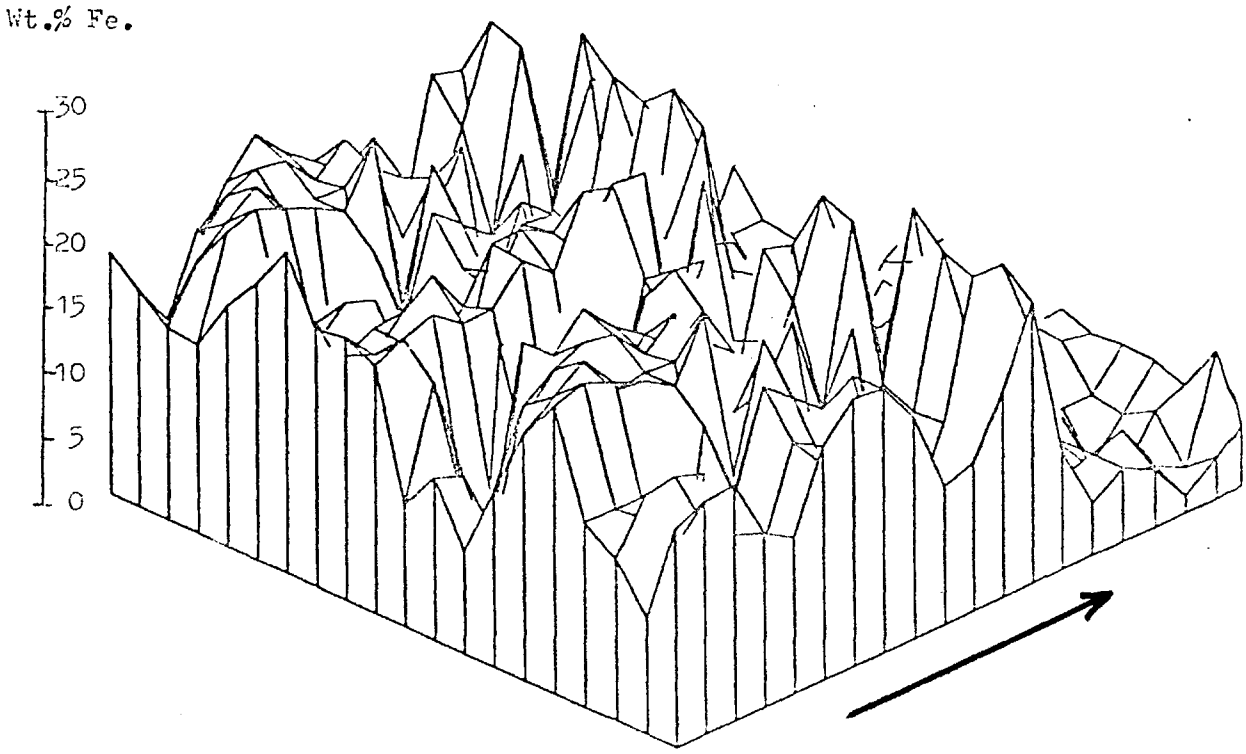

Figure 6.17: Co, 1301, Second Grid.

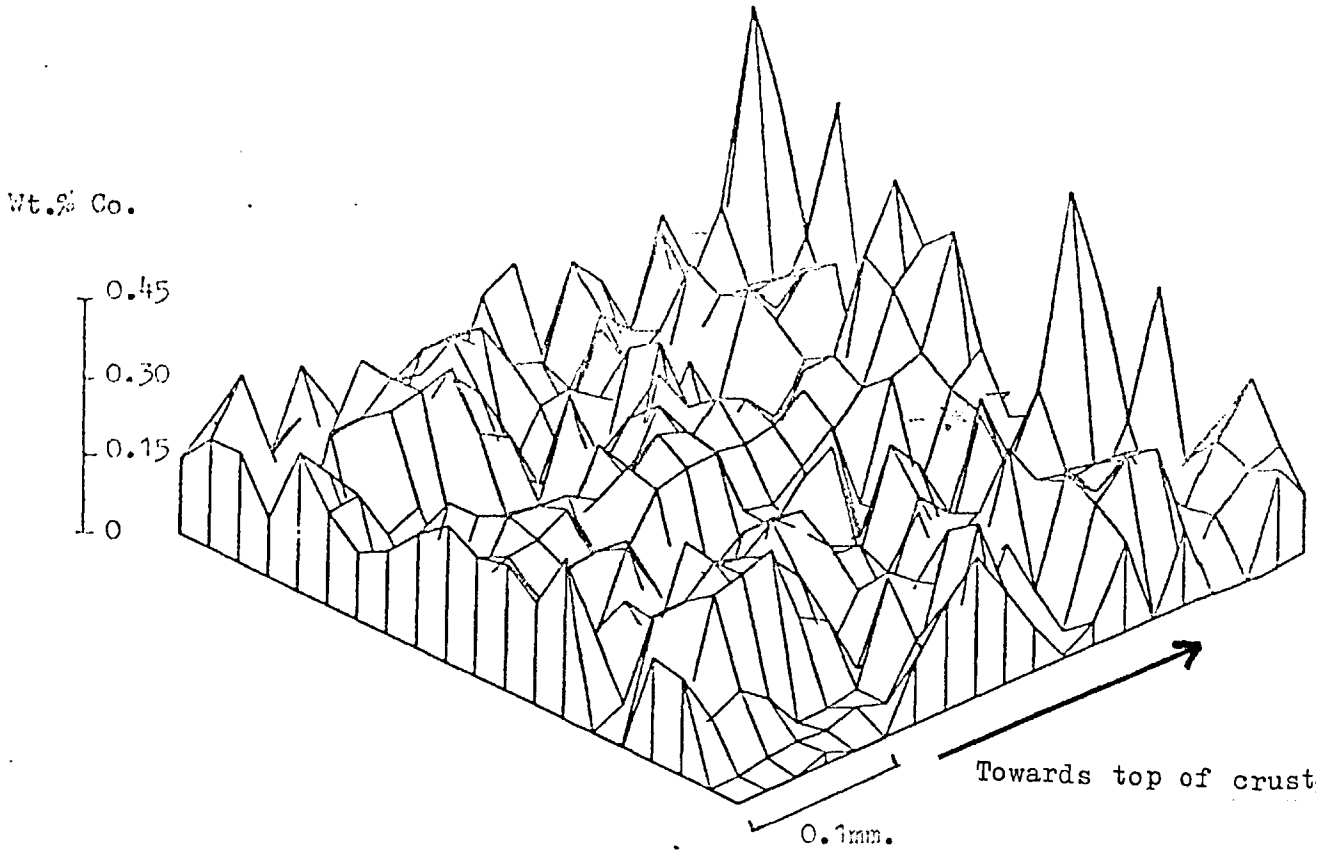

Figure 6.18: Co, 1301, Second Grid.
Cut-off= 0.15%.

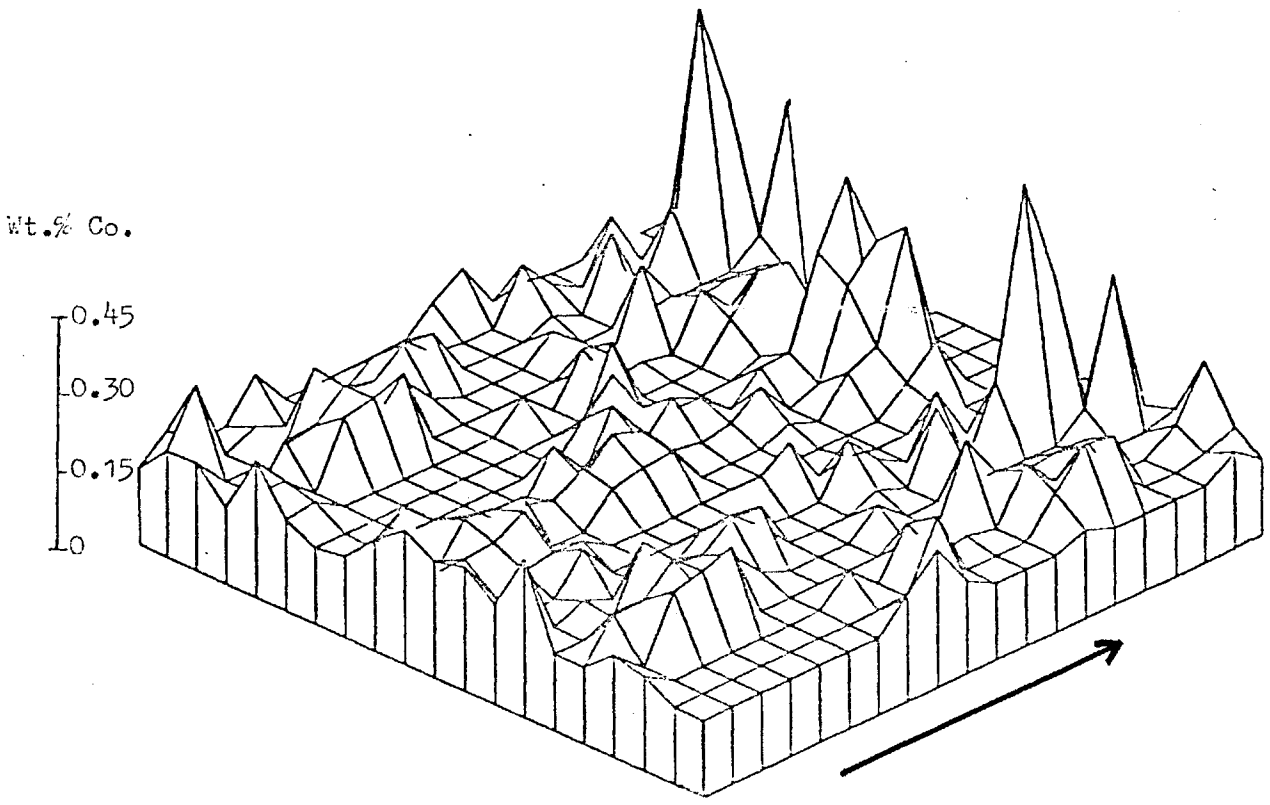

Figure 6.19: Ti, 1301, Second Grid.

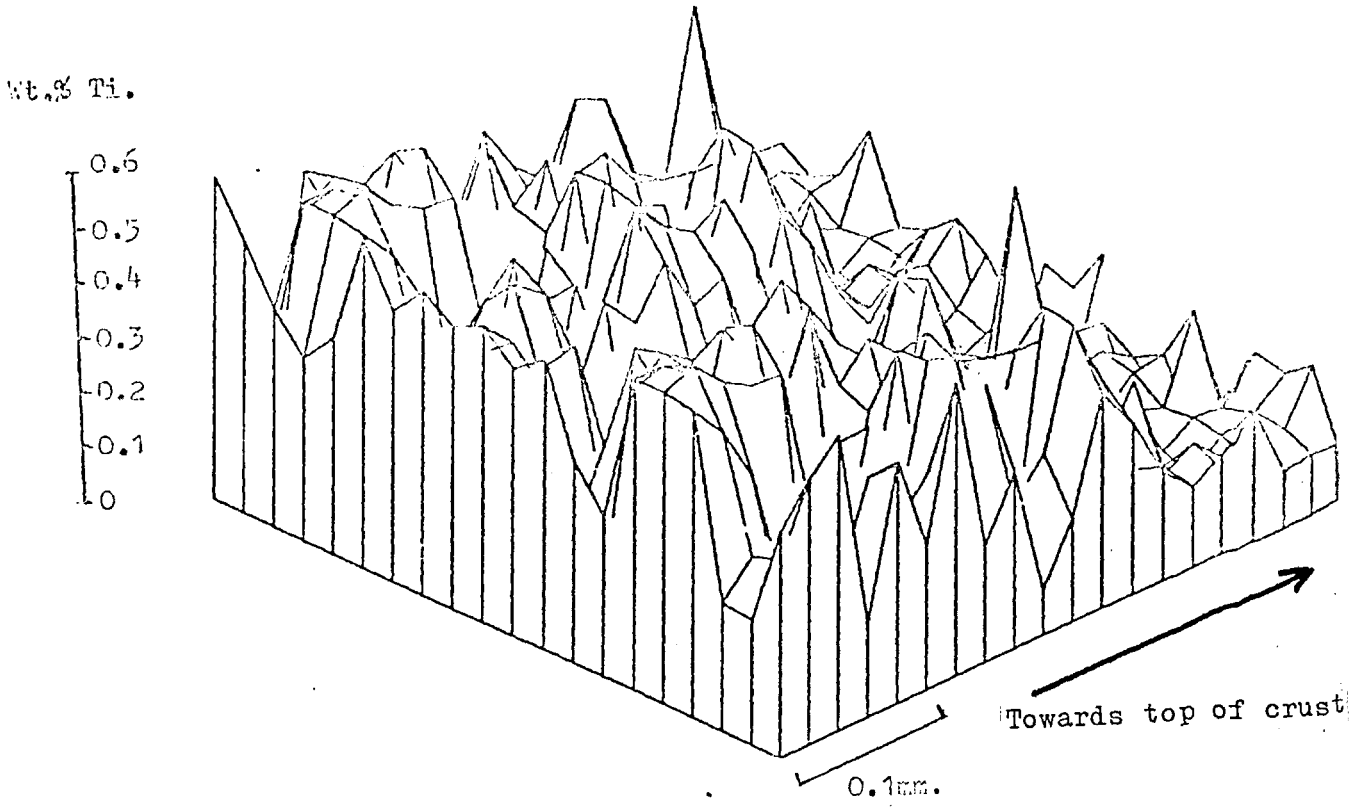

Figure 6.20: Ca, 1301, Second Grid.

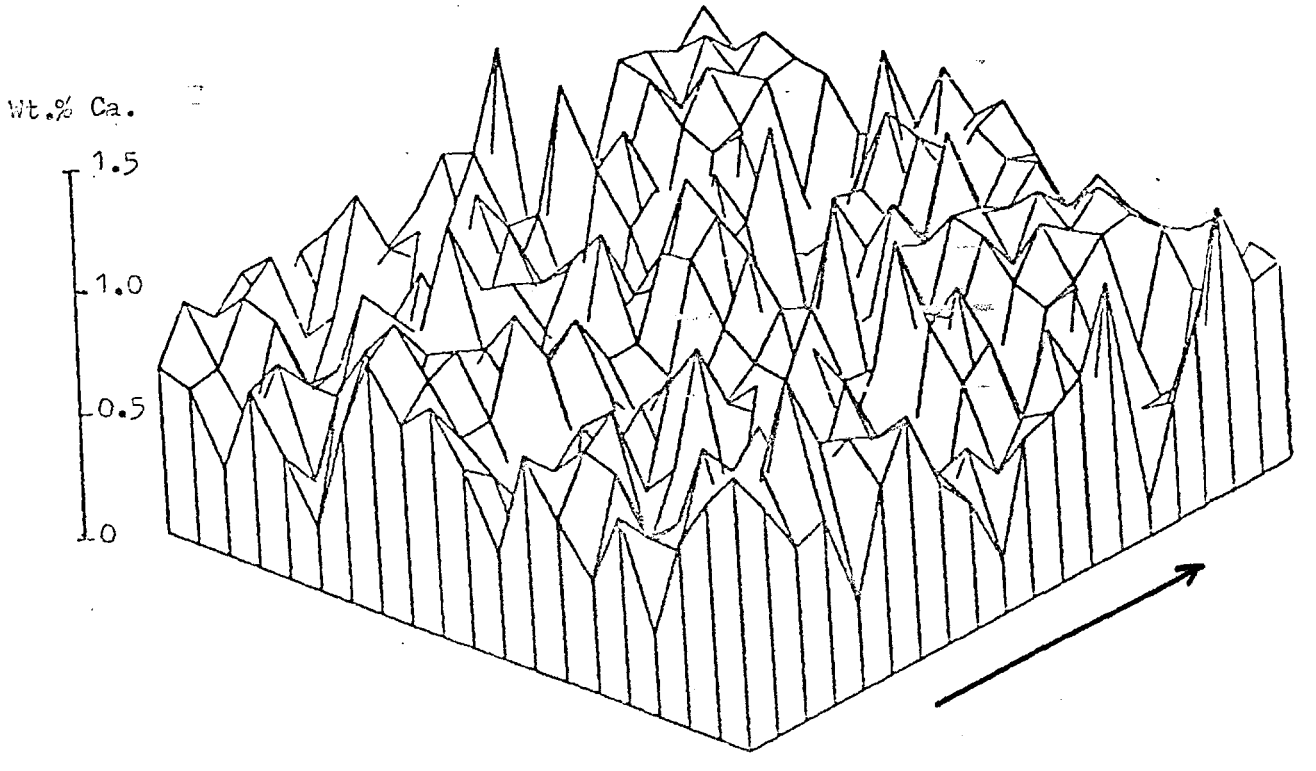

Figure 6.21: Al, 1301, Second Grid.

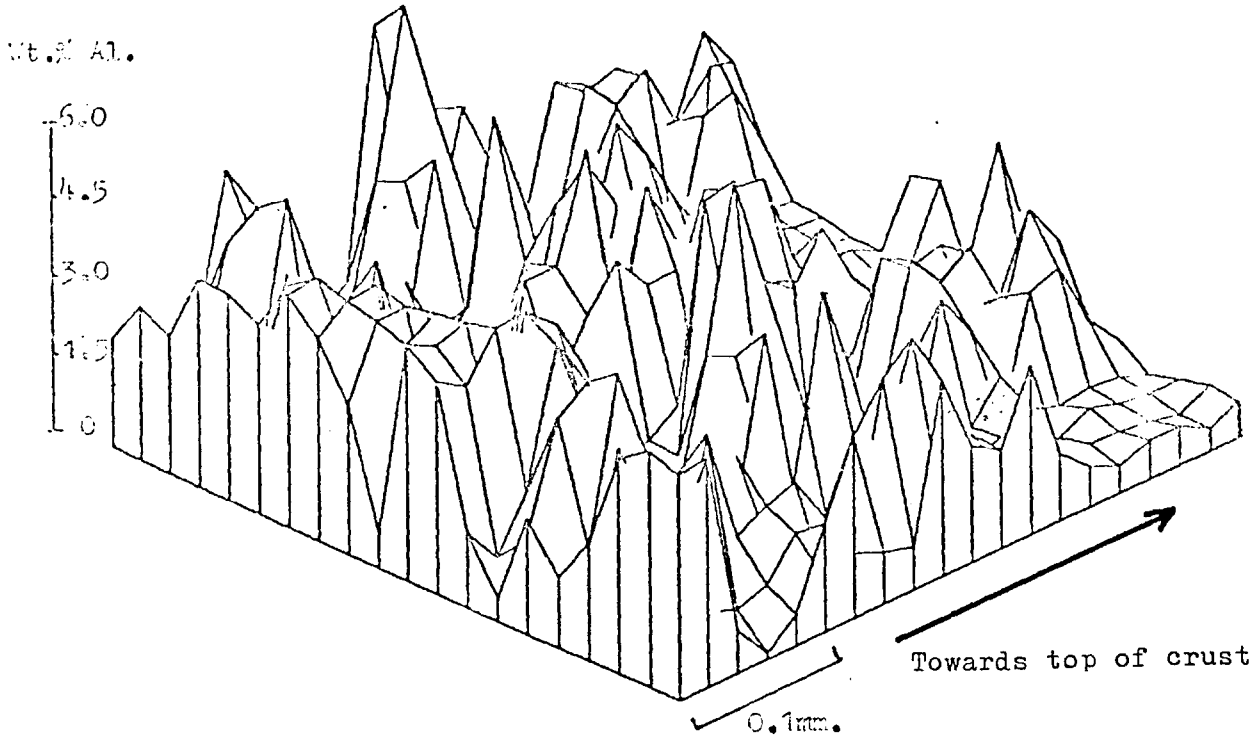

Figure 6.22: Si, 1301, Seoond Grid.

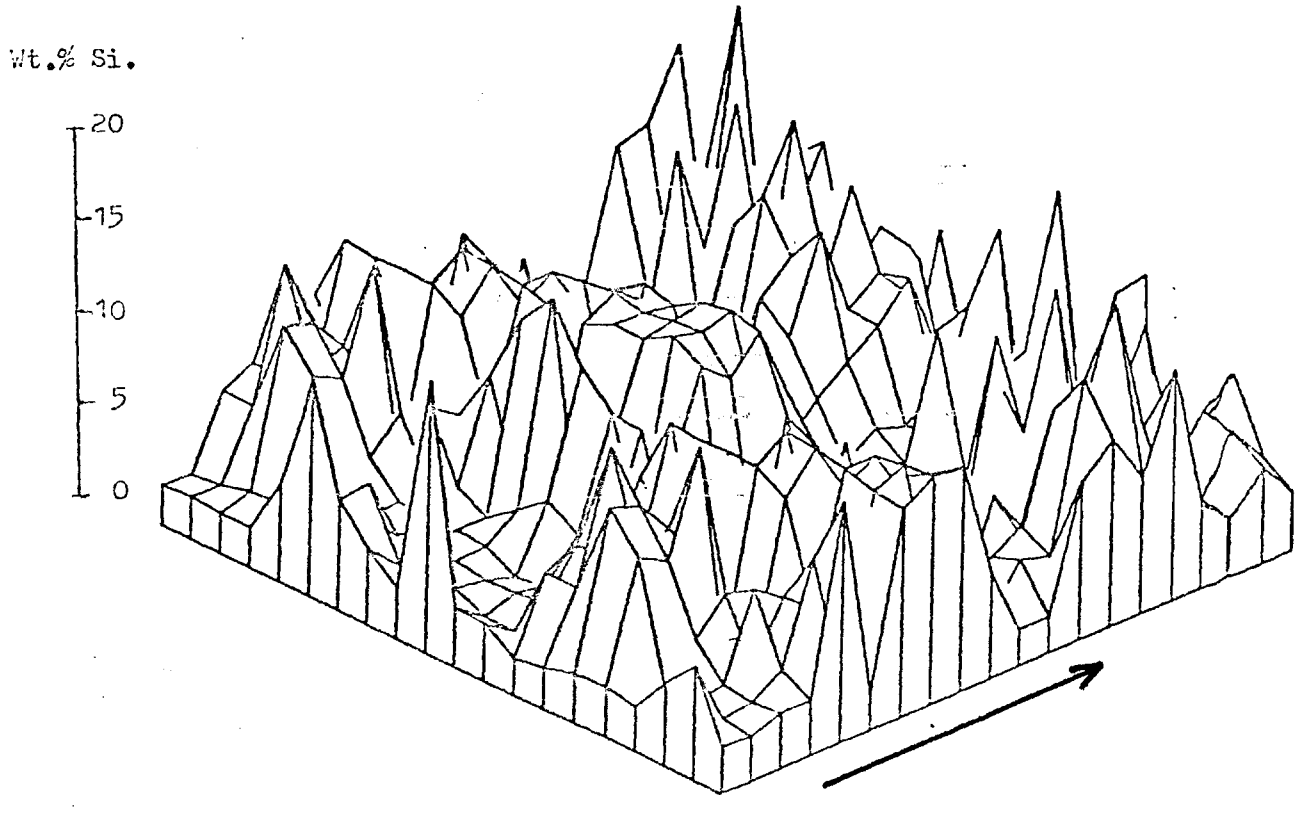

to have a greater number of analyses showing high concentrations in the vein, but there does not appear to be a clear overall increase in Co concentration in the vein. The iron concentrations show the reverse distribution to Mn, being higher in the pod structures (15-25%) and lower in the vein (2-10%) (Figure 6.16). Ti shows a similar distribution to iron. In the vein it is present at about 0.1 to 0.2%; in the pods it is present at about 0.4 to 0.6% (Fig. 6.19). Ca shows a relatively even distribution around 0.5-1% (Fig.6.20) and shows no increase in either the vein or the pods. Al and Si show irregular distributions (Figs.6.21 and 6.22) with no apparent preference for either the vein or the pods.

A series of more quantitative analyses was carried out with the E.D. system in an attempt to characterise the vein more fully and to compare it with the material of Zone 1, to which it bears some resemblance (high Mn, Ni and Cu, and low Fe). The vein is referred to as zone 4 in the E.D. data, and table 6.1 summarises these data. No distinction is made here between the two types of oxide mineral which constitute the crack infilling.

The chemical composition of zone 4 is similar to zone 1. Si and Al are a little higher in zone 4 than in zone 1 (4.32% and 1.6% compared with 3.12% and 1.14%). Mn is slightly lower (43.1% compared with 47.3%) and Fe is higher, 3.16% compared with 1.89%. Co and Cu are only slightly increased in zone 4 compared to zone 1, but the increase in Ni is much larger, 0.92% in zone 4 compared with 0.69% in Zone 1.

This vein of high Mn content is very bright in the

backscattered electron image (plate 6.2). This indicates a relatively high density compared to the material around it. Also in the fracture, material that was very dull in the backscattered electron image was found (zone 3 in table 6.1). This was characterised by very high silicon and aluminium contents and low concentrations of Mn. Ni, Cu and Co were not detected. This suggested the material is composed of clay.

Discussion

The crust selected from station 1301 for probe analysis had a macrogranular, knobby surface (Type A, Chapter 3). The section appeared to have been cut between knobs, so it may not give a true representation of the surface form, i.e. some of the top may not have been sectioned.

It was suggested in Chapter 4 that a reduction in the redox potential of the depositional environment may have been responsible for the change in mineral composition of the top few mms. of some crusts from 1301. The data from the electron probe show that there is a sharp demarcation between the surface zone with its high Mn/Fe ratio, indicative of todorokite-containing material, and the inner zone which has a lower Mn/Fe ratio, indicative of δ-MnO_2-containing material. Therefore, the electron probe data support the idea that a sudden change in the depositional environment brought about the change in mineralogy and hence the chemical composition of the oxide material being deposited.

The similarities in chemical composition between zone 1 and the fracture-filling (Zone 4) of this crust may indicate that the source(s) of the metals for the oxides in the two

zones had the same or very similar compositions. This implies that the fracture-filling formed at about the same time as the top few mms. of the crust. The relatively small differences in composition between the two zones probably reflect the different processes responsible for their formation. The solution forming the top few mms. of the crust was able to percolate through a fracture system (Heye, 1975) in the crust. Such a fracture system would be relatively restricted compared to outside the crust, so continuous equilibration of the solution percolating through the fracture system with the external solution probably would not be possible. The original composition of the solution would have changed as it percolated through the crust. The oxides formed from it would therefore also change in composition.

Station 1317

The crust from station 1317 consisted of three layers (Chapter 5), the top and bottom having Mn/Fe ratios averaging about 0.86, and the middle layer showing a marked depletion in Mn bringing the Mn/Fe ratio down to 0.43. A grid consisting of 1350 points (10 x 135), 200μ apart was performed for Mn and Fe on this crust. This did not traverse the whole section, but went from the top surface to the bottom of the middle layer. Figure 6.23 shows the map for Fe. The distribution appears to be fairly constant at about 30%, except in the top of the middle layer, where there is a marked trough in the Fe level, down to about 20%. The quantitative energy dispersive analyses do not agree with these figures. While the distribution of Fe given by

Figure 6.23: Fe, 1317.

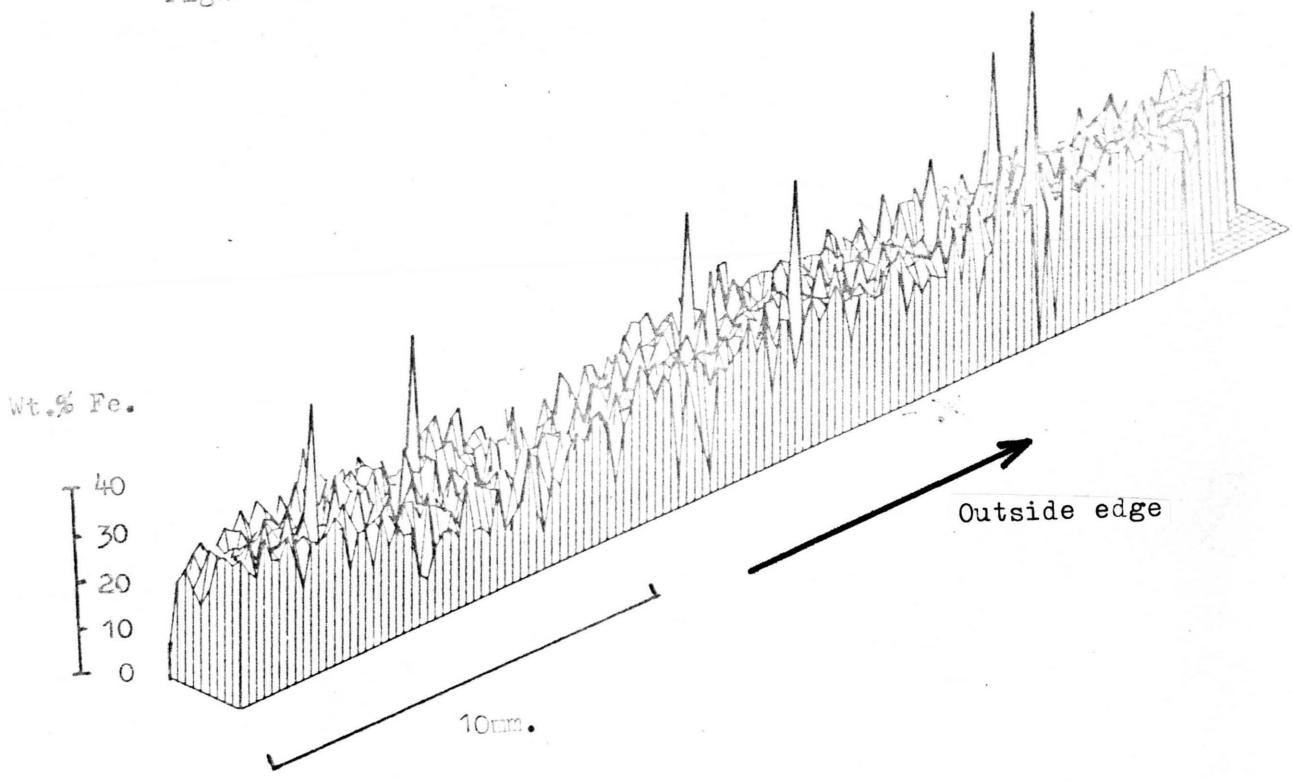

Figure 6.24: Mn, 1317.

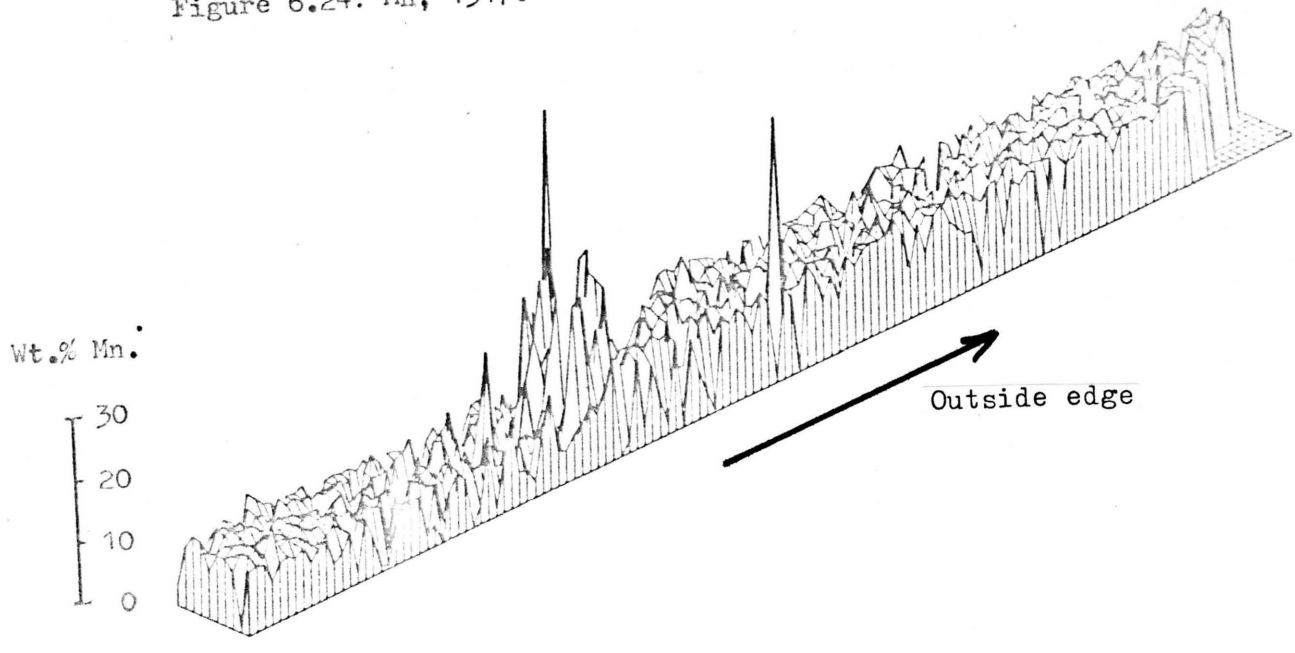

the grid agrees with the bulk geochemical data (Chapter 5), there seems to be a constant error in the grid data, causing the Fe concentrations to be too high (compare figure 6.23 with table 6.2).

Figure 6.24 shows the map for Mn. The most striking aspect of this distribution is the high values (greater than 20%) in an area corresponding to the top of the middle layer. In the upper layer of the crust, the Mn content is generally about 12-15%. In the middle layer, apart from the high values, Mn is about 8-10%.

Energy dispersive analyses were carried out to characterise the structures causing the high Mn values at the top of the middle layer. For the purposes of describing and discussing the analyses, they can be divided into four groups:

Group 1 is analyses of the top layer.

Group 2 is analyses of the middle layer not associated with the high Mn values.

Group 3 is analyses of the middle layer associated with the high Mn values.

Group 4 is analyses of the bottom layer.

Table 6.2 summarises the data for the four groups. Analyses of detrital material have been excluded in order to obtain a clearer picture of the differences occuring in the oxide phase.

In group 1, the Mn/Fe ratio varies quite widely but averages just over 1. Mn, Co and Ni were found to be higher in general near the outside (top) edge, and are higher overall in group 1 than in group 4 (the bottom layer). Si

and Al are lower than in group 4; perhaps these elements are higher in group 4 through incorporation from weathering of a volcanic substrate. Group 4, on the other hand, has lower contents of Mn and Fe, and Ni was not detected (i.e. less than about 0.12%).Cobalt is only slightly lower. In group 2, there is a large change in the composition of the oxide phase: Mn decreases to less than 10% compared with 20% in group 1 and 12% in group 4. The iron content is slightly lower than in group 1 and similar to group 4, at about 16%. Ni is below the detection limit (i.e. less than about 0.12%), but Co is similar to both groups 1 and 4 at about 0.4%. Si is much greater than in group 1 and appreciably higher than in group 4. Al is also greatly increased over group 1, but is very similar to group 4. The analyses for group 3 are the most striking in table 6.2. The structure giving rise to these analyses were arcuate, colloform growth forms (plates 6.3 and 6.4). The bright layers were found to have higher Mn/Fe values than the duller areas. The average Mn/Fe value in the structures as a whole is 7.79, much higher than in groups 1,2 and 4. This is caused by an increase in Mn content to an average of nearly 29% and a drop in Fe to an average of 6.9%. Ni shows a large increase to 1.2%, and Cu is above the detection limit, the only zone in which it is so. Co remains at about the same level as in groups 1, 2 and 4. Magnesium shows a marked enhancement in group 3 (2.2%) over the other areas (about 0.7%). Al is slightly higher than in groups 2 and 4 and much higher than in group 1. The Si content of group 3 is the lowest of all the groups (2.1%)

Element	Means, wt %				Maxima				Minima			
	Group 1	Group 2	Group 3	Group 4	Group 1	Group 2	Group 3	Group 4	Group 1	Group 2	Group 3	Group 4
Na	1.07	1.15	0.84	0.9	2.60	6.54	1.48	1.25	0.39	0.24	0.15	0.27
Mg	0.82	0.63	2.2	0.77	1.11	0.86	3.91	0.98	0.35	0.18	0.45	0.48
Al	0.42	1.07	1.18	1.05	1.08	1.87	2.14	1.83	0.12	0.61	0.38	0.62
Si	2.97	4.25	2.06	3.75	6.95	7.23	4.04	6.32	1.85	2.84	0.52	2.45
S	0.28	0.2	0.15	0.29	0.53	0.88	0.70	0.62	0.09	0.06	0.06	0.07
Ca	1.86	0.96	0.8	1.13	2.58	1.63	1.56	1.47	0.89	0.23	0.32	0.36
Mn	20.1	9.75	28.1	12.5	28.8	17.9	48.7	15.5	9.51	0.31	11.8	8.85
Fe	17.5	15.5	6.86	15.1	21.4	28.30	17.7	20.0	13.8	10.50	1.46	12.1
Co	0.43	0.42	0.38	0.39	0.76	0.59	0.76	0.54	0.27	0.20	0.18	.24
Ni	0.22	N.D.	1.23	N.D.	0.33	N.D.	2.3	N.D.	0.18	N.D.	0.18	N.D.
Cu	N.D.	N.D.	0.37	N.D.	N.D.	N.D.	0.51	N.D.	N.D.	N.D.	0.25	N.D.
P	0.25	0.14	0.13	0.14	0.3	0.28	0.18	0.20	0.17	0.07	0.08	0.08
Cl	N.D.	0.45	N.D.	0.64	N.D.	0.64	N.D.	0.94	N.D.	0.19	N.D.	0.41
Mn/Fe	1.17	0.67	7.74	0.84	1.65	1.14	32.0	1.19	0.46	0.02	0.68	0.50

Table 6.2. Summary of E.D.S. probe data, 1317.

N.D.:not detected.

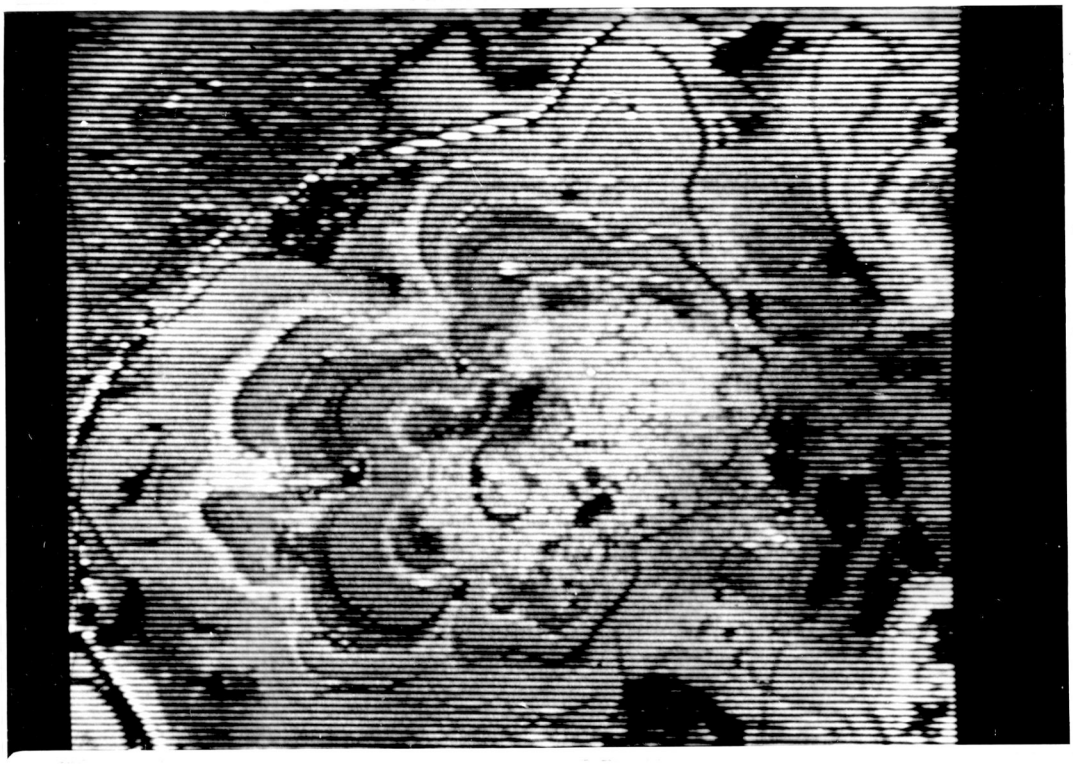

Plate 6.3: Back-scattered electron image of colloform growth structures, specimen from 1317. ⊢⊣ 20μ

Plate 6.4: Back-scattered electron image of colloform growth structures, specimen from 1317. ⊢⊣ 20μ

Discussion

The origin of the middle layer in the crusts from 1317 (Group 2 in the above description) is thought to be volcanic (Chapter 5). The data described above do not conflict with the data used to arrive at this conclusion; indeed they confirm the marked drop in Mn/Fe ratio in this layer found by the bulk analyses discussed in chapter 5.

The presence of the arcuate colloform structures showing markedly different compositions from the rest of the middle layer, and examples of which are shown in plates 6.3 and 6.4, requires some comment. Optically, the bright zones seen in plates 6.3 and 6.4 show marked anisotropy, probably indicating that crystalline todorokite or birnessite is the mineral form present. There was no sign of any clay material associated with these growth forms, so it is unlikely that diagenetic reactions with non-ferromanganese oxide phases can account for their presence. Post-depositional recrystallisation prompted by some factor or factors unknown seems to have been responsible for the formation of these structures.

Station 1321

The specimen from this station was selected because it contained todorokite in the bottom part, which, on a bulk scale, showed enhanced values of Ni and Cu compared to the top (1% and .16% compared with .28% and .035%). An analysis grid was performed across the bottom edge, as shown in plate 6.5, where it traversed some very varied structures. The grid itself was a rectangle of 578 points (34 x 17), 30μ apart. The area traversed was 1.02 mm. by 0.51 mm. Figures

Plate 6.5: Back-scattered electron image of the grid area, specimen from 1321.
⊢⊣ 100μ

6.25 and 6.26 show the maps for Mn. The layering which is visible in plate 6.5 is not reflected in the Mn distribution since there is no Mn variation corresponding to the visual variation. The most striking aspect is a plateau of high values corresponding to the very bright area in the upper centre of the grid. The Mn concentration here appears to be in excess of 30%. The maps of copper concentrations are shown in figures 6.27 and 6.28. A comparison of figures 6.26 and 6.28 shows that the Cu distribution follows very closely that of Mn, with values of Cu exceeding 0.5% in the bright area where Mn exceeds 30%. Elsewhere in the grid, Cu appears to be about 0.2 to 0.3%. Ni shows a similar pattern. The values within the bright area are around 2%, whereas outside they are about 1 to 1.5% (Figures 6.29 and 6.30). Fe shows the opposite distribution to Mn, being low in the bright patch (about 3-4%), and higher outside (greater than 5%) (Figure 6.31). The overall level of Fe in the grid area is quite low, generally being less than about 10%. Co (figures 6.33 and 6.34) seems to follow Fe in being low in the bright area (about 0.3%). Outside it, values approach 0.5%. A comparison of figures 6.31 and 6.34 suggests that Co is high where Fe is high. Si shows a very erratic distribution (Fig.6.32). The high values (greater than about 10%) seem to correspond to dark zones in plate 6.5. These are probably areas of clay between the oxide layers. The general level of Si associated with the oxide material is about 2-4%. Figure 6.37 shows the Al distribution. There is some correspondence between high Al values (greater than about 2%) and high Si values,

Figure 6.25: Mn, 1321.

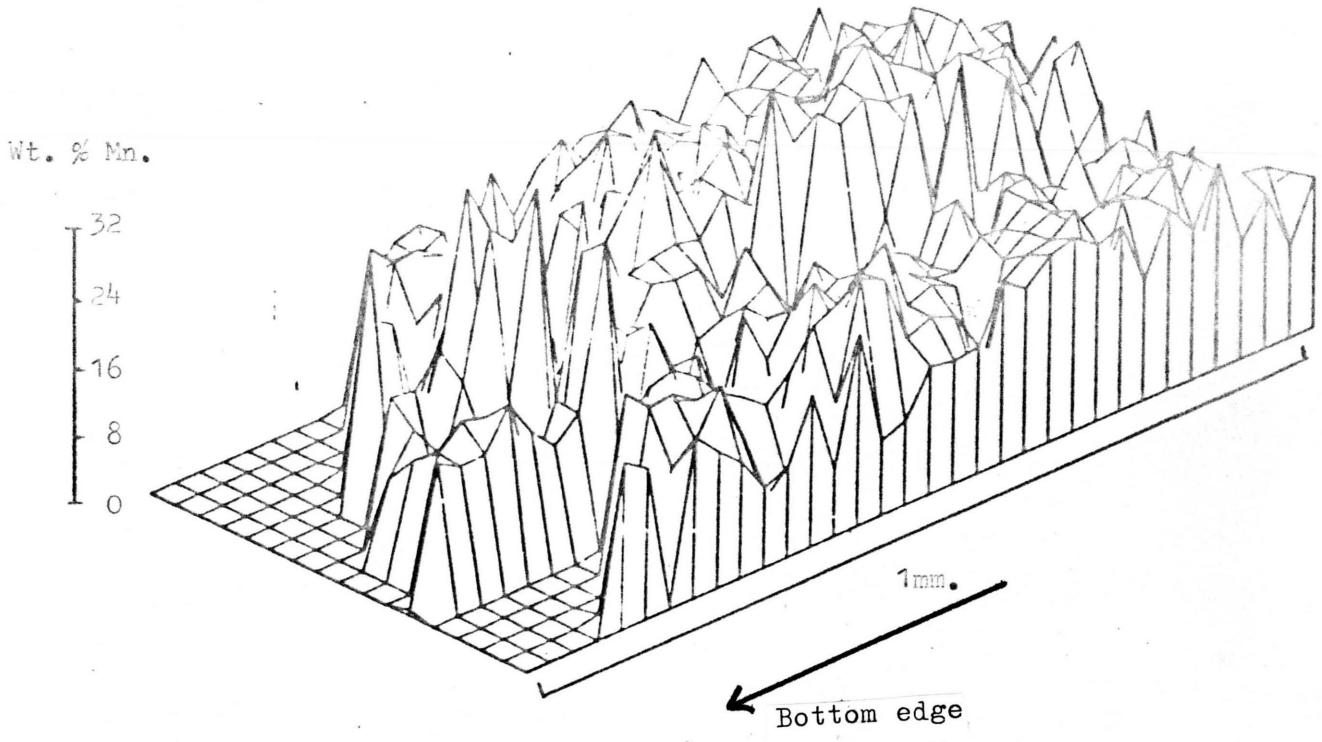

Figure 6.26: Mn, 1321; Cut-off=25%.

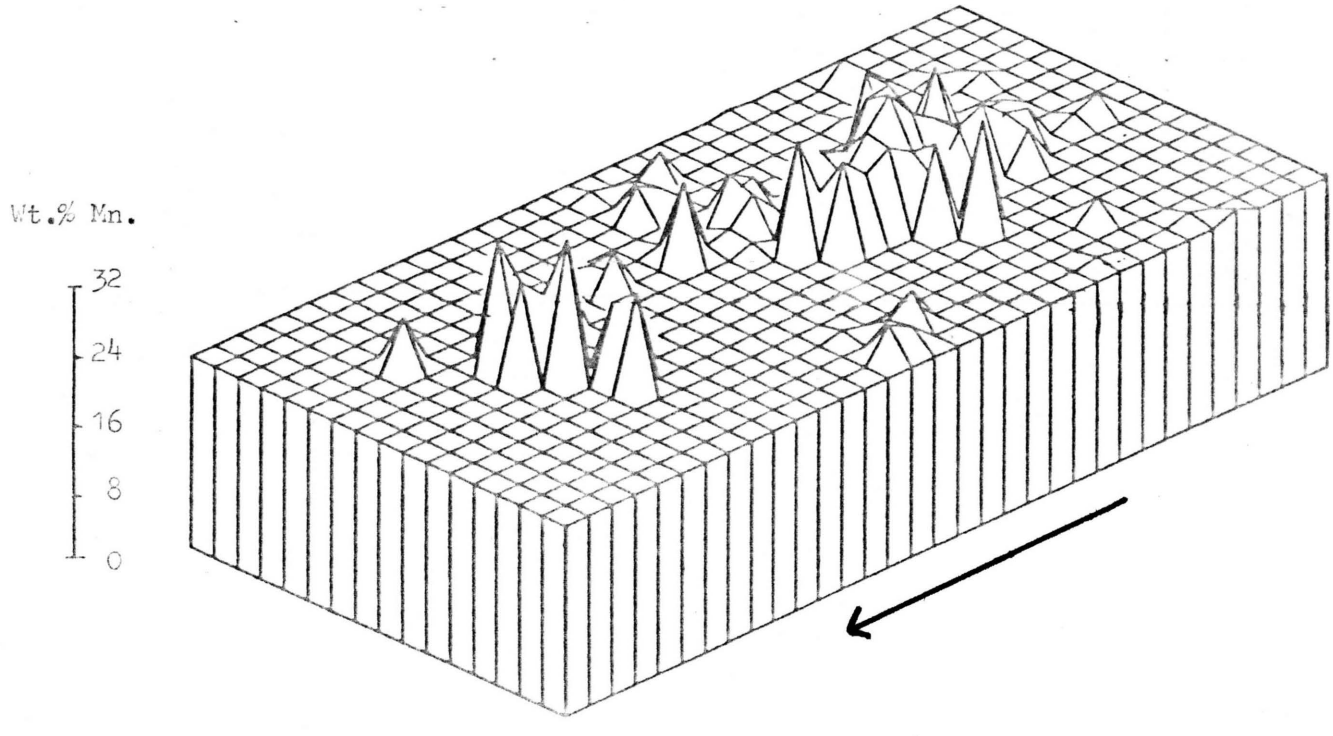

Figure 6.27: Cu, 1321.

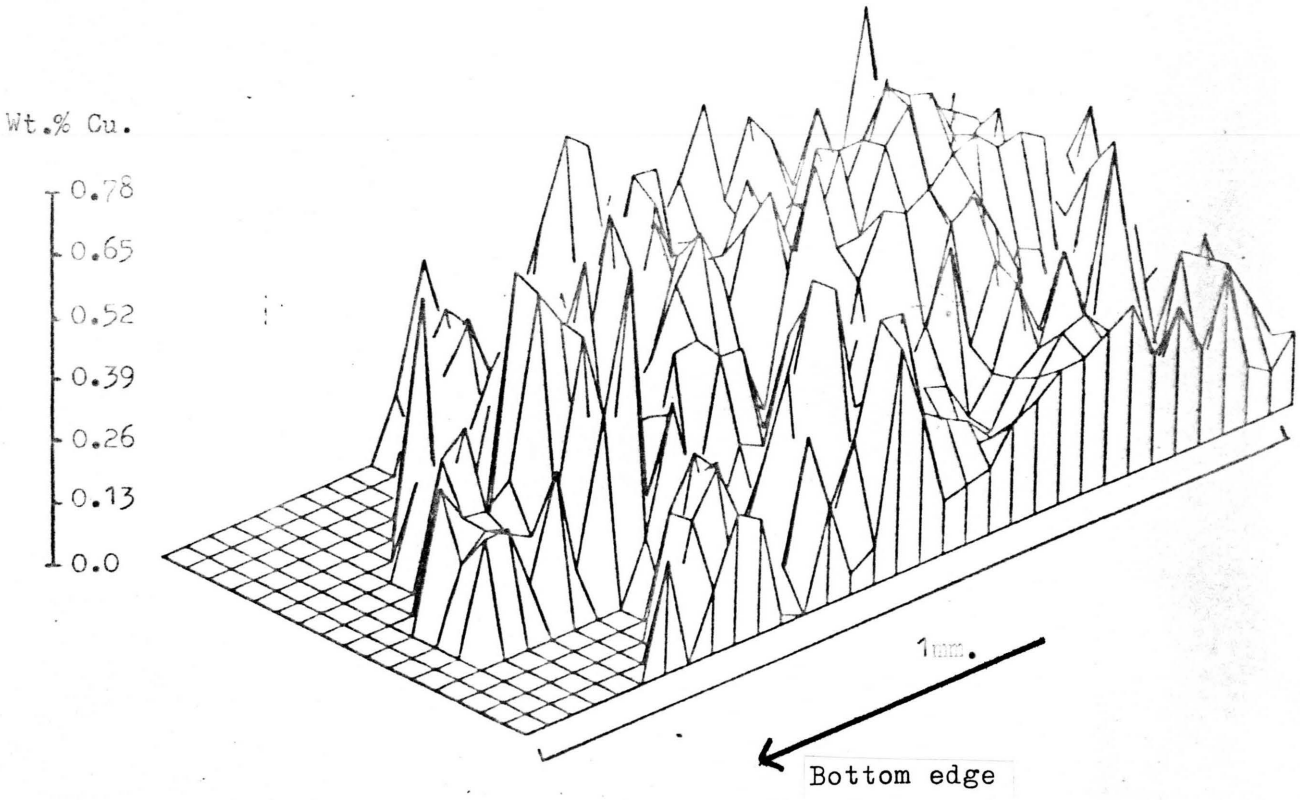

Figure 6.28: Cu, 1321; Cut-off=0.4%

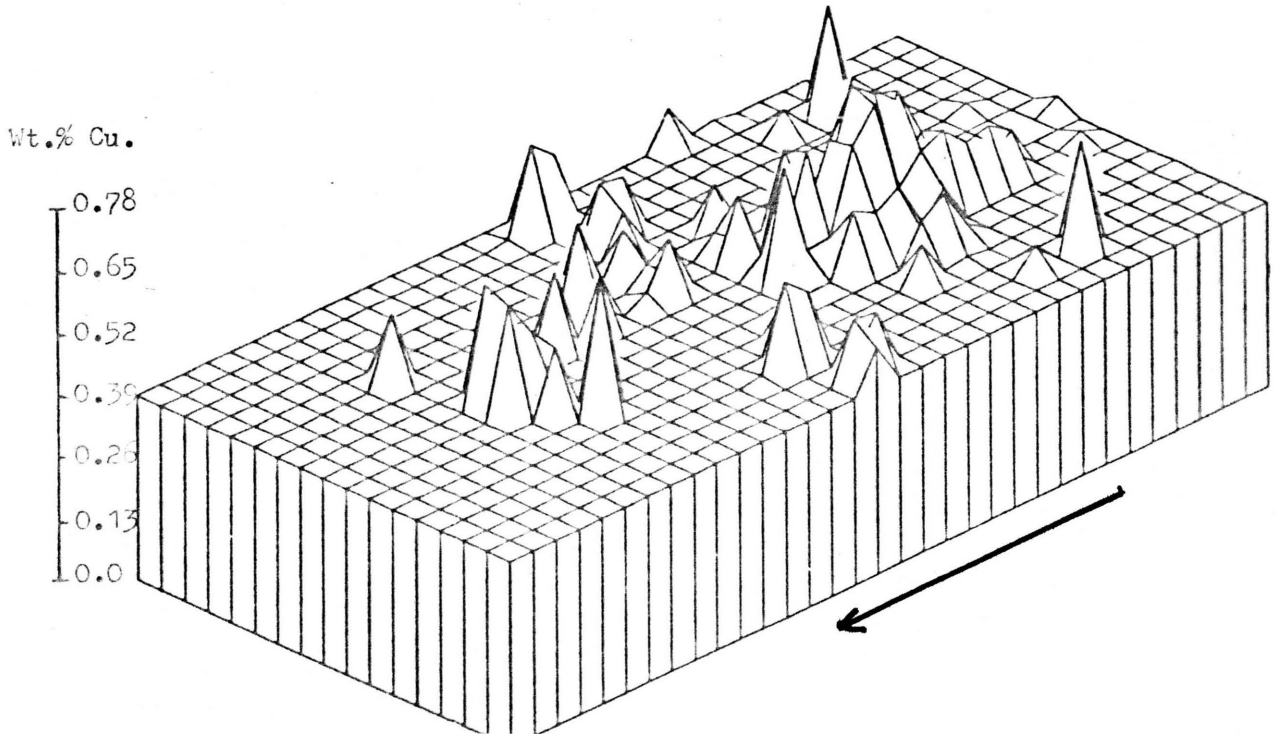

Figure 6.29: Ni, 1321.

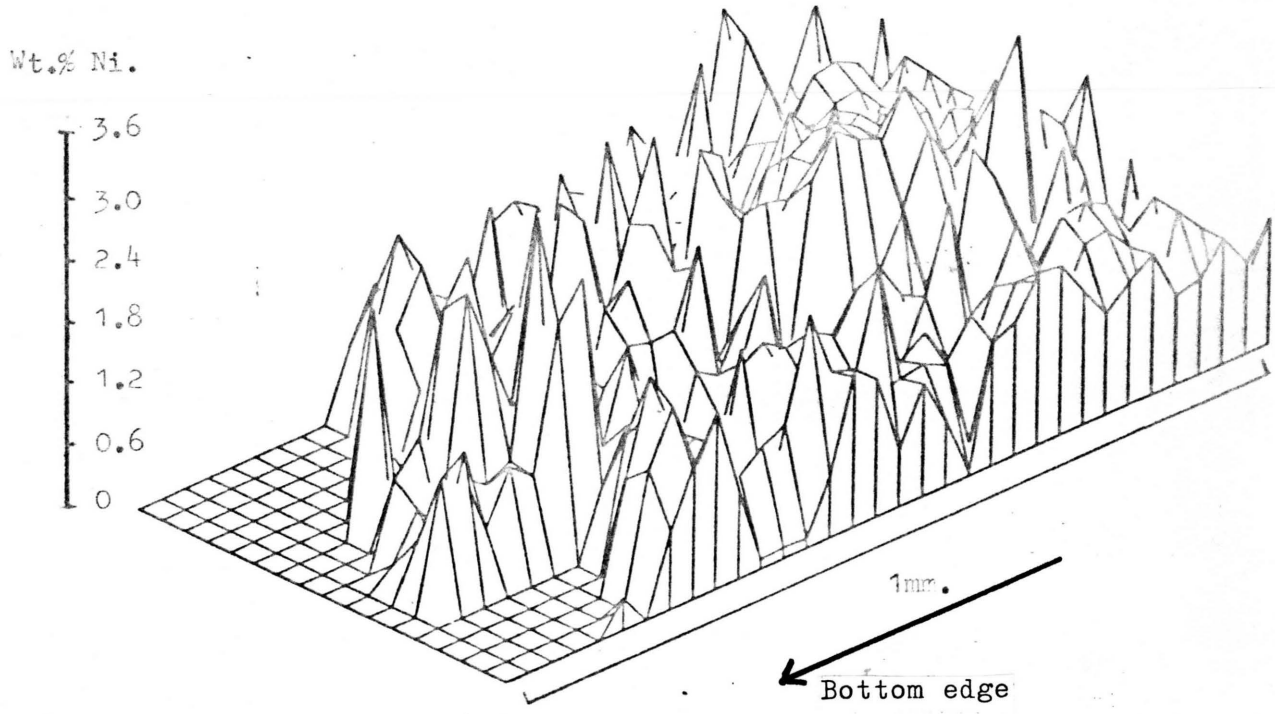

Figure 6.30: Ni, 1321; Cut-off=1.2%.

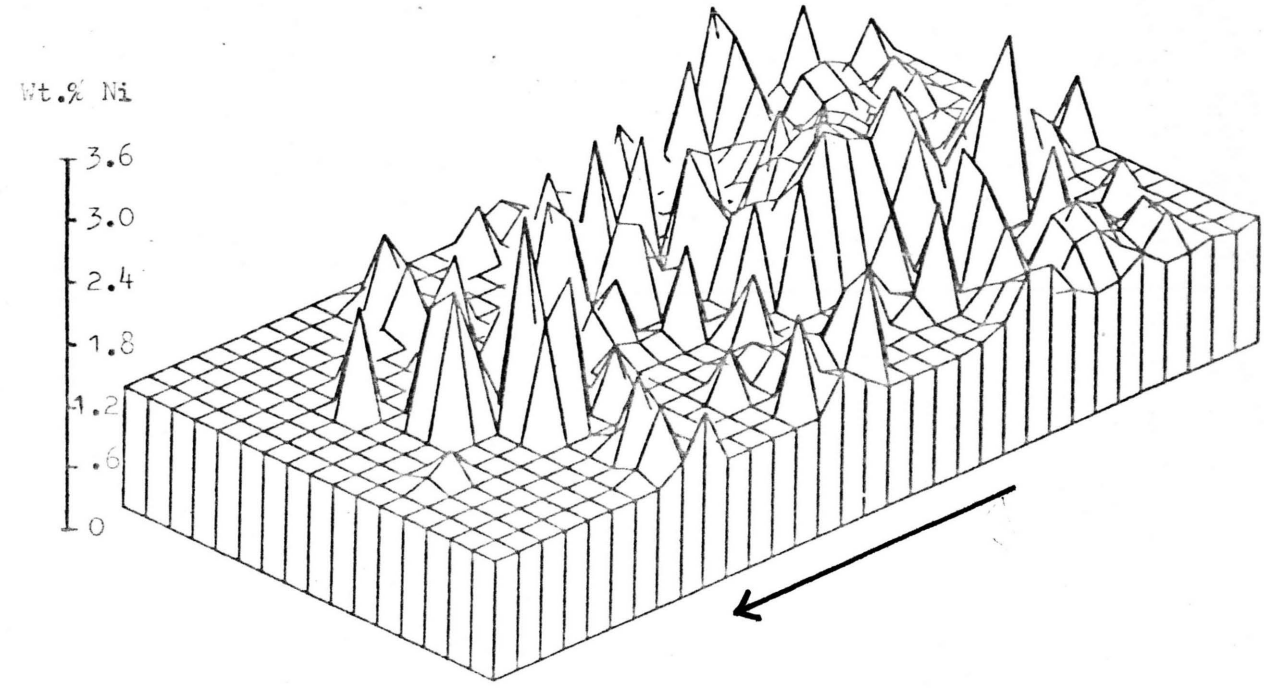

Figure 6.31: Fe,1321.

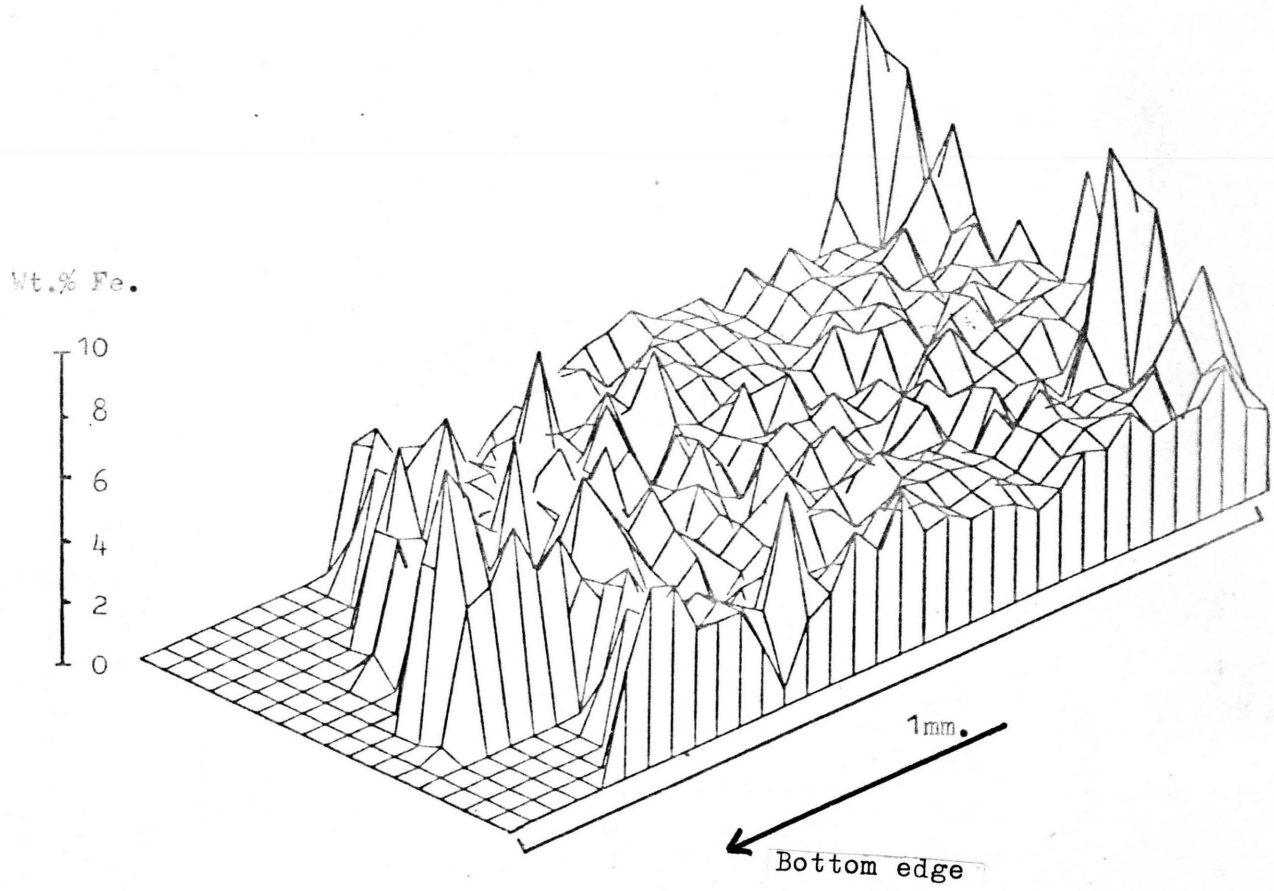

Figure 6.32: Si,1321.

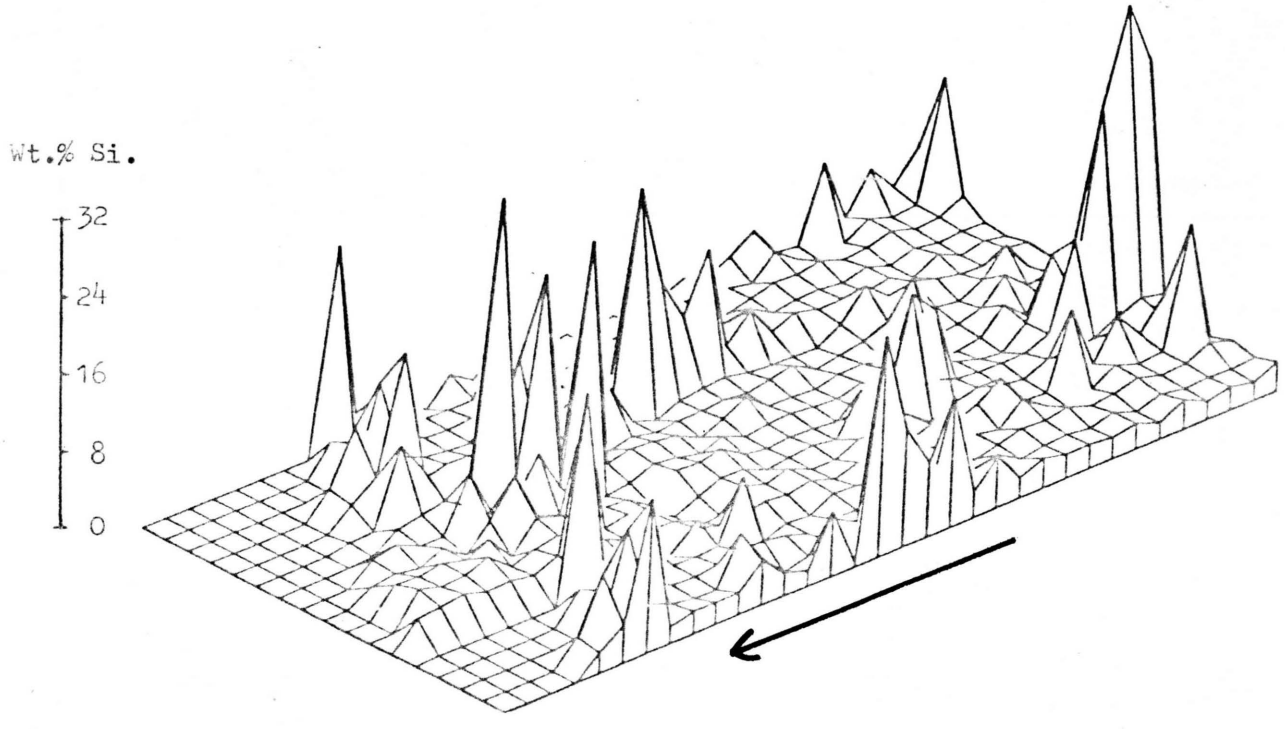

Figure 6.33: Co, 1321.

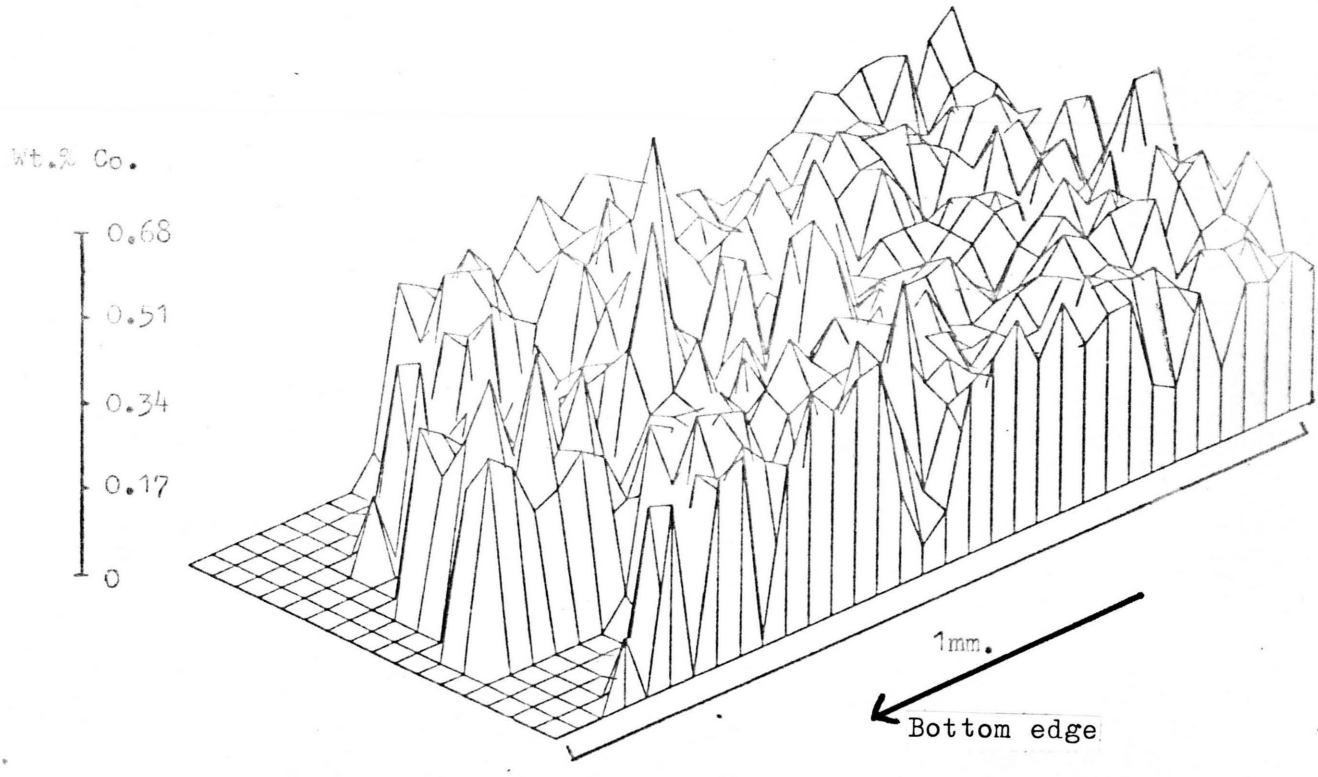

Figure 6.34: Co, 1321; Cut-off= 0.35%.

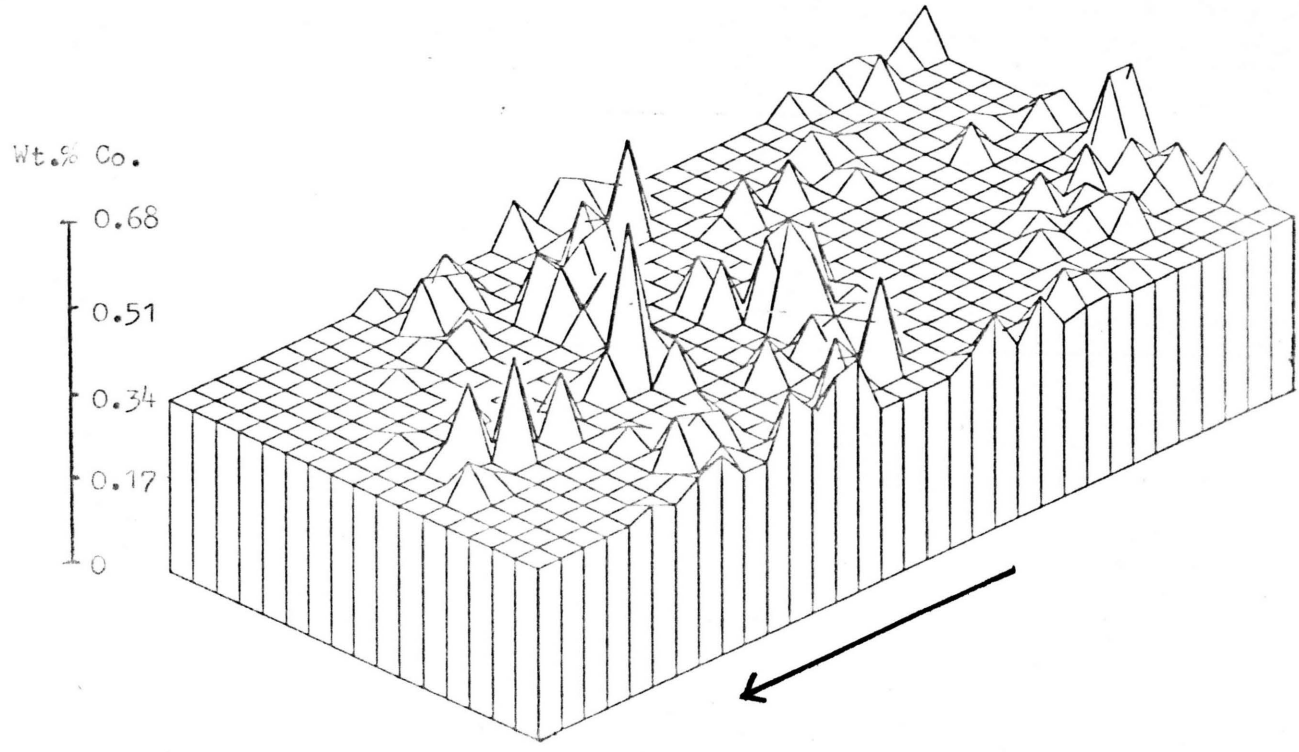

Figure 6.35: Ca, 1321.

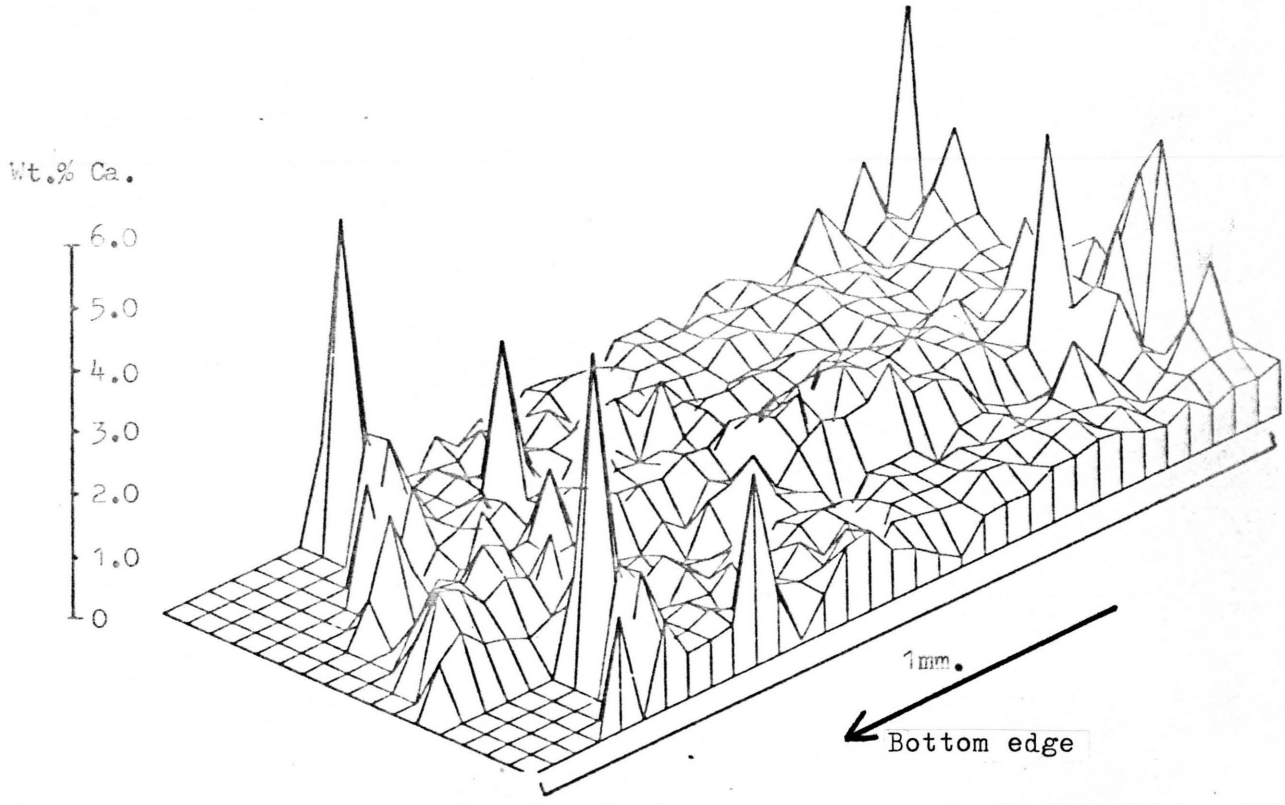

Figure 6.36: Ca, 1321; Cut-off=0.8%.

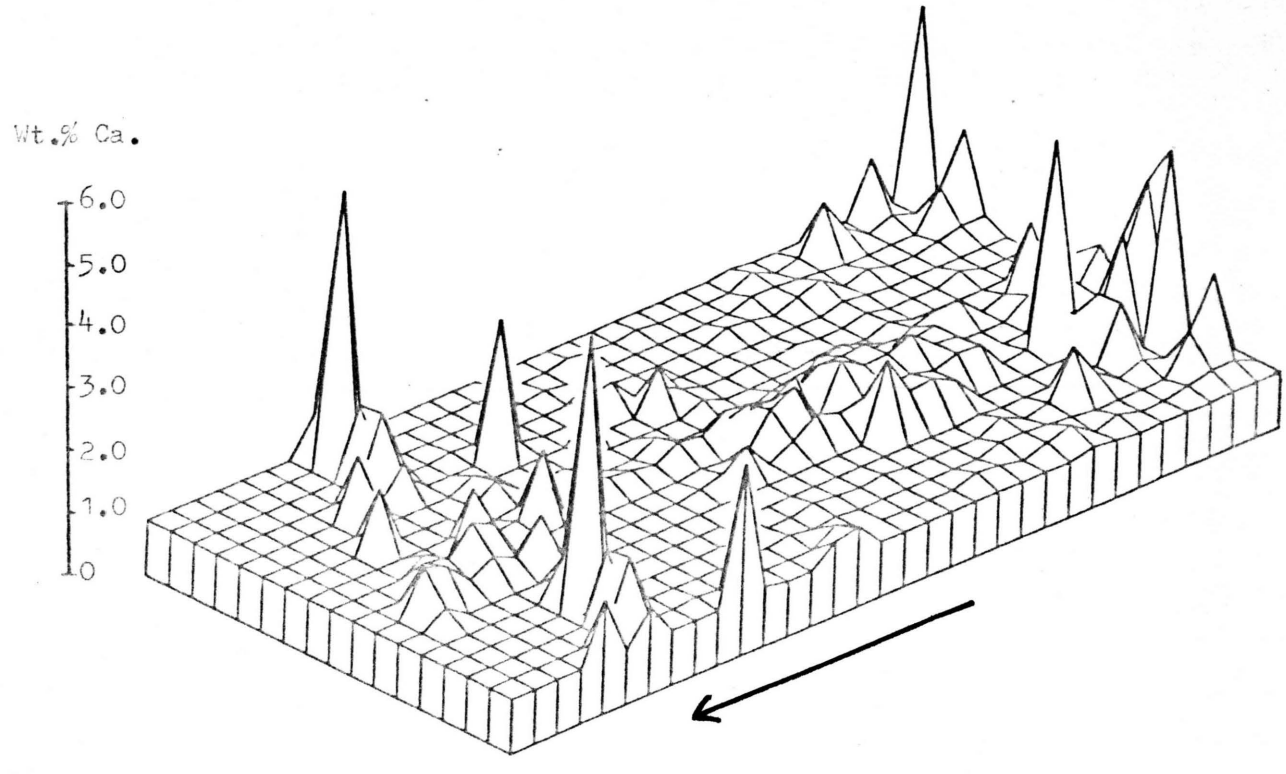

Figure 6.37: Al, 1321.

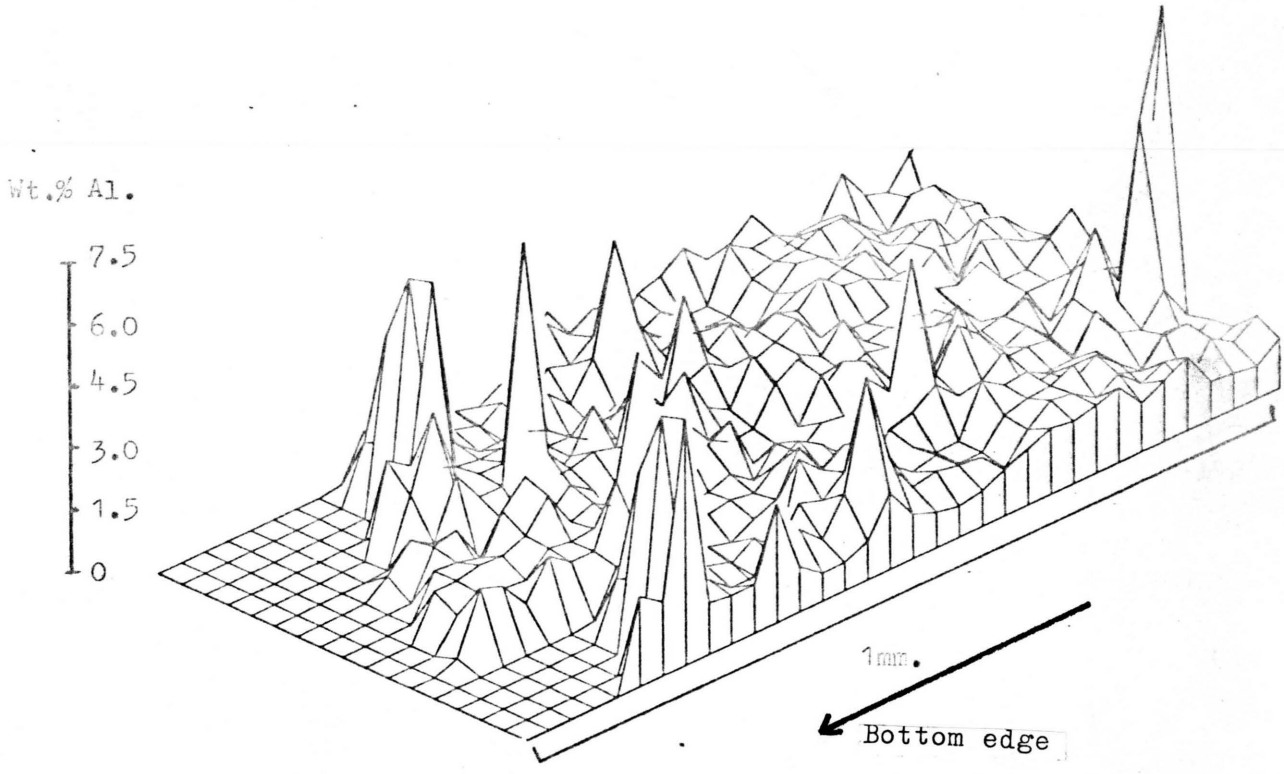

which supports the suggestion that these are attributable to clay. Ca shows a similar distribution to Al and Si (Fig. 6.35), which suggests the high Ca values (greater than about 1.5%) correspond to detritally derived minerals incorporated into the crust. In the oxide phase, Ca shows some enrichment to over 1% in the bright zone where Mn, Ni, and Cu were enhanced.(Figure 6.36). Outside here the Ca levels are about 0.5 to 0.8%.

Quantitative energy-dispersive analyses were carried out to investigate the crust composition on a larger scale than the grid area. Table 6.3 summarises the results of 58 E.D. analyses of this crust. The analyses fall into three groups. Group 1 consists of 41 analyses from the bottom half of the crust where the structure is stratiform (plate 6.5). Group 2 consists of 11 analyses of cuspate pod growths from the top half of the crust. Group 3 consists of six analyses of silicate material found in the crust. Group 1 has the highest Mn/Fe ratio, generally between 4 and 5; in group 2, it is less than or about 1. Ni and Cu also attain their highest levels in group 1, 1.9 and 0.39% respectively. In groups 2 and 3, Cu is not detectable (i.e. less than about 0.1%), while Ni is about 0.3 to 0.4%. Mg reaches its highest levels in group 1, nearly 3%, while in groups 2 and 3, it is less than 1%. K, Si and Al are all highest in the detrital group where Mn, Fe, Cu and Ni are lowest. Co and Ti are higher in group 2 than in group 1.

Discussion

It was suggested in chapter 4 that the changes in chemistry and mineralogy in this specimen were brought

Element	Means, wt. %			Maxima			Minima		
	Group 1	Group 2	Group 3	Group 1	Group 2	Group 3	Group 1	Group 2	Group 3
K	0.34	0.27	1.31	0.60	0.56	2.07	0.17	0.16	0.36
Mg	2.81	0.89	0.79	4.93	1.63	1.94	1.21	0.36	0.18
Si	2.06	3.72	14.9	7.53	6.60	24.5	0.45	2.40	9.53
Al	1.53	0.84	3.86	2.52	2.07	4.91	0.64	0.41	3.07
Ca	0.97	1.48	1.11	1.65	2.11	1.75	0.61	0.83	0.39
P	0.15	0.37	0.26	0.36	0.58	0.43	0.07	0.18	0.10
Ti	0.46	0.70	0.55	0.98	0.85	1.29	0.13	0.56	0.22
Mn	23.5	13.9	5.43	42.8	16.0	9.21	15.1	11.2	0.24
Fe	4.96	13.5	7.25	10.2	18.3	9.74	0.93	8.73	2.68
Co	.46	0.53	0.35	.76	0.70	0.41	0.20	0.39	0.26
Ni	1.87	0.35	0.31	4.46	0.56	0.52	0.48	0.23	0.19
Cu	.39	N.D.	N.D.	0.67	N.D.	N.D	0.26	N.D.	N.D

Table 6.3 Summary of E.D.S. data for 1321

N.D. not detected.

about by a change in the redox potential of the bottom environment to more oxidising conditions. Alternatively the crust may have become detached from its rock substrate and was resting on sediment at the time of collection. Two possible modes of accretion on the bottom of the crust may operate in these circumstances: active accretion by diagenetic remobilisation of Mn from the sediment, and reaction between ferromanganese oxyhydroxides and the sediment (Lyle et al., 1977), and its pore water.

Price & Calvert(1970), and Calvert & Price (1977), suggest that diagenetic remobilisation of Mn is an important source of this element to growing nodules in several regions of the World Ocean. However, Bender (1971) and Elderfield (1976), have shown that remobilisation of Mn in the sediment column is not likely on the scale which would be necessary if the Price & Calvert theory of Mn enrichment of nodules is totally correct. The conclusions of Boudreau & Scott (1978), support this. They have shown that there is no significant flux of Mn to the sediment surface if the depth of the oxic zone in the sediment exceeds 40 cms. Therefore in an open ocean environment such as the Somali Basin, where the oxic layer probably everywhere exceeds 40 cms., a diagenetic flux of Mn is not considered a significant source of the metal to the sediment surface. Calvert & Price, (1977) suggest that Pacific Ocean ferromanganese oxide deposits precipitated directly from seawater have Mn/Fe ratios of about 1.0, and that deposits with a Mn/Fe ratio of greater than 1.5 have received substantial amounts of Mn from the underlying sediment by diagenetic remobilisation.

The energy dispersive analyses of the bottom half of a crust from this station (1321), which may have been resting on a sediment substrate, show Mn/Fe ratios of about 4 to 5, which could indicate a substantial contribution to the crust from remobilisation. However station 1321 is located on a group of seamounts in the Somali Basin. Sediment cover on seamounts is likely to be thin and patchy because of current scour, so it is unlikely that remobilisation of Mn occurs to any significant extent. In view of this and the more detailed work of Bender (1971) and Elderfield (1976), remobilisation of Mn from depth in the sediment column is regarded as an unlikely cause of the changes seen in the crust from 1321.

If active accretion of Mn-rich material from the sediment is not occurring, then perhaps post-depositional reaction between the oxides and the sediment occurs. Greenslate et al., (1973) suggest that marine organisms are an important source of Mn in areas of high surface biological productivity since these organisms are able to incorporate transition metals in their tests and/or soft parts. As the tests are deposited, they begin to dissolve, and release their transition metal contents, which may then be available for incorporation into ferromanagese oxide deposits. However, Greenslate et al., (op.cit.), have shown that the Fe content of marine organisms is at least an order of magnitude higher than their Mn content and if these organisms form the major supply of Mn to nodules in certain areas then some mechanism must be operating which inhibits the increased supply of Fe from being incorporated

into the oxides.

Table 6.3 shows a pronounced depletion in the Fe content of Group 1 (analyses of the bottom half) to 5% compared to the average Fe content of Group 2 (the top half) of 13.5%. A process whereby available Fe is not only prevented from becoming incorporated into the oxide phase, but is actively removed from it, must therefore be envisaged in order to account for the presence of the Mn-rich, Fe-poor bottom halves of crusts from 1321. Such a process was put forward by Lyle et al., (1977) to explain the low Fe content of nodules from the Bauer Deep. It is also used later (pp 202-203) to account for the presence of a manganese-rich, iron-poor fracture filling in a crust from station 1301. Lyle et al., (op.cit.), suggested that the iron from Fe-Mn oxyhydroxides is incorporated into iron-rich smectite by reaction with opal. The Mn originally associated with the iron oxyhydroxides is not accepted by the smectite structure and crystallises as todorokite micronodules. They also suggest that trace metals such as Ni and Cu, which may occur in the biogenic opaline silica in relatively high amounts, (Greenslate et al., 1973), may be released during this process and may subsequently become incorporated in the todorokite micronodules as they form. These micronodules may become incorporated in the bottom of the crust as this process proceeds.

This process is thought to occur at or near the sediment surface, and could explain why two of the crusts from 1321 were different from the other two. The presence of the sediment is necessary for the reactions producing the metal-enriched todorokite present on the bottom of the two crusts.

The other two crusts examined from this station contained no todorokite, perhaps because they remained attached to their rock substrates until collection. This prevented contact with opaline silica in any surrounding sediment, so therefore no todorokite was formed.

Electron probe microanalysis and the petrology of some features of two ferromanganese oxide crusts.

Introduction

Crusts from stations 1301 and 1315 showed certain features which merited closer detailed investigations. These features were healed cracks, and in 1315, void-infillings. Optically, these features were discontinuous with the surrounding oxide material which made up the rest of the crusts, and it was thought that detailed optical and chemical studies would yield information concerning the paragenesis of these secondary features.

Results:1301

The feature of interest here is a horizontal fracture cutting across oxide material which is structureless, fragmented and isotropic. This fracture is shown in plain light in plate 6.6 and polarised light in plate 6.7. It is a secondary feature, extending about three-quarters of the way across the section. It has been filled with clay and anisotropic oxide minerals. The electron probe has been used to investigate the nature of the infilling materials and their relation to the groundmass.

Optically, there appear to be two different types of oxide mineral in the groundmass. One is a very pale grey to white oxide material which is essentially isotropic or

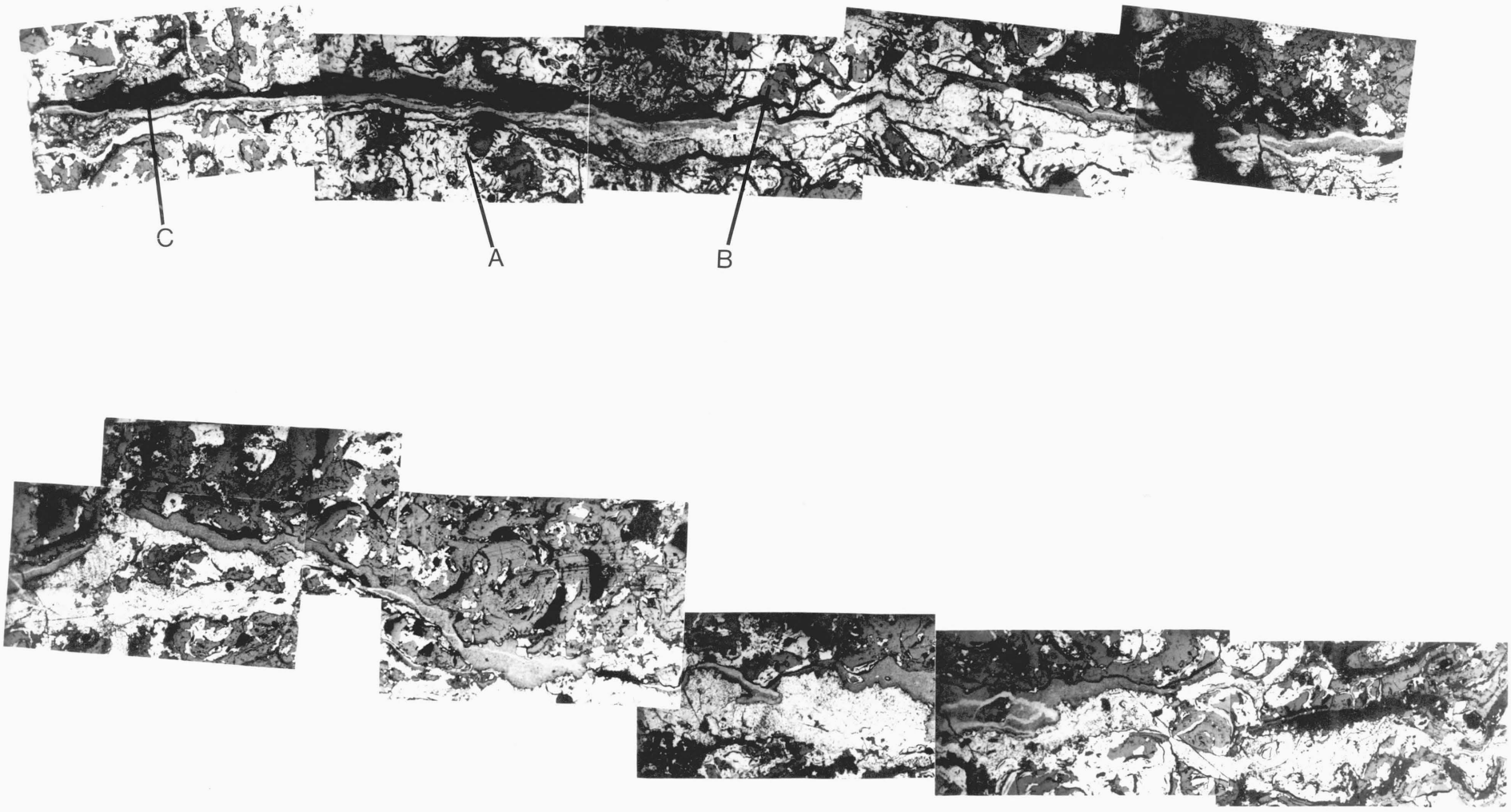

Plate 6.6: Horizontal healed crack, 1301: plain light. ⊢—⊣ 0.2mm.

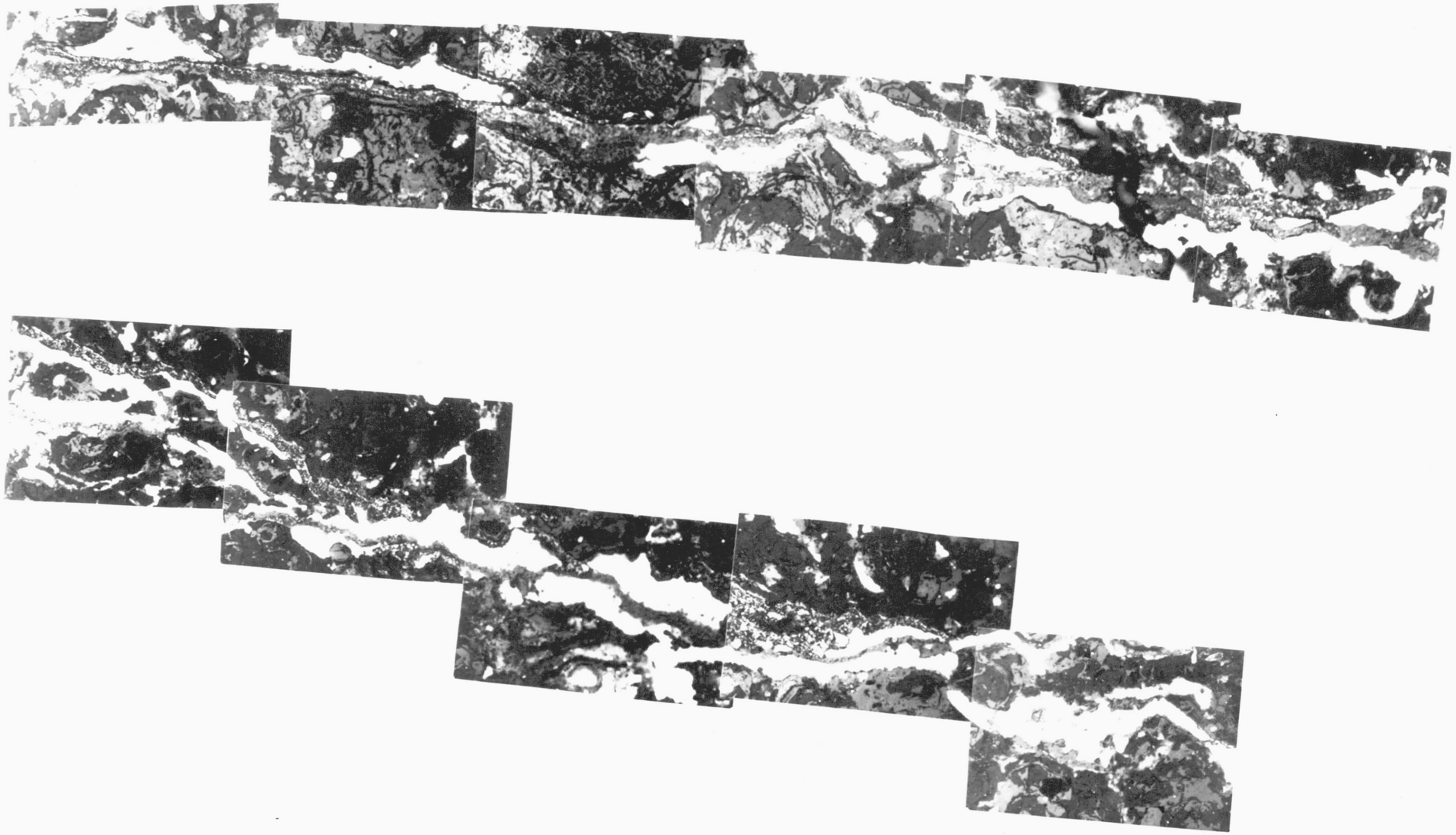

Plate 6.7: Horizontal healed crack, 1301: polarised light. ⊢—⊣ 0.2mm.

very weakly anisotropic, examples of which are labelled A in plate 6.6. This is dark grey in crossed Nicols. The other type (labelled B) is dark grey in plain light and remains dark grey in crossed Nicols. Chemically, these two materials are very similar indeed, about 21-23% Fe, 7-9. Mn, .1 to .2% Ni, about .9% Al and about 5% Si in each. There is no discernible change in chemistry from one side of the crack to the other. Inside the crack, there appears to be two different oxide minerals. One is white to pale grey and strongly anisotropic. It forms veins within the other mineral, which is a darker grey, and shows a less pronounced degree of anisotropy than the first mineral. The two minerals differ significantly in their chemical composition. The first contains about 40% Mn, 2% Fe, 1.6% Ni, 0.5% Cu, 0.5% Al, and 0.8% Si. The second mineral contains about 31% Mn, 3.6% Fe, 1.8% Ni, 0.4% Cu, 1.9% Al, and 5.5% Si. Apart from oxide minerals in the crack, there is a silicate mineral (labelled C) present. This is white, with a speckled appearance in plain light, and appears to be present mainly on the edge of the crack. The chemical analysis gives a composition of about 8% Fe, 1% Mn, 0.1% Ni, 0.02% Cu, 4% Al, and 18% Si, suggesting the presence of an iron smectite-type mineral.

Discussion

Healed cracks containing metal-enriched minerals have been noted in ferromanganese oxide deposits before (Sorem & Fewkes, 1977; Burns & Burns, 1978a), though no detailed study of them has been made. Sorem & Fewkes (1977) noted that a fracture-filling exhibited anisotropy and they

suggested this indicated the presence of todorokite and birnessite. Burns & Burns (1978a), found values of Cu, Ni and Mn in oxide material lining a healed fracture greatly enhanced over values for these metals on either side of the crack. Neither Burns & Burns (op.cit.) nor Sorem & Fewkes (1977) suggested why cracks specifically might possess these features. Burns & Burns, however, suggested a reaction scheme whereby todorokite is formed in deposits during a post-depositional process from clays, biogenic silica, organic matter and pre-existing iron-manganese oxyhydroxides (e.g. δ-MnO_2). They further suggested that metal enrichment occurs by adsorption of Ni and Cu from organic complexes, already adsorbed onto the surfaces of clay particles, onto the todorokite. The primary requirement for these reactions is sea water which contains the constituents for the reaction and acts as the transporting agent to the reaction sites in the deposits. This process is not greatly at variance with that proposed by Heath & Dymond (1977) or Lyle et al., (1977). These authors suggest that small-scale diagenetic processes within the sediment may be responsible for the presence of todorokite in certain deposits. The main difference is that phillipsite (an iron-poor mineral) is formed in the reaction of Burns & Burns, 1978a), while iron-rich smectite is formed by the reaction of Heath & Dymond (1977) and Lyle et al., (1977). Both theories are similar inasmuch as they both postulate post-depositional reactions between ferromanganese oxides and external agents.

Raab, (1972) describes internal fractures in ferromanganese

oxide deposits as "generally filled with clay, but occasionally the fractures are clay-free and lined with an overgrowth of ferromanganese oxide". The present fracture contains both clay and oxide material. The oxide does not line the walls continuously but sometimes passes through the clay. Heye, (1975) carried out a detailed study of the occurrence of cracks in ferromanganese oxide deposits. He argued that cracks within nodules and crusts are self-propagating features and eventually result in the complete break up of the deposits on the sea bed. One can therefore visualise a crust or nodule as possessing a complete network of fractures of varying dimensions throughout its structure. Seawater, containing dissolved organic matter, dissolved oxygen, with a particulate load consisting of clay material and fragments of tests, both siliceous and calcareous would therefore be able to percolate through most parts of a deposit containing such a fracture system. A little of the finer particulate matter is likely to be deposited over a period of time in the cracks, thereby enabling the reactions envisaged by Lyle et al., (1977) and Burns & Burns (1978a) to take place. This would produce the relatively enriched crystalline manganese oxide minerals inside the cracks, if the theories of either Burns & Burns (1978a) or Lyle et al., (1977) are correct.

If this process does indeed occur, then it serves to explain the occurrence of Cu-Ni-Mn enriched crystalline oxide minerals inside the crack in plates 6.6 and 6.7. It is not clear why there are two types of oxide mineral. The presence of an iron-rich silicate (a smectite?) in close

proximity to those minerals, rather than an iron-poor one indicates that reaction processes similar to those suggested by Heath & Dymond (1977) and Lyle et al., (1977) might have occurred here rather than those of Burns & Burns (1978a)

Results: 1315

The crust studied from this station appeared to have two distinct layers, each about 1.5 - 2 mms thick. They were very similar in appearance and structure to each other, but with a distinct discontinuity separating them. The interface between the top and bottom layers is botryoidal in form. While the top layer nearly always follows the form of the bottom layer, there are occasional hollows in the surface of the bottom layer which have not been filled by the top layer. The hollows contain deposits of oxide material relatively rich in anisotropic minerals. Plates 6.8 and 6.9 show a typical example of this. Table 6.4 shows the differences in the chemical composition between the isotropic and the anisotropic material. The latter is seen to be enriched in Mn (36.7% compared with 19.9%), Ni (2.5% compared with 0.5%), Cu (0.2% compared with 0.06%) and Mg (2.8% compared with 1.1%). The growth of these infillings probably occurred at a different time to both upper and lower layers because there is a lack of continuity between these layers and the infillings. This suggestion is supported by the differences in the chemical compositions of the isotropic material filling the void, and of the isotropic material of the upper layer. If they were formed at the same time, then the source of the metals would probably be the same, so the compositions would be

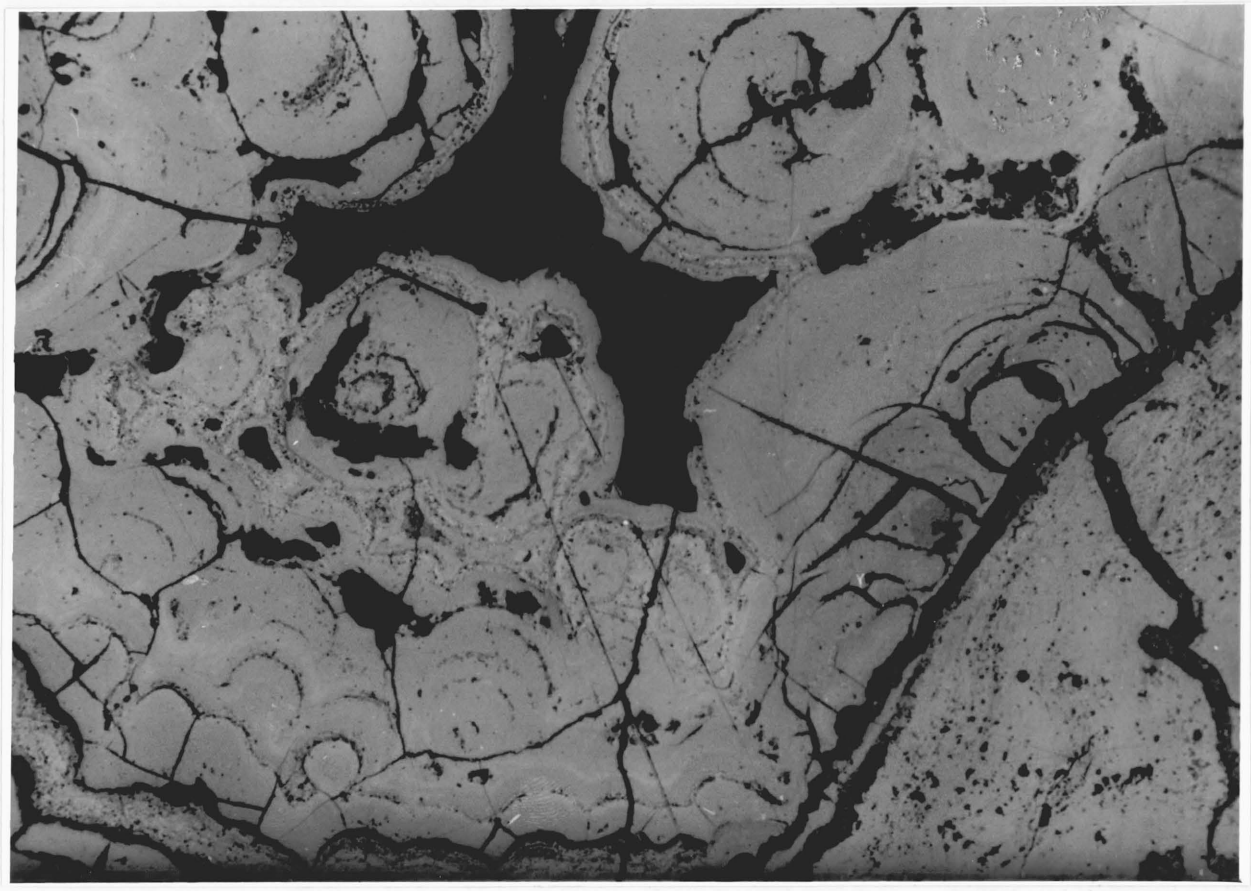

Plate 6.8: Photomicrograph of part of a void-filling from a specimen from 1315.(Plain light). ⟵⟶ 50μ

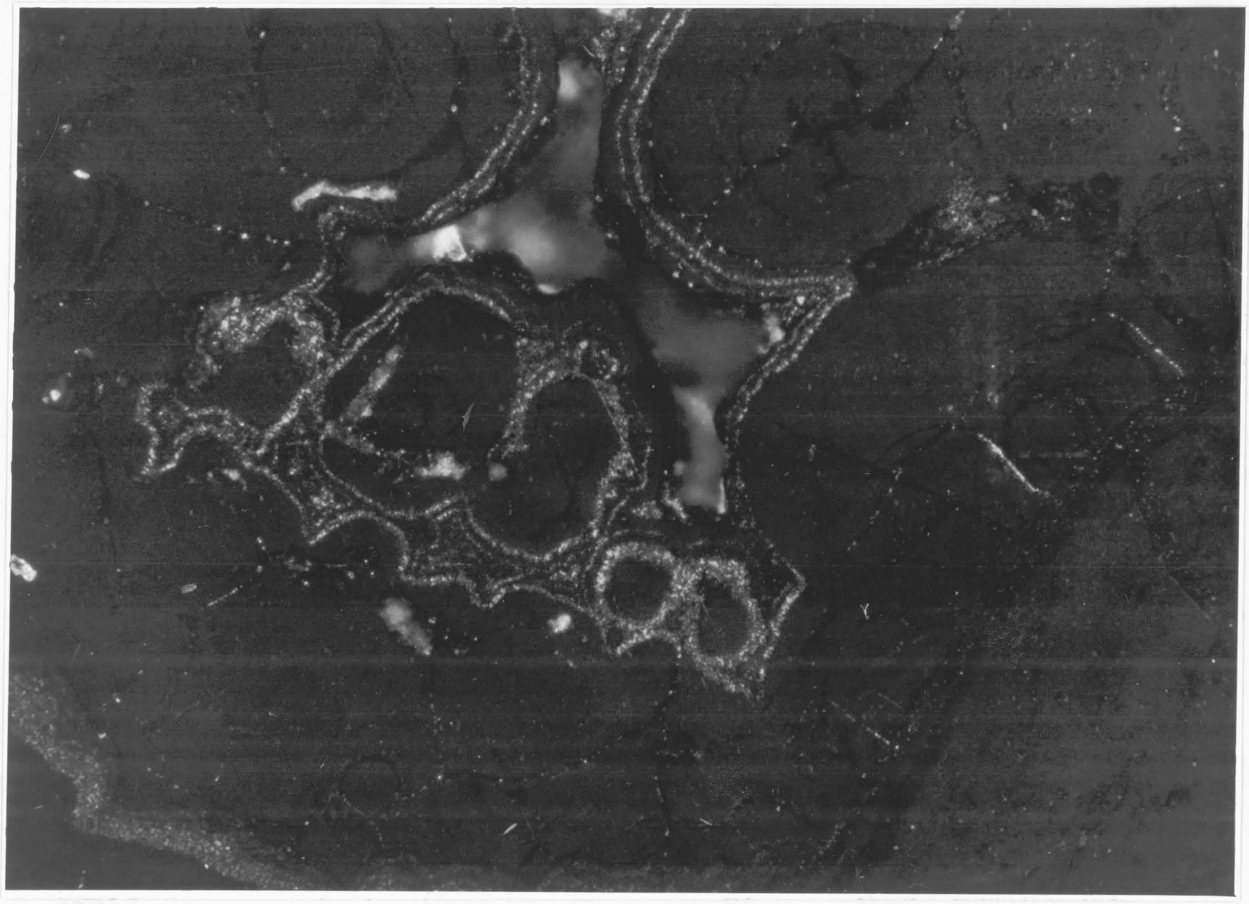

Plate 6.9: Same area as shown in Plate 6.8, polarised light.

similar. Table 6.4 shows the differences between the top layer and the isotropic void-filling. The top layer, overlapping the void, contains less Fe(11.7% compared with 16.1%),less Ni (.3% compared with .5%), more Co (0.9% compared with 0.6%), less Cu (not detected), less Si (0.8% compared with 1.45%), and less Al (.17% compared with .49%) than the isotropic void filling. These differences indicate an origin for the void-filling different from the origin of the top layer.

Plates 6.10 and 6.11 show a vertical crack in the bottom layer lined with anisotropic material. This crack stops sharply at the interface with the top layer, indicating that the formation of this crack definitely predates the formation of the top layer. The occurrence of anisotropic minerals as a fracture filling was noted in the crust from 1301. The crack in the crust from 1315, however, is not completely filled: the crack walls themselves appear to consist of anisotropic minerals. Table 6.5 shows the results of an electron probe investigation into this feature. Three zones are recognised. One is isotropic grey material outside the crack, constituting the groundmass, inside the crack walls there is a dark grey zone, bordered by much paler whitish material. Offshoot cracks from the main crack can be seen, also with anisotropic material making up the crack walls. The main difference between the dark grey zone and the white zone in the crack walls is that the Al and Si contents of the former (1.8% and 3.1%) are higher than the latter (1.3% and 1.6%).

The Mn content of the dark grey zone is much lower

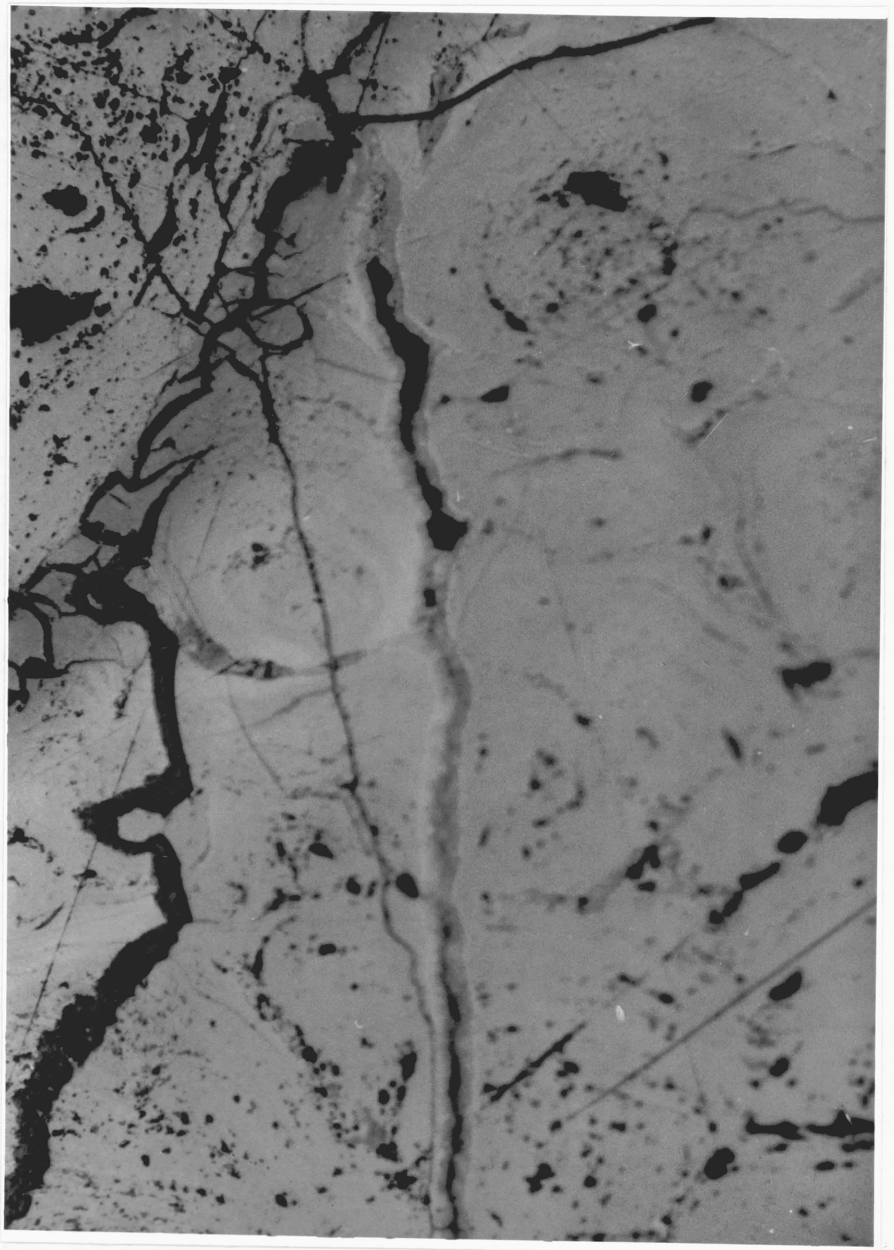

Plate 6.10: Vertical crack in a specimen from 1315. (Plain light). ⟵⟶ 50μ

Plate 6.11: Same crack as in Plate 6.10. (Polarised light).

	Top outside void, n = 2	Btm outside void, n = 4	Inside void	
			Isotropic n = 12	Anisotropic n = 12
Mn	19.6	18.4	19.9	36.7
Fe	11.7	14.4	16.1	3.8
Ni	0.3	0.35	0.48	2.5
Co	0.9	0.75	0.59	0.53
Cu	not detected	0.09	0.06	0.20
Ca	1.9	1.8	2.1	1.25
Si	0.8	2.2	1.4	0.46
Al	0.17	0.68	0.49	0.81
Mg	0.6	0.86	1.1	2.8
K	0.25	0.52	0.27	1.1
P	0.33	0.35	0.4	0.08
S	0.39	0.48	0.5	0.66
Mn/Fe	1.7	1.3	1.3	27.8

Table 6.4 Average E.D.S. analyses of the void environment and void filling in plates 6.8 and 6.9.

(22.4% compared with 36.6%) than the white zone, although the Mn/Fe ratio is not greatly diminished (12.9 compared with 16.3). The grey material of the fracture walls show less strong anisotropy than the white substance. This is similar to the observation of the infilling of the crack of 1301, and the variations in the chemical composition between the strongly anisotropic and the less strongly anisotropic minerals in both 1315 and 1301 are similar.

Discussion

It was described and discussed earlier how the fracture in 1301 was filled with a mixture of silicate material and crystalline anisotropic oxides. The fracture in 1301 is thought to be part of a network of fractures, allowing seawater to percolate through and contribute to the formation of the fracture filling. The crack in 1315 is different from that in 1301: it is narrow and vertical, whereas the crack in 1301 was horizontal and relatively wide. However, the presence of smaller cracks, branching off from the main one, also lined with crystalline anisotropic oxides supports the suggestion that there is probably a fracture system, at least in this sample from 1315, allowing the percolation of seawater into it. The seawater is probably responsible for the formation of the crystalline oxides in and adjacent to cracks by transporting material necessary for the crystallisation process to the reaction site. The absence of any siliceous material (organic or inorganic) in the cracks of 1315 is noteworthy, since this is required for the production of crystalline metal-rich oxide in the theories of Lyle et al., (1977)

	OUTSIDE CRACK	INSIDE CRACK	
	Greyish white, n = 5	Dark Grey, n = 3	Whitish-grey n = 6
Mn	19.7	22.4	36.6
Fe	17.5	1.74	2.31
Mn/Fe	1.12	12.9	16.3
Ni	0.31	1.42	2.35
Co	0.47	0.10	0.34
Cu	0.07	0.12	0.36
Ca	2.14	0.38	0.81
Si	1.56	3.13	1.58
Al	0.73	1.80	1.34
Mg	0.87	2.21	2.79
K	0.28	1.00	1.11
P	0.37	0.02	0.05
S	0.56	0.08	0.25

Table 6.5 Average E.D.S. analyses of the crack in a specimen from station 1315 illustrated in plates 6.10 and 6.11.

and Burns & Burns (1978a). If either of these theories is correct then the present crystalline oxides inside this crack in 1315 cannot have been formed by a crystallisation process involving such siliceous matter. In the process envisaged by Burns & Burns (1978a), the iron from the pre-existing oxides is reduced to Fe^{2+} at least once before being reoxidised and precipitated. The Fe content of the crack is approximately an order of magnitude lower than in the groundmass (table 6.5). If a process of recrystallisation occurs in a way similar to that envisaged by Burns & Burns, then the redox potential of the crack environment would have to be low enough to maintain the Fe as soluble Fe^{2+} during its removal, and this would cause the Mn to be reduced to the soluble Mn^{2+} and removed also. This manifestly is not so (table 6.5). Therefore it must be concluded that a process of recrystallisation is probably not occurring, and that the crystalline metal-rich oxides in the crack have been deposited directly from metal-rich fluids percolating through the crack.

The similarities between the anisotropic crack lining and the anisotropic material in the void filling suggest a similar mode of formation for both. If the suggestion that the crack lining was formed by direct deposition from fluids percolating through it is correct, then perhaps the void-filling, at least the anisotropic part, was also formed by direct deposition from metal-rich fluids flowing through the voids. The amorphous, isotropic, relatively metal-poor oxides are envisaged as being deposited by normal sea water flowing through the voids. The void infilling probably

postdates both upper and lower layers. Therefore it probably postdates the crack in the lower layer, which appears to have been formed before the formation of the upper layer. So while it is suggested that the origin of the crystalline metal-rich layers in the infilling is similar to the origin of the crystalline metal-rich deposits of the crack wall, the void-filling must have been deposited at a later date from different fluids.

Summary.

At station SHI30I, the probe data suggest a sudden change in the depositional environment, which is reflected in the changed composition of the deposited oxide of the top few mms. The similar compositions of this top layer and a fracture-filling at depth in the crust suggest that they may have been deposited from the same fluid. This indicates the possible importance of fractures for transporting fluids from outside the crust to inside. Possible post-depositional recrystallisation of pre-existing oxides lining the crack, as they react with water and fine suspended matter percolating through the crack, is suggested as an alternative reason for the change in composition of these oxides. The presence of an iron-rich silicate mineral also within the crack suggests that reaction processes similar to those suggested by Heath & Dymond (I977), and Lyle et al.,(I977) may have occurred.

At station SHI3I5, the absence of such silicate material in the vicinity of similar oxides adjacent to cracks and in void fillings suggests that these oxides were formed by direct deposition from metal-rich fluids percolating through the crust and not by post-depositional reaction processes.

At station SHI32I, it is thought that the todorokite present on the bottom of certain crusts was caused by post-depositional reaction of pre-existing ferromanganese oxides with sedimentary components such as opaline silica, and not by remobilisation of Mn from the sediment followed by subsequent incorporation of the metal into the crusts.

CHAPTER 7

SCANNING ELECTRON MICROSCOPE STUDIES OF FERROMANGANESE OXIDE CRUSTS FROM THE NORTH WEST INDIAN OCEAN.

Introduction and previous work

To understand the genesis of ferromanganese oxide deposits, it is essential to understand the mechanism of incorporation of authigenic, biogenic, and detrital components into these deposits. It has become increasingly recognised in recent years that the scanning electron microscope (SEM),particularly one which can be used in an analytical manner, can play a significant role in obtaining this understanding. The S.E.M. has been used with success to study the microstructure and microchemistry of many nodules from the Pacific (Fewkes, 1973; Margolis & Burns, 1976; Dugolinsky et al., 1977; Burns & Burns, 1978a, 1978b, 1978c, 1979; Lalou et al., 1979) with particular reference to establishing the role of biogenic material in nodule origin (Margolis et al., 1979; Dudley, 1979; Nesteroff, 1979; Bignot & Dangeard, 1979).

Fewkes (1973) studied a collection of nodules from the N.Pacific and concluded that non-crystalline material, floc-like in appearance, is colloidal in origin. He

suggested that crystalline materialwas derived not only from primary depositional processes on the outside of the deposits, but also from secondary recrystallisation processes occurring inside the deposits. Vassiliou & Blount (1977) found phillipsite crystals lining cavities in nodules from the Argentine Basin, and concluded they were authigenic in origin. The work of Burns & Burns (1978a, b, and c, 1979) is perhaps outstanding in its demonstration of the close association of biogenic siliceous debris with authigenic manganese mineral formation and authigenic phillipsite formation. They suggest a secondary recrystallisation process occurs inside deposits because of the thermodynamic instability of heterogeneous assemblages of biological and amorphous oxide materials.

Several workers have found the remains of organisms within ferromanganese oxide deposits (Frederick-Jantzen et al., 1975; Harada & Nishida, 1976), but it was not clear whether the organisms played a passive role, as a dilutant to ferromanganese oxide accretion, or a more active one by influencing nodule structure and composition. Recent results from several workers indicate a positive role for biogenic material in the growth of ferromanganese oxide deposits. Bignot & Dangeard (1979) feel that the scarcity of remains ascribable to fungi and bacteria is not in keeping with a fundamental part for them in the genesis of such deposits. However, the abundance of nannofossils such as coccoliths and diatom frustules within many deposits leads these authors to suggest that they make an important contribution to ferromanganese oxide deposit genesis. Dudley, (1979),

comes to the conclusion that biological activity during some phase of deposit accretion is of significance in determining the final composition and structure of the deposit. Nesteroff, (1979) states that deposits from 2000-3000 m. grow by the deposition on their surface of calcareous plankton debris. He suggests that their deposition is followed by replacement of the calcite by ferromanganese hydroxides. This diagenesis continues inside the deposits, where all the skeletal structures disappear, resulting in a texture identical to the one observed in nodules from below the carbonate compensation depth. Margolis et al., (1979) conclude that biogenic material within nodules from the equatorial Pacific provides nucleation sites for secondary growth of manganese oxides. They suggest that this may be the principal reason why nodules from here are enriched in Cu and Ni relative to nodules from elsewhere in the Pacific, and contain less abundant benthic fauna.

Nearly all the samples so far studied with the S.E.M. have come from the Pacific Ocean, particularly the ore-grade zone. A few have come from the Atlantic Ocean, but very little work has been published on S.E.M. investigations of deposits from the Indian Ocean. The primary reason for employing the S.E.M. on the present samples was to determine if there was any evidence on a micro-scale in support of the suggestions of previous chapters that volcanic activity, and secondary recrystallisation may have been responsible for influencing the chemistry of some of the specimens.

Method

Horizontal fracture surfaces for investigation were

obtained by gently breaking the crusts by hand so that fracturing would occur as much as possible along natural breaks. The fragments thus broken off were mounted horizontally on stubs and coated with gold for examination with the scanning electron microscope. The machine used was a JEOL JSM35, fitted with an energy dispersive detection system for qualitative study of the X-ray spectrum.

Results: 1317

Plate 7.1 shows a low magnification picture of the top surface of a crust from 1317. It shows a rippled form. Plate 7.2 shows a higher magnification picture of the same area. Coccosphere fragments are visible and the hollows are seen to be festooned in a fibrous algal growth. Closer inspection of the contents of these hollows shows large quantities of biological debris (Plates 7.3 & 7.4). Bristles of the siliceous organism Chaetoceros lorezianus (?) can be seen in plate 7.3, and in plate 7.4 fragments of the coccospheres Emiliania huxleyi and Gephyrocapsa oceanica can be seen. Of particular note is the good state of preservation of the calcareous debris, and the obvious baldness of the elevated areas of the crust, compared to the hollows. On the bottom of this surface layer, there are no signs of biological remains. Plate 7.5 shows the structure of the oxide particles at this point. Thin needle-like structures of unknown origin are present (labelled A). Also found in this zone were numerous clusters of material, an example of which is shown in plate 7.6. Their origin and significance are not known, but they are very similar to the birnessite clusters of Fewkes (1973). Plate 7.7 shows a long rod-like

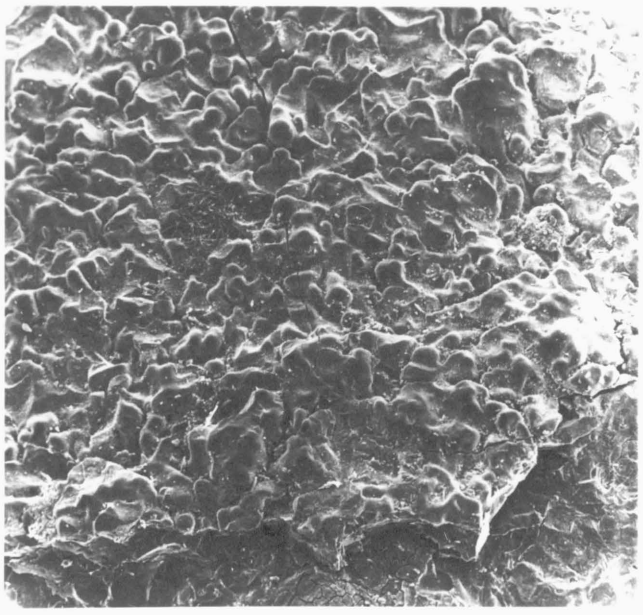

Plate 7.1: Top surface of a crust from station 1317, x20

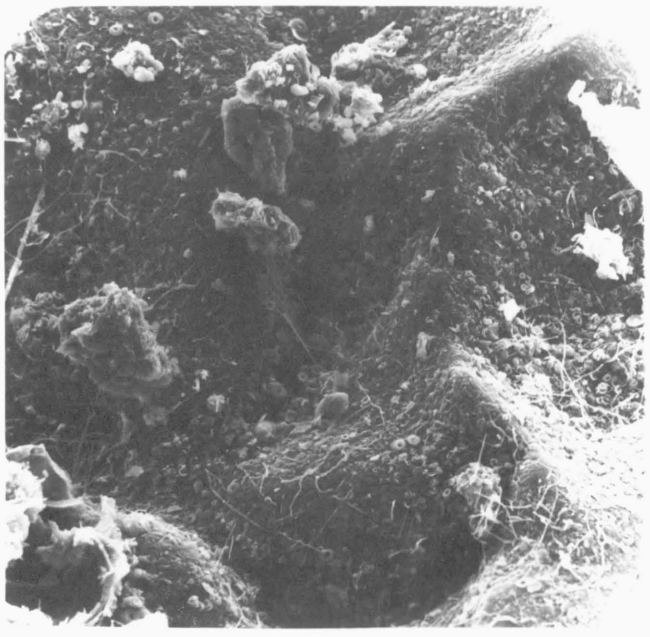

Plate 7.2: Close up of Plate 7.1, x330

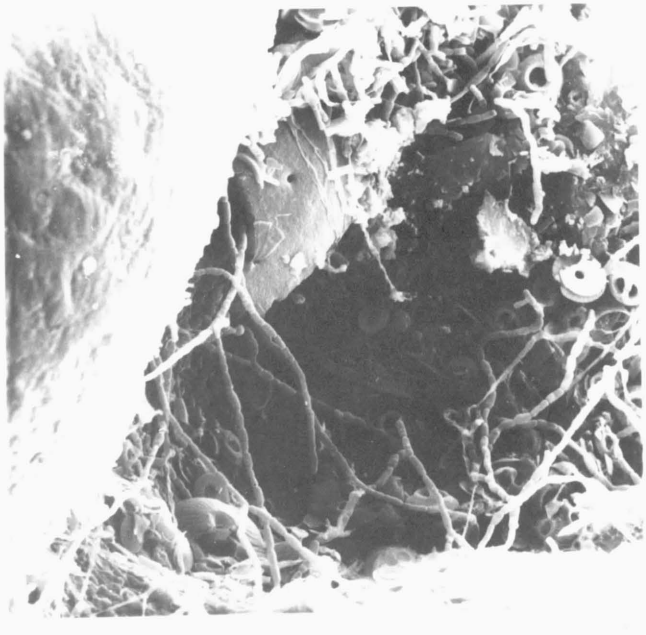

Plate 7.3: x1200

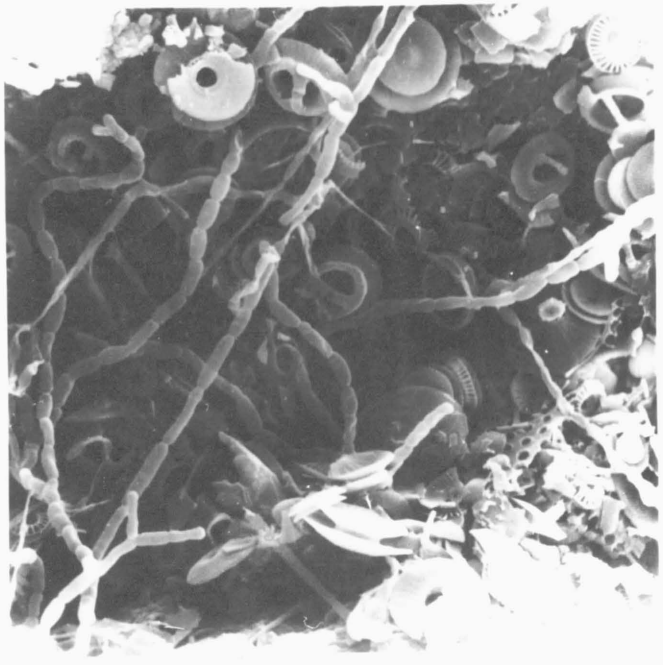

Plate 7.4: x2200

Biological remains in a hollow on the top surface of a crust from 1317.

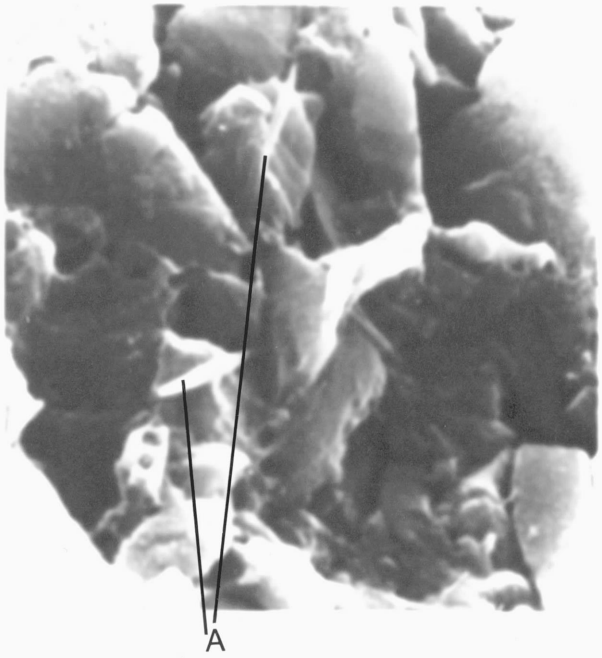

Plate 7.5: Oxide material, bottom of surface layer of a crust from 1317, x9000

Plate 7.6: Clusters of oxide material, bottom of surface layer of a crust from 1317, x3600

Plate 7.7: Object rich in Si, from 1317, x1000

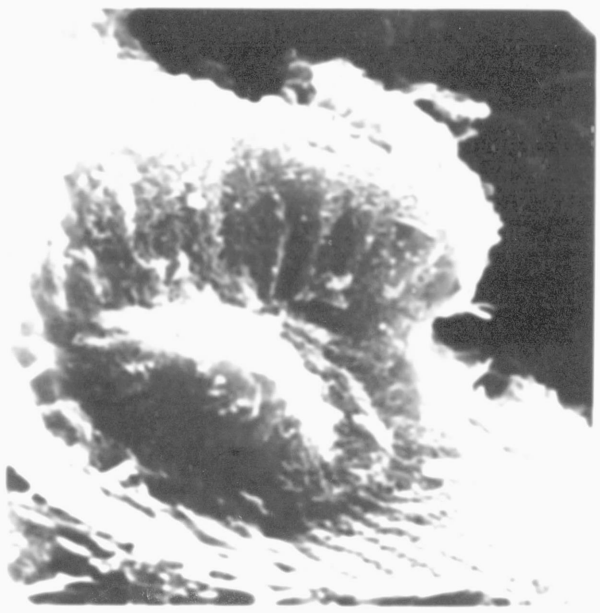

Plate 7.8: Coccolith(?) cast, from 1317, x12000

crystal protruding out of the oxide material. This is similar in appearance to the authigenic phillipsite crystals of Burns & Burns (1978a,b,c), and indeed, the analysis showed much Si but little Fe or Mn. There is no sign of any authigenic oxide material in its vicinity.

Below the top layer of 1317 was the middle layer, which featured in its upper part anisotropic cuspate columnar growths, very rich in Mn, Ni and Cu, which were discussed in Chapter 6. Plate 7.8 shows a cast of a coccolith in oxide material. The X-ray spectrum shows that the Mn content is very high, much higher than Fe. There are also relatively high quantities of Ni,Cu, and Mg in the cast material. This is in keeping with the observation of Dudley, (1979), who found foram tests completely replaced by relatively pure manganese oxides containing as much as 0.5% Cu, and only a trace of Fe. If coccoliths replaced by manganese oxides, such as that shown in plate 7.8, were relatively abundant in the upper part of the middle layer of 1317, then this might account for the presence of the colloform structures described in Chapter 6. The different shapes and sizes of the structures seen in the polished section might be accounted for by the different orientation of individual coccoliths with respect to the vertical axis of the section. Plate 7.9 shows the setting of plate 7.8, The bulbous botryoids to the left of the cast have a chemical composition which is completely different to the cast. The Mn content is less than the Fe, and Ni and Cu are not detectable. In the centre of the middle layer, further evidence of biological influence was the structure shown in plate 7.10. This object showed

Plate 7.9: Setting of plate 7.8, x1100

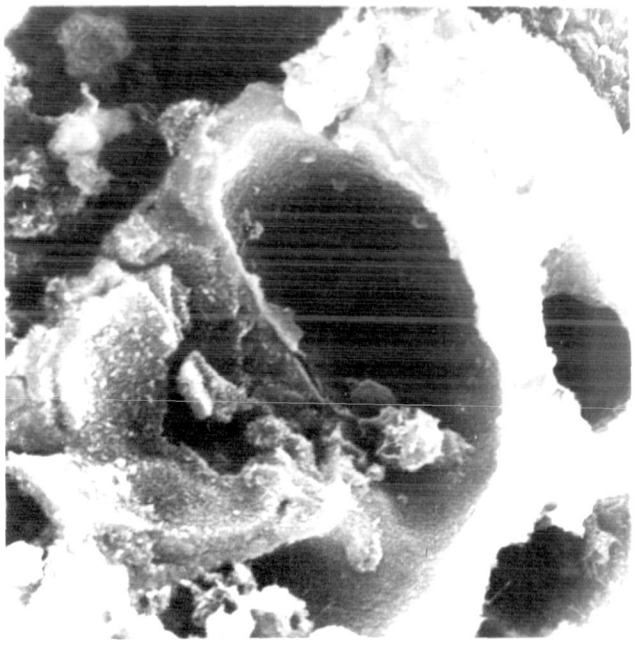

Plate 7.10: Structure of possible biological origin, middle layer of 1317, x3300

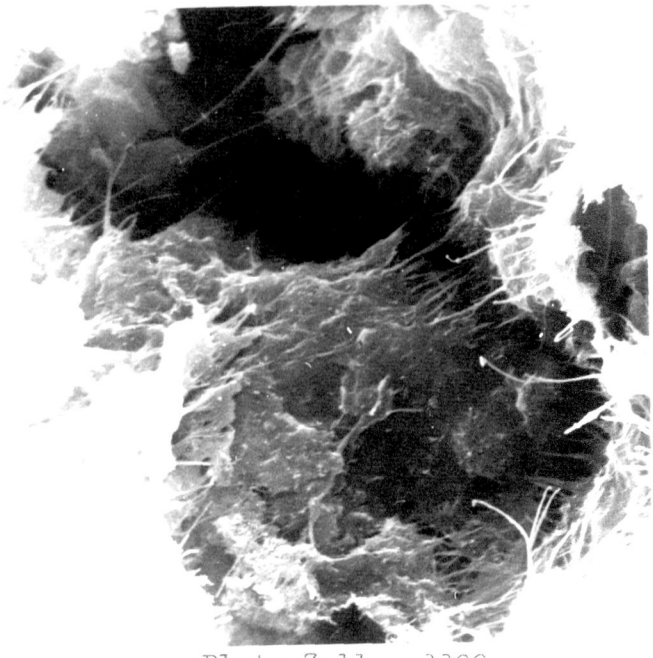

Plate 7.11, x3300

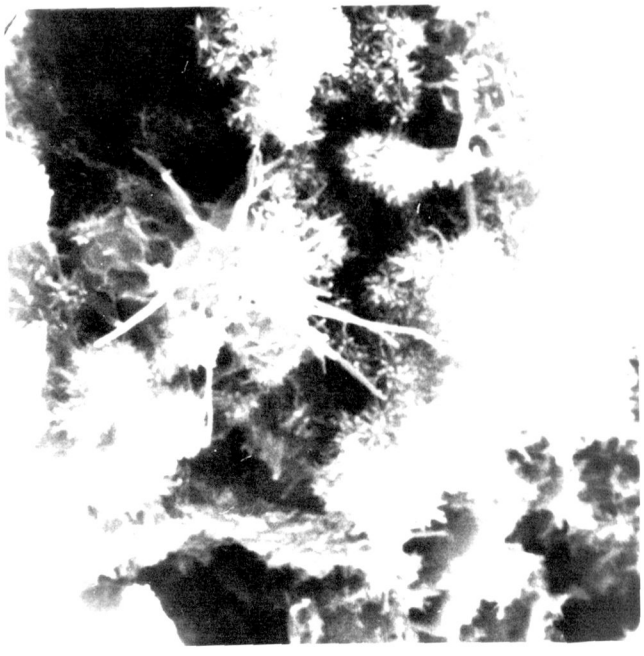

Plate 7.12, x9000

Fibrous iron oxide material from the middle layer of 1317.

no enrichment of Mn, Ni, or Cu, but the iron content was greatly in excess of Mn. In the bottom part of the middle layer, there was no sign of any biological or clastic debris, but there was much evidence of authigenic iron oxide formation.

Plates 7.11 and 7.12 show fibrous growths of iron oxide material found in this zone. The spectrum showed Fe to be the most abundant element. There was very little Mn, but there was a little Al. The bulk X-ray diffraction pattern of the bottom of the crust showed todorokite peaks, but no sign of any crystals that could be todorokite were found with the S.E.M.

1301

A todorokite-bearing crust (Type A, Chapter 3) was chosen from station 1301 for study with the S.E.M. The top 6 mms., where the todorokite was found previously (Chapters 4 and 5), were sampled. Again, biological remains were much in evidence (Plate 7.13) on the top surface. Also a honeycomb-like structure was found, very similar in appearance to that found by Bignot & Dangeard (1979) (Plate 7.14). Just below the surface, sphere-like structures were found (Plates 7.15 and 7.16). These are very similar in appearance to those found by Lalou et al., (1979), and they are also very similar in composition viz: high Mn, with some Ni and Cu. The surface upon which they are resting shows a relatively low Mn content and a high Fe content. No clues as to their origin or their significance were found. As with 1317, no crystalline material attributable to todorokite was seen, either on the surface or further inside the crust. In a

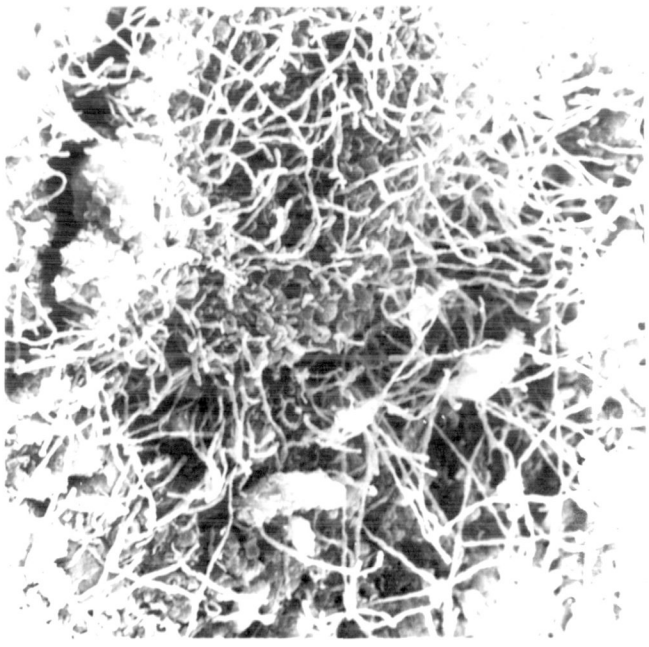

Plate7.13: Top surface of a crust from 1301, x940

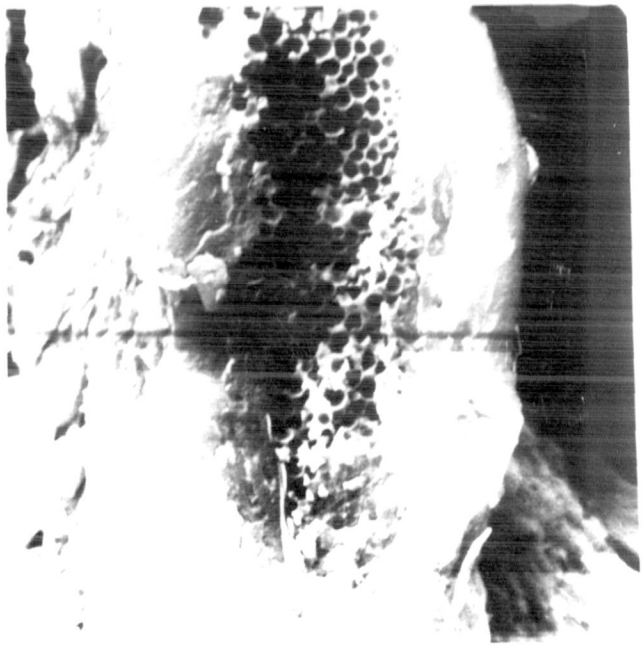

Plate7.14: Honeycomb structure from 1301, x3000

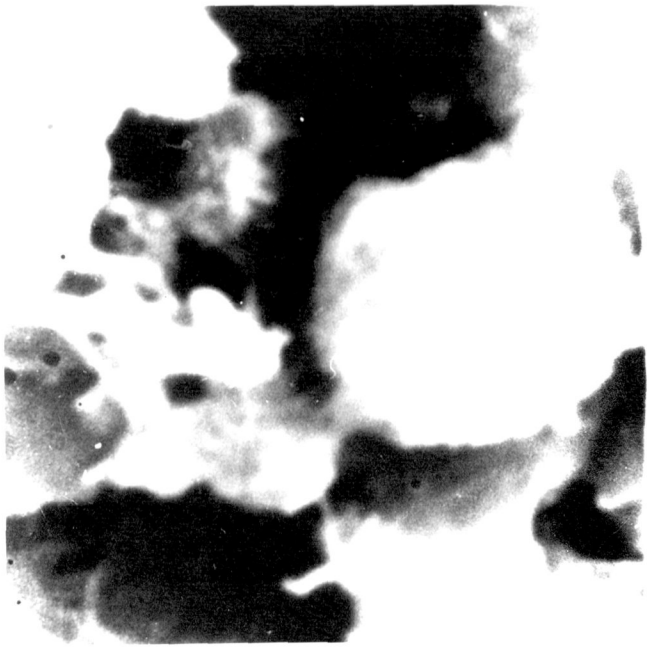

Plate 7.15, x10,000

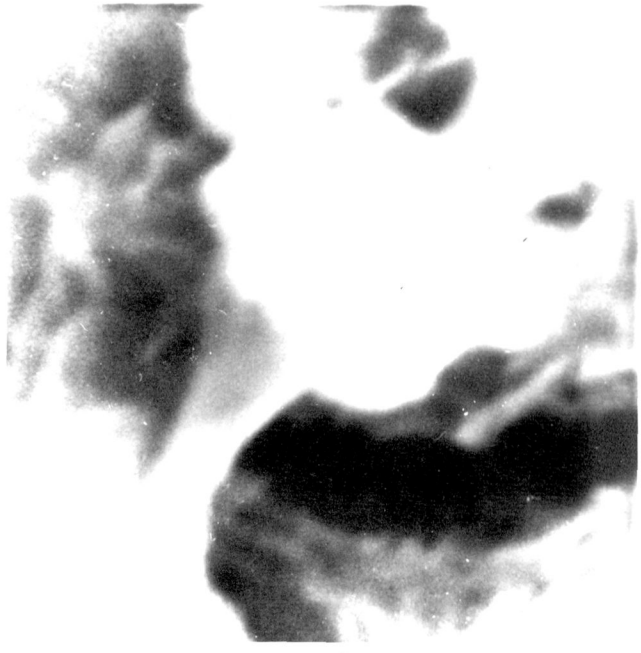

Plate 7.16, x11,000

Sphere-like oxide material from 1301.

layer beneath the spheres, needle-like iron oxide crystals were found (plates 7.17 and 7.18). The analysis showed much Fe, very little Mn, and a little Ni. Towards the bottom of the sampled zone, globular structures were found again, very similar in appearance to those found near the top (plates 7.15 and 7.16). Their composition is rather different, however. The dominant X-ray peaks are Ni and Cu, with some Al and Fe. The Mn content is relatively low. The surrounding area is higher in Fe content but with very little Ni and Cu.

Discussion

There was little evidence of detrital material in the specimens studied. No clay minerals were identified. This sparseness of detrital minerals could be caused by the rate of oxide accretion being much greater than the rate of deposition of detrital minerals. However, in view of the slow accretion rate of pelagic ferromanganese oxide deposits compared to accompanying sediments (Ku & Broecker, 1969; Heye, 1975; Anderson, 1978; Greenslate, 1978), this does not seem likely. A possible reason for this lack of incorporation of detrital minerals is that they are swept off the surface of the deposit, as they settle, by bottom currents. As they are swept along, they may abrade the surface of the deposit. This would account for the smoothness of elevated portions, seen in plates 7.2 and 7.3, and the accumulation of coarse material, such as skeletal remains, in the sheltered hollows. Therefore, the theory of Nesteroff (1979), whereby deposits from 2000 to 3000 m grow by the deposition on their surface of calcareous debris, which is subsequently replaced by

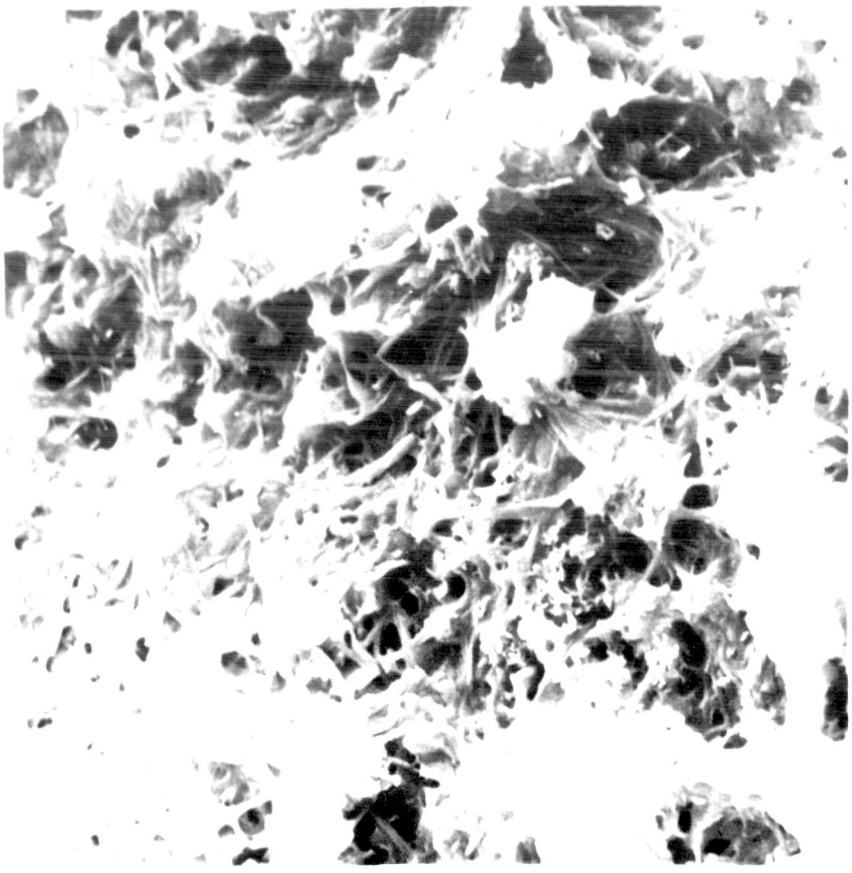

Plate 7.17: Fe-rich material from 1301, x2400

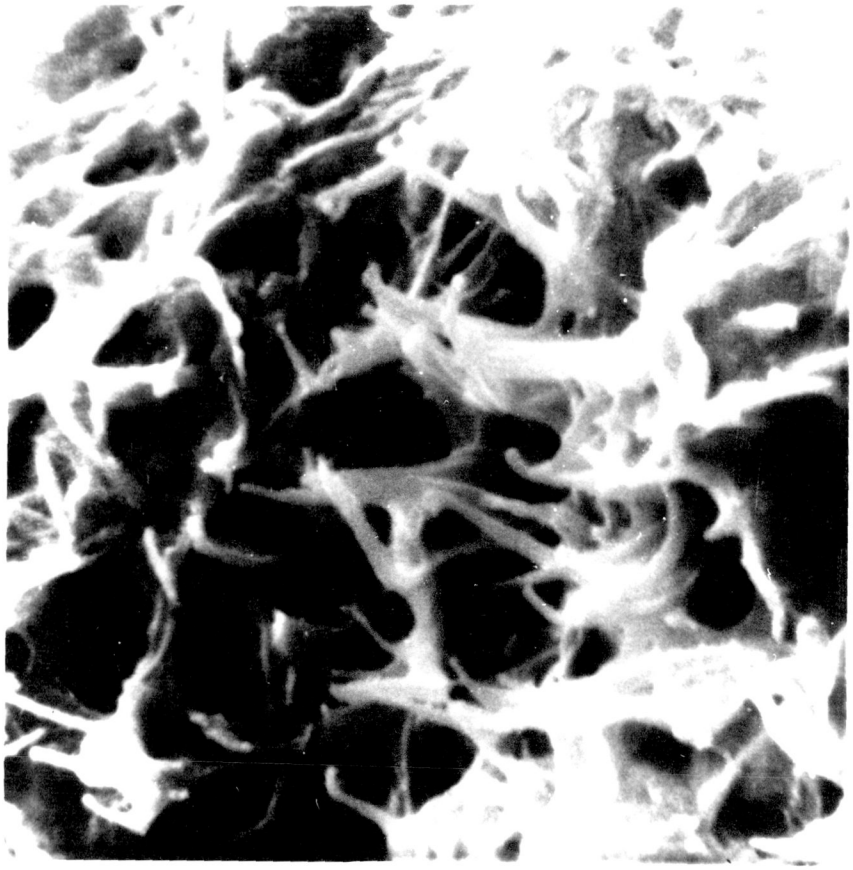

Plate 7.18: Fe-rich material from 1301, x9400

ferromanganes oxides, may only apply here to skeletal remains which are swept into sheltered hollows in the surface. Accumulation on the elevated portions may continue by the direct precipitation of ferromanganese oxide particles. The lack of biological remains within the crusts is difficult to reconcile with this observation. However, it might be explained in the following way. If this process has been in operation long enough to allow an appreciable increase in thickness of the crusts, it can be visualised that the elevated areas would coalesce and that the sheltered hollows would become cavities entrapped within the specimen. The contents of the cavities thus formed might then slowly dissolve or become replaced by ferromanganese oxides. If dissolution occurs, then any siliceous biological debris or clay minerals might assist in the formation of Cu-Ni rich todorokite (Lyle & Dymond, 1977; Burns & Burns, 1978a). If replacement occurs, then casts such as those seen in plates 7.8 and 7.10 would be seen. The disparity between the compositions of the features shown in plates 7.8 and 7.10 does not necessarily mean that they have a different genesis. Dudley, (1979), has noted a high Fe content associated with foram tests, possibly attributable to an Fe-rich cement used in the construction of the test. This may explain the high Fe content of the feature seen in plate 7.10. Dudley, (op. cit.) has also found foram tests completely replaced by relatively pure Mn oxides with only a trace of Fe. Such replacement of calcareous material may explain the high Mn content of the feature shown in plate 7.8.

There was no sign at depth in the crusts of fossil

residues definitely attributable to fungi. This is in agreement with the conclusion of Bignot & Dangeard (1979). The algal growth on the surface (plates 7.3, 7.4, and 7.13) was probably alive at the time of collection. The X-ray spectrum was identical to the oxide material behind it. It was felt that this was because the electron beam was passing through the algal cell material and impingeing on the oxide material surrounding it rather than because of any intrinsic mineralisation of the algal substance itself.

The appearance of the features shown in plates 7.15 and 7.16 is suggestive of a biological origin. The globules are apparently attached to each other by threads reminiscent of a biological secretion. How the globules were formed and why they have such widely varying compositions cannot be explained on the basis of the available data.

The lack of abundant identifiable biological remains may indicate that biological activity has had little overall effect on the composition and structure of these deposits. However, where such remains have been found, their local effect, particularly on composition, has been profound. No clear trend in these effects was seen; the composition of the oxide material associated with biological remains is very different from the oxide material of colloidal origin forming the rest of the crust: the former is markedly enriched in either Mn or Fe, whereas the latter shows no enrichment of either of these metals over the other.

Evidence of authigenic mineral formation is shown in plates 7.6, 7.11, 7.12, 7.17 and 7.18. The similarity between the feature seen in plate 7.6 and that found by

Fewkes (1973) is very striking. Fewkes thought that the feature he found was birnessite and attributed the formation of such crystalline material to the changes in the geochemical environment on the ocean floor. The feature shown in plate 7.6 was found in the top layer of 1317, which is thought to have a relatively homogenous oxide fraction (Chapters 4, 5 and 6), so the significance of its presence is not clear. The fine, fluffy crystals shown in plates 7.11 and 7.12 are from the bottom of the middle layer of 1317, which is relatively enriched in iron compared with the top and bottom of the crust. This layer is thought to have a volcanic origin (Chapter 5), so the material shown in plates 7.11 and 7.12, which appeared to be predominantly Fe oxide, may have precipitated from volcanic exhalations. The features in plates 7.17 and 7.18 were found on the underside of the todorokite-bearing top layer of a crust from station 1301. This substance bears some resemblance to the substrate of some of Fewkes' (1973) crystalline oxide material. Fewkes tentatively identified it as montmorillonite, though the X-ray spectrum of the present material showed mainly iron oxide with very little manganese oxide present, which would suggest that it is not montmorillonite.

To summarise, little detrital material was found in the ferromanganese oxide crusts studied in this work. No clay minerals were identified. This sparseness of detrital debris is thought to be because it is swept off crust surfaces by bottom currents. This may abrade and smooth the crust surfaces, and cause accumulation of coarse particles in hollows in the surfaces. Dissolution of incorporated biological debris

may bring about the formation of Cu-Ni rich todorokite. Replacement of tests by oxide material brings about marked fractionation of Mn from Fe: the replacing oxide has either a very high Mn content or a very high Fe content. Crystalline authigenic oxide material was uncommon in the ferromanganese crusts studied in this work. Possibly iron oxide crystal formation may occur when the deposit has a volcanic contribution. In other situations, the main method of growth is by deposition of amorphous colloidal ferromanganese oxide particles.

APPENDIX I

Sample preparation and analytical procedures

i) Introduction

All elements analysed in both nodules and sediments were determined by flame atomic absorption spectrophotometry, on a Perkin Elmer 403 and a Pye Unicam SP90. The hollow cathode lamps were operated at the manufacturers' recommended settings. The fuel/oxidant mixture of the flame was adjusted to optimise machine sensitivity.

Total carbonate in the sediment samples was determined with a calcimeter, standardised against Analytical Reagent calcium carbonate. The values thus obtained were assumed to be calcium carbonate.

ii) Sample Preparation

a) Ferromanganese oxides

All the North West Indian Ocean crusts had been collected by dredge haul and had been washed free of nearly all associated sediment while being brought up to the ship.

The nodules from 1323, 1578 and 1564 had been obtained from sediment cores but had already been washed free of sediment before being given to the author.

Samples were drilled out of the N.W.Indian Ocean crusts at various depths with a 2 mm. hand drill with a stainless steel bit. Analysis of such a bit has shown that no noticeable contamination of the samples should arise from this procedure. While the drilling gave rise to a fine powder, coarse fragments were usually chipped off by the bit, so the samples required crushing. This was done with an agate mortar and pestle. To minimise cross contamination between samples, both pestle and mortar were thoroughly washed with 50% HCl , deionised water and acetone between grinding each sample. At all stages of the procedure, care was taken to minimise loss of the finest fraction of the samples as dust to the atmosphere.

The nodules were sectioned with a hacksaw blade. Half was put inside for future work, a quarter was ground up for mineralogical analysis, and a quarter was prepared for chemical analysis.

b) Sediments

The sediment samples were supplied to the author in a variety of forms. Several cores had to be opened for sampling. The samples obtained from here were taken from the centres of the cores rather than the sides, to minimise the effect of smearing. The wet samples thus obtained were freeze-dried for 24-48 hours and then ground up as described previously. Some samples were supplied as a powder requiring no further preparation before analysis. The rest of the samples were obtained in a dried uncrushed state in a plastic container, e.g. polythene bag, sealed box. These were crushed without further drying.

iii) Bulk Chemical Attack

Approximately 250-300mg. of each sample were weighed out accurately into separate, numbered P.T.F.E. beakers which had previously been dried and weighed accurately. The beakers and their contents were then placed in desiccators and dried to constant weight, this usually taking 2 - 3 days. This preliminary desiccation procedure was only required for ferromanganese oxide samples, because of their tendency to absorb atmospheric moisture when in a finely divided state. After 5 mls. of 6M. HCl had been added to the beakers, they were placed on a hotplate and heated gently for about 2 hours to breakdown the manganese oxides prior to the addition of the main reagents. This pre-treatment was not necessarily with sediment samples. The beakers were then cooled and the following reagents added to each: 8 mls.of 40% hydrofluoric acid, followed by 6 mls.of a 50-50 mixture of concentrated nitric and perchloric acids.

After addition of all the reagents, the beakers were returned to the hotplate and evaporated to dryness. The beakers were then removed from the heat and a further 2 mls. of perchloric acid were added. The contents were evaporated to dryness again. While still warm, 5 mls. of 6M HCl were added to dissolve the small pellet of residue in the beaker. The resulting solutions, when cold, were transferred to separate, numbered 25 ml. volumetric flasks. The beakers were rinsed thoroughly with deionised water and the washings also transferred to the flasks. The contents were then made up to 25 mls. with deionised water, giving a final

solution which was very nearly 1M with respect to HCl. The solutions were then analysed by AAS, by comparing them with standard solutions made up in 1M HCl. The principles and method of operation of AAS are well known and will not be described. However, some work was done to establish the extent of calcium interference on certain elements.

iv) Calcium interference : effects and correction procedure.

a) Introduction

Compared to other spectral methods, atomic absorption spectrophotometry is relatively free from interferences. However certain interferences do exist. Within a flame, light is absorbed not only by the element being determined, but also by the flame and by other elements which may be present. If the spectral line of the element being determined cannot be resolved from those of other elements, a positive analytical error results because of the addition of the two signals. This is known as spectral interference. A particular type of this interference known as molecular absorption has been encountered in this study. The source of this absorption is the high concentration of Ca (up to 38%) in the sediment samples. The ferromanganese oxides, rarely exceeding 2% Ca, were generally not subject to this interference.

b) Effects of the interference:

In this study, molecular absorption by Ca has been recorded on the resonance lines of Ni (232 nm) Co (240.7nm), Cu (324.7nm), Cd (228.8 nm), Pb (283.2 nm) and Zn (213.8 nm). Horder (1979) also found this interference on Ba (553.6nm).

The effect of the molecular absorption can be seen from Table A1.1, in which the results are presented of analyses of a surface sediment from the North West Indian Ocean by AAS for the elements in question, with and without the application of the Ca interference correction procedure described below.

c) Method of correction

The correction method used was that developed by Horder (1979). This entailed preparing pure interference standards with zero content of the element being determined, and measuring these on the resonance line of thatelement. Since the amount of interfering element in the sample is known, its equivalent signal (determined from the standards) can be subtracted from the total signal. This method can also be used for multi-element interferences, if the combined effect is additive.

In this study, the molecular absorption is probably nearly all attributable to the large concentrations of Ca present, and not from the other potential interferents such as Fe or Al. Therefore the method used was based on a single rather than a multi-element interference effect.

Ca standard solutions covering the range of Ca values found in the samples were measured on the resonance lines in question and the absorbances caused by the known concentrations of the calcium were recorded. From a correction graph of absorbance against Ca content, it was possible to determine the absorbance due to molecular absorption of a particular trace element at a particular Ca concentration. All the samples were corrected against

Table A1.1

Analysis of a surface sediment from the N.W.Indian Ocean by AAS with and without the application of the Ca interference correction procedure.

Element	Without Correction (ppm)	With Correction (ppm)	Analytical precision (%error)
Ni	280	174	15.3
Co	224	73	50.3
Cu	264	238	2.4
Cd	56	15	1.0
Pb	280	73	16.0
Zn	192	122	18.0

Wt. % Ca. in sample = 28.67%

All data are expressed on a C.F.B.

such graphs and the value due to molecular absorption was deducted from the total absorbance before the results were recalculated to a carbonate-free basis.

This method of correction has been applied to all the sediment samples analysed in this study. It does not take into account any other interelement molecular absorption effects which might occur in these samples and is therefore only a first order correction method.

d) Deuterium background correction

The deuterium background correction is an alternative correction method to the one employing interference standards which was described above. It was employed by Koirtyohann & Pickett(1965) and Billings(1965), who considered it particularly useful for Cd, Zn, and Ba. Its merits have been discussed by Angino & Billings(1967) and Zander (1977), but controversy exists concerning its validity in all analytical situations. The method employs a hydrogen (deuterium) lamp as well as the normal hollow cathode lamp. Using the hollow cathode lamp, the element plus background absorbances are measured. Then, by employing a switching mechanism to superimpose the deuterium spectrum along the optical path of the hollow cathode lamp's sharp line spectrum, the background absorbance is measured at an adjacent wavelength. The difference between the two signals is the absorbance due to the element, the background correction having removed the effect of the molecular absorption. However, Koirtyohann & Pickett (1965) point out that fine structure in the background, perhaps unresolved, may also cause error. For example, Na may interfere in the

determination of Mg in Na salts since a sodium line at 285.3nm is very close to the analytical Mg line at 285.2nm. The sodium line would absorb part of the continuous radiation passed by the monochromator set to detect Mg, thus causing too large a correction to be made.

Horder (1979) has compared the Ca interference standard correction method with the deuterium background correction method for Ni and Cd. He also attempted a comparison for Cu but was prevented in this by a serious degradation of the signal-to-noise ratio. He suggested the behaviour of Co is probably similar to that of Ni, Zn to that of Cu, and Pb to that of Cd. He concluded that the deuterium background correction produces unsuitable measurements of the background absorption for Ni, Cd, and Cu. He put forward the following reasons:-

1. Instability of the intensity of the deuterium source.

2. Difficulty in matching the intensities of the deuterium and hollow cathode lamps.

3. The resultant high noise levels.

4. The difficulty of obtaining exact super-position of the two spectra along the optical path of the spectrophotometer.

It was decided to extend this study to cover more of the affected elements. The elements chosen were Co and Zn, and Ni was restudied. The main analysis line of Co at 240.7nm is very close to a fairly strong Ca line at 239.9nm. It was hoped that the effect of this would become clear as the study proceeded. The method chosen was similar to that

of Horder (1979): a number of sediment samples were taken and analysed for Co, Zn, and Ni using first the Ca interference standard correction method and then using the deuterium background correction method. The results are shown in figures A1.1, A1.2 and A1.3.

For Co, (Fig. A1.1), the deuterium background correction method gave such large corrections that there was little or none of the original signal left. Only a few samples had signals left to be plotted. This is probably because of the proximity of the Co line to a Ca line, mentioned above. It is in this situation that the deuterium correction method fails, by making too large a correction. The spread of the remaining data clearly indicates that the deuterium correction method is not adequate to analyse for Co in a high Ca matrix.

From a study of Fig. A1.2, it appears that there is a difference in the amount of absorbance caused by the background absorption measured by the two methods for Zn. At low Zn levels (usually associated with high Ca levels), it appears that either the deuterium background correction method under-corrects or the Ca interference method over-corrects. At higher zinc levels (greater than about 0.5 µgms./ml.), generally associated with lower Ca levels, this appears to be reversed.

For Ni, (Fig. A1.3), the picture is less clear. At low Ni values (high Ca levels), values for Ni fall on both sides of the equivalence line. More points seem to be above it than below it i.e. the calcium interference corrected values are higher than the deuterium background

Figure A1.1: D_2- corrected values vs. Ca- corrected values, for Co.

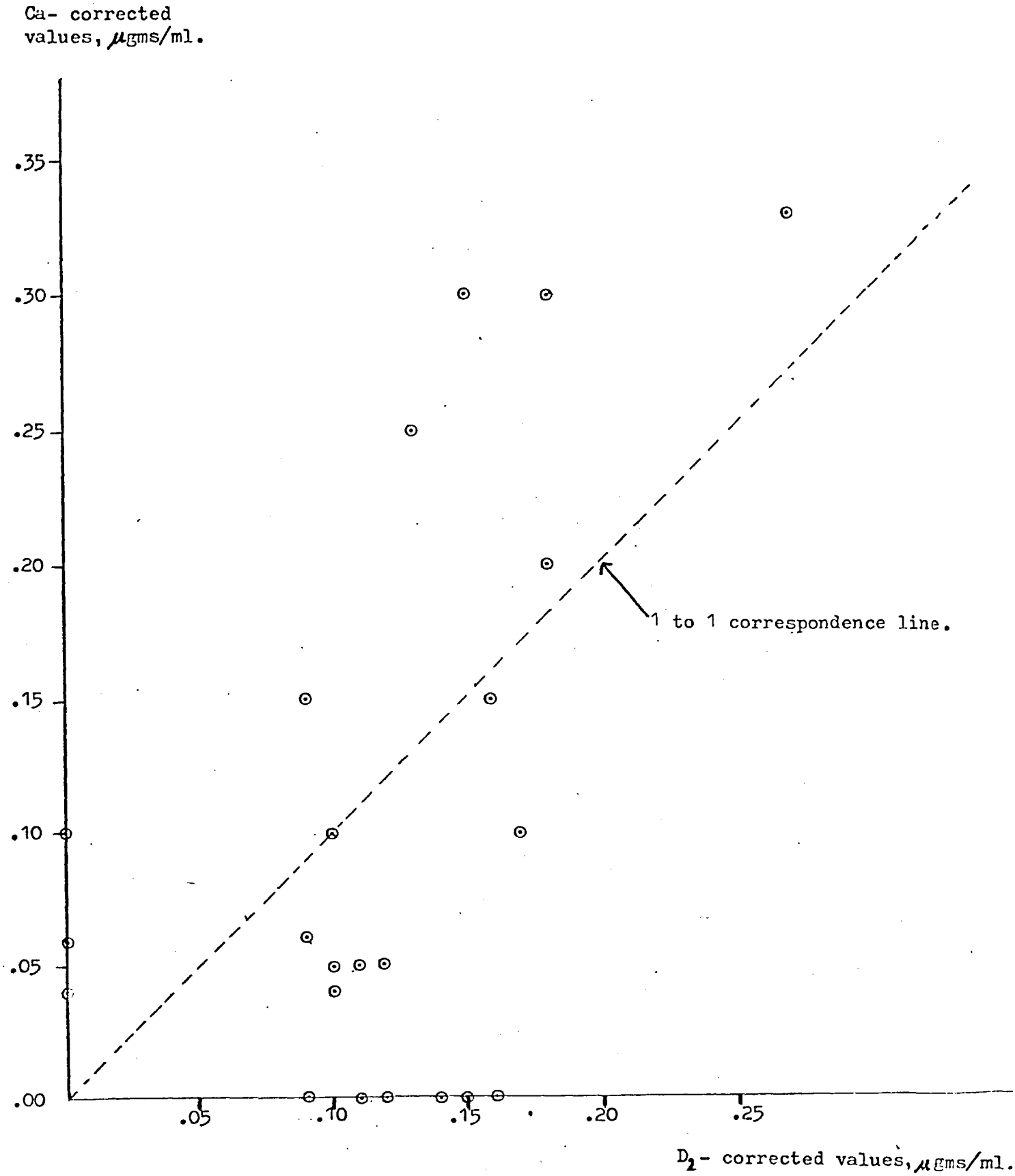

Figure A1.2: D_2- corrected values vs. Ca- corrected values, for Zn.

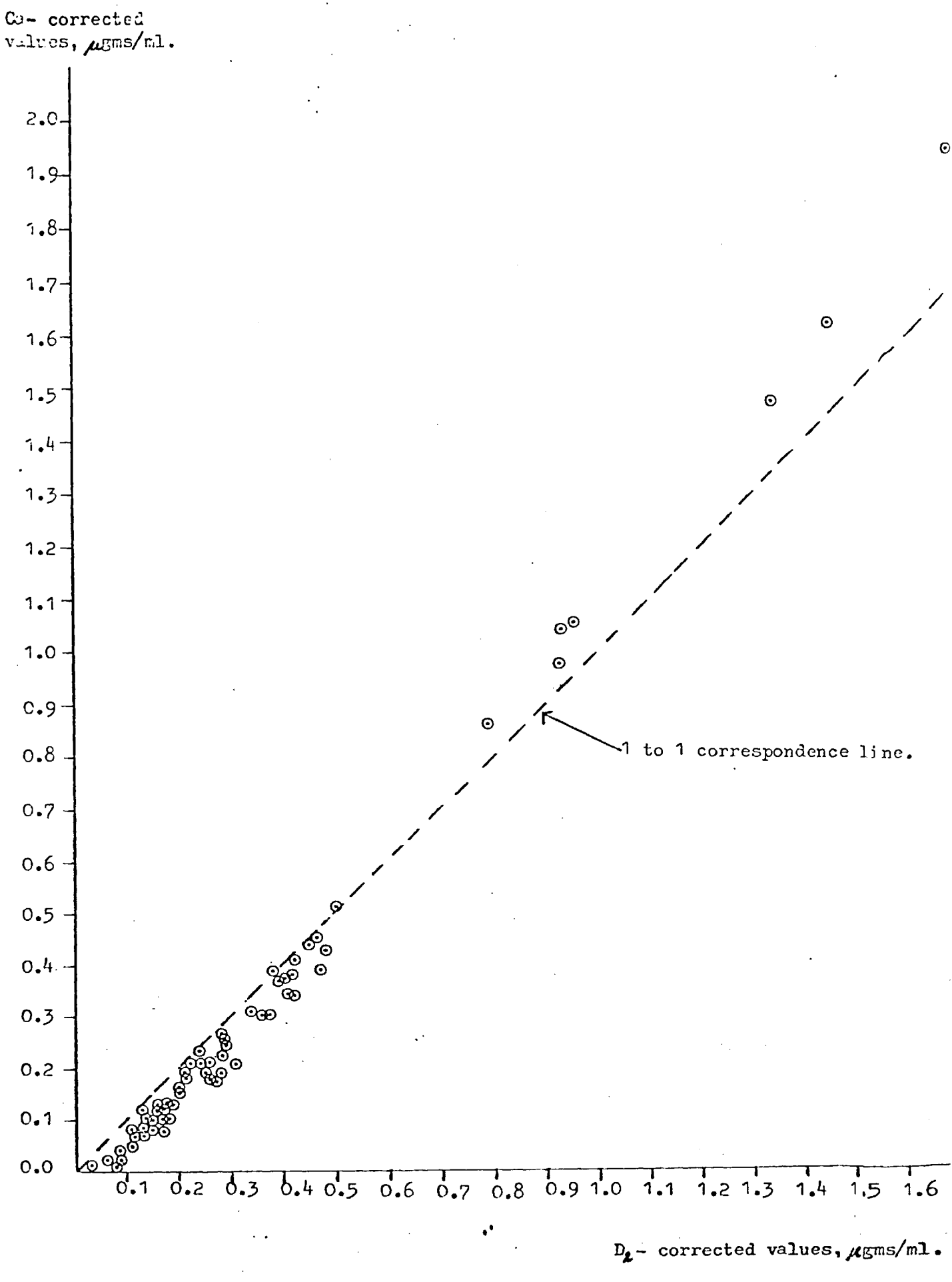

Figure A1.3: D_2- corrected values vs. Ca- corrected values, for Ni.

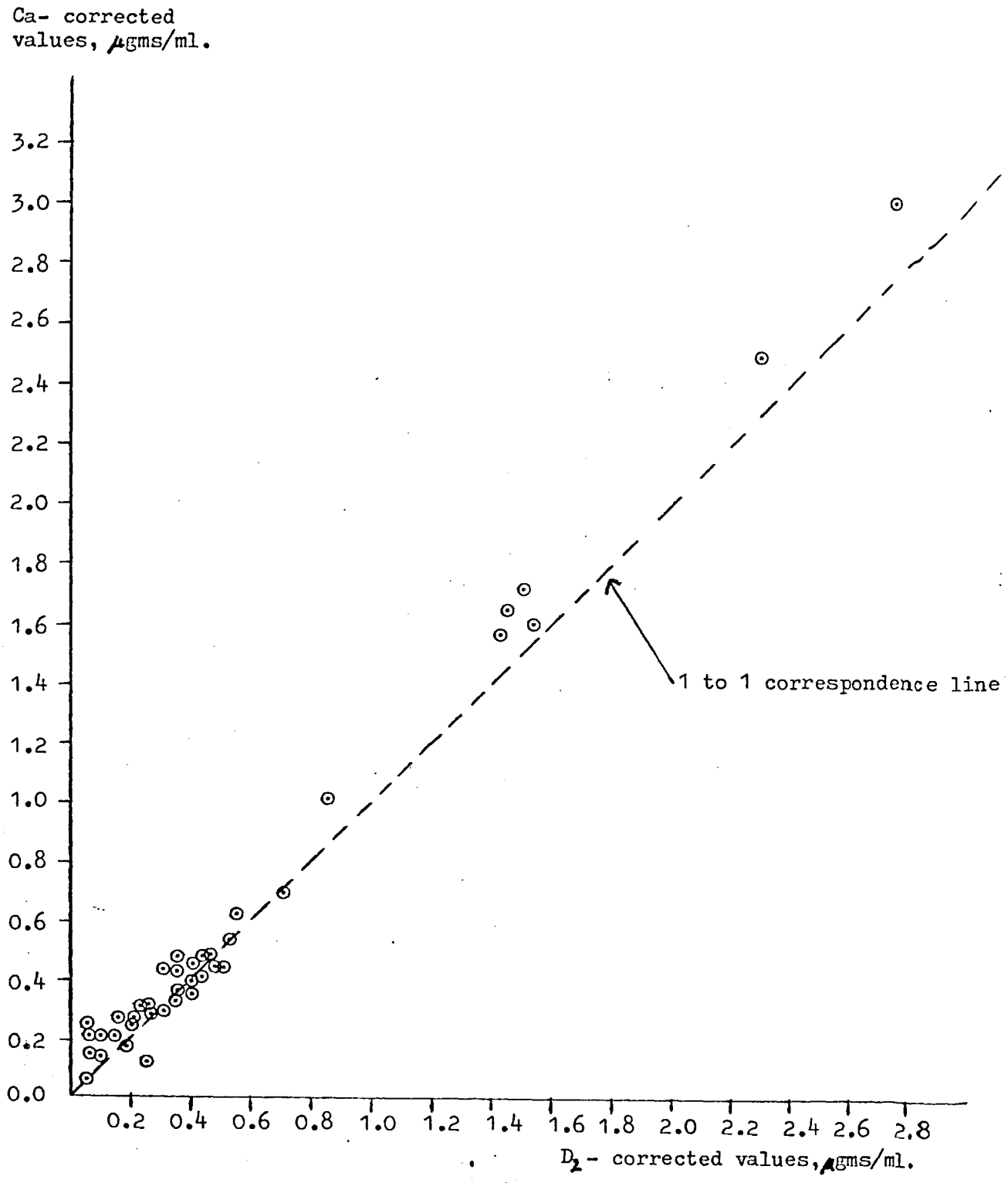

corrected values. This is opposite to the results of Horder (1979), who found that for Ni, the deuterium background corrected values were larger than the Ca interference corrected values.

Since only one detecting device is used (a phototube), it is essential to ensure that the beams from the hollow cathode and deuterium lamps are exactly superimposed(Zander, 1977). In the instrument used by Horder, a Perkin Elmer 403 Spectrophotometer, this was not possible. Consequently, "some miscorrection must be expected" (Horder, 1979). The machine used by the author, an IL 351, is more sophisticated and superpositon of the beams was possible. Consequently, the accuracy of the correction is probably greater, leading to a more accurate estimation of the Ni content of the samples.

In conclusion, it appears that for Co, the deuterium background correction method cannot be used in high Ca samples because it over corrects. The calcium interference correction method probably gives better results. For zinc there is little to choose between the two methods: below about 0.5 µgms/ml.Zn, the deuterium background correction method appears to undercorrect with respect to the Ca interference correction method, and above 0.5 µgms/ml.Zn, the opposite seems to occur. The significance of the differences in the values for Zn in geochemical terms is seen in figure A1.4. This depicts the down-core plot for Zn for core SH1305, using Zn values calculated by the Ca interference correction method and the deuterium background correction method. The values for the Zn

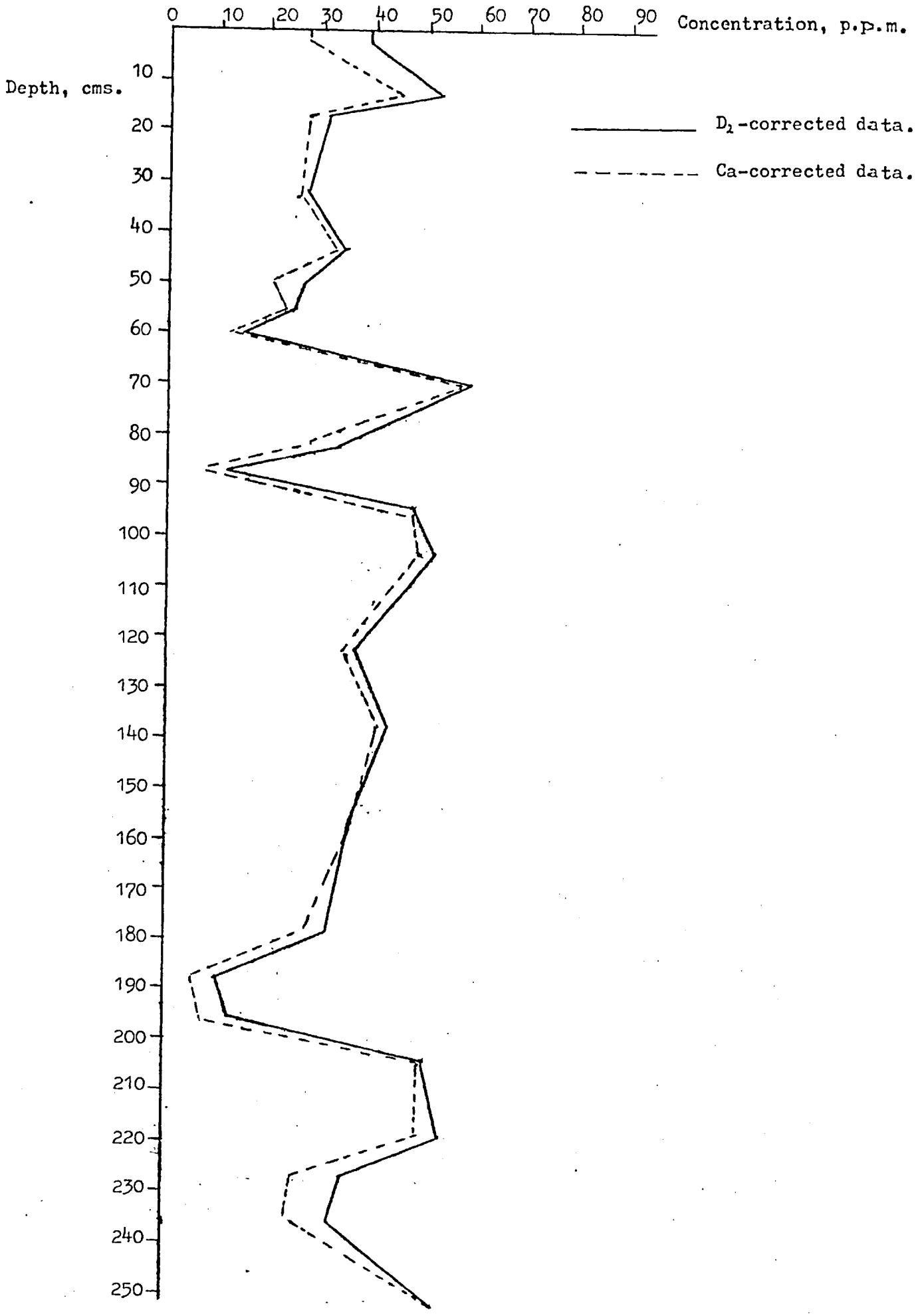

Figure A1.4: Comparison of Zn content (expressed on a total sediment basis) in core SH1305, determined by Ca- corrected a.a.s. and by D_2 - corrected a.a.

content sometimes differ quite widely e.g. 27 ppm and 38 ppm in the surface for the Ca-corrected and the deuterium-corrected values respectively. However, the overall geochemical interpretation of the data is not affected since the trends are the same for the two sets of values. For Ni, there are again only small differences between the Ca-corrected values and the deuterium-corrected values. The geochemical interpretation of the data is therefore not likely to be significantly different if either the Ca-interference corrected data or the deuterium background-corrected data are considered.

v) Calcium carbonate determination

It is necessary to obtain accurate Ca CO_3 values for the sediment samples for use in the carbonate-free correction, particularly at the higher Ca CO_3 concentrations (>80%) (Dymond et al., 1976). The Ca CO_3 contents of the sediments have been determined from CO_2 values obtained by an acid dissolution process using a Collins calcimeter. The volume of gas evolved when a known amount of sample reacts with an excess of acid is measured. The equation for the reaction is

$$CaCO_3 + 2HCl = CaCl_2 + H_2O + CO_2$$

The calcimeter is similar to the apparatus used by Hulsemann (1966); in the calcimeter, the liberated CO_2 displaces a column of water rather than a column of mercury as in the method of Hulsemann (op.cit.). The water is displaced from a calibrated tube, thus allowing the amount of liberated CO_2 to be read off directly in cms^3. The sample and water column were allowed to equilibrate to

room temperature in a water bath before the reading was taken. The apparatus is calibrated using Analar $CaCo_3$ and the values obtained were corrected for volume differences in reaction vessels, differences in sample weights, and variations in room temperature and barometric pressure. The wt. of $CaCO_3$ is calculated as follows:-

0.2 gms Analar $CaCO_3 \longrightarrow 44$ cms^3 CO_2

$$\therefore \text{wt. \% } CaCO_3 = n \times \frac{44.0}{Cs} \times A \times W \times T \times P \times V$$

where n = volume of CO_2 evolved from sample

Cs = volume CO_2 obtained from Analar $CaCO_3$ for a particular sample batch.

A = correction factor for molecular weight of CO_2,

$= \frac{100.08}{44.08}$ in $CaCO_3$

W = correction for difference in sample weight,

$= \frac{0.20}{\text{recorded sample wt.}}$

T = Correction for variation in room temperature,

$= \frac{\text{Initial temperature}}{\text{Temperature at measurement}}$

P = correction for variation in barometric pressure

$= \frac{\text{Initial pressure}}{\text{Pressure at measurement}}$

V = correction for volume of reaction vessel

$= \frac{V_O}{V_A}$ V_O = 100cms^3 (a 100ml. Quickfit conical flask)

V_A = Actual volume.

It has been suggested that this method may dissolve

amounts of $MgCO_3$ (dolomite). However, Horder (1979) reports that dolomite is only dissolved by the acid used in the determination (25% HCl) if the reaction vessel is heated, and suggests that Mg is present in forms other than a discrete carbonate phase. Since the sediments studied come from an oxidising, open ocean environment, it is unlikely that the gas evolved contained any H_2S which might have been evolved from the attack of sulphide minerals by the acid, and is therefore CO_2 liberated from the dissolution of the calcium carbonate in the sediments.

Results

The standard used was the U.S.G.S. National Bureau of Standards Argillaceous Limestone, NBS1b. The mean value of $CaCO_3$ in this standard was found to be 91.43% (16 measurements) with a standard deviation of 0.82%. The precision of the method, quoted at the 95% confidence level (i.e. two standard deviations) is therefore ± 1.64% $CaCO_3$. The variation between the reported Ca CO_3 content of NBS 1b and those determined here i.e. the accuracy was ±0.3%.

APPENDIX 2

Accuracy and Precision

The accuracy and precision of the methods used have been determined using international standards. Four ferromanganese oxide standards were available, covering a range of compositions; these had been analysed at eight other laboratories in Europe and America so their compositions were well established. Table A2.1 shows the results of the present analyses compared with the recommended values. The only problem appears to be Al which consistently seems to be 20% lower than the recommended values. The reason for this is not known; Moorby (1979), using the same standards, did not experience this. The Al values for the sediment standards (analysed over the same period) are very close to the recommended values. Since the error seems to be consistent, then the Al values for the whole data set should be internally consistent. Therefore since the purpose of the study was an attempt to understand ferromanganese oxide deposit genesis in the North West Indian Ocean, the Al values of the samples have not been adjusted. All other accuracies are better than 10% and are considered satisfactory.

Because of the wide range of sediments analysed (from 0% calcite to 97% calcite) it was difficult to find a standard

Table A2.1 Concentrations of major and trace elements in ferromanganese oxide standards used in this study, together with values of analytical accuracy for each metal.

Standard	No.of detmns.	Result	Mn %	Fe %	Co	Pb	Ni %	Cu %	Zn	Al %	Ti	Ca %	Mg %	Cd	Li
		Actual	29.5	5.2	1600	350	1.46	1.48	1570	3.18	3700	1.78	n.d	n.d	n.d
I	13	Found(±2σ)	27.1	4.8	1594	367	1.37	1.45	1420	2.46	3581	1.72	1.96	22	134
			±1.83	±.48	±176	±27	±.14	±.16	±132	±.29	±856	±.47	±.64	±3	±22
		Accuracy,%	-8.1	-7.7	-0.4	+4.9	-6.2	-2.0	-9.6	-22.6	-3.2	-3.4	--	--	--
		Actual	22.3	13.2	2900	750	0.76	0.51	820	2.81	9300	1.93	n.d	n.d	n.d
II	11	Found(±2σ)	21.28	11.89	2790	812	0.70	0.50	738	2.21	9087	1.85	1.34	8	39
			±1.3	±.73	±388	±86	±.06	±0.06	±42	±.48	±1313	±.3	±.13	±2	±8
		Accuracy	-4.6	-9.9	-3.4	+8.3	-7.6	-2.1	-10	-21.3	-2.3	-4.1	--	--	--
		Actual	19.1	6.7	1700	490	0.95	0.8	1010	4.98	5000	1.45	n.d	n.d	n.d
III	10	Found(±2σ)	18.59	6.32	1653	510	0.90	0.8	875	4.10	4495	1.51	1.80	12	93
			±1.0	±.46	±140	±109	±0.03	±0.05	±5.7	±.65	±929	±.59	±.09	±2	±12
		Accuracy	-2.7	-5.7	-2.8	+4.1	-4.8	+0.5	-13.4	-17.7	-10.1	+4.1	--	--	--
		Actual	31.8	4.6	1700	330	1.52	1.52	1580	2.8	3000	1.66	n.d	n.d	n.d
IV	13	Found(±2σ)	30.42	4.46	1752	350	1.45	1.50	1575	2.09	2925	1.59	2.05	25	151
			±3.1	±.45	±253	±4.7	±.15	±.16	±154	±.28	±384	±.34	±.18	±2	±17
		Accuracy	-4.3	-3.0	+3.1	+6.1	-4.6	-1.3	-0.3	-25.3	-2.5	-4.2	--	--	--
		Average inter-batch replicate sample precision,%	7.1	8.3	12	13.1	8.0	9.8	7.8	15.7	18.0	26.0	14.2	15.8	15.3
		Average element accuracy %	-4.9	-6.6	-0.9	+5.8	-5.8	-1.2	-8.3	-21.7	-4.6	-1.9	--	--	--

n.d: not determined. Co,Pb,Zn,Ti,Cd and Li are expressed in p.p.m.

Table A2.2 Concentrations of major and trace elements in sediment standards used in this study, together with values of analytical accuracy for each metal.

Standard	No. of detmns.	Result	$CaCO_3$ %	Ca %	Mn	Fe	Ni	Co	Ti	Al %	Mg %	Cu	Zn	Pb	Cd
		Actual	--	1.48	4500	5.62	120	58	5190	9.4	1.99	105	130	33	4
		Found($\pm 2\sigma$)	--	1.68	4301	5.67	137	94	4798	9.18	2.02	113	148	67	4
Red	6			±.25	±480	±0.18	±14	±14	±444	±1.3	±0.3	±5	±8	±32	±2.9
Clay		Accuracy,%	--	13.5	4.4	0.9	12.4	62	7.6	2.3	1.5	7.6	13.8	100	0
		Precision,%	--	14.9	11.1	3.1	10.2	14.9	9.2	14.1	14.8	4.4	5.4	47.7	72.5
		Actual	91.72	35.84	1370	0.53	17	10	-	0.62	0.22	2.4	19	9	1
NBSIb	21	Found($\pm 2\sigma$)	91.43	36.79	1550	0.55	14	9	ND	0.66	0.20	4.5	17	12	1.5
Limestone			±1.64	±4	±194	±0.03	±11	±14		±0.06	±0.02	±2	±8	±16	±1.5
Standard		Accuracy,%	0.3	2.6	11	3.8	17.6	10	--	6.5	9.1	87.5	10.5	33	50
		Precision,%	1.8	10.9	12.5	5.4	78.6	155	--	9	10	44.4	47.1	133	100

N.D. Not Detected

All metals are expressed in p.p.m. unless otherwise stated.

which would fairly represent this range. Two standards were used: an argillaceous limestone, NBS 1b, and a red clay standard supplied by the Institute of Oceanographic Sciences. Since the more calcareous the sediment, the lower the trace metal content, then to present average accuracies and precisions over such a wide range of calcite contents would have little meaning. Table A2.2 shows the analytical data for the clay and limestone standards, together with the precision and accuracy for each element in each standard. The precisions on the trace metals (Ni, Co, Cu, Zn, Pb, and Cd) are much worse for the limestone than for the clay. This is probably for two reasons: the actual contents are lower and the calcium interference effects are stronger. Because of these effects, the accuracies for Ni, Cu, Pb and Cd are all worse than 15% in the limestone whereas only Co and Pb fall into this category in the clay. While the correction method employed is reasonably efficient, with such low amounts of the metals present in the limestone standard the signal to noise ratio is still relatively poor even after correction, thus causing the poor accuracies and precisions on these metals. Very few of the sediment samples had such low metal contents; consequently the data quality overall should be better than is implied from the limestone standard.

In conclusion, it seems that while the major elements are analysed well by the methods used, caution must be used when discussing the minor elements Ni, Co, Cu, Zn, Pb and Cd because of their relatively poor precisions and accuracies.

APPENDIX 3

Minerological analysis

i. Sample Preparation

The samples were acquired and prepared as described in subsection ii(a) of Appendix 1. A portion of each sample was placed in a small agate mortar and ground until the powder became quiet under the pestle. The pestle and mortar were thoroughly cleaned with concentrated HCl and deionised water between each sample. There was usually insufficient material for cavity mounts to be used so smear mounts were prepared. No difficulties were encountered from preferred orientation of the crystallites.

ii. Analysis

The analyses were carried out on a Phillips PW1010/80 diffractometer using Fe Kα radiation at a tube setting of 34KV and 28mA. The radiation was filtered using a Mn filter and passed through a 2^{o} divergent slit and a 0.1^{o} receiving slit. Counting was by means of a proportional counter. The samples were scanned a $\frac{1}{2}^{o}$/minute through a range of 2θ from 5^{o} to 55^{o} and 80^{o} to 90^{o}. The peaks obtained on the diffracograms were compared against those given for recognised minerals in the ASTM index.

APPENDIX 4

Sample preparation and operating conditions for the electron probes.

Sections for probe analysis were prepared by the method of Sorem & Foster (1973). Selected crusts were first impregnated with Araldite. This inhibited crumbling and flaking of the crusts during cutting and polishing. After the resin had set the crust was cut and cast in more resin. The crust was cut again, and polishing of the section thus obtained followed the final product was a 2.5 cms. diameter polished block containing the crust section to be examined. Before insertion into the probe, the blocks were coated with carbon under vacuum. Because of the high porosity of the samples, the initial evacuation of the probe to an operational vacuum took up to two hours. To reduce this, the backs of the blocks were cut off so that there was less sample to evacuate. The section was then kept in a desiccator until required in order to reduce the water content. Finally, the section was kept under vacuum in the carbon coating unit overnight before use. With these precautions, it was found that evacuation of the probe to an operational condition was achievable in less than

five minutes.

For the Geoscan, the operating conditions were 15KV, and a specimen current of 50 - 100nA, depending on the element being determined. The higher the concentration of the element, then the lower the current and the shorter the analysis time. For Fe and Mn, the current was 50-55nA., and the analysis time was 10 seconds. For Cu, Ni and Co, the current was 100 nA. and the analysis time was 100 seconds. Severe specimen damage occurred when these latter conditions were used, so with the method used on the Geoscan (Chapter 6), the minor elements were always done last. Because of this specimen damage, the quality of the data for these metals is relatively poor compared with Fe and Mn. With the Microscan MK5, the operating conditions were 15 KV, a specimen current of 6-8nA. and a counting livetime of 100 seconds.

BIBLIOGRAPHY

Ahrens, L.H., Willis,J.P., & Osthuizen, C.O.(1967). Further observations on the composition of manganese nodules with particular reference to some of the rarer elements. Geochim. Cosmochim. Acta 31, 2169-2180.

Anderson, M.E.(1978). Accumulation rates of manganese nodules and sediments: an α-track method. Unpubl. M.S. Thesis. U.C.S.D. (Scripps Institute of Oceanography) 113 pp.

Andrushenko, P.F. & Skornyakova, N.(1969). The texture and mineralogical composition of ferromanganese concretions from the southern part of the Pacific Ocean. Oceanol 9, 229-242

Angino, E.E., & Billings, G.K. (1967). Atomic absorption spectrometry in geology. Elsevier.

Arrhenius, G.(1952). In: Reports of the Swedish Deep Sea Expedition volume 5, p112.

Arrhenius, G.(1963). Pelagic sediments. In: "The Sea" (M.N.Hill, ed.), 665-727. Interscience, New York.

Arrhenius, G. & Bonatti, E., (1965). Neptunism and volcanism in the ocean. Prog. Oceanogr. 3 pp7-22.

Arrhenius, G., Mero.J.L. & Korkish,J. (1964). Origin of oceanic manganese nodules. Science 144, 170.

Aston,S.R. & Chester,R.(1973). Influence of suspended particles on the precipitation of iron in natural waters. Est. & Coastal. Mar. Sci. 1, 225-231.

Aston, S.R., Chester, R., Johnson,L.R. & Padgham,R.C.(1973). Eolian dust from the lower atmosphere of the eastern Atlantic and Indian Oceans, China Sea and Sea of Japan. Mar. Geol. 14, p15.

Aumento, F. (1969). The Mid-Atlantic Ridge near 45° N.V: Fission track and ferromanganese chronology. Can. Jour. Earth Sci. 6, 1431-1440.

Avraham, Z.B. & Bunce, E.T.(1977). Geophysical study of the Chagos-Laccadive Ridge, Indian Ocean. Jour. Geophys. Res. 82 (8), 1295-1305.

Baker, B.H. (1963). Geology and mineral resources of the Seychelles Archipelago. Geol. Surv. Kenya Memoir No.3., Ministry of Commerce and Industry, Kenya.

Barnes, S.S.(1967). Minor element composition of ferro-manganese nodules. Science 157 63-65.

Bender, M.L. (1971). Does upward diffusion supply the excess manganese in pelagic sediments? Jour. Geophys. Res. 76, 4212-4215.

Bender, M.L. & Schultz,C. (1969). The distribution of trace metals in cores from a traverse across the Indian Ocean. Geochim.Cosmochim. Acta 33, 292-297.

Berger, W.H., Adelseck, C.G. & Mayer, L.A. (1976). Distribution of carbonate in surface sediments of the Pacific Ocean. Jour. Geophys. Res. 81(15) 2617-2627.

Bezrukov, P.L. & Andrushenko, P.F. (1974). The geochemistry of ferromanganese nodules from the Indian Ocean. Int. Geol. Rev. 16 1044-1061.

Bhat, S.G., Krishnaswamy, S., & Lal, D. (1973). Radiometric and trace element studies of ferromanganese nodules. Symposium on hydrogeochemistry and biogeochemistry, vol.1, 443-462, Clarke Co., Washington.

Bignot, G & Dangeard,L.(1979). Traces nanobiotiques dans les nodules polymétalliques des fonds oceanique actuels.C.N.R.S. Colloque International No.289: "Sur la genèse des nodules de manganèse." Gif-sur-Yvette, 25-30th September,1978 C.Lalou(ed),in press.

Billings, G.K.(1965). Light scattering in trace element analyses by atomic absorption. Atomic Absorp. News. 4, 257-261.

Biscaye, P.E., Kolla, V. & Turekian, K.K. (1976). Distribution of calcium carbonate in the surface sediments of the Atlantic Ocean. Jour. Geophys.Res 81, 2595-2603.

Bischoff, J.L. & Dickson, F.W. (1975). Seawater-basalt interactions at 200°C and 500 bars: implications for the origin of seafloor heavy mineral deposits and regulation of seawater chemistry. Earth Planet. Sci. Letts. 25, 385-397.

Bonatti, E.& Nayudu,Y. (1965). The origin of manganese nodules on the ocean floor. Amer.Jour. Sci. 263, 17-39.

Bonatti, E., Kraemer, T. & Rydell, H.(1972). Classification and genesis of submarine iron-manganese deposits. In: "Ferromanganese deposits on the ocean floor" (D.R.Horn, ed). 149-165. Lamont-Doherty Geol.Obs.,N.Y.

Bostrom,K.(1973). The origin and fate of ferromanganoan active ridge sediments. Stockh. Contrib. Geol. 27(2) p243.

Bostrom,K, & Fisher, D.E. (1971). Volcanogenic U,V, and Fe in Indian Ocean sediments. Earth Planet.Sci.Lett. 11, 95-98.

Bostrom, K., Kraemer,T. & Gartner,S.(1973). Provenance and accumulation rates of opaline silica, Al, Ti, Fe, Mn, Cu, Ni, and Co in Pacific pelagic sediments. Chem. Geol. 11,123-148.

Bostrom, K., Peterson, M.N.A., Joensuu,O. & Fisher, D.E. (1969). Aluminium-poor ferromanganoan sediments on active oceanic ridges. Jour. Geophys. Res. 74, 3261-3270.

Boudreau, B.P. & Scott, M.R. (1978). A model for the diffusion-controlled growth of deep-sea manganese nodules. Am.Jour. Sci. 278, 903-929.

Boyle, E.A., Sclater, F.R. & Dymond, J.M. (1977). The distribution of dissolved copper in the Pacific Earth Planet. Sci. Letts. 37, 38-54.

Broecker, W.S. & Broecker, S. (1974). Carbonate dissolution on the western flank of the East Pacific Rise. In: Studies in Palaeooceanography pp. 44-57, Hay, W.W. (ed.) Soc. Econ. Palaeo. Miner. Spec. Paper No. 70.

Bunce, E.T., Langseth, M.G., Chase, R.L. & Ewing, M.(1967). Structure of the W.Somali Basin. Jour. Geophys. Res. 72, 2547.

Burkle, L.H., Venkatarathnam, K. & Booth, J.D.(1974). Sediment transport by Antarctic Bottom Water in the Western Indian Ocean. Eos (Trans. Am. Geophys. Un) 55, (4), 312.

Burns, R.G. (1976). The uptake of cobalt into ferromanganese nodules, soils and synthetic Mn (IV) oxides. Geochim. Cosmochim. Acta. 40, 95-102.

Burns, R.G. & Brown, B.A.(1972). Nucleation and mineralogical controls on the composition of manganese nodules. In "Ferromanganese deposits on the ocean floor" (D.R.Horn, ed.) 51-60. Lamont-Doherty Geol.Obs. N.Y.

Burns, R.G. & Burns, V.M. (1977). Mineralogy of ferromanganese nodules. In "Marine Manganese Nodules" (G.P.Glasby ed). Chap.7. Elsevier.

Burns, V.M. & Burns, R.G. (1978a). Post depositional metal enrichment processes inside manganese nodules from the north equatorial Pacific. Earth Planet. Sci. Letts. 39, 341-348.

Burns, R.G. & Burns, V.M. (1978b) Authigenic todorokite and phillipsite inside deep-sea manganese nodules. Am. Min. 63, 827-831.

Burns,V.M. & Burns, R.G. (1978c). Diagenetic features observed inside deep-sea manganese nodules from the north equatorial Pacific.Scan.Elect.Micr. 1, 245-252.

Burns, V.M., & Burns, R.G. (1979). Observations of processes leading to the uptake of transition metals in manganese nodules C.N.R.S. Colloque international No.289: "Sur la genèse des nodules de manganèse. "Gif-sur-Yvette. 25-30 September, 1978. C.Lalou, ed. In press.

Burns, R.G. & Fuerstenau, D.W. (1966). Electron-probe determination of inter-element relationships in manganese nodules. Am. Miner. 51, 895-902.

Burns, R.G., Sung, C.-M., Schwartz, K.B., Sung,W. & Burns, V.M. (1975). Chemical stratigraphic mapping of manganese nodules by electron microprobe: evidence of late stage Ni and Cu enrichments in nodules from the N.E. equatorial Pacific. Geol. Soc. Am. Abstr. Progs. 7 (7) 1014-1015.

Buser, W.& Grutter, A. (1956). Uber die natur der manganknollen. Schweiz Min. Petrogr. Mitt.36, 49-64.

Calvert, S.E. & Price, N.B.(1977). Geochemical variations in ferromanganese nodules and associated sediments from the Pacific Ocean. Mar. Chem. 5, 43-74.

Calvert, S.E., Price, N.B., Heath, G.R., & Moore, T.C. (1978). Relationship between ferromanganese nodule composition and sedimentation in a small survey area of the Equatorial Pacific.Jour. Mar. Res. 36 No.1. 161-183.

Cann. J.R. (1969) Spilites from the Carlsberg Ridge, Indian Ocean. Jour. Petrol.10 1-19.

Cann, J.R. & Vine F.J. (1966). An area on the crest of the Carlsberg Ridge: petrology and magnetic survey. Phil. Trans. Roy. Soc. A259, 198-217.

Carroll,D.(1958). Role of clay minerals in the transportation of iron. Geochim. Cosmochim.Acta. 14, 1-27.

Chayes, F. (1960). On the correlation between variables of constant sum. Jour. Geophys. Res. 65, 4185-4193.

Chester,R. & Aston,S.(1976). The geochemistry of deep-sea sediments. In: J.P.Riley & R. Chester (eds). Chemical Oceanography Vol.6. 281-390. Academic Press, London.

Colley,N.M., Cronan, D.S. & Moorby, S.A.(1979). Some geochemical and mineralogical studies on newly collected ferromanganese oxide deposits from the N.W. Indian Ocean.C.N.R.S. Collogue International No. 289: Sur la genèse des nodules de manganèse. Gif-sur-Yvette, 25-30 September, 1978; C.Lalou(ed.) In press.

Corliss, J.B., (1971). The origin of metal-bearing submarine hydrothermal solutions. Jour.Geophys. Res. 76, 8128-8138.

Crerar, D.A. & Barnes,H.L. (1974). Deposition of deep-sea manganese nodules. Geochim.Cosmochim. Acta 38, 279-300.

Cronan, D.S. (1967). The geochemistry of some manganese nodules and associated pelagic deposits. Unpubl. Ph.D.Thesis, Univ. London, 342 pp.

Cronan, D.S. (1972) Regional geochemistry of ferromanganese nodules in the World Ocean. In: "Ferromanganese deposits on the ocean floor". (D.R.Horn,ed.) 19-30. Lamont-Doherty Geological Obs. N.Y.

Cronan, D.S. (1975a) Manganese nodules and other ferromanganese oxide deposits from the Atlantic Ocean. Jour. Geophys. Res. 80, 3831-3837.

Cronan, D.S. (1975b). Zinc in marine ferromanganese nodules. Trans. Inst. Min. Met. 84, 1330-1332.

Cronan, D.S. (1976). Manganese nodules and other ferromanganese oxide deposits. In: J.P.Riley & R.Chester (eds.) Chemical Oceanography Vol.5, 217-263. Academic Press, London.

Cronan, D.S. & Tooms, J.S. (1968). A microscopic and electron probe investigation of manganese nodules from the north-west Indian Ocean. Deep Sea Res. 15, 215-223.

Cronan, D.S. & Tooms, J.S.(1969). The geochemistry of manganese nodules and associated pelagic deposits from the Pacific and Indian Oceans. Deep Sea Res. 16, 339-359.

Dudley, W.C. (1979). Biogenic influence on the composition and structure of marine manganese nodules. C.N.R.S. Colloque International No. 289: Sur la genèse des nodules de manganèse. Gif-sur-Yvette, 25-30 September 1978; C.Lalou, ed. In press.

Dugolinsky, B.K., Margolis, S.V. & Dudley W.C. (1977). Biogenic influence on the growth of manganese nodules. Jour. Sed.Pet. 47, 428-445.

Dunham,A.C. & Glasby G.P.(1974). Petrographic and electron microprobe investigation of some deep-and shallow-water manganese nodules. N.Z. Jour.Geol.Geophys. 17, 929-953.

Dymond,J., Corliss, J.B. & Stillinger, R.(1976). Chemical composition and metal accumulation rates of metalliferous sediments from sites 319, 320, and 321. Init.Rpts. D.S.D.P. 34, pp 575-588, R.S.Yeats & S.R.Hart et al.,(eds.), U.S.Govmt.Print.Office, Washington D.C.

Dymond, J. & Veeh, H.H.(1975). Metal accumulation rates in the south east Pacific and the origin of metalliferous sediments. Earth Planet. Sci. Letts. 28, 13-22.

Elderfield, H.L.(1976) Manganese fluxes to the oceans. Mar. Chem. 4, 103-132.

Ewing, M., Eittreim, S., Truchman, M., & Ewing, J.I. (1969). Sediment distribution in the Indian Ocean. Deep Sea Res. 16, 231-248.

Fein, C.D. & Morgenstein, M.(1973). Microprobe analysis of manganese crusts from the Hawaiian Archipelago. In: Ferromanganese deposits on the ocean floor. 85-92. Unpubl. Phase 1 report. Seabed Assessment Program. I.D.O.E., N.S.F., Washington D.C.

Fewkes, R.H. (1973). External and internal features of marine manganese nodules as seen with the S.E.M., and their implications in nodule origin. In: "The origin and distribution of manganese nodules in the Pacific, and prospects for exploration." pp 21-30; M.Morgenstein (ed.) Hawaii Inst. Geophys., Honolulu, Hawaii.

Fisher, R.L., Engel,C.G. & Hilde, T.W.C.(1968). Basalts dredged from the Amirante Ridge, W.Indian Ocean. Deep Sea Res., 15, 521-534.

Fisher, R.L., Bunce, E.T. et al.(1974). In: "Initial Reports of the Deep Sea Drilling Project" 24, U.S. Govmt. Printing Office, Washington D.C.

Fisher, R.A. & Yates, F.(1964). Statistical tables for biological, agricultural and medical research. 146 pp. Oliver & Boyd, Edinburgh.

Fordham, A.W. (1970). Sorption and precipitation of iron on kaolinite: III: The solubility of iron (III) hydroxide precipitated in the presence of kaolinite. Austr. Jour. Soil Res. 8, 107-122.

Frederick-Jantzen, C.M., Herman, H. & Herley,P. (1975). Micro-organisms on manganese nodules. Nature 258, 270.

Frondell, C., Marvin, U.B. & Ito, J. (1960). New occurrence of todorokite. Amer. Mineral. 45, 1167-1173.

Frost, M.T. (1977). A new interactive computer program to process electron microprobe data. Min. Mag. 41, 414-416.

Frost,M.T., O'Hara, K., Suddaby, P., Grant, G., Reid, A.F., Wilson, A.F. & Zuiderwyk,M.(1976). A description of two automated control systems for the electron microprobe. X-ray Spect. 5, 180-187.

Fuerstenau, D.W., Herring, A.P. & Hoover, M.(1973). Characterisation and extraction of metals from sea-floor manganese nodules. Trans. Soc. Min. Eng.(A.I.M.E.) 254, 205-211.

Fujita, T.(1971). Concentrations of major chemical elements in marine plankton. Geochem. Jour. 4, 143-156.

Giovanoli, R., Burki, F. & Scheiss, P. (1973). Investigation of manganese nodules. Reprint 33a, Univ. Berne. Inst. Inorg. Anal. Phys. Chem. (unpubl.).

Glasby, G.P.(1970). The geochemistry of manganese nodules and associated pelagic deposits from the North-West Indian Ocean. Unpubl. Ph.D. Thesis. Univ. London. 629pp.

Glasby, G.P. (1973). The role of submarine volcanism in controlling the genesis of manganese nodules. In: Oceanogr. & Mar. Biol. Ann. Rev. 11, 27-44; H.Barnes (ed.) Hafner Publ. Co. N.Y. 383 pp.

Glasby, G.P. (ed.) (1977). Marine manganese deposits. Elsevier, 523 pp.

Goldberg, E.D. (1954). Marine geochemistry 1: Chemical scavengers of the sea. Jour. Geol. 62, 249-265.

Goldberg, E.D.(1961). Chemistry of the oceans. In: "Oceanography." (M.Sears, ed), 583-597. A.A.A.S., New York.

Goldberg, E.D.(1965). Minor elements in sea-water. In: "Chemical Oceanography" (J.P. Riley and G.W.Skirrow, eds.) 1, 163-196.

Goldberg, E.D. & Arrhenius, G.O.S. (1958). Chemistry of Pacific pelagic sediments. Geochim. Cosmochim. Acta 15, 153-212.

Goldberg, E.D. & Griffin, J. (1970). The sediments of the northern Indian Ocean. Deep Sea Res. 17, 513-538.

Goodell, H.G., Meylan, M.A. & Grant, B.(1970). Ferromanganese deposits of the southern Pacific Ocean, Drake Passage and Scotia sea. In: "Antarctic Oceanology 1." (J.L. Reid, ed.), Antarctic Res. Ser. 15, 27-92. Amer. Geophys. Un., Baltimore.

Greenslate, J.(1978). Marine manganese concretion growth rates: non-radiometric considerations. Geophys. Res. Let. 5, 237-240.

Greenslate,J., Frazer, J.Z., & Arrhenius, G.(1973). Origin and deposition of selected transition elements in the sea-bed. In: "The origin and distribution of manganese nodules in the Pacific, and prospects for exploration." (M.Morgenstein, ed.), 45-70. Hawaii Inst. Geophys. Honolulu, Hawaii.

Griffin, J.J., Windom, H., & Goldberg, E.D.(1968). The distribution of clay minerals in the world oceans. Deep Sea Res. 15, 433-459.

Grutter, A. & Buser, W.(1957). Untersuchungen an mangansedimenten. Chimia 11, 132-133.

Harada, K. & Nishida, S.(1976). Biostratigraphy of some marine manganese nodules. Nature 260, 77P-771.

Heath,G.R. & Dymond, J. (1977). Genesis and transformation of metalliferous sediments from the East Pacific Rise, Bauer Deep and Central Basin, northwest Nazca plate. Bull. Geol. Soc. Am. 88, 723-733.

Heezen, B.& Thorpe,M.(1965). Physiography of the Indian Ocean. Phil. Trans. Roy. Soc. 259A. 137-149

Hekinian, R. (1968). Rocks from the mid-oceanic ridge in the Indian Ocean. Deep Sea Res. 15, 195-214.

Helsley, C.E. & Steiner, M.B. (1969). Evidence for long intervals of normal polarity during the Cretaceous period. Earth Planet.Sci. Letts. 5, 325-332.

Hem, J.D.(1978). Redox processes at surfaces of manganese oxide and their effects on aqueous metal ions. Chem. Geol. 21, 199-218.

Hem, J.B.(1978a). Reactions of metal ions at surfaces of hydrous iron oxide. Geochim.Cosmochim. Acta. 41 527-538.

Herzenberg, C.L. & Riley, D.(1969). Interpretation of the Mossbauer spectra of marine iron-manganese nodules Nature, 224, 259-260.

Heye,D (1975). Wachstumverhaltrisse von manganknollen. Geol. Jahrb., E5, 3-122.

Heye, D. & Marchig, V.(1977). Relationship between the growth rate of manganese nodules from the central Pacific and their chemical constitution. Mar. Geol. 23, M19-M25.

Holeman, J.H. (1968). The sediment yield of the major rivers of the world. Water Resources Res. 4, 737-747.

Honjo,S.(1978). Sedimentation of materials in the Sargasso Sea at a 5,367m. deep station. Jour. Mar. Res. 36, 469-492.

Horder, M.F.(1979). Geochemical investigations on deep sea sediments from the Indian Ocean. Unpubl. Ph.D. thesis, Univ. of London.

Horn, D.R., Horn, B.M. & Delach, M.N. (1973). Copper and nickel content of ocean ferromanganese deposits and their relation to properties of the substrate. In:"The origin and distribution of manganese nodules in the Pacific and prospects for exploration. "(M. Morgenstein, ed), 77-84. Hawaii Institute Geophys. Honolulu, Hawaii.

Horowitz, A.(1970). The distribution of Pb, Ag, Sn, Ti and Zn in sediments on active ocean ridges. Mar. Geol. 7, p241.

Hulsemann, J. (1966). On the routine analysis of carbonates in unconsolidated sediments. Jour. Sed. Petrol. 36, 622-625.

Jenkyns, H.C. (1970). Fossil manganese nodules from the West Sicilian Jurassic. Eclog. Geol. Helv. 63, (741-774).

Kennett, J.P. & Watkins, N.D. (1975). Deep sea erosion and manganese nodule pavement development in the South and Indian Oceans. Science, 188, 1011-1013.

Kobletz-Mishke, O.J., Volkovinsky,V.V. & Kabanova, J.G.(1970). Plankton primary production of the World Ocean. In: "Scientific Exploration of the South Pacific" (W.S. Wooster, ed.), 183-193, Nat. Acad. Sci., Washington D.C.

Koirtyohann, S.R. & Pickett, E.E.(1965). Background correction in long path atomic absorption spectrophotometry. Anal. Chem. 37, 601-603.

Kolla, V., Bé, A.W.M., & Biscaye, P.E. (1976a). Calcium carbonate distribution in the surface sediments of the Indian Ocean Jour. Geophys. Res. 81, 2605-2616.

Kolla, V., Henderson, L., & Biscaye, P.E.(1976b). Clay mineralogy and sedimentation in the western Indian Ocean. Deep Sea Res. 23, 949-961.

Kolla,V., Sullivan,L., Streeter, S.S. & Langseth, M.G.(1976c). Spreading of Antarctic Bottom Water and its effects on the floor of the Indian Ocean inferred from bottom water potential temperature, turbidity and sea-floor photography. Mar. Geol. 21, 171-189.

Krauskopf, K.B.(1956). Factors controlling the concentrations of 13 rare metals in seawater. Geochim.Cosmochim. Acta 9, 1

Krauskopf, K.B.(1957). Separation of manganese from iron in sedimentary processes. Geochim. Cosmochim. Acta, 12, 61-84.

Krey,J. (1973). Primary production in the Indian Ocean. In: "The Biology of the Indian Ocean". (B.Zeitschel, ed.), 115-126. Springer-Verlag, New York.

Ku, T-L. & Broecker, W.S. (1969). Radiochemical studies on manganese nodules of deep-sea origin. Deep Sea Res. 16, 625-637.

Lalou,C., Brichet,E. & Jehanno, C.(1979). Techno encrustation: II-structural and chemical study. In: C.N.R.S. Colloque International No. 289: Sur la genèse des nodules de manganèse. Gif-sur-Yvette. 25-30 September,1978. C.Lalou (ed.) In press.

Landergren,S.(1964). On the geochemistry of deep-sea sediments. Rpts. Swedish Deep-Sea Exp. 10 Spec. Invest. 5, 154pp.

Leatherland, T., Burton, J., McCartney, M. & Culkin, F. (1973). Concentrations of some trace metals in pelagic organisms and Hg in north-east Atlantic Ocean water. Deep Sea Res. 20, 679-683.

Levinson, A.A.(1960). Second occurrence of todorokite. Amer. Mineral. 45, 802-807.

XX See bottom of page.

Lyle, M., Dymond, J. & Heath, G.R.(1977). Copper-nickel-enriched ferromanganese nodules and associated crusts from the Bauer Basin, northwest Nazca Plate. Earth Plan. Sci. Letts. 35, 55-64.

Margolis, S.V. & Burns, R.G. (1976). Pacific deep-sea manganese nodules : their distribution, composition and origin. Ann. Rev. Earth Planet. Sci. 4, 229-263.

Margolis, S.V., Dugolinsky, B.K. & Dudley, W.C.(1979) Microchemistry and morphology of biogenic, detrital and authigenic phases in Pacific manganese nodules. In: C.N.R.S. Colloque International no.289. Sur la genèse des nodules de manganèse. Gif-sur-Yvette, 25-30 September. 1978. C.Lalou, (ed.) In press.

Martin, J.H. (1970) The possible transport of trace metals via moulted copepod exoskeletons. Limnol.Oceanogr. 15, p756.

Martin, J.H. & Knauer, G.A. (1973). The elemental composition of plankton Geochim. Cosmochim. Acta. 37, 1639-1653.

Matthews, D.H., Vine, F.J. & Cann, J.R. (1965). Geology of an area of the Carlsberg Ridge, Indian Ocean. Bull. Geol. Soc. Am. 76, 675-682.

XX Lyle, M.W. & Dymond,J.(1976). Metal accumulation rates in the South East Pacific- errors from assumed bulk densities. Earth Planet.Sci. Letts.30, 164-168.

McKenzie, D.P. & Sclater, J.G.(1971). The evolution of the Indian Ocean since the late Cretaceous. Geophys. Jour. Roy. Astr. Soc. 24, 437-528.

McMurtry, G.M. (1974). The mineralogy and geochemistry of sediments from the Nazca Plate. Geol. Soc. Am. Abstr. with Progs. 6, 218-219.

McMurtry, G.M. & Burnett, W.C. (1974). Hydrothermal metallogenesis in the Bauer Deep of the S.E. Pacific Nature 254, 42-44.

Mero,J.L. (1965). The mineral resources of the sea. Elsevier, Amsterdam.

Moorby, S.A. (1978). Geochemistry and mineralogy of some ferromanganese oxides and associated deposits from the Indian and Atlantic Oceans. Unpubl. Ph.D.Thesis, Univ.London. pp 378.

Moóre, C. & Bostrom, K.(1978). The elemental compositions of lower marine organisms. Chem. Geol. 23, 1-9.

Mottl, M.J. & Holland, H.D. (1978). Chemical exchange during hydrothermal alteration of basalt by seawater. 1. Experimental results for major and minor components of seawater. Geochim. Cosmochim. Acta. 42, 1103-1117.

Muir, I.P. & Tilley, C.E.(1964). Basalts from the northern part of the rift zone of the Mid-Atlantic Ridge. Jour. Petrol. 5, 409-434.

Murray, J. & Renard, A.F. (1891). Report on the scientific results of the exploring voyage of H.M.S. Challenger. 3, 525 pp. H.M.S.O. London.

Nesteroff, W.D. (1979). Une origine biologique pour les nodules de manganèse. Ultrastructure, geochimie et rôle des organismes du plancton dans leur edification. In: C.N.R.S. Colloque International No.289: Sur la genèse des nodules de manganèse. Gif-sur-Yvette, 25-30 September, 1978. C.Lalou (ed). In press.

Nicholls, G.D., Curl,H. & Bowen, V.T. (1959). Spectrographic analysis of marine plankton. Limnol. Oceanogr. 4, 472-478.

Oldnall, R.J.(1975). Possible sources of metals in pelagic sediments with special reference to the Bauer Basin.Unpubl. M.S.Thesis. Univ. of Hawaii. H.I.G. Publication 75-14.

Opdyke, N.D. & Glass, B.P. (1969). The palaeomagnetism of sediment cores from the Indian Ocean. Deep Sea. Res. 16, 249-261.

Ostwald, J. & Frazer, F.W. (1973). Chemical and mineralogical investigations on deep-sea manganese nodules from the Southern Ocean. Mineral. Deposita 8, 303-311.

Payne, R.R. & Connelly,J.R. (1972). Pleistocene manganese pavement production: its relationship to the origin of manganese in the Tasman Sea. In: "Ferromanganese deposits on the ocean floor." 81-92. (D.R. Horn (ed)).Lamont-Doherty. Geol. Obs. ew York.

Le Pichon, X. (1960). The deep water circulation in the south west Indian Ocean. Jour. Geophys. Res. 65, 4061-4074.

Le Pichon, X. & Heirtzler J.R.(1968). Magnetic anomalies in the Indian Ocean, and sea floor spreading. Jour. Geophys. Res. 73, 2101-2117.

Piper, D.Z. & Williamson, M.E.(1977). Composition of Pacific Ocean ferromanganes nodules. Mar.Geol. 23, 285-303.

Price, N.B. & Calvert, S.E.(1970). Compositional variations in Pacific Ocean Fe-Mn nodules and their relationships to sediment accumulation rates. Mar. Geol. 9, 145-171.

Qasim, S.Z.(1977). Biological productivity of the Indian Ocean. Ind. Jour. Mar. Sci. 6, 122-137.

Raab, W. (1972). Physical and chemical features of Pacific deep sea manganese nodules and their implications to the genesis of nodules. In: "Ferromanganese deposits on the ocean floor". (D.R.Horn, ed.), 31-49. Lamont-Doherty. Geol. Obs., New York.

Rateev, M.A., Gorbunova, Z.N., Lisitzin, A.P. & Nosov,G.L. (1969). The distribution of clay minerals in the ocean. Sedimentology 13, 21-43.

Sayles, F.L., Ku,T.L. & Bowker, P.C. (1975). Chemistry of ferromanganoan sediments of the Bauer Deep. Bull. Geol. Soc. Am. 86, 1423-1431.

Sayles, F.L., Ku, T.L. & Bowker, P.C. (1976). Elemental accumulation rates in the Bauer Deep - a correction. Authors' MS, 3pp.

Sclater, R.F.,Boyle, E. & Edward, J.M. (1976). On the marine geochemistry of nickel. Earth Planet. Sci. Letts. 31, 119-128.

Seibold, E.(1972). Sedimentary regimes on continental margins and in abyssal cones. Procs. 24th I.G.C. Ottawa,1972.

Sharma, G.S.(1968). Some inferences on the equatorial undercurrent in the Indian Ocean based on the physical properties of the waters. Jour.Mar. Biol. Assoc. India 10, 224-236.

Sillen, L.G.(1961). The physical chemistry of seawater. In: "Oceanography." M.Sears (ed.) 549-581. A.A.A.S. Washington D.C.

Sorem, R.F. & Foster, A.R. (1973). Mineralogical, chemical and optical procedures and standards for study of growth features and economic potential of manganese nodules. Unpubl. Phase 1 Report, Seabed Assessment Program. I.D.O.E./N.S.F., Washington D.C.

Sorem, R.F. & Fewkes, R.H.(1977). Internal characteristics. In: "Marine manganese deposits". G.P.Glasby(ed.) pp 523; Elsevier.

Sorem, R.K., Fewkes, R.H., McFarland, W.D. & Reinhart,W.R. (1979). Physical aspects of the growth environment of manganese nodules in the 'Horn Region', east Equatorial Pacific Ocean. C.N.R.S. Colloque International No.289. Sur la Genèse des Nodules de Manganèse. Gif-sur-Yvette 25-30 September, 1978. C.Lalou (ed). In press.

Sozanski, A.G. & Cronan, D.S. (1976). Environmental differentation of morphology of ferromanganese oxide concretions in Shebandowan Lake, Ontario. Limnol. Oceanog. 21, 894-898.

Straczek, J.A., Horen,A., Ross,M.& Warshaw, C.W.(1960). Studies of the manganese oxides, IV: todorokite. Am. Miner. 45, 1174-1184.

Stumm, W & Morgan, J.J. (1970). Aquatic chemistry. 583pp. Wiley Interscience.

Thompson, G. & Bowen, V.T. (1969). Analyses of coccolith ooze from the deep tropical Atlantic. Jour. Mar. Res. 27, p32.

Tooms, J.S., Summerhayes, C.P. & Cronan, D.S. (1969). Geochemistry of marine phosphate and manganese deposits. Oceanogr. Mar. Biol. 7, 49-100.

Turekian, K.K. (1965). Some aspects of the geochemistry of marine sediments. In "Chemical Oceanography". J.P.Riley & G.Skirrow (eds). Academic Press.

Turekian, K.K. (1967). Estimates of the average Pacific deep sea clay accumulation rate from material balance calculations. In:"Progress in Oceanography" M.Sears. (ed). 4, 227-244.

Turekian, K.K. & Wedepohl, K.H.(1961). Distribution of the elements in some major units of the earth's crust. Bull. Geol. Soc. Am. 72, 175-192.

Udintsev,G.B. et al.,(1975). Geological-Geophysical Atlas of the Indian Ocean. Pergamon Press. London.

Van der Weijden, C.H., & Kruissink, E.(1977). Some geochemical controls on lead and barium concentrations in ferromanganese deposits. Mar. Chem.5, 93-112.

Vassiliou, A. & Blount, A.M. (1977). Crystallographic data for authigenic phillipsite from manganese nodules. Min. Dep. 12, 171-174.

Vergès, E.(1979). Conditions d'accumulation des metaux Al, Fe, Mn, Ni, Cu, Co, Ca et Mg dans les sédiments superficiels de l'océan indien: implications geochimiques. Unpubl. Ph.D thesis. Paris University 86pp.

Wadsley, A.D. (1952). The structure of lithiophorite, (Al, Li) $MnO_2(OH)_2$. Acta Cryst. 5, 676-680.

Wadsley, A.D.(1964) Inorganic, non-stoichiometric compounds. In: "Non-Stoichiometric Compounds." Ed. L.Mandelcorn. Academic Press, London; pp 98-209.

Warren, B.A. (1974) Deep flow in the Madagascar and Mascarene Basins.Deep Sea Res. 21, 1-21.

Watkins, J.D. & Kennett, J.P.(1973). Regional sedimentary discomformities and upper Cenozoic changes in bottom water velocities between Australasia and Antartica. In: "Antarctic Oceanology II." (D.E. Hayes, ed.) 273-293. Antarctic Res. Ser. 19

Weser, O.E. (1972). Sedimentological aspects of strata encountered in leg 23 in the N.Arabian Sea. Initial Reports D.S.D.P. 23, 503-520.

Willis, J.P. (1970). Investigations on the composition of manganese nodules. with particular reference to certain trace elements. Unpubl. MSc.Thesis, Univ. Cape Town. 111pp.

Winterhalter, B. & Siivola, J.(1967). An electron microprobe study of the distribution of Fe, Mn, and P in concretions from the Gulf of Bothnia, Northern Baltic Sea. Comptes Rend. Soc. geol. Fin 39, 161-172.

Wiseman, J.D.H.(1965). Calcium and magnesium carbonate in some Indian Ocean sediments. Prog. Oceanogr. 3, 373-384.

Wyrtki, K.(1971) Oceanographic Atlas of the International Indian Ocean Expedition (K.Wyrtki, ed.) U.S. National Science Foundation, Washington D.C.

Zander, A.T. (1977). Factors influencing accuracy in background-corrected atomic absorption spectrometry. Intern. Lab.(Jan/Feb) pp15-24.

ADDENDUM Ib

Tabulated analyses of ferromanganese oxide crust samples.

Units are as follows:

Ca: Wt.%

Mn: Wt.%

Fe: Wt.%

Ni: ppm.

Co: ppm.

Ti: ppm.

Al: Wt.%

Mg: Wt.%

Cu: ppm.

Zn: ppm.

Pb: ppm.

Cd: ppm.

Li: ppm.

Sample	Principal Oxide Mineral	Ca	Mn	Fe	Ni	Co	Ti	Al	Mg	Cu	Zn	Pb	Cd	Li
SH 1301A Bulk	δMnO_2	1.8	16.3	20.2	2045	1750	4348	1.17	1.0	529	506	997	5	--
0-4mm	δMnO_2	1.83	15.8	19.8	1720	1693	3960	1.01	1:01	396	904	946	6	--
12-16mm	δMnO_2	1.83	17.1	20.0	2020	1702	5227	1.05	1.0	511	498	884	6	--
22-25mm	δMnO_2	1.68	13.4	19.4	1700	1684	5130	1.44	0.95	568	530	1054	6	--
SH1301B 0-4mm	Str.todorokite	1.16	24.3	9.4	3841	1821	2842	1.88	2.04	2167	546	488	5	38
4-6mm	Wk.todorokite	1.1	18.9	17.0	4380	2135	4048	1.51	1.72	1938	723	837	6	12
6-14mm	δMnO_2	1.46	11.0	23.0	1957	1826	5784	1.71	1.32	1015	692	1316	5	11
25-30mm	δMnO_2	1.28	11.0	23.1	2144	2081	5280	1.73	1.15	1114	694	1153	5	9
SH1301C 0-4mm	Str.todorokite	1.02	21.2	13.1	4174	2048	4043	1.85	1.88	2229	578	668	6	37
4-8mm	Wk.todorokite	1.1	16.4	19.2	5390	3208	6273	1.81	1.61	2135	819	1093	7	29
14-18mm	δMnO_2	1.1	9.8	23.4	1707	1964	6042	2.0	1.1	997	616	1118	6	8
35-40mm	δMnO_2	1.23	10.7	22.5	2010	2431	5897	2.2	1.25	1090	594	1185	7	9
SH1301D 0-5mm	Wk.todorokite	1.31	21.0	17.3	4265	2135	4219	1.70	1.46	1633	650	928	8	42
3-10mm	δMnO_2	1.26	11.8	24.1	2178	2007	6310	1.43	1.02	900	710	1158	6	8
15-25mm	δMnO_2	1.07	11.6	23.3	2028	1789	5606	1.67	1.01	1121	666	1193	7	11
H1301E 0-5mm	δMnO_2	1.70	15.8	19.5	2283	2634	6958	1.40	1.13	410	502	1000	9	7
15-18mm	δMnO_2	1.71	13.7	21.0	1711	2281	6501	1.48	1.02	684	488	719	7	10
32-38mm	δMnO_2	1.29	15.7	20.4	2837	2184	6076	2.35	1.20	1033	495	990	6	9
H1301F 0-4mm	δMnO_2	2.54	15.2	20.3	1636	1690	4797	1.19	1.05	359	512	1004	6	4
4-8mm	δMnO_2	1.67	16.6	20.2	2024	1951	4802	0.94	1.07	491	523	1050	8	6
8-11mm	δMnO_2	1.76	16.9	19.3	1905	1528	4911	1.01	1.04	616	442	906	5	5
13-18mm	δMnO_2	1.54	15.3	20.4	1810	1867	5994	1.33	1.02	741	460	1147	5	5
25-30mm	δMnO_2	2.21	14.9	21.7	1794	1794	5214	1.45	1.00	779	522	1065	5	4
32-37mm	δMnO_2	1.8	12.3	19.7	1343	1670	4705	1.54	1.01	728	504	1065	6	5
43-47mm	δMnO_2	1.8	13.2	20.3	1600	1886	4627	2.00	1.07	949	469	983	5	6
52-55mm	δMnO_2	3.8	12.2	18.6	2071	1690	4732	3.0	1.22	1062	476	800	5	10

Sample	Principal Oxide Mineral	Ca	Mn	Fe	Ni	Co	Ti	Al	Mg	Cu	Zn	Pb	Cd	Li
SH1301G Bulk	Goethite+δMnO_2	1.7	14.7	22.1	1744	2682	8282	1.0	1.06	690	503	1045	5	5
SH1301H 0-3mm	Str.todorokite	1.04	22.4	8.6	3694	1353	2708	1.77	1.90	2278	500	463	4	41
3-6mm	Wk.todorokite	1.35	20.2	15.4	4964	2104	4318	1.73	1.61	2280	687	815	5	27
6-11mm	δMnO_2	1.18	13.0	22.1	2370	1940	5662	1.41	1.13	1130	720	1130	5	10
15-25mm	δMnO_2	1.4	11.0	22.8	1937	1830	5490	1.71	1.04	1025	689	1153	3	7
33-3 mm	δMnO_2	1.4	9.5	20.3	1644	1634	4638	2.13	1.03	1065	615	1160	3	8
SH1301I 0-3mm	Str.todorokite	1.0	20.5	10.6	5026	1856	3414	1.81	2.0	2600	602	570	6	38
3-6mm	Wk.todorokite	1.13	21.9	13.5	4901	2200	4200	1.70	1.68	2370	630	743	4	29
15-20mm	δMnO_2	1.27	10.7	20.9	2146	1818	5791	1.77	1.09	1150	663	1074	3	8
28-33mm	δMnO_2	1.27	10.0	23.0	1960	1614	4906	1.79	1.11	1245	701	1175	3	10
SH1301J 0-4mm	δMnO_2	2.01	14.6	18.6	1717	1606	4646	1.06	1.02	378	473	906	5	7
8-12mm	δMnO_2	2.0	15.4	18.7	2168	1607	4671	1.12	1.06	670	506	851	3	5
26-32mm	δMnO_2	1.6	12.5	22.2	1437	1603	5211	1.61	1.03	698	494	1060	3	5
44-50mm	δMnO_2	1.5	12.8	18.8	1997	1663	4484	2.22	1.20	996	474	869	3	9
60-65mm	δMnO_2	1.4	9.1	17.1	1730	832	5034	3.79	1.23	1045	427	497	4	16
SH1303 Bulk	δMnO_2	2.2	18.1	22.3	2270	1831	--	0.44	--	255	510	1150	--	--
SH1307A Bulk	δMnO_2	1.93	16.1	19.9	2582	3373	6981	1.62	1.08	846	524	1162	7	--
0-5mm	δMnO_2	1.72	14.4	21.0	1683	3033	6967	1.06	0.95	520	512	1181	5	--
23-27mm	δMnO_2	1.71	15.0	17.8	2430	2840	7520	2.02	1.02	1130	445	1033	6	--
45-51mm	δMnO_2	1.70	12.7	16.0	2310	2615	7000	2.50	1.09	1115	416	800	6	--
SH1307B 0-5mm	δMnO_2	2.36	16.0	21.3	1820	2664	7390	0.88	1.04	474	580	1140	6	2
15-20mm	δMnO_2	1.60	14.3	19.7	2185	2378	7070	2.18	1.04	825	545	1000	5	9
	glassy rind	3.72	0.32	8.42	198	105	5613	8.94	2.53	315	280	47	5	48
	Basalt	8.58	0.40	7.8	180	119	5725	8.41	3.45	197	113	56	4	10

Sample		Principal oxide mineral	Ca	Mn	Fe	Ni	Co	Ti	Al	Mg	Cu	Zn	Pb	Cd	Li
SH1307C	Bulk	δMnO_2	1.76	14.1	20.2	1880	2816	7390	1.29	1.03	469	502	1091	--	6
		glassy rind	1.83	0.71	9.71	276	186	6700	8.73	2.12	383	315	112	7	60
		basalt	8.0	0.31	8.0	133	118	5325	8.28	3.70	163	124	74	6	7
SH1307D	0-4mm	δMnO_2	2.18	14.5	20.4	1610	2300	5810	0.87	0.97	484	590	1028	7	5
	10-15mm	δMnO_2	1.77	13.4	19.5	1850	2020	6433	2.15	1.01	625	530	934	7	6
	20-25mm	δMnO_2	1.80	12.8	18.2	1690	1690	5853	2.48	1.07	610	540	709	7	10
SH1307E	0-5mm	δMnO_2	2.12	16.5	20.7	2120	3660	8012	0.98	1.02	420	526	1202	6	5
	15-20mm	δMnO_2	1.7	14.9	17.7	2510	3158	8226	1.87	1.16	989	480	1118	7	8
	25-30mm	δMnO_2	2.80	15.8	18.3	2777	3377	8144	1.63	1.10	880	490	1054	5	8
		Substrate	2.15	14.0	16.1	2825	2810	7771	3.22	1.39	1208	485	843	6	16
SH1307F	0-4mm	δMnO_2	2.38	19.5	20.4	2336	4065	7541	0.59	0.98	477	590	1243	6	3
	4-8mm	δMnO_2	1.84	15.4	21.1	1692	2674	6900	1.01	0.96	831	520	1168	7	4
	16-20mm	δMnO_2	2.01	13.4	21.5	2400	2940	8327	1.68	1.10	1320	546	1020	6	9
SH1315	Bulk	δMnO_2	2.56	23.4	14.2	4400	9080	5883	0.42	1.19	374	535	2592	7	--
	0-3mm	δMnO_2	2.38	22.4	13.1	4590	9617	6100	0.35	1.16	358	511	2117	7	7
	3-5mm	δMnO_2	2.35	21.5	14.4	4930	8185	6830	0.68	1.22	484	641	2177	10	17
		Substrate	17.4	0.24	9.5	195	101	8576	3.39	1.94	136	292	54	2	14
SH1317A	0-4mm	δMnO_2	2.0	18.7	19.9	2663	3531	6200	0.53	1.0	353	600	1600	6	2
	12-16mm	δMnO_2	1.36	9.8	18.5	1470	3215	6990	2.87	1.0	682	501	1353	5	8
	21-25mm	δMnO_2	1.87	18.7	19.4	2704	3585	6463	0.77	0.98	528	603	1593	5	3
SH1317B	0-5mm	δMnO_2	2.31	18.8	19.3	2300	3441	6040	0.45	0.94	242	580	1680	5	3
	9-13mm	δMnO_2	1.47	7.77	18.9	1234	3032	6992	3.08	1.00	658	519	1481	6	9
	19-25mm	δMnO_2	2.07	13.5	22.8	1322	4397	7981	1.7	1.04	744	757	2063	5	5

Sample	Principal oxide mineral	Ca	Mn	Fe	Ni	Co	Ti	Al	Mg	Cu	Zn	Pb	Cd	Li
SH1317C 0-5mm	δMnO_2	2.15	18.3	19.0	2831	3000	5537	0.37	0.96	258	607	1637	4	1
9-13mm	δMnO_2	1.42	7.7	22.0	1402	2341	7872	2.76	1.02	607	567	1760	2	8
20-25mm	Wk todorokite	1.48	19.4	15.8	9234	3362	5664	1.53	1.73	1563	945	1237	8	24
SH1318A Bulk	δMnO_2	3.06	19.3	16.5	3073	9332	7900	0.39	1.14	196	501	2235	6	2
	Substrate	35.3	0.37	0.64	160	114	642	0.30	0.42	31	40	48	---	4
SH1318B Bulk	δMnO_2	4.74	17.6	15.5	3001	9750	7500	0.55	1.10	204	500	1855	8	2
	Substrate	29.4	1.47	3.16	435	512	1490	0.78	0.68	70	97	151	1	6
SH1321A 0-4mm	δMnO_2	2.14	17.4	20.2	2645	5429	6960	0.72	1.02	267	650	1670	6	3
10-14mm	δMnO_2	1.50	12.6	22.2	2331	3542	7952	1.27	1.22	510	606	1573	4	5
16-20mm	δMnO_2	1.40	10.8	20.5	2355	4366	8860	1.93	1.21	616	557	1613	6	15
SH1321B 0-6mm	δMnO_2	2.15	17.3	19.0	2757	4191	6310	0.55	0.98	350	596	1684	6	3
10-15mm	Wk todorokite	1.6	20.8	14.3	10333	4385	6859	1.85	2.03	1625	995	1262	10	33
SH1321C 0-10mm	δMnO_2	2.12	17.0	19.7	2479	5063	7135	0.63	1.0	253	544	1750	7	5
20-30mm	δMnO_2	1.84	18.4	17.4	4093	3920	7418	1.22	1.1	772	569	1542	8	9
SH1321D 0-4mm	δMnO_2	1.87	16.2	17.8	4206	3894	6698	1.56	1.32	561	636	1293	11	19
7-11mm	δMnO_2	2.0	19.7	19.1	3820	3873	7158	0.94	1.07	608	619	1588	6	5
15-20mm	wk.todorokite	1.93	20.7	16.3	6584	3715	6933	1.27	1.39	1000	723	1653	9	18
SH1323 0-4mm	δMnO_2	1.62	8.1	25.9	1343	2979	9090	1.49	1.25	429	588	1355	5	9
12-16mm	δMnO_2	1.52	6.46	26.7	1272	2233	10700	1.85	1.22	459	537	1380	6	11
SH1325 0-4mm	δMnO_2	1.67	18.5	19.3	2516	5065	6845	0.83	1.02	404	595	1777	11	2
15-18mm	δMnO_2	6.86	5.53	15.3	1780	2305	11100	4.12	1.03	257	473	580	3	16
SH1326 0-5mm	δMnO_2	1.8	19.1	17.9	2820	6324	11300	0.9	1.02	539	492	1280	6	5
9-14	δMnO_2	1.83	18.0	17.6	2883	5282	12200	1.23	1.05	918	490	1333	5	5
20-24mm	δMnO_2	1.66	16.9	19.0	2844	4503	11400	1.77	1.09	1219	466	1374	6	7

Sample		Principal oxide mineral	Ca	Mn	Fe	Ni	Co	Ti	Al	Mg	Cu	Zn	Pb	Cd	Li
SH1370A	0-2mm	δMnO_2	3.5	14.9	20.9	1912	2294	5200	0.51	0.88	618	524	669	5	1
	3-6mm	δMnO_2	2.92	15.9	21.4	2072	2125	4907	0.57	0.89	795	510	594	4	1
	7-8mm	δMnO_2	1.82	16.5	20.1	2164	1960	3791	0.48	0.71	970	504	600	5	1
	8-10mm	δMnO_2	2.87	15.4	21.8	2036	1975	4730	0.59	0.91	1053	513	569	5	1
SH1370B	0-4mm	δMnO_2	3.0	16.2	21.8	1842	1564	3737	0.53	0.88	892	534	575	5	1
	4-6mm	δMnO_2	2.98	16.0	22.1	1825	1411	3650	0.54	0.93	983	541	559	6	1
	8-12mm	δMnO_2	2.28	16.3	22.7	1852	1320	2964	0.60	0.92	1237	524	482	4	2
	12-15mm	δMnO_2	2.87	14.3	24.2	1594	1067	2758	0.82	0.91	1459	637	465	5	1
D6269	Top	δMnO_2	1.58	16.2	18.8	2873	1410	6186	1.58	1.11	1536	540	904	10	7
	Equatorial	δMnO_2	1.72	15.4	18.8	2081	1829	7087	1.70	1.04	1074	541	1054	5	11
	Equatorial	δMnO_2	1.75	14.4	15.3	2662	1970	8465	1.91	1.20	1113	492	1006	4	17
	Bottom	δMnO_2	1.89	15.4	16.6	2658	3104	8974	2.11	1.15	978	532	1045	5	14
	Bottom	δMnO_2	2.62	15.7	14.7	3533	2706	9579	1.88	1.23	1335	570	1181	5	25
	Bottom	δMnO_2	1.54	17.6	14.8	5524	2218	8154	2.27	1.52	2052	684	964	5	41
D6273A	0-4mm	δMnO_2	1.90	17.3	16.8	3465	1654	5943	1.14	1.05	1369	657	1039	5	13
D6273A	4-10mm	δMnO_2	1.86	15.4	18.1	2667	1826	7138	1.69	1.11	1162	579	1102	4	14
D6273B	0-4mm	δMnO_2	1.7	21.4	12.5	8277	1008	4434	1.55	1.30	3072	940	773	10	46
	4-10mm	δMnO_2	1.61	17.1	15.8	4152	1415	6052	1.56	1.17	2208	695	1128	6	23
	10-14mm	δMnO_2	1.55	16.7	16.8	3403	1546	5620	1.90	1.13	1998	661	1169	5	20
	14-20mm	δMnO_2	1.87	17.7	14.9	4803	1132	5407	1.44	1.15	1726	675	864	6	24
Lalou	Bulk	δMnO_2	1.8	12.3	19.9	1456	2160	11100	2.63	1.37	953	539	1000	5	9
SH1564	Bulk	Str.todorokite	1.51	29.1	7.47	11800	1200	2536	1.80	2.16	6438	1506	322	23	24
SH1578	Bulk	Str.todorokite	1.44	30.7	10.0	10600	455	1024	0.98	1.74	6830	1558	109	26	295

ADDENDUM Ia

Tabulated analyses of sediment samples.

Units are as follows:

Depth: corrected metres.

$CaCO_3$: Wt.%

Ca: Wt.%

Mn: ppm.)
Fe: Wt.%)
Ni: ppm.)
Co: ppm.)
Ti: ppm.) Expressed on a
Al: Wt.%) carbonate-free-basis.
Mg: Wt.%)
Cu: ppm.)
Zn: ppm.)
Pb: ppm.)
Cd: ppm.)

Sample	Location	Depth	$CaCO_3$	Ca	Mn	Fe	Ni	Co	Ti	Al	Mg	Cu	Zn	Pb	Cd	Water Depth.
1	SH 1315	0-3cms	97.0	38.1	7953	5.15	277	469	--	2.24	4.0	83	145	300	69	I200m.
2	SH 1315	10-13cms	96.2	38.4	7677	4.23	314	341	--	1.83	3.7	81	126	191	63	
3	SH 1315	20-23cms	96.4	37.8	8733	4.49	449	388	--	2.01	4.5	88	182	383	96	
4	SH 1315	32-35cms	96.4	38.1	10470	5.87	435	509	--	2.48	4.4	141	165	457	63	323Im.
5	SH 1308	0-3cms	86.8	35.6	2722	3.12	142	47	--	4.89	2.04	236	138	101	17	
6	SH 1308	10-13cms	87.1	34.9	912	3.19	117	49	--	5.15	2.42	205	110	82	15	
7	SH 1308	20-23cms	86.3	34.4	2321	3.61	174	42	--	5.70	2.42	246	115	94	18	
8	SH 1308	30-33cms	87.2	35.2	2324	4.15	159	48	--	6.53	2.81	257	131	94	32	
9	SH 1323B	0-3cms	85.3	35.0	6679	4.11	285	118	4400	4.88	3.18	169	134	104	33	2940m.
10	SH 1323B	10-13cms	90.0	34.8	6805	4.57	294	154	4880	4.99	3.89	170	144	193	63	
11	SH 1323B	20-23cms	86.4	34.9	7581	4.14	303	113	4330	4.76	3.36	184	141	103	49	
12	SH 1323B	30-33cms	90.0	35.8	6846	4.10	455	165	--	4.68	4.21	196	149	187	66	
13	SH 1323B	40-43cms	86.7	35.1	5407	4.33	358	84	5100	5.05	3.30	143	133	84	46	
14	SH 1323B	50-53cms	89.6	34.9	5410	4.26	420	106	--	5.05	3.74	142	149	144	58	
15	SH 1313	0-3cms	70.6	28.1	2730	4.39	163	54	4630	7.0	2.07	258	124	78	9	4404m.
16	SH 1313	10-13cms	80.1	31.7	3188	4.63	191	43	4820	7.63	2.65	247	158	110	13	
17	SH 1313	20-23cms	79.9	31.5	3534	4.71	192	55	4920	7.8	2.65	198	150	92	15	
18	SH 1313	30-33cms	82.4	32.4	2416	4.91	143	57	5100	7.7	2.65	202	151	173	13	
19	SH 1313	40-43cms	80.7	31.9	1321	5.0	132	49	5240	8.30	2.70	185	143	67	12	
20	SH 1313	50-53cms	70.5	28.0	2305	5.8	150	37	6100	8.71	2.75	261	164	97	7	
21	SH 1313	56-59cms	67.6	26.3	3403	5.52	176	57	5660	8.34	2.60	304	156	97	8	
22	SH 1300	0-3cms	29.2	12.7	3628	5.32	243	42	5183	7.9	3.50	152	148	74	4	46I5m.
23	SH 1300	10-13cms	32.3	13.6	2987	5.46	201	44	5374	8.3	3.43	123	145	67	4	
24	SH 1300	20-23cms	32.8	13.9	2469	5.48	183	37	5461	8.17	3.28	111	143	70	4	
25	SH 1300	30-33cms	3.2	1.8	2475	5.42	196	51	5294	7.71	3.10	131	140	60	4	
26	SH 1300	40-43cms	11.3	5.2	1012	5.22	114	46	4946	8.21	2.60	86	123	61	7	

Sample	Location	Depth	$CaCO_3$	Ca	Mn	Fe	Ni	Co	Ti	Al	Mg	Cu	Zn	Pb	Cd	Water Depth
27	SH 1318	0-3cms	96.2	37.9	1883	1.92	718	210	--	1.76	4.40	63	334	552	29	I358m.
28	SH 1318	10-13cms	94.5	38.2	1090	1.34	126	117	--	1.28	4.21	42	90	279	37	
29	SH 1318	20-23cms	95.70	37.0	1104	2.23	370	269	--	2.76	5.36	53	173	230	39	
30	SH 1318	29-31cms	94.4	36.7	410	2.01	188	99	--	2.72	4.27	73	133	300	43	
31	SH 1323A	0-3cms	88.6	34.6	981	3.80	129	39	--	5.76	3.02	160	156	141	97	2800m.
32	SH 1323A	10-13cms	87.6	35.1	768	3.5	89	25	--	5.31	2.75	176	128	120	48	
33	SH 1323A	20-23cms	87.9	35.2	1351	2.83	134	83	3708	4.45	2.45	181	124	143	20	
34	SH 1323A	30-33cms	87.4	35.2	2731	2.68	246	48	4431	4.10	2.25	148	123	151	16	
35	SH1323A	40-43cms	86.0	34.9	585	3.47	162	56	4114	5.10	2.64	109	117	79	35	
36	SH 1323A	50-53cms	85.7	34.3	510	3.08	139	54	3766	4.6	2.59	131	155	125	46	
37	SH 1323A	60-63cms	86.3	34.2	566	3.31	114	59	3616	4.8	2.7	130	121	126	51	
38	SH 1323A	70-73cms	85.7	35.3	593	3.0	70	92	3685	4.5	2.44	153	113	119	52	
39	SH 1323A	82-84cms	86.9	34.6	903	3.56	100	73	--	5.35	2.56	155	139	176	49	
40	SH 1305	0-5cms	77.6	28.7	3625	4.0	174	73	4193	6.57	2.28	238	122	73	15	4369m.
41	SH 1305	10-15cms	78.0	29.7	10850	4.13	447	68	4018	6.86	2.66	284	198	64	10	
42	SH 1305	16-19cms	69.7	28.1	1106	2.8	130	41	2854	5.0	1.78	113	88	70	14	
43	SH 1305	30-34cms	77.1	30.9	2036	3.55	137	35	3680	5.96	2.36	139	112	58	10	
44	SH 1305	36-39cms	73.2	29.5	3784	3.0	160	40	3257	5.22	1.77	166	100	69	10	
45	SH 1305	41-46cms	76.6	30.8	4438	3.34	181	21	3251	5.43	1.91	183	106	49	9	
46	SH 1305	49-50cms	77.5	31.3	1308	3.37	91	67	3538	5.74	2.06	146	98	56	11	
47	SH 1305	54-56cms	82.8	34.2	2822	3.44	166	63	--	5.80	2.51	163	117	41	19	
48	SH 1305	56-61cms	86.2	34.8	1294	1.08	47	115	--	1.3	2.21	71	69	38	23	
49	SH 1305	67-73cms	55.8	21.1	2892	5.05	176	59	4540	7.31	2.13	187	126	72	13	
50	SH 1305	80-82cms	79.4	31.0	5260	4.15	180	58	4175	6.78	2.34	237	137	68	13	
51	SH 1305	86-90cms	85.5	34.4	2751	1.08	69	28	--	1.30	2.02	106	71	74	29	
52	SH 1305	93-98cms	65.1	24.4	2720	4.95	152	24	4876	7.32	2.23	237	131	79	16	

Sample	Location	Depth	$CaCO_3$	Ca	Mn	Fe	Ni	Co	Ti	Al	Mg	Cu	Zn	Pb	Cd	Water Depth.
53	SH 1305	100-106cms	65.5	26.1	3425	4.9	182	75	5060	8.21	2.26	252	134	44	9	
54	SH 1305	121-125cms	76.4	30.3	5457	4.34	214	85	4277	6.90	2.75	245	144	53	15	
55	SH 1305	135-140cms	69.5	26.9	1066	4.50	128	19	4474	7.25	2.49	162	132	54	9	
56	SH 1305	156-162cms	71.4	28.9	2348	4.67	166	66	4900	7.31	2.61	192	133	68	4	
57	SH 1305	175-181cms	77.4	31.2	2405	3.16	93	60	3375	5.45	2.32	155	109	72	8	
58	SH 1305	186-191cms	88.7	35.5	1404	1.07	80	61	4557	1.78	4.49	66	98	66	18	
59	SH 1305	195-198cms	87.4	35.0	1500	1.11	125	5	4206	1.23	3.61	60	50	43	44	
60	SH 1305	204-208cms	61.1	24.8	2257	4.1	134	33	4307	6.2	2.01	206	126	57	8	
61	SH 1305	215-220cms	64.3	24.8	2716	5.04	141	59	5118	7.43	2.70	237	144	68	7	
62	SH 1305	225-229cms	81.2	32.0	5015	4.46	155	74	4568	7.53	2.61	235	136	93	10	
63	SH 1305	235-237cms	82.8	32.1	8378	4.30	232	116	4480	7.41	2.70	281	134	84	12	
64	SH 1305	242-246cms	76.7	30.2	1906	4.33	152	56	4858	7.50	2.58	197	133	69	11	
65	SH 1305	251-254cms	62.4	25.4	1655	4.84	148	37	4849	7.34	2.47	205	140	74	4	
66	SH 1306	0-5cms	88.8	35.7	2213	3.54	108	18	4982	4.66	2.37	454	155	65	61	3983m.
67	SH 1306	20-23cms	85.7	33.9	2303	2.83	184	29	3894	4.36	2.13	144	100	71	16	
68	SH 1306	40-45cms	85.9	34.1	1094	2.77	128	57	3811	3.94	1.85	133	77	64	18	
69	SH 1306	59-64cms	86.1	34.6	1225	3.02	67	58	3983	4.89	2.12	157	77	106	25	
70	SH 1306	80-85cms	84.9	34.1	2197	2.51	89	50	3600	3.87	1.75	178	93	20	44	
71	SH 1306	98-102cms	85.6	34.4	1768	2.96	93	55	3780	4.39	2.02	148	104	23	44	
72	SH 1306	117-122cms	88.9	35.9	2180	3.42	185	64	--	5.11	2.43	232	125	46	32	
73	SH 1306	137-142cms	84.8	34.4	1476	2.72	117	22	3493	4.0	1.78	160	78	27	38	
74	SH 1306	148-154cms	81.1	32.6	621	2.89	79	47	3100	4.67	1.88	118	101	51	29	
75	SH 1306	166-171cms	87.3	35.1	1812	3.07	158	59	--	4.45	2.40	161	97	111	32	
76	SH 1306	185-189cms	83.0	33.3	1714	2.44	59	51	3223	3.79	1.74	141	88	58	50	

Sample	Location	Depth	$CaCO_3$	Ca	Mn	Fe	Ni	Co	Ti	Al	Mg	Cu	Zn	Pb	Cd
77	2°44.6'N61°15'E	0-1cm	24.9	10.3	894	4.3	330	37	3787	5.93	2.08	267	162	71	1
78	2°44.6'N61°15'E	101-102cms	12.7	4.9	1495	5.1	172	45	4469	6.54	2.2	206	294	72	2
79	2°44.6'N61°15'E	201-202cms	21.3	8.9	3721	5.0	375	48	4737	7.32	2.60	302	239	77	1
80	2°44.6'N61°15'E	bottom	21.9	8.5	4214	5.7	216	44	4700	7.17	2.63	262	149	74	1
81	5°47.5'N61°47'E	0-1cm	56.0	22.7	1772	2.44	111	34	2343	3.61	1.52	110	72	64	3
82	5°47.5'N61°47'E	bottom	54.0	21.4	1088	3.32	113	18	3385	5.03	2.07	94	115	85	2
83	2°55.3'N59°52.8'E	4700m	40.5	17.2	6285	5.34	200	40	4657	7.2	2.57	247	200	76	3
84	1°54'N56°10'E	4800m	47.2	19.2	8132	4.7	315	64	4900	6.9	2.36	261	201	68	3
85	5°34.5'N61°57'E	0-1cm	77.2	31.0	2683	3.70	135	57	3375	5.6	2.5	203	136	70	7
86	5°34.5'N61°57'E	bottom	59.8	24.7	2000	3.97	109	40	3622	5.25	2.54	97	106	70	2
87	5°34.5'N61°56'E	0-1cm	65.5	26.4	1439	2.19	81	38	2184	3.32	1.54	113	1.29	57	3
88	5°34.5'N61°56'E	bottom	65.3	26.9	1218	3.79	105	22	3853	5.76	2.45	114	114	58	1
M79/1	9°50'N57°54.6'E	0-2cms	65.1	26.8	4900	2.94	170	39	3400	3.34	2.22	150	85	52	11
M79/1	9°50'N57°54.6'E	6-8cms	68.2	28.2	2605	3.15	99	33	3291	4.3	2.37	156	91	66	9
M79/1	9°50'N57°54.6'E	10cms	76.3	31.3	5457	4.88	109	16	3165	4.12	3.64	170	135	59	2
M79/2	6°21.4'N60°56.2'E	0-3cms	72.0	29.5	1419	2.15	97	44	2188	2.69	1.61	115	84	19	13
M79/2	6°21.4'N60°56.2'E	5-6cms	77.2	31.4	5625	2.81	149	39	2891	3.45	2.06	152	85	51	9
M79/2	6°21.4'N60°56.2'E	15-16cms	77.9	31.7	6014	3.22	127	38	3238	4.0	2.25	189	73	83	13
M79/2	6°21.4'N60°56.2'E	22-25cms	82.7	33.8	1010	5.14	108	119	7227	6.62	3.85	192	62	49	12
M79/2	6°21.4'N60°56.2'E	39cms	70.0	28.9	7227	5.04	142	49	4122	5.74	3.61	172	141	72	7
M79/2	6°21.4'N60°56.2'E	43cms	59.9	25.1	858	3.97	106	42	4480	5.37	2.67	97	108	71	5
M79/2	6°21.4'N60°56.2'E	51cms	61.8	25.4	908	3.80	115	33	3802	5.29	2.62	78	64	65	6
M79/3	6°20.6'N60°56.7'E	0-3cms	67.1	27.7	1451	2.18	107	60	2124	2.56	1.89	112	62	63	14
M79/3	6°20.6'N60°56.7'E	22-25cms	78.0	31.7	1867	3.69	74	65	3878	4.76	2.71	174	65	62	10

Sample	Location	Depth	$CaCO_3$	Ca	Mn	Fe	Ni	Co	Ti	Al	Mg	Cu	Zn	Pb	Cd
M79/3	6°20.6'N60°56.7'E	35cms	68.8	28.6	665	3.38	111	60	2534	4.38	2.63	103	127	68	10
M79/3	6°20.6'N60°56.7'E	44-48cms	69.1	28.2	772	4.44	128	33	4652	6.78	3.33	98	132	47	5
M79/3	6°20.6'N60°56.7'E	95-97cms	68.0	27.9	635	3.48	130	45	2972	4.81	2.31	62	187	62	11
M79/3	6°20.6'N60°56.7'E	120cms	68.2	28.3	617	3.69	112	17	3965	5.23	2.68	84	172	48	7
M79/4	3°46'N63°50.7'E	0-3cms	50.2	20.7	2617	5.13	103	54	3819	5.54	2.72	212	138	63	5
M79/4	3°46'N63°50.7'E	30-33cms	48.7	20.3	2840	4.92	96	39	4355	5.68	2.59	210	106	56	4
M79/4	3°46'N63°50.7'E	56-58cms	51.1	21.2	824	4.73	99	39	4325	5.64	2.58	125	127	45	2
M79/4	3°46'N63°50.7'E	60cms	50.5	21.0	932	4.67	122	42	4264	5.47	2.68	131	146	60	7
M79/4	3°46'N63°50.7'E	67cms	53.2	21.9	1016	4.97	85	42	3795	5.73	2.65	135	103	72	6
M79/5	1°38.8'S67°50.7'E	0-3cms	79.6	32.2	1889	3.22	93	45	2694	3.27	2.17	187	63	39	4
M79/5	1°38.8'S67°50.7'E	14-17cms	76.2	31.1	1392	2.43	59	31	2695	2.63	1.93	143	66	69	18
15558	8°59'N51°44'E	3985	61.6	25.4	10300	3.54	258	57	4435	5.28	2.52	164	174	55	--
15559	8°54'N51°37'E	3797	33.8	14.7	1142	4.84	172	44	5352	6.32	3.11	74	295	60	2
15560	8°58.5'N52°02'E	4350	75.2	31.5	1796	3.35	153	65	4407	4.76	2.46	109	105	28	--
15561	8°58'N52°20'E	4722	9.1	5.4	500	5.63	109	50	7909	6.83	2.61	73	164	47	2
15563	9°11'N52°23.5'E	4499	61.4	26.7	1794	3.78	161	41	4741	5.64	2.80	137	129	26	3
15565	9°02'N54°40.5'E	4852	29.0	12.9	4179	4.10	220	61	4749	6.24	2.46	186	149	56	1
15568	8°59'N54°47'E	4950	18.6	8.6	5310	3.89	249	63	4573	5.56	2.46	217	166	53	1
15569	8°58.5'N56°02'E	4001	71.4	28.8	7193	3.57	291	88	4109	5.20	2.28	221	165	46	4
437	5°52'N53°51'E	5031	62.2	25.2	1230	3.60	204	32	4180	5.10	3.28	130	182	53	3
439	0°55'N51°38'E	5041	18.7	8.5	1179	4.82	124	55	5437	7.08	2.10	170	141	46	2
4310	0°22'S54°33'E	4806	48.9	20.1	3695	4.38	188	51	4863	6.71	2.17	196	209	51	—
4312	1°38'S53°20'E	4733	31.1	13.0	2348	4.31	218	60	5398	6.72	2.05	247	174	48	--
4315	2°55'S55°43'E	3692	90.7	35.6	3740	3.75	289	96	5327	5.68	3.22	289	1768	161	27

Sample	Location	Depth	$CaCO_3$	Ca	Mn	Fe	Ni	Co	Ti	Al	Mg	Cu	Zn	Pb	Cd
4369	2°49'N59°41'E	4184	64.4	26.0	5090	4.39	188	56	4600	6.19	2.56	225	593	53	3
10036	7°48'N56°13.1'E	4680	40.1	16.9	14850	4.02	501	53	4266	5.74	2.25	285	204	50	2
10037	7°45.1'N54°45.5'E	5102	55.2	23.4	2430	4.2	125	56	4530	5.76	2.81	158	640	42	7
10038	7°5.4'N55°57'E	4250	75.7	30.5	2000	4.1	177	87	4400	6.06	2.76	161	453	41	10
10040	6°55.4'N54°41.7'E	5106	56.8	24.1	767	3.73	153	35	4300	5.60	3.01	162	167	19	2
10042	4°27.3'N51°08'E	5049	38.2	17.9	1350	3.88	131	49	5310	6.18	2.28	131	128	26	2
10043	3°13.7'N52°23.3'E	5115	6.3	3.75	416	3.96	98	45	5102	6.29	1.86	163	126	43	1
10044	3°13.3'N52°39.8'E	5123	40.2	18.1	522	4.08	187	54	4900	6.36	2.26	130	196	38	2
10045	3°7.9'N52°37.9'E	5126	0.0	1.5	1796	4.81	112	60	5660	7.03	1.90	143	129	41	1
10046	2°56.1'N50°16.1'E	5004	49.5	21.0	597	4.42	131	46	5050	6.50	2.52	153	192	55	2
10047	0°56.8'N53°18.3'E	5101	49.3	20.2	8986	4.20	124	95	4680	6.29	2.03	237	136	37	2
10048	0°14.5'S6°3.5'E	4576	68.0	26.4	6134	4.47	247	75	4600	6.87	2.09	300	212	25	2
10049	1°5.4'N53°30'E	5104	17.3	8.0	5356	4.36	192	47	4800	6.70	1.8	204	139	48	3
10050	1°56.7'N53°59.3'E	5126	0.0	0.8	1310	4.71	135	56	5100	6.31	1.94	169	133	50	1
10051	1°49'N56°51.2'E	4782	36.1	15.4	5442	4.57	261	55	4813	7.09	2.08	249	164	63	2
10052	1°37'N54°40.7'E	5426	0.0	1.8	8170	4.45	275	65	4210	6.4	2.08	369	175	44	1
09015	7°24'N72°36'E	3341	3.6	2.0	847	3.9	65	54	3820	7.85	2.01	43	130	47	1
09156	6°4'N69°48.2'E	4583	9.9	4.8	2416	4.77	194	54	4502	7.19	2.91	149	151	50	3
09158	6°39'N64°10.3'E	4814	14.1	6.2	4147	5.52	260	62	5233	7.88	3.26	170	163	48	2
09159	8°44.4'N62°59.5'E	4576	33.7	14.2	4205	5.02	258	60	4880	7.27	3.41	190	155	47	3
09160	12°3.1'N63°8.8'E	4268	56.2	22.8	2628	4.8	201	71	4570	7.33	3.91	98	153	71	2
12321	4°42'S50°2'E	5077	20.5	10.2	2010	5.35	145	68	6270	9.06	1.82	166	140	47	2
12322	0°18'N50°25'E	5077	5.72	2.9	2080	4.94	128	64	5700	7.76	1.91	176	130	46	0
12323	4°29'N 51°13'E	4825	0.0	1.3	3804	4.65	256	61	7071	6.82	2.37	188	223	45	1
12324	4°29'N51°10'E	4954	57.2	23.4	1155	4.14	138	68	5100	6.57	2.74	154	157	41	0
12325	3°37'N52°11'E	5136	55.8	23.0	1126	3.66	147	45	4530	5.74	3.05	138	165	43	0

Sample	Location	Depth	$CaCO_3$	Ca	Mn	Fe	Ni	Co	Ti	Al	Mg	Cu	Zn	Pb	Cd
12326	0°47'N55°E	4795	47.6	19.6	4642	4.83	252	53	5211	7.58	2.20	237	199	43	0
12327	1°44'N57°50'E	4446	73.6	29.9	2151	2.8	133	68	2970	4.39	2.5	197	129	76	4
12328	3°57'N60°36'E	3087	85.3	34.6	1990	2.4	183	68	3310	3.23	2.65	204	639	75	7
12329	2°59'N65°12'E	3864	81.9	31.8	3810	4.02	176	55	3000	5.46	2.76	264	187	94	8
12330	2°50'N67°43'E	3834	79.2	32.0	3247	4.0	265	92	3059	4.5	2.70	303	188	43	5
12331	2°30'N69°52'E	3941	77.2	31.8	4703	3.6	154	66	3000	5.49	2.42	286	136	92	0
12332	0°47'N74°36'E	3115	88.0	33.9	1770	2.46	83	75	4215	3.55	7.68	209	167	21	13
12335	6°14'N71°E	3314	33.6	14.1	370	4.08	120	50	3455	6.20	2.12	93	152	42	2
14095	4°18'S64°49'E	4513	56.3	24.1	14900	3.64	458	39	3173	4.81	2.34	497	247	39	5
14096	2°50'S66°18'E	4135	70.9	29.5	5593	4.16	217	28	3316	5.57	2.2	313	588	124	10
10497	2°26.5'S66°59'E	3713	73.4	31.1	2808	3.12	132	19	2357	3.95	2.41	226	165	64	7
14098	0°38'S69°27'E	3893	78.5	31.8	3754	4.59	213	27	4278	6.77	2.85	283	232	56	12
14100	3°52'N65°31'E	3682	58.7	26.1	2832	4.74	179	39	4955	6.72	2.95	116	208	36	8
14101	7°31'N59°50.5'E	2390	89.1	34.3	1242	3.20	247	18	4457	4.2	4.0	219	338	--	18
14102	10°15'N57°11'E	3915	75.4	31.5	3702	3.30	167	81	3389	4.8	2.85	203	236	90	4
14103	11°26.5'N56°14'E	4232	73.1	29.5	1041	3.76	138	26	3904	5.21	3.68	175	216	130	7
19177	7°35'N74°13'E	2770	54.7	22.8	1746	3.71	104	33	3716	5.76	2.58	108	148	57	3
19178	8°7'N73°15'E	2188	65.9	29.2	3690	3.26	201	23	3544	5.33	2.84	91	176	91	4
19179	8°9'N70°38'E	4136	39.1	16.4	2500	5.07	207	46	5000	7.65	3.22	166	156	84	1
19180	8°9'N69°15'E	4651	43.8	18.7	2070	5.57	164	37	5844	6.57	3.36	130	132	32	0
19181	8°14'N 66°57'E	4610	17.3	7.4	1768	5.37	195	58	4956	7.67	3.54	133	150	44	2
19182	8°16'N64°05'E	4173	57.1	25.9	2318	4.45	170	21	4375	6.40	3.08	140	147	54	3
19183	8°7'N62°47'E	4451	50.0	21.4	5189	5.19	314	50	5381	7.40	3.44	214	178	42	8
19184	7°26'N61°04'E	3471	68.3	29.1	1261	4.55	136	41	4730	6.72	3.44	91	167	35	5

Sample	Location	Depth	$CaCO_3$	Ca	Mn	Fe	Ni	Co	Ti	Al	Mg	Cu	Zn	Pb	Cd
19185	6°42'N59°20'E	2867	76.5	32.3	992	1.45	119	6	1733	2.04	2.64	81	106	26	11
19186	6°50'N60°12'E	3813	52.3	23.8	1725	4.23	107	38	4284	5.45	3.61	130	109	50	3
19188	6°52'N60°40'E	3356	82.1	33.7	5672	3.47	297	28	3236	4.54	3.47	207	218	67	6
19189	6°37'N59°48'E	2915	78.3	32.7	1283	2.31	92	32	2372	3.0	3.14	115	148	92	5
19190	6°10'N57°51'E	4136	68.9	28.0	3105	3.92	151	16	4084	5.6	3.0	215	154	71	6
19191	5°58'N55°04'E	5125	33.8	15.5	1320	3.90	148	38	4173	5.8	3.05	131	156	59	2
19192	4°43'N52°05'E	5112	0.0	1.6	1928	4.5	113	43	5256	6.3	2.3	164	124	42	2
19193	2°59'N51°28'E	5106	0.0	1.0	1154	4.36	108	56	5470	6.27	2.3	134	117	41	3
19194	0°29'S53°41'E	4859	53.9	22.9	3710	4.42	197	39	4685	6.31	2.54	202	163	41	4
19196	3°34'S51°51'E	5062	17.3	8.5	9453	4.55	423	64	4909	7.03	2.03	277	272	54	5
19197	3°24'S50°46'E	4984	4.3	2.5	769	4.32	107	44	5430	7.18	2.11	123	111	38	2
19198	3°11'S50°49'E	4609	20.0	9.0	1341	4.64	112	51	5246	7.92	1.75	147	126	52	2

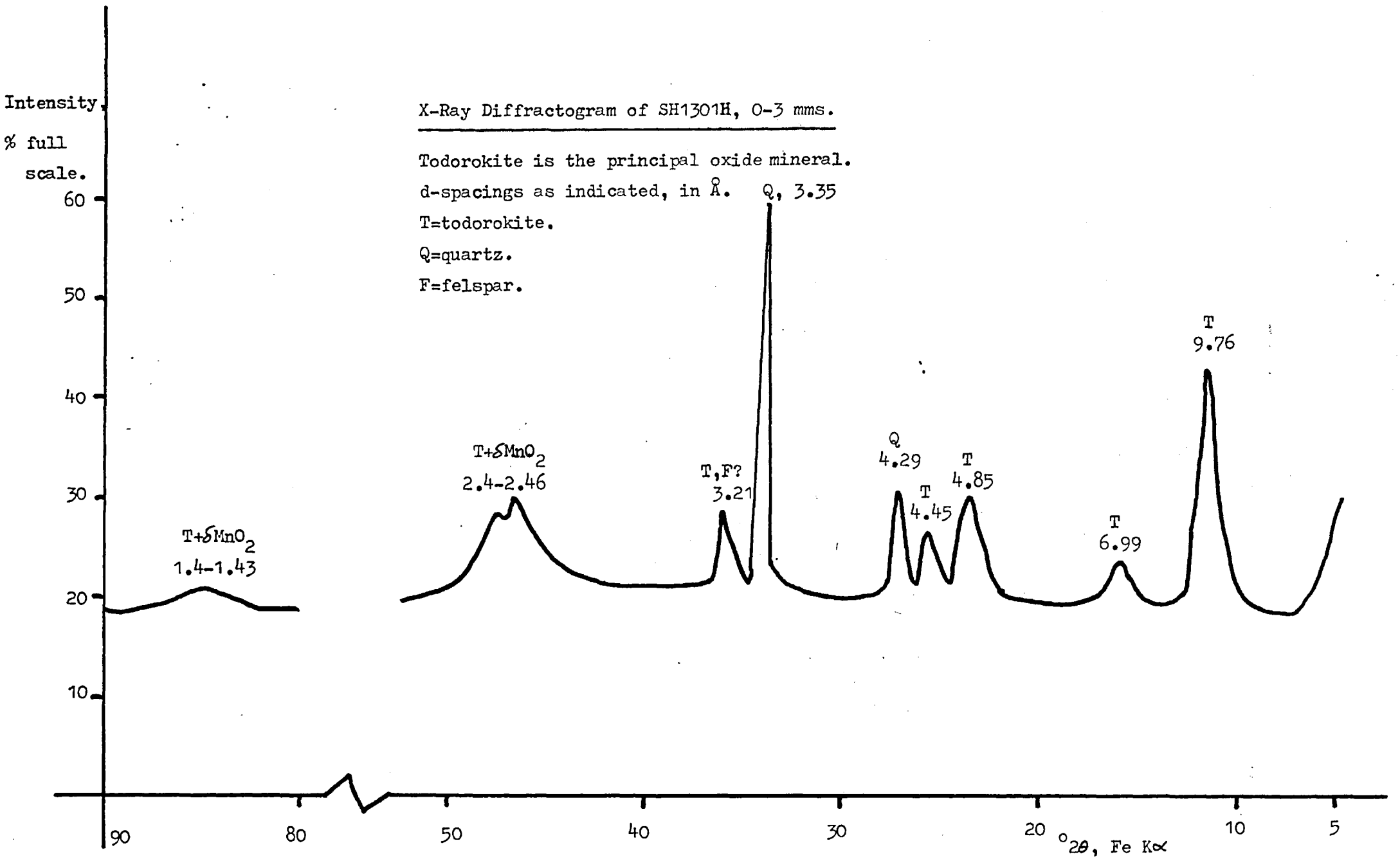
X-Ray Diffractogram of SH1301H, 0-3 mms.
Todorokite is the principal oxide mineral.
d-spacings as indicated, in Å.
T=todorokite.
Q=quartz.
F=felspar.
Intensity, % full scale.
60
50
40
30
20
10
T+δMnO2 1.4-1.43
T+δMnO2 2.4-2.46
T,F? 3.21
Q, 3.35
Q 4.29
T 4.45
T 4.85
T 6.99
T 9.76
90
80
50
40
30
20
10
5
°2θ, Fe Kα

X-Ray Diffractogram of SH1307C Bulk

δMnO_2 is the principal oxide mineral.

d-spacings as indicated, in Å

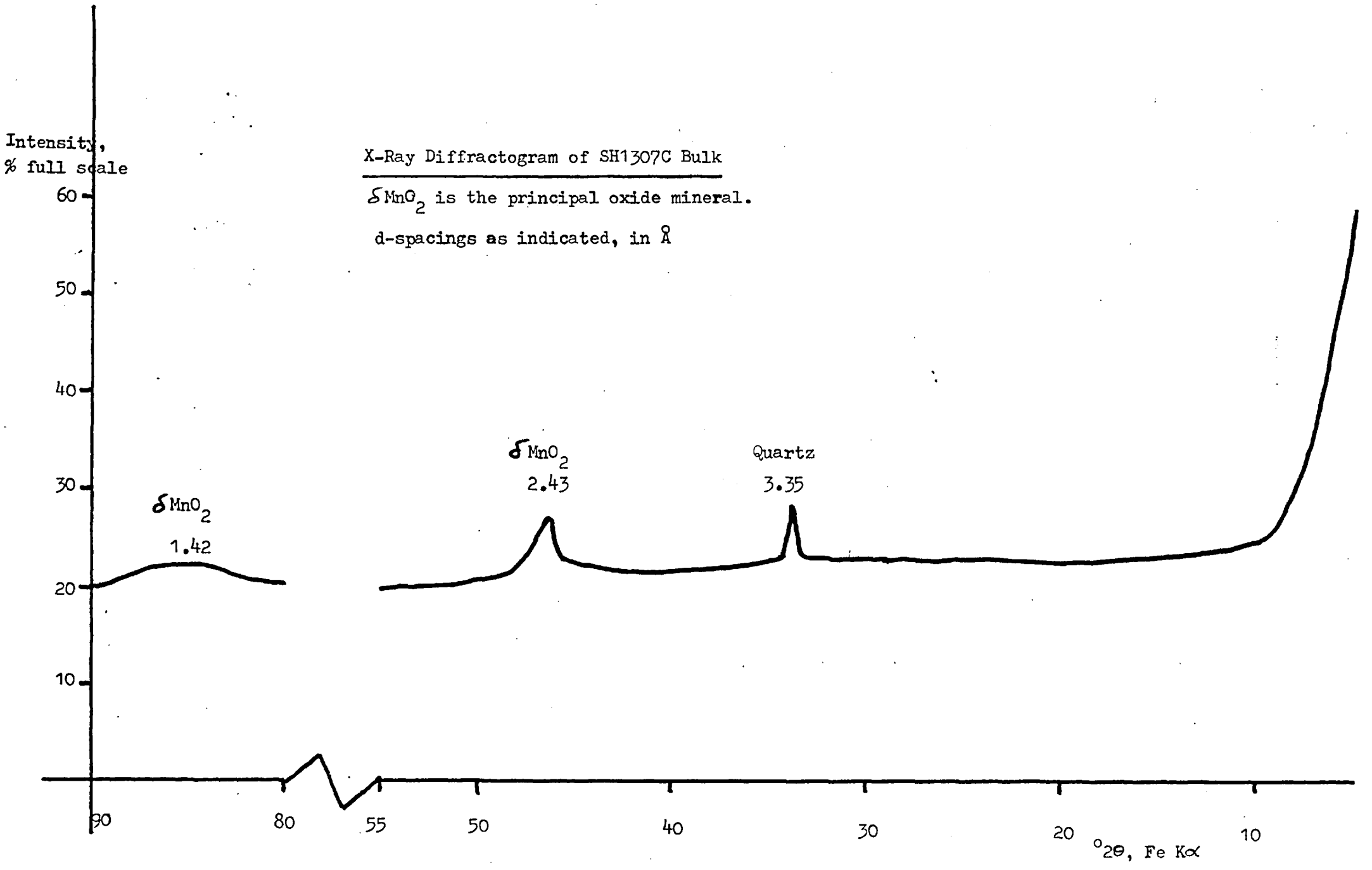

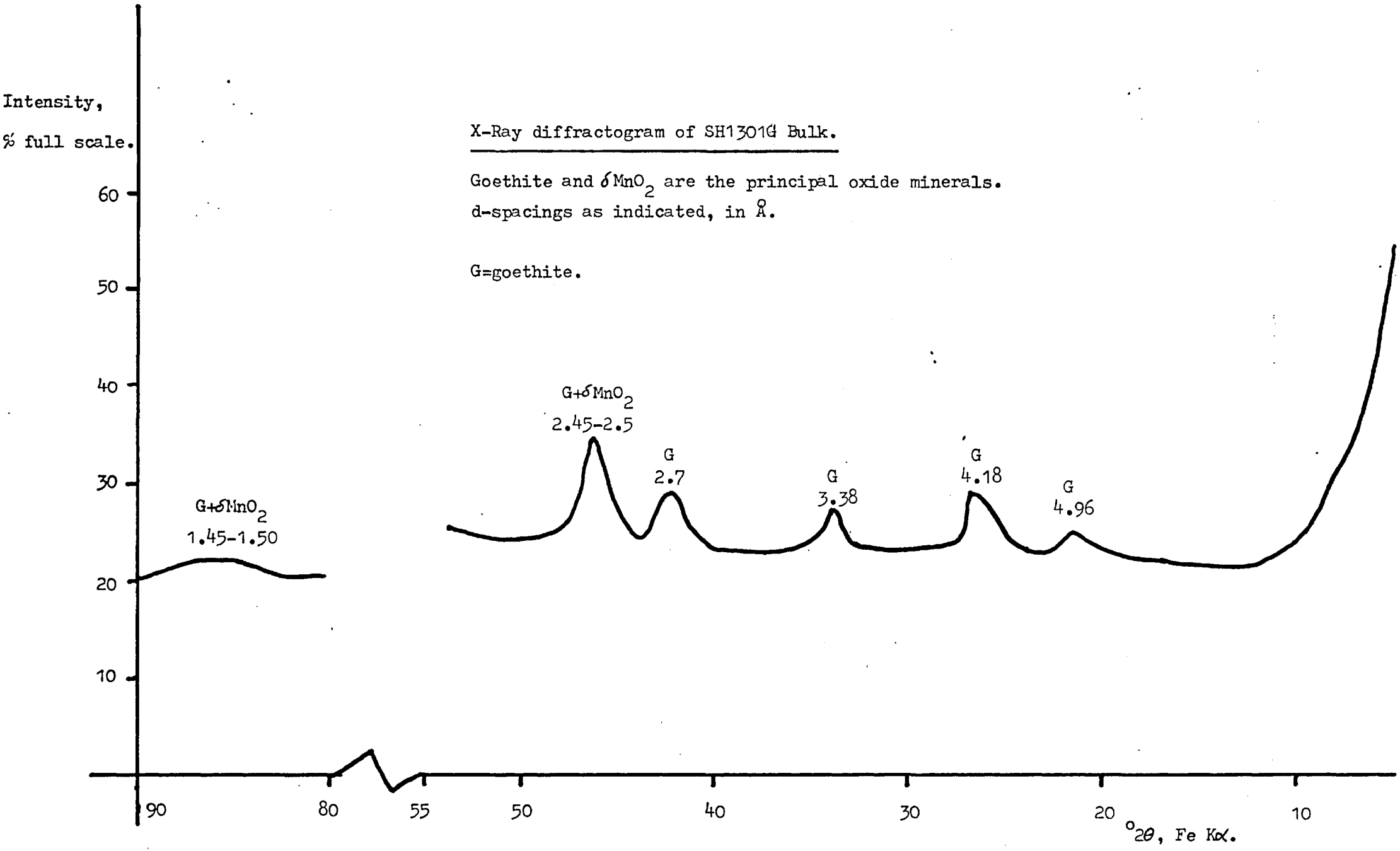
Intensity,
% full scale.
60
50
40
30
20
10
X-Ray diffractogram of SH1301G Bulk.
Goethite and δMnO2 are the principal oxide minerals.
d-spacings as indicated, in Å.
G=goethite.
G+δMnO2
1.45-1.50
G+δMnO2
2.45-2.5
G
2.7
G
3.38
G
4.18
G
4.96
90
80
55
50
40
30
20
10
°2θ, Fe Kα.